Modelling the M-Effect in H.R.C. Fuses

D. A. BEAUJEAN

Ph.D. March 1991

STATEMENT

The work submitted in this thesis has been carried out entirely by the candidate, under the supervision of Dr. M. G. Jayne, at the Department of Electronics and Information Technology, The Polytechnic of Wales, and has not been accepted for, nor currently submitted for any other degree.

.....
Candidate

.....
Director of Studies

MODELLING THE M-EFFECT IN H.R.C. FUSES.

DAVID ALEXANDER BEAUJEAN.

A thesis submitted in partial fulfilment of the requirements of the Council for National Academic Awards for the degree of Doctor of Philosophy.

March 1991

The Polytechnic of Wales

in Collaboration with Brush Fusegear Ltd.

ACKNOWLEDGEMENTS

I should like to thank Dr. J.D. Davies, Director of The Polytechnic of Wales and Professor P.A. Witting, Head of Department, Electronics and Information Technology, for permitting this work to be undertaken.

I am also indebted to the following people:

My Director of Studies, Dr. M.G. Jayne, Principal Lecturer in the Department of Electronics and Information Technology, Polytechnic of Wales for his patience and professional advice at each stage of the investigation.

Mr. P.G. Newbery, Technical Director, Brush Fusegear Ltd. for his support throughout the project. In particular I should like to thank two members of his engineering staff, Mr. John Peak, Chief Engineer - L.V. Fuses and Mr. Harold Handcock, Senior Engineer - H.V. Fuses for their sound advice and practical assistance.

To my colleagues in the Polytechnic of Wales who have contributed at various stages, and also Dr. J.C. Newby, Department of Mathematics and Statistics, Brunel University.

I am thankful to Miss C.E. Rees, Department of Science and Chemical Engineering, Polytechnic of Wales, for help in preparing the micrographs and also to Miss C. Bell, a member of the secretarial staff in the Department of Electronics and Information Technology for typing this thesis.

My final thanks to go to my wife and children for the patience they have shown during the many hours I have spent on the investigation, which otherwise would have been spent with them.

MODELLING THE M-EFFECT IN H.R.C. FUSES

D.A. BEAUJEAN, B.Sc.(Lond.), M.Sc.(Wales), C.Eng., M.I.E.E.

SYNOPSIS

The long-time operation of the modern high rupturing capacity fuse using notched strip elements and M-effect alloy, is governed by the inter-relationship between the element current distribution, the corresponding element temperature distribution, and the M-effect diffusion rate. This thesis describes a novel method which has been developed to model these complex effects, and hence determine fuse-link pre-arcing behaviour.

The method is based on modelling both temperature and diffusion as electrical analogues and to utilise a computer circuit analysis software package to simulate the resulting circuitry. Although such packages have been available for several years, they have never been used, as far as it is known, to model fuse operation. The model enables fuse parameters to be studied to depths previously not possible, and offers unrivaled possibilities in the fields of fuse design and fuse applications.

Examples of temperature distribution and diffused element concentrations and their variation with both current and time are shown, and comparisons of calculated and experimental results given. The cooling effect of the granular filler and its variation with filler depths is also studied.

The data for the diffusion model is obtained from fuse elements which have been heat treated under both constant temperature and constant current conditions and then extensively analysed using both optical and scanning electron microscope, S.E.M., techniques. Measurements from the micrographs obtained enable both the diffusion coefficient and activation energy of the system to be determined. The effects of varying the quantity and composition of the M-effect alloy and their impact on fuse operation are also presented.

The model is used to predict the time-current characteristic for fuse elements both with and without M-effect and comparisons with experimental data made. Finally, the possible ageing of fuses utilizing M-effect is studied and fuse service-life predictions made.

CONTENTS

CHAPTER 1

INTRODUCTION

1.1 Introduction

The fuse is the most widely used of all electrical safety devices, and occupies a major role in the protection scheme for electrical systems. Under short circuit conditions the modern high rupturing capacity (h.r.c.) fuse is in many ways superior to other circuit breaking devices. It has a high breaking capacity (some designs tested up to 200kA at 13kV), requires no calibration throughout its service life, and provides reliable discrimination with circuit breakers and other fuses over the complete fault current range. It is generally non-deteriorating, relatively cool running, silent in operation, emits no harmful flames or gases and requires no maintenance. It limits the current to a value considerably lower than the prospective fault current and forces the current gradually to zero, usually within the first half cycle of fault current, minimizing both the arcing or switching voltages generated and the energy let through into the faulty circuit. It is of a deceptively simple construction, yet embraces a very high degree of technology and its operation is considerably more complex than may at first be appreciated. Correctly specified, the fuse offers an unequalled degree of protection at a cost which is small compared to that of the system and equipment

protected, and its continued improvement is reflected in the steady stream of amendments to the relevant international standards.

1.2 The Evolution of the Fuse

As far as is known, the fuse was the earliest protective electrical device. Probably the first record of the use of fuses was in 1864 when they were used to protect cables [1], but it was the invention of the incandescent lamp in the eighteen eighties and the subsequent demand for public lighting which necessitated the rapid development of reliable protective equipment. In 1879 S.P. Thompson [2] produced a fuse which consisted of two iron wires connected together by a ball of low melting point metal, as shown in Fig. 1.1. Passing a sufficiently high current through the fuse, caused the ball to melt, breaking the circuit.

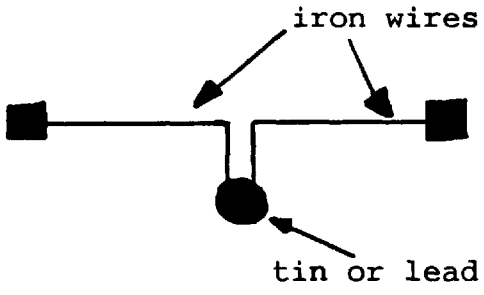

Fig. 1.1
(After Newbery and Wright [11])

In 1883 C.V. Boys and H.H. Cunyngham [3] patented a fuse which consisted of two leaf springs soldered together as shown in Fig. 1.2. Above a certain current the solder melted and the strips sprang apart breaking the circuit.

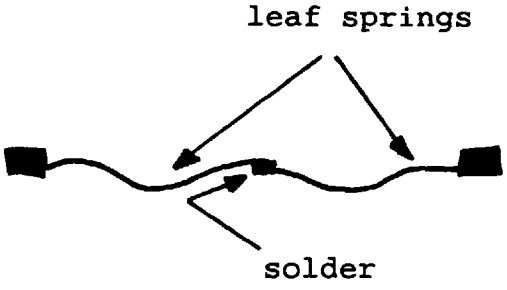

Fig. 1.2
(After Newbery and Wright [11])

In 1887 A.C. Cockburn [4] attempted to put the subject of fuse design and operation on a sound scientific basis by studying the effects of fusing current on the heat conducted away to the fuse terminals, and also by studying the properties of materials likely to be suitable for use as fuse elements. Although investigations such as this considerably increased fuse understanding, the majority of early fuses still basically consisted of an open wire between terminals, the wire being typically made from a low melting point metal such as lead or tin. Increased power demand led, however, to higher fault levels, resulting in increasingly violent fuse operation.

The first enclosed element fuse was described by T. A. Edison in 1880 [5]. In this design a wire element was placed in a glass tube in an attempt to limit the emission of gas and flame which occurred during fuse operation. The glass tube was later replaced by an asbestos tube, a design still widely used on low fault level domestic circuits. The breaking capacity achievable with this design, however, was inadequate for the majority of industrial applications, and further improvements were necessary.

In 1893 W.M. Mordey [6] patented what may be considered the forerunner of the modern cartridge fuse. This patent described a fuse with "one or more copper wires enclosed in a short glass tube and surrounded by a non-conducting and incombustible powder which effectually quenches the arc". The move to copper elements with their relatively high melting temperature and the use of an arc absorbing medium greatly increased the breaking capacity of the fuse and was a major advance in fuse design. In 1905 Oelschläger [7] showed that the performance of the fuse could be further increased by the use of elements of varying cross-section.

Steady improvements in the type and size of arc absorbing filler and the configuration of the fuse elements were made throughout the 1920's and 1930's and in 1939 J.W. Gibson [8] reviewed the design and operation of h.r.c. fuses and their electrical performance in the light of the newly issued British Standard on fuses, BS 88 (1939). Gibson showed that the fuse element material should, ideally, have a low value of resistivity, high melting point, low specific heat and resist oxidation to ensure a long service life. Silver met these requirements the closest, although because of cost considerations, copper was also used.

One possible disadvantage of fuses using silver or copper elements is the relatively high melting temperature of these metals. This means that under low over-current conditions, the fuse may 'thermally soak' up to temperatures of several hundred degrees before operating, which may cause

overheating of itself and adjacent equipment. This problem was overcome by Metcalf [9] when in 1939 in his paper entitled 'A new fuse phenomenon', he showed that the operation of the fuse could be improved by the addition of a small globule of low melting point metal, such as tin or lead, or a combination of the two, to the centre of a silver or copper fuse element. The fuse element dissolved in the low melting point metal at a temperature considerably lower than the melting temperature of the fuse material, and he concluded ".... the melting point of the fuse wire is reduced to nearly one third of its normal value simply by the application of a globule of solder to the centre of the wire". He called this effect the **"M-effect"** and is, in essence, **the modification of the electrical parameters of a fuse by the addition of a small quantity of a low melting point metal or alloy to the centre of the fuse elements.**

H.R.C. fuse design, particularly for use on high voltage circuits (over 1000 volts) was pioneered by Gibson and others in the 1950's. Designs utilising silver elements of varying cross-section with "M-effect" alloy at their centres and surrounded with high purity silica sand as the arc extinguishing material proved to be the most successful in meeting the then newly issued British Standard on high voltage fuses, BS 2692 (1956).

Although the basic configuration of the h.r.c. fuse has remained unchanged since the mid 1950's, design improvements have greatly increased fuse performance over their complete operating range and have allowed much larger current ratings to be achieved from a given body size.

1.3 The Design of the Modern H.R.C. Fuse

Fig. 1.3 shows a typical modern h.r.c.fuse in section. The ceramic barrel and copper end-caps which enclose the fuse have to withstand very high pressures and temperatures which occur at the moment of operation. Instantaneous pressures of 1000 p.s.i. and arc temperatures of 10,000°K are not uncommon.[10] The heart of the h.r.c. fuse is the current carrying elements. Elements are typically made from silver, silver plated copper or plain copper wire or strip. The length of these elements determine the voltage capability of the fuse, the number and cross-sectional area of the elements determine its current carrying capacity and the shape of the elements, together with their spacing and configuration determine the electrical characteristics of the fuse.[11] Early fuses used silver wire as the fusible elements. The main disadvantage of this design was under short circuit conditions the whole element would melt simultaneously and, due to the dissipation of the circuit's inductive energy, an arc, broken only by molten element globules, drawn out along the complete length of the wire. This produced an unacceptably high switching voltage which was impressed across the whole system causing flashovers or insulation damage. Modern h.r.c. fuses use strip elements

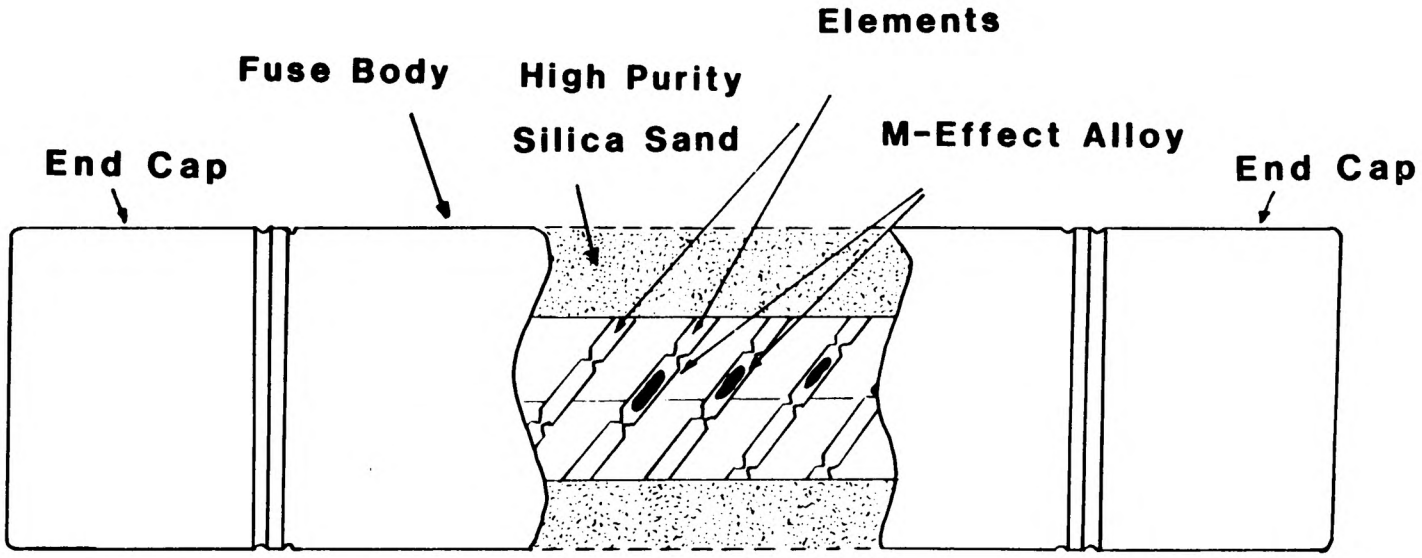

DESIGN OF A MODERN H.R.C. FUSE

Fig. 1.3

which have varying cross-sections or restrictions in the form of notches or holes punched in a regular pattern along their length.(Fig. 1.4) The current density and thus temperature at these restrictions is much higher than that in the bulk strip and thus under short circuit conditions these restrictions melt first. A series of short arcs are thus drawn out and the current reduced to zero in a controlled manner, greatly reducing the switching voltage. The majority of modern fuses use strip elements with wire being used only for the lowest current ratings, such as 1 or 3 ampere fuses where the use of strip of such small cross-sectional area would be impractical. In the case of fuses having elements which are of greater length than the fuse body, the elements are helically wound, upon a ribbed ceramic former, known as a 'star core', otherwise the elements are suspended between the endcaps inside the fuse barrel. The elements are surrounded by a compacted mass of silica sand of high purity and closely controlled mesh size. The thermal and electrical properties of this filler, along with its shape and degree of compaction, has a major influence on fuse performance [12,13]. By a suitable choice of element and notch size, silica sand filler, body and endcap parameters, fuses with the operating characteristics required to suit particular applications may be produced.

M-effect alloys which usually consist of various tin formulations are used on the majority of British designed fuses.

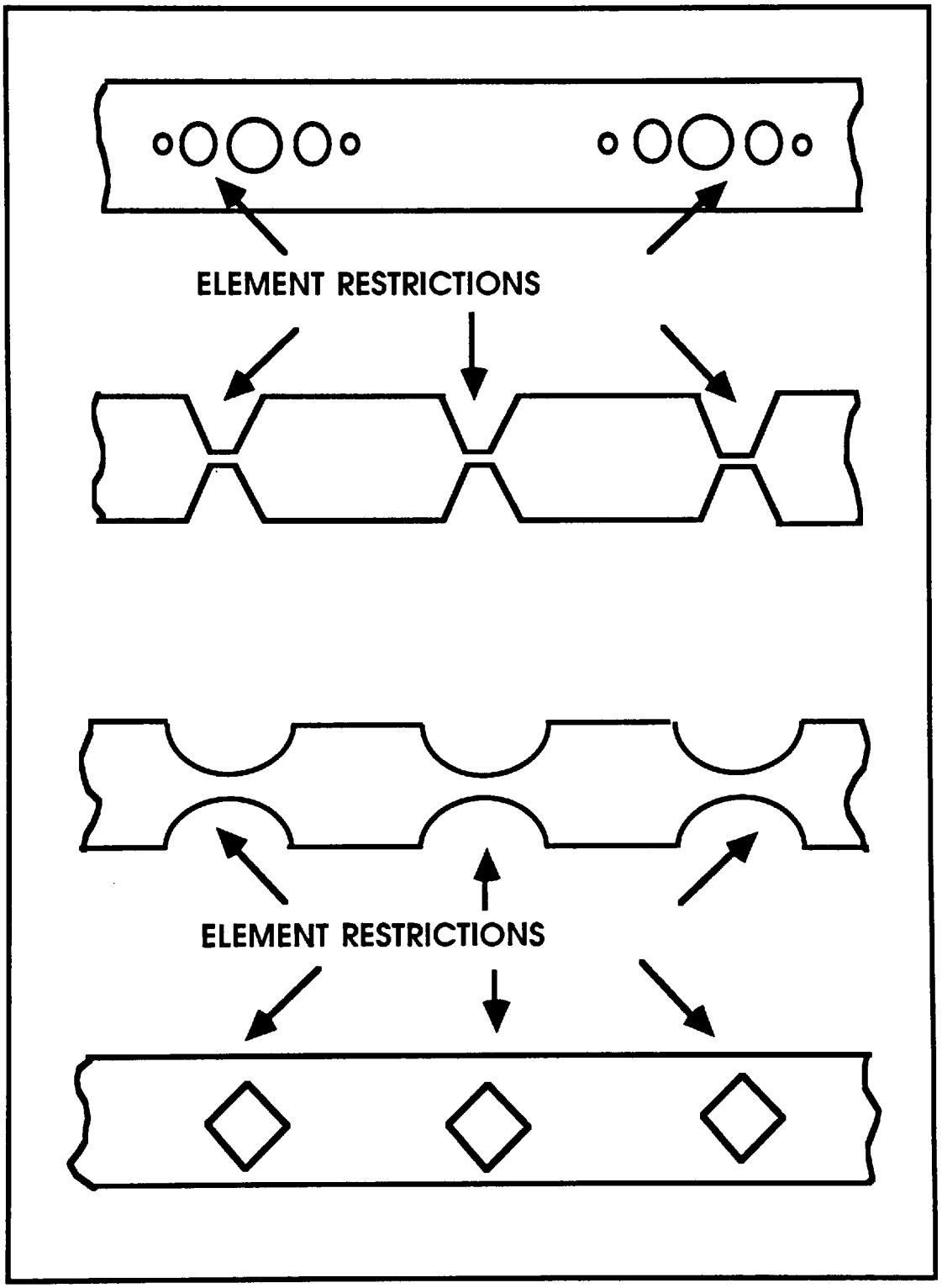

Some Fuse Element Designs

Fig. 1.4

M-effect fuses have a lower watt's loss at rated current and thus run cooler than equivalent fuses without M-effect, and also have the major advantage that the maximum temperature reached during operation is considerably lower.[14] This substantially reduces the risk of the fuse overheating and the barrel cracking due to the resulting differential expansion of the barrel and the granular filler. It also prevents the fuse overheating any temperature sensitive surroundings, such as enclosed resin bonded switchgear, both carrying normal full load current and during operation on low fault currents.

Not all fuse manufacturers use the M-effect, and their fuses tend to run and operate at appreciably higher temperatures. These manufacturers claim that the use of the M-effect alloy causes the fuse to deteriorate over a long period of time. This reduces its useful life and in some situations may lead to it operating on currents less than its minimum breaking current (see section 1.4.1) and thus subjecting it to a condition which may cause catastrophic failure.

Although fuse manufacturers have utilised the M-effect for many years its use has been on an empirical basis. Little work of a quantifiable nature has been carried out to explain M-effect action, or to predict the effect of the M-effect process on fuse operation, and the possibility of fuse deterioration through its use is a question which has not yet been fully resolved.

Studying and predicting the operating characteristics of fuses, and in particular fuses using this "M-effect" alloy addition to their elements will form the basis of this thesis, but before discussing this in detail it is necessary to briefly outline the modes of operation of fuses and to introduce some of the terminology associated with fuse design.

1.4 Modes of Fuse Operation

In its normal load current carrying role the fuse must carry rated load current and permitted overloads for an indefinite time without deterioration. Under fault conditions, however, the fuse must disconnect the circuit as quickly as possible absorbing the many kilojoules of resultant arc energy within itself and limiting, as much as possible, the energy let through into the faulty circuit [8,15]. There are two distinct periods in fuse operation, namely the "melting" or "pre-arcing period" and the "arcing period".

1.4.1. The Pre-Arcing Period

Every fuse must have some electrical resistance, determined by its element configuration and general construction. Under constant load current conditions, ohmic heating will cause the fuse temperature to rise, and eventually stabilise at some constant temperature where the heat input is balanced by the heat losses to the surroundings by conduction and convection. A typical 11kV distribution fuse may dissipate 100 watts at its rated current resulting in a barrel temperature rise of approximately 40°C.[10] If the load

current is then increased, the fuse temperature will again rise and re-stabilise at some higher temperature. If the current is continued to be increased in this way, then eventually a current will be reached where the ohmic heat input into the fuse exceeds the heat losses. When this point is reached, thermal equilibrium cannot be established and the fuse temperature continues to rise until the element melting temperature is reached. Once the sections of element have melted and broken up, then, under the action of the applied voltage, arcs are drawn out between the remaining sections of elements. These arcs are eventually extinguished by the arc quenching action of the fuse filler.[12]

The greater the current applied to a fuse, the faster the fuse temperature rise and the shorter the time taken for the fuse to reach its melting temperature. All fuses, therefore, have an inverse minimum current/time operating characteristic (Fig. 1.5). The curve is assymptotic at a particular value of current, and, theoretically, the pre-arcing time is infinite at this value, known as the **"minimum-fusing-current"**. For practical purposes, this minimum fusing current, which is the maximum current at which thermal equilibrium can exist, is taken as the current which will melt the fuse in a long, but definite time - typically 4 to 6 hours.[11]

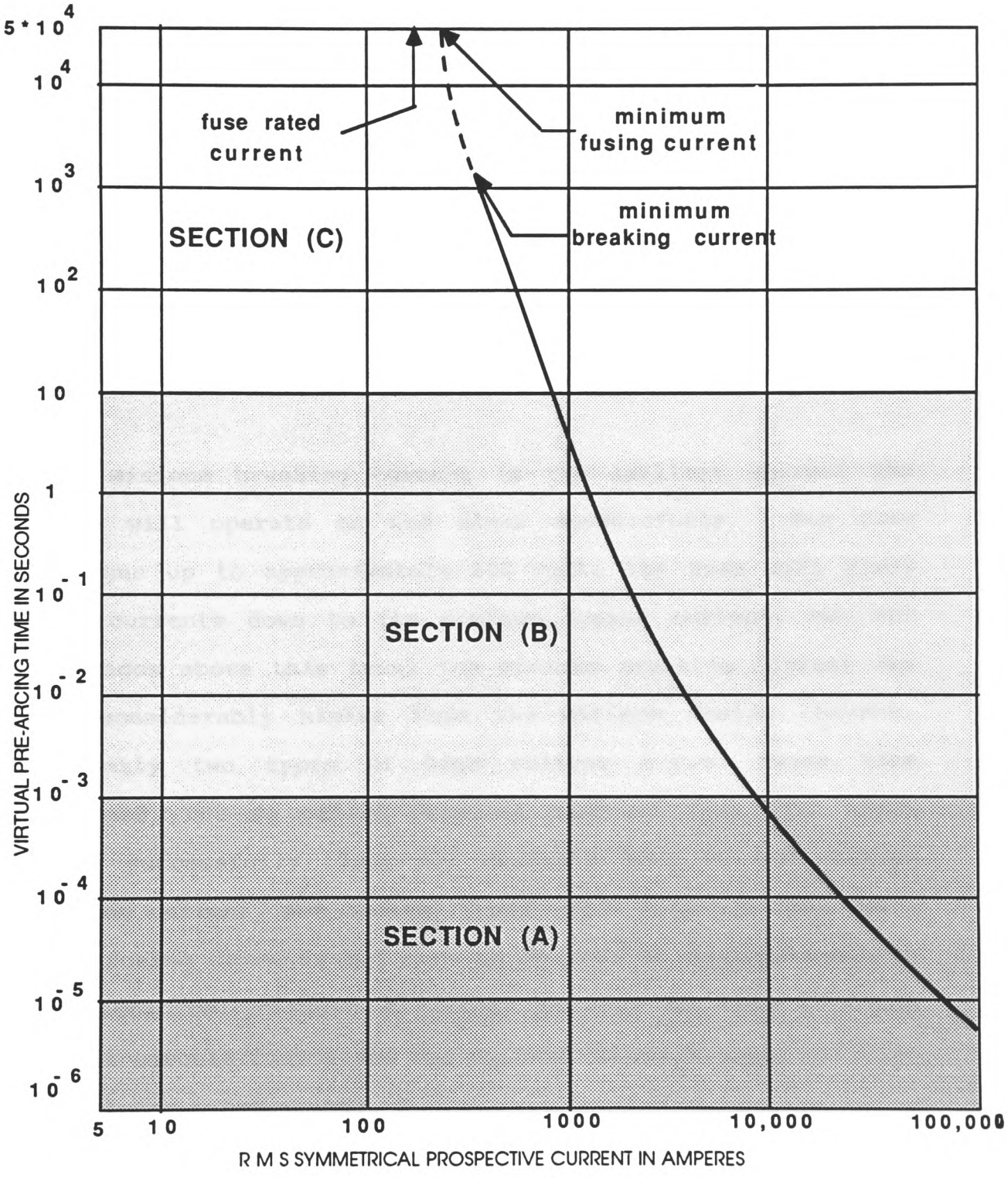

Time-Current Characteristic for an H.R.C. Fuse

Fig. 1.5

The **minimum fusing current** should not be confused with either the the **fuse rated current** or the fuse **minimum breaking current.**

The **fuse rated current** is the current the fuse can carry indefinitely, without exceeding permitted temperature rise limits. It obviously has to be less than the minimum fusing current, but there is no fixed relationship between the two. Typically the ratio minimum fusing current / rated current is between 1.3 and 2.

The **minimum breaking current** is the smallest current the fuse will operate on and clear successfully. For fuse designs up to approximately 600 volts the fuse will clear all currents down to its minimum fusing current, but for voltages above this level the minimum breaking current may be considerably higher than the minimum fusing current. Recently two types of high voltage h.r.c. fuses have emerged, the so called **"general purpose" fuse** [14] which will successfully clear all currents down to its **minimum fusing current**, and **back-up fuses** which will not clear very low fusing currents and have to be used in conjunction with a mechanical circuit breaking device, the fuse clearing short circuit faults and the switch/circuit-breaker clearing the lower overcurrents.

1.4.2 The Arcing Period

In the case of low level faults, say up to about three times the minimum fusing current, the elements reach melting temperature gradually over a period of many seconds or minutes.[11] The centre of the fuse elements tend to be the highest temperature, since heat is conducted away from the relatively massive fuse ends, and eventually one element, because of slight dimensional differences, will melt first at its centre, transferring its current to the other parallel elements. Each element then melts in turn until when the last element melts, the full system voltage appears across the break. This element then breaks up into a number of small arcs in series and the vapourised element is absorbed by the silica sand forming a silica-sand slag known as 'fulgurite' (see Fig. 1.6).[12] The remaining elements then restrike, arc and extinguish in turn, since at low fault currents the arcs are unstable and cannot exist in parallel simultaneously [8]. The fuse eventually clears the current after several cycles of arcing.

At high fault currents, typically values of current which will melt the fuse in a few milliseconds, the element restrictions all reach melting temperature approximately simultaneously, the heat losses being negligible during the short times involved.[17] The elements melt at several points along their length and multiple arcs are drawn out. These arcs burn back and clear more or less at the same

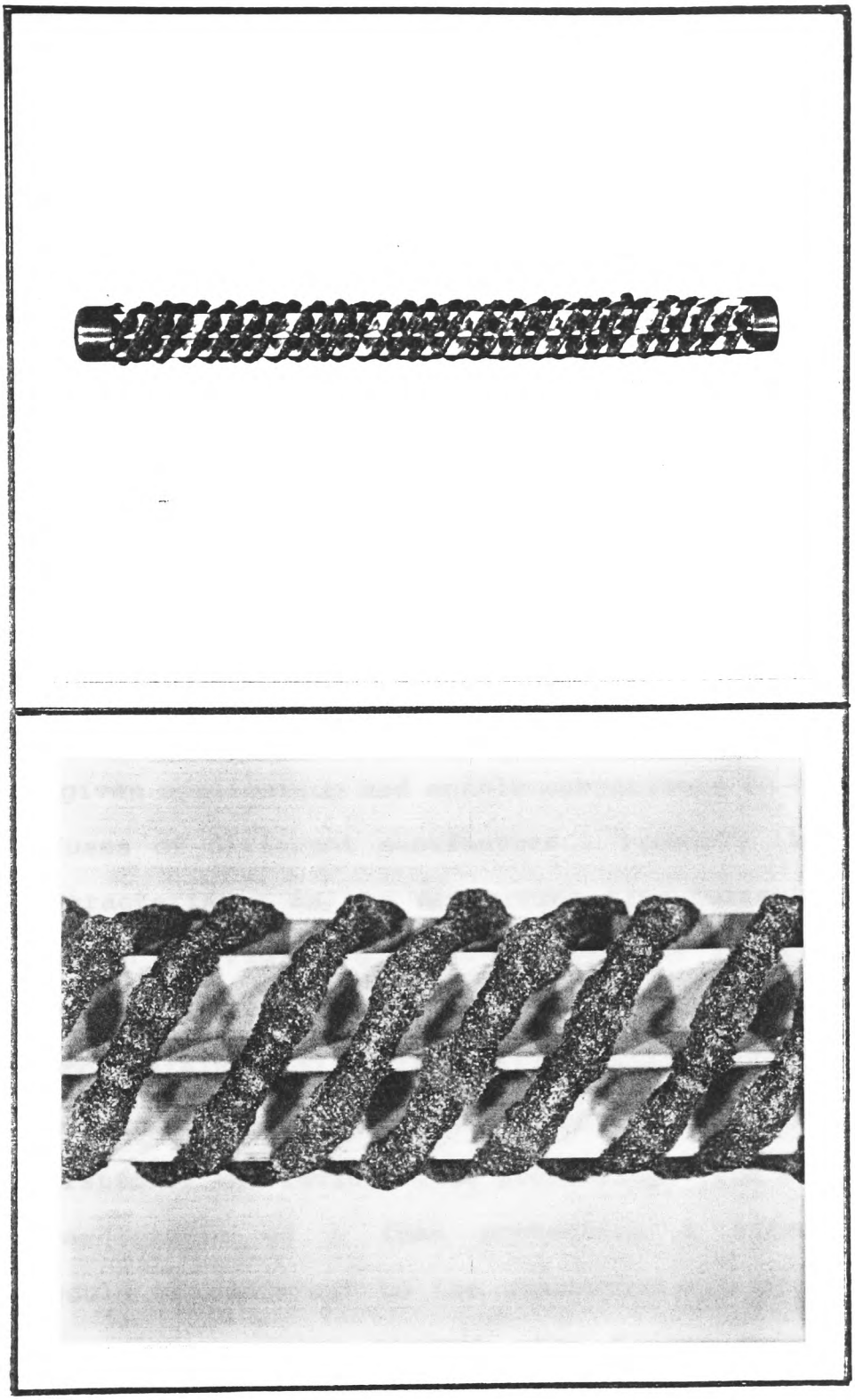

(a)

(b)

Elements from an Operated Fuse showing the Formation of Silver/Sand 'Fulgurite'

(a) Complete 12 kV. Star Core after Fuse Operation

(b) Enlarged Section of Part of the Fulgurite

Fig. 1.6

time, normally within the first half cycle of arc current, minimising the quantity of energy let through into the fault.

The amount of 'fulgurite' produced during arc interruption is directly related to the energy absorbed by the fuse (approximately 2.15kJ per gram of fulgurite [8,12]), and an examination of the fuse after operation can yield considerable information about the type and severity of the fault current.

1.5 The Fuse Time-Current Characteristic

The characteristics of a fuse determine its suitability for use in a given application and enable comparisons to be made between fuses of different manufacture. Probably the most useful characteristic is the **pre-arcing time-current curve** [18],as shown in Fig. 1.5, which shows the relationship between the **applied fault current** and the fuse **pre-arcing time** (approximately equal to the melting time). Ideally the fuse characteristic should be tailored to suit the characteristic of the device it is protecting. For example, the characteristic of a fuse protecting a transformer circuit would be different to the characteristic of a fuse protecting, say, a motor circuit, the former being much shallower than the latter [15](Fig. 1.7). In general, the fuse must accept, without deterioration or exceeding permitted temperature rise limits, periodic overloads and current surges associated with transformer and capacitor inrush currents, motor starting currents, and other pulsed

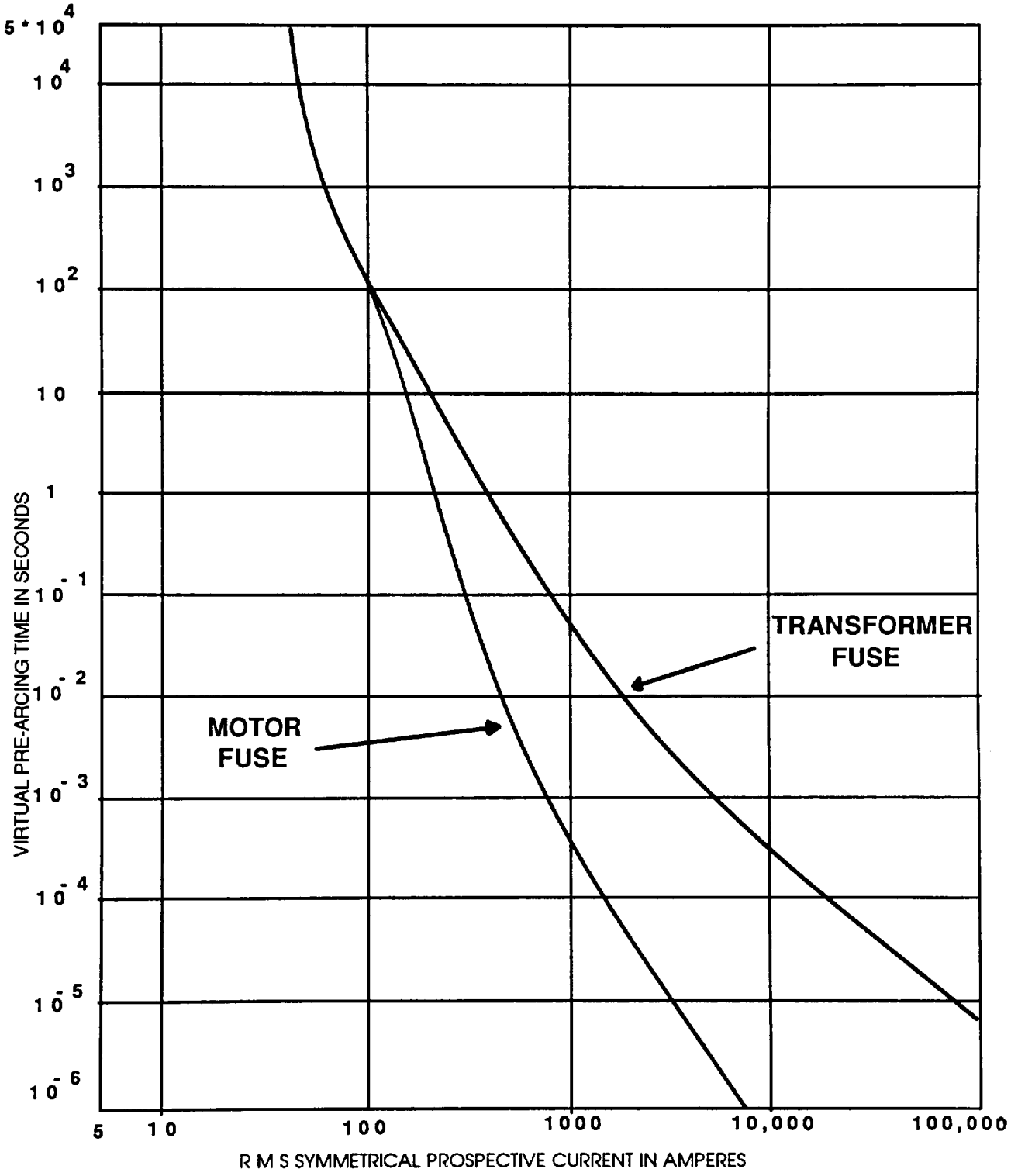

Time-current Characteristics Of Fuses To Protect Motor & Transformer Circuits

Fig. 1.7

overloads but operate quickly in the event of a fault. The final design of the fuse must, therefore, embrace all the requirements to achieve the optimum shaped time-current characteristic whilst at the same time meet the stringent breaking capacity specifications. The shape of the characteristic is, in the main, determined by the number, cross-sectional area, shape and spacing of the elements. Other factors, however, such as filler type, rated current watts loss and barrel and endcap temperatures must also be taken into account.

The time-current characteristic can be roughly divided into three time sections, A, B and C as indicated in Fig. 1.5

For pre-arcing times up to approximately one millisecond (section A), the element heating is adiabatic (constant I^2t) and all element restrictions reach melting temperature simultaneously, there being virtually no heat loss to either the remainder of the element or other fuse components. The time-current characteristic is thus a straight line up to approximately one millisecond [17].

For pre-arcing times between one millisecond and approximately ten seconds (section B), heat is conducted away from the element restrictions firstly to the remainder of the element, and then to the granular filler and end connections. The element restrictions thus take longer to melt than under adiabatic heating and the characteristic bends away from the straight line.

For pre-arcing times greater than approximately ten seconds (section C), heat is conducted away through the elements to the end caps and connecting cables and also through the granular filler to the fuse barrel and hence by convection to the surrounding air. These heat losses slow down considerably the rate of rise of restriction temperature and the time-current characteristic thus bends further away from the adiabatic straight line.

The slope of the characteristic is further modified for times greater than a few seconds by using "M-effect" alloy. The increased element melting speed achieved by adding a low melting point metal or alloy to the centre of each element reduces the long-time melting current without modifying the short circuit performance [14].

1.6 The Modelling of Fuse Operation

In the event of a high current fault, that is, one which will cause the fuse to melt in times of less than approximately one millisecond, adiabatic heating of the element causes the element restrictions to quickly reach the melting temperature of the element material. The operation of fuses under these conditions has been considerably researched and both analytical and numerical mathematical models for predicting pre-arcing behaviour obtained [17,19,20]. For longer pre-arcing times, however, when heat loss to the filler has to be taken into account, these models lack accuracy due to the complex nature of the heat loss equation. No models currently exist for

successfully predicting pre-arcing times longer than a few seconds and the time-current characteristic for longer times is either determined experimentally, or interpolated from existing practical data on similar designs.

The remainder of this thesis will consider the pre-arcing characteristics of fuses, and in particular the investigation of the long-time operation of fuses using the M-effect. A novel model for predicting the long-time pre-arcing characteristic of fuses using the M-effect will be developed and compared with experimental data. Once installed, fuses are expected to have a life expectancy of many years in a fault free circuit, and the novel models developed by the author will be used to predict any fuse degradation due to the use of the M-effect.

The development of a new model would not only allow the fuse design engineer to determine the outcome of any design modifications without the need for recourse to expensive, time-consuming experimentation, but would also allow the prediction of long term effects which at present can only be determined by extracting fuses from service and subjecting them to destructive examination.

CHAPTER 2

MODELLING FUSE OPERATION

2.1 Introduction

Fuse operation has been modelled by several researchers. Both analytical and numerical methods have been used, in some cases a mixture of the two, with varying degrees of success. In general, however, the simplifying assumptions made in formulating the the model prevented a reasonable degree of accuracy being achieved over the whole pre-arcing time-current characteristic, that is, from operation with short-circuit faults to that with the minimum fusing current, for even the simplest of designs. Indeed, many of the models only considered short-circuit operation, and made no attempt to evaluate fuse behaviour under long-time operating conditions. A brief survey of such attempts will now be given.

2.2 Previous Attempts at Modelling Fuse Behaviour

Early attempts at fuse modelling were based on the analytical solution using classical techniques of the complex heat equations which describe fuse operation. Ikeda and Yoneta [21], Novotny [26], and Schubert [22], all attempted to obtain solutions in this way, but in doing so had to make considerable simplifying assumptions. In general, accurate determination of heat losses from the fuse element to the surroundings was not possible in all but the

shortest time periods, and whilst reasonable results were obtained for fast operating times, accuracy diminished for longer time periods. The model of Ikeda and Yoneta also only applied to long wire elements in air, and this could not be used on the vast majority of fuses in which the elements are surrounded by a granular filler.

Guile and Carne [23] published a paper describing a method for calculating the temperature distribution along a wire in a long fuse barrel. The calculations assumed the resistivity and thermal properties of the wire were independent of temperature, and that there was no radial heat loss from the wire. The temperature rise of the wire could be predicted to within 20% for short operating times, but predictions were not valid for times longer than approximately one millisecond.

Guile [24,25] published two further papers on analytical solutions to the heat equations, covering both wire and strip elements. Again simplifying assumptions on heat loss meant that reliable results could only be obtained for very short operating times.

Wilkins [19] used a semi-analytical model to determine element temperature distribution for notched strip fuse elements, and the resulting analytical equations solved on a computer using an iterative method. The equations used were those developed by Guile [25] in which the notched strip was

replaced by an "equivalent round uniform wire", upon which the thermal calculations were then based. The model first calculated the element temperature distribution after a fixed time interval for a given applied current. If the maximum temperature obtained was less than the element melting temperature, then the temperature was recalculated for the next time interval. This process was repeated until the element's melting temperature was reached, and the melting time determined. The model was unique in that it contained a "correction term" to allow for fuses using an M-effect alloy. For these fuses it is not sufficient to consider that operation will occur if the temperature exceeds the melting point of the M-effect material. Even if this temperature is exceeded the rate of diffusion of the alloy through the element may be so slow that operation will not occur for some time. To allow for this Wilkins estimated the time for the alloy to diffuse through the element and from this computed an "effective melting temperature". This new temperature was then used as the element melting temperature in the model. Good agreement was claimed to be obtained with experimental results for pre-arcing times of several seconds. No results obtained using this model have, however, ever been published and thus the accuracy of the model is not known.

Recently, computer based models for predicting fuse behaviour have been developed. Leach, Newbery and Wright [17] used a step numerical technique based on finite difference methods to analyse current density and heat flow in the fuse element. Account was taken of the electrical

resistance change with temperature and the spatial variation of current density which exists with notched strip elements. Axial heat flow from restrictions and radial heat flow to the filler was also considered, as was the temperature variation of the fuse body and end caps. Published results indicate that this model gave good agreement (within $\pm$ 10%) with experimental results up to pre-arcing times of approximately one second, but accuracy reduced for longer pre-arcing times due to the complicated heat loss equations.

Wilkins and McEwan [20,27] used a finite difference method very similar to that developed by Leach, Newbery and Wright to study pre-arcing currents in both uniform section and notched fuse elements, but in both cases their investigations were restricted to very short pre-arcing times (<100 milliseconds) as heat loss was not taken into account.

Xinzhong and Wang Ji-Mei [28] used a finite element technique to calculate the temperature rise of fuse-links and used a heat dissipation factor to account for any heat loss. They allowed for M-effect action in a similar way to Wilkins by determining an "effective melting time" for the alloy. Results within 10% were claimed for short pre-arcing times.

Hofmann and Lindmayer [29,30] used a semi-numerical, semi-experimental method to predict the time-current characteristics of plain, unnotched copper element fuses using M-effect. They used the commercial finite element

package ADINAT (A Finite Element Program for Automatic Dynamic Non-linear Analysis of Temperature) [31] to predict fuse element temperature rise, but modified the fuse element resistivity values by taking into account changes due to diffusion of the M-effect alloy into the base element. These diffusion depths were not, however, calculated by the program, but obtained from experimental measurements and injected into the program at appropriate points. Reasonable agreement was obtained with experimental results. All tests were, however, performed in air and no account was taken of the cooling effects of the fuse filler.

These numerical methods based on finite difference and finite element techniques offer the best possibilities of modelling fuse operation. The model of Leach, Newbery and Wright in particular gave results within $\pm$10% for pre-arcing times up to about one second, and although it lacked accuracy for longer times the model was capable of giving a reasonable guide to fuse performance over a range of operating times on notched silver strip elements. This model is, however, based on the assumption that the notched sections are the hottest part of the element and that fuse operation will eventually occur due to one or more of these restrictions melting and thus breaking the circuit. For melting times up to approximately one second this is indeed the operating mechanism, but for longer times this is not necessarily the case. Most British fuses use M-effect alloy to modify their operating characteristics, and for pre-arcing times greater than a few seconds operation occurs due to the alloy diffusing through the bulk strip. Experimental

results presented later in this thesis (see Section 4.4) will show that in this case, fuse operation is not initiated at a notch or other similar current restriction, but at the position of the M-effect alloy, which is usually at the centre of the fuse element, mid-way between two notches. Since the models of neither Wilkins and McEwan nor Leach, Newbery and Wright allowed for M-effect action they cannot be applied to the majority of fuse designs for long melting times when M-effect action predominates. The model of Hofmann and Lindmayer, whilst allowing for M-effect action, did not predict the diffusion depth of the M-effect alloy, but relied on this information being available from other sources. In view of this, it was felt by the author that a new model was required which would closely simulate M-effect action and thus allow fuse operating times greater than a few seconds to be determined with a reasonable degree of accuracy.

2.3 M-Effect Operation

A simplistic description of M-effect action may be obtained by considering a deposit of tin or tin-alloy (the M-effect material) applied to the surface of a silver element (Fig. 2.1a). Electric current passing through the element produces ohmic heating and this heat is conducted to the M-effect material. The resistivity of the latter is such that only a small percentage of the total current actually passes through it, and thus very little direct ohmic heating occurs. As the current is increased, the temperature of the element increases until, eventually, the M-effect material melts. Once in a molten state, the alloy readily dissolves

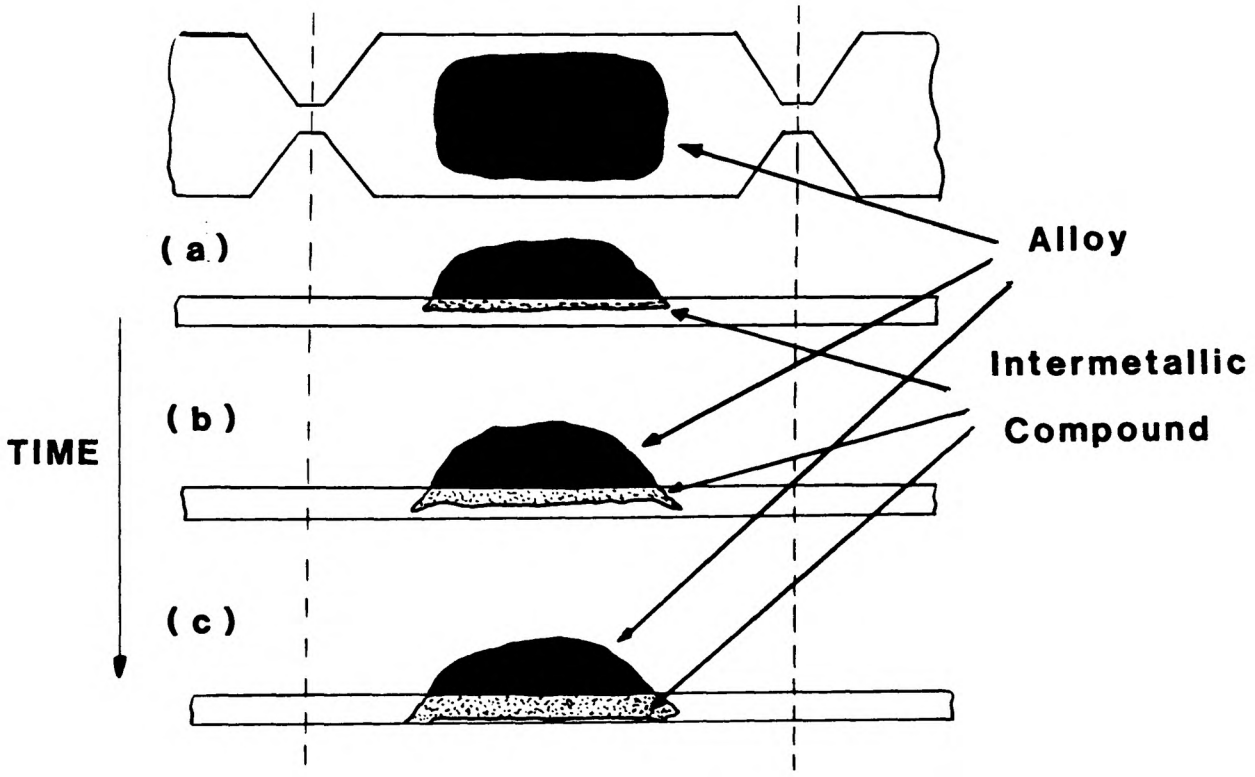

Schematic Representation Of M-effect Action
Showing The Diffusion Of The Low Melting Point
Alloy Through The Fuse Element.

Fig. 2.1

the silver element, or more correctly, diffuses through it. Whilst diffusing through the silver, tin/silver compounds are produced which have an electrical resistivity considerably higher than both the silver and the M-effect material [32]. The majority of the current is thus diverted through the reduced silver element cross-section (Fig. 2.1b). Experimental measurements (see Section 4.4) have shown that this results in a higher current density and the corresponding increase in temperature produces a local hotspot. The M-effect material temperature also rises and, as a consequence, its rate of diffusion through the silver element increases since diffusion rate is temperature dependent [33]. This cumulative process continues with increasing current density in the silver producing higher temperatures (see Section 4.4) and thus faster diffusion rates. Eventually the M-effect material diffuses completely through the silver element and fuse operation occurs (Fig. 2.1c).

Modelling the M-effect thus not only requires the current distribution and the temperature rise of the fuse element to be determined, but also the rate of diffusion of the M-effect alloy through the fuse element.

Before attempting to model the M-effect, it is necessary, therefore, to consider the underlying theory of current distribution, mass diffusion and temperature rise in a fuse element.

2.3.1 Current Flow in a Fuse Element

In order to study the generation and flow of heat in a fuse element it is necessary that the current density at various points within the element be known. Leach [34] has shown that the current in a notched element will, to a first approximation, vary in two dimensions only, as shown in Fig. 2.2, the current being essentially constant in the third dimension. In the M-effect region, however,the current will vary in three dimensions. The calculation of current flow thus involves the solution of Laplace's equation for a three dimensional system.

Laplace's equation for a three dimensional region of non-uniform conductivity may be written as [35]:

$$\frac{\partial}{\partial x}[\sigma\frac{\partial E}{\partial x}]+\frac{\partial}{\partial y}[\sigma\frac{\partial E}{\partial y}]+\frac{\partial}{\partial z}[\sigma\frac{\partial E}{\partial z}]=0 \qquad -- (2.1)$$

where, in the case of an electrical system, σ is the electrical conductivity and E the electrical potential. Writing ρ the resistivity for $1/\sigma$, equation (2.1) becomes

$$\frac{\partial}{\partial x}[\frac{1}{\rho}\frac{\partial E}{\partial x}]+\frac{\partial}{\partial y}[\frac{1}{\rho}\frac{\partial E}{\partial y}]+\frac{\partial}{\partial z}[\frac{1}{\rho}\frac{\partial E}{\partial z}]=0 \qquad -- (2.2)$$

The solution of this equation will give the electric potential at points within a current carrying conductor, from which the components of the current density in the x, y and z directions, given by :

$$Jx=\frac{1}{\rho}\frac{\partial E}{\partial x}: \qquad Jy=\frac{1}{\rho}\frac{\partial E}{\partial y}: \qquad Jz=\frac{1}{\rho}\frac{\partial E}{\partial z}:$$

can be obtained at any point in the field.

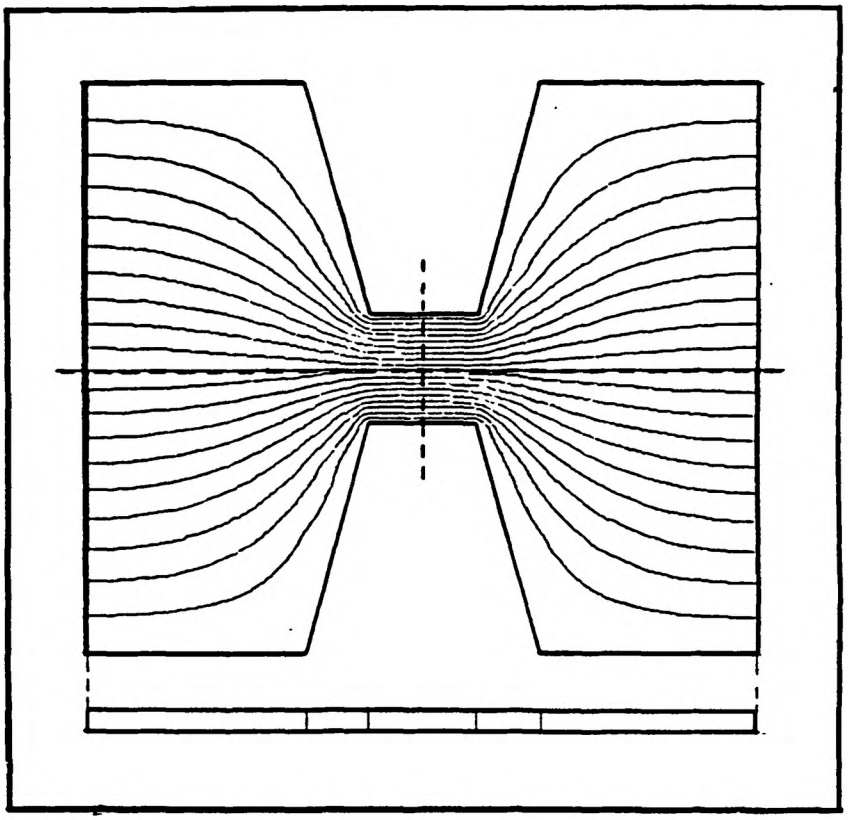

Current In A Flat Strip Varies To A First Approximation In Two Dimensions Only.

(After Leach [34])

Fig. 2.2

2.3.2 Mass Diffusion in Solid/Liquid Systems

Diffusion may be defined as the net transfer of material from a region of high concentration to one of low concentration. Diffusion occurs as a result of continuous thermal or random molecular motion. The rate of transfer of material (the solute) through a unit cross-section of a medium is known as the flux (F). If a mass M of solute transfers by diffusion through a section of area A in a time t then for one dimensional diffusion [36]:

$$F = \frac{M}{At} = \frac{D(C_1 - C_2)}{x} \qquad - - (2.3)$$

where F is the rate of mass transfer per unit area, D is the diffusion coefficient for the solute in the medium and C_1 and C_2 are the solute concentrations a distance x apart.

This expressions is a form of Fick's first law of diffusion (1855)[37] which may be more generally stated as .....'the rate of transfer of a diffusing substance through a unit cross-sectional area of the diffusion medium is proportional to the concentration gradient in the direction of transfer', that is to say:

$$F(x) \alpha \frac{\partial C}{\partial x} \qquad - - (2.4)$$

or

$$F(x) = -D\frac{\partial C}{\partial x} \qquad - - (2.5)$$

where F(x) is the rate of transfer at a point x, the negative sign indicating that diffusion occurs in the opposite direction to that of increasing concentration.

Fick's first law applies to steady state conditions where there is no change of concentration with time. In order to solve non steady-state problems, Fick's second law of diffusion, often referred to as the diffusion equation, is used which relates solute concentration to both distance and time.

For one dimensional diffusion, this may be stated mathematically as:

$$\frac{\partial C}{\partial t} = D\frac{\partial^2 C}{\partial x^2} \qquad \text{- - (2.6)}$$

or for the more general three dimensional case

$$\frac{\partial C}{\partial t} = D\left(\frac{\partial^2 C}{\partial x^2} + \frac{\partial^2 C}{\partial y^2} + \frac{\partial^2 C}{\partial z^2}\right) \qquad \text{- - - (2.7)}$$

Equation (2.7) is known as Fick's second law of diffusion [37] and enables the concentration of the solute to be determined at any position in the system, at any point in time, provided the value of D, the diffusion coefficient, is known. D is not, however, a constant, but usually varies with temperature according to the relationship [33]:

$$D = D_o \exp.\left(\frac{-Q}{RT}\right) \qquad \text{- - (2.8)}$$

where Do is the diffusion constant for the medium, T the absolute temperature, R the universal gas constant, and Q, the activation energy, a constant for the diffusing system.

Combining equations (2.7) and (2.8) permits the depth of penetration of the diffusion interface to be calculated, and provided the temperature is known, the depth of diffusion of the solute through the medium for any given time.

2.3.3 Heat Flow within a Fuse Element

The relative rates of heat generation, heat absorption and heat conduction which occur during the fuse pre-arcing period determine the rate of rise of temperature, and hence the fuse operating characteristics (see section 4.4). Heat is generated by ohmic heating and heat transfer throughout the fuse is predominantly conductive. The basic one dimensional equation for the rate of transfer of heat through an area A with a constant temperature difference is given by Fourier's Law.

$$q = -KA\frac{\partial T}{\partial x} \qquad \text{- - (2.9)}$$

where q is the rate of heat transfer, $\frac{\partial T}{\partial x}$ the temperature gradient in the direction of heat flow and K the thermal conductivity of the material.

If the temperature is not constant, but varies with time, then the general equation for conductance in three dimensions must be used and is given by [25]:

$$\frac{\partial}{\partial x}\left(\frac{K\partial T}{\partial x}\right)+\frac{\partial}{\partial y}\left(\frac{K\partial T}{\partial y}\right)+\frac{\partial}{\partial z}\left(\frac{K\partial T}{\partial z}\right)+Q=\rho C_p\frac{\partial T}{\partial t} \qquad \text{- - (2.10)}$$

where Q is the rate of heat production per unit volume and ρ and Cp are respectively the density and specific heat of the material.

If K, ρ and Cp are assumed constant, then this general equation reduces to:

$$\nabla^2 T + \frac{Q}{K} = \frac{1}{\alpha}\frac{\partial T}{\partial t} \qquad \text{- - (2.11)}$$

where α is the thermal diffusivity given by

$$\alpha = \frac{K}{\rho C_p}$$

Solution of this equation gives the temperature at any point in the fuse element.

Provided the theory outlined above adequately describes the M-effect mechanism, then the three inter-related equations (2.2), (2.7) and (2.11) define the current, diffusion depth and temperature at the position of the M-effect alloy at any point in time. This offers the possibility, that by solving these equations, taking into account the relevant boundary conditions, the rate of diffusion of the M-effect alloy through the silver element may be calculated.

2.4 Modelling the M-Effect

In view of the difficulties in obtaining solutions to these complex equations using classical techniques, a numerical approach was adopted. Numerical modelling methods are based

on iterative techniques in which each variable is calculated on a step-by-step basis at discrete points in time. In the case of fuse operation, this would enable the key variables of current, temperature and element composition to be calculated at various times from current application to the alloy completely diffusing through the element and subsequent fuse operation.

The portion of the fuse element containing the M-effect alloy was considered to consist of a large number of small sub-volumes or cells, each possessing uniform properties throughout the sub-volume at any given instant in time (Fig. 2.3). These properties included temperature, electrical resistivity, thermal conductivity and coefficient of diffusion. The electrical, thermal, and diffusion gradients between centres of the cells were considered to be uniform. Within the fuse element, heat production is dependent upon the current density and resistivity of each cell. This resistivity is a function of both the temperature and composition (which varies due to alloy diffusion) of each cell. In this way change of electrical resistivity, thermal conductivity, specific heat and current density with temperature and varying element composition can be made on a step by step basis.

Provided the mesh size chosen is reasonably fine and hence the cells sufficiently small, the accuracy of such a numerical method can be very high. A flow diagram showing the essential components of the model is given in Fig. 2.4 and the procedure is as follows:

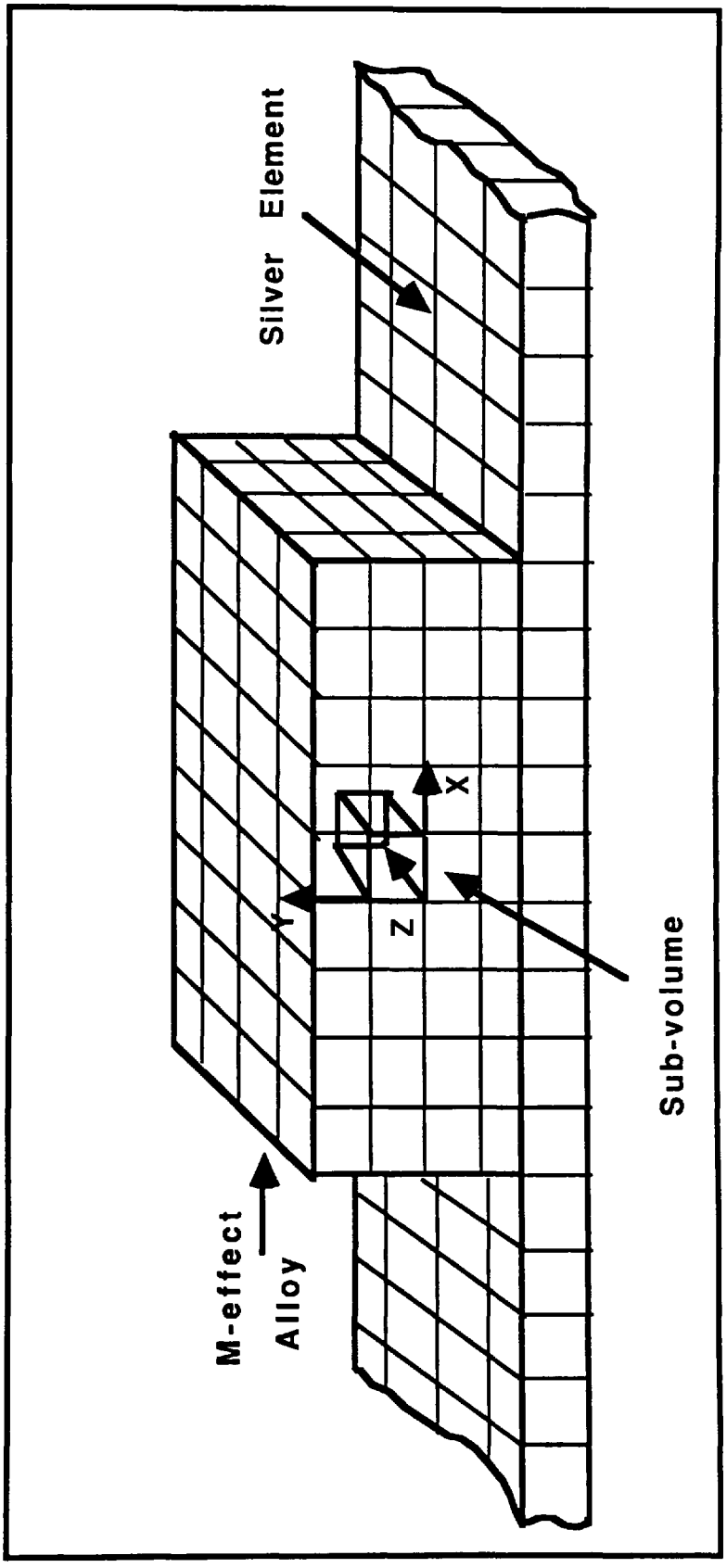

Modelling The M-effect

Fig. 2.3

1. Divide the element into a number of small cells.

2. For the known conditions existing in each of the cells at the beginning of each step in the calculation, determine the current distribution in the element.

3. Calculate the energy generated within each cell and the transfer of heat between adjacent cells during the step under consideration and hence determine the temperature distribution at the end of the step.

4. Using this value of temperature, calculate the depth of diffusion of the alloy through the element during the step under consideration, and hence the new composition of the cell.

5. Determine the properties of each of the cells comprising the fuse element for the temperatures at which they are operating at the end of the step. This gives the initial conditions for the start of the next step in the calculation.

The usual method of solving such a problem would be to convert the partial differential equations relating current, temperature and mass diffusion to finite difference equations and to use an iterative procedure in which repeated calculations of temperature and composition changes

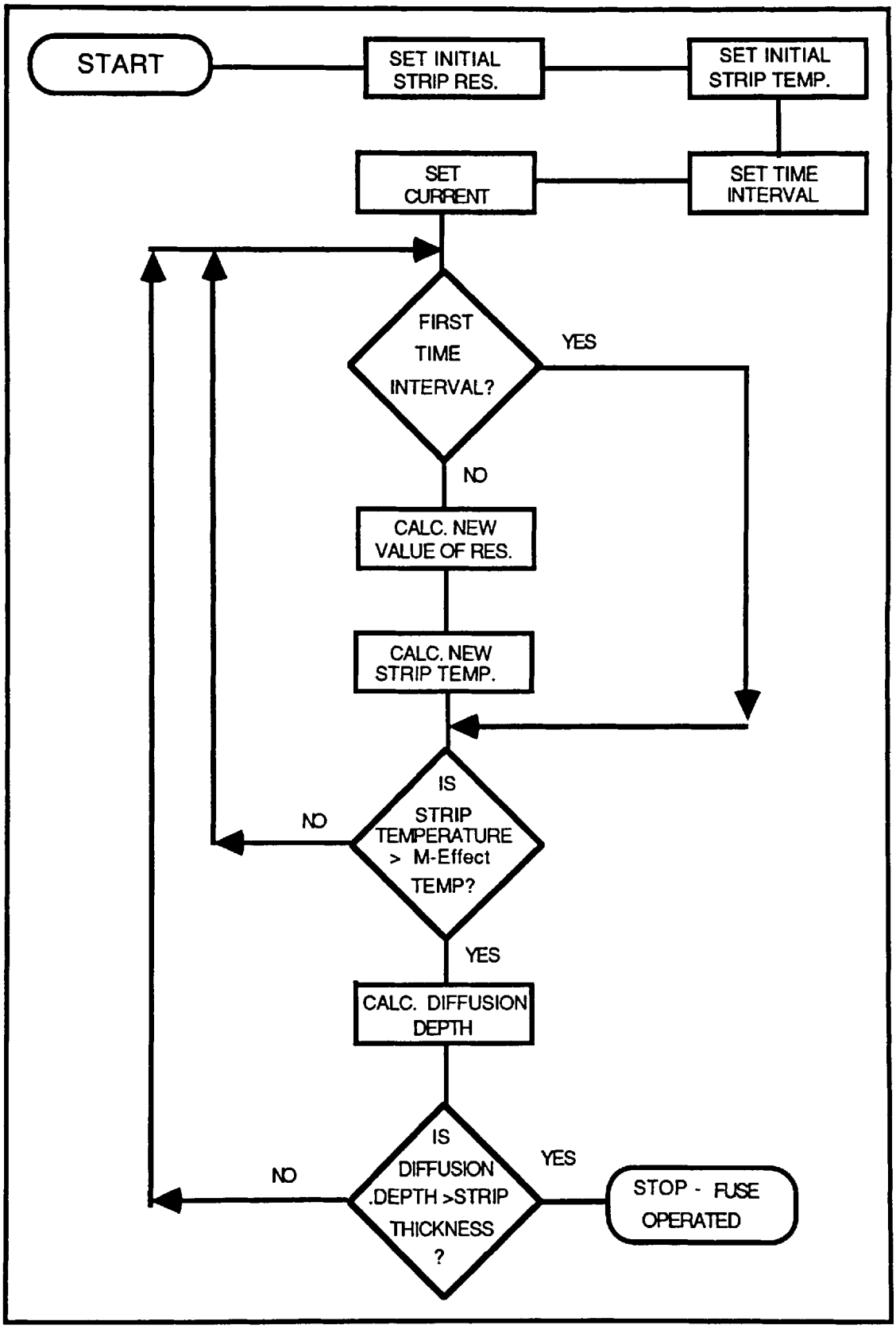

Flowchart Of A Computer Program To Determine Fuse Operation Under M-effect Conditions

Fig. 2.4

occurring throughout the element are made. When the desired degree of accuracy is obtained, another time interval is taken. This is a double iteration with respect to space and time, and a computer program could be written in a high level language to perform these calculations.

Writing such a program, however, requires a high degree of programming skill to not only ensure the problem is solved, but also that the solution is achieved within a reasonable computing time. The ability to study the effect of key variables requires them to be easily changed between simulations and this also requires the program to be user interactive, providing prompts for variables to be entered.

An alternative approach is to adapt a suitable commercial computer simulation software package. These packages are optimised to provide efficient calculation of the iterative loops and also provide a friendly operating environment with error messages identifying problem areas. This approach considerably simplifies the analysis by removing the need to generate from first principles an efficient high level computer program.

The three key parameters in M-effect action have been identified as the current flowing through the fuse element, the temperature rise of that element and the rate of diffusion of the M-effect alloy through the element as a result of this temperature rise. Chapter 3 will show that these are analogous systems which may be fully described by differential equations of similar form, and thus by a

suitable change of variables, it will be shown that temperature rise and diffusion rates may be modelled using a computer aided design (C.A.D.) electrical circuit simulation package. In view of the availability of a C.A.D. package which could be suitably adapted, this second approach was adopted.

CHAPTER 3

MODELLING USING ASTEC3 SOFTWARE

3.1 Analogous Systems

A closer examination of the three key variables of current, temperature and element composition show that all three variables can be represented by partial differential equations of a similar form.

For example, the two basic laws of electricity are

Coulomb's Law $\sigma = C^*E$

and Ohm's Law $jx = \frac{-1}{R^*}\frac{\partial E}{\partial x}$

where σ is the charge density, jx is the electric current density (charge flux, or diffusion of charge per unit time and area), C^* is the capacitance per unit volume and R^* the resistivity. Thus the equation for the one dimensional movement of electricity may be written as:

$$\frac{\partial^2 E}{\partial x^2} = R^*C^*\frac{\partial E}{\partial t} \qquad \text{- - - - (3.1)}$$

which is analogous to that for the one dimensional conduction of heat (assuming no heat generation).

$$\frac{\partial^2 T}{\partial x^2} = \frac{1}{\alpha}\frac{\partial T}{\partial t} \qquad \text{- - - - (3.2)}$$

and also the one dimensional diffusion of mass

$$\frac{\partial^2 C}{\partial x^2} = \frac{1}{D}\frac{\partial C}{\partial t} \qquad \text{- - - - (3.3)}$$

This similarity between thermal and diffusive systems was recognised by Fick [37] who first put diffusion on a quantitative basis by adapting the mathematical equation of heat conduction derived some years earlier by Fourier [39]. Indeed, many problems in engineering involve the determination of potentials existing at various points in a field, and the flow of substance between these potentials. In electrical engineering it would be the flow of charge in a conductor or the flux in an electric or magnetic field. It could, however, equally well be the determination of temperature at various points in a thermal field, the flow of liquid in a cooling system or the mass diffusion of one substance through another.

Most fields can be described mathematically by a form of Laplace's equation.

$$\nabla^2\psi = 0 \qquad \text{- - - - (3.4)}$$

Where ψ is the scalar value of a variable in the field. Each field is of the form:

Flow Density = Constant x Potential Gradient

or Flux $\equiv \frac{\text{Flow Rate}}{\text{Area}}$ = transport property x Potential Gradient

For example,

Flux Density	= Permittivity x Voltage Gradient
Current Density	= Conductivity x Potential Gradient
Rate of Mass Transfer per unit area	= Diffusion Coefficient x Concentration Gradient

Rate of Heat Transfer per unit area = Thermal Conductivity x Temperature Gradient

Computer aided design (CAD) packages are now available covering all fields of engineering and in particular electrical engineering, where various circuit simulation packages enable the current and voltage at various points in a network to be determined. Owing to the similarity of the systems under discussion, a suitable change of variables allows these CAD packages to be modified to also determine the movement of heat and material in thermal and diffusive fields. A CAD package which is suitable for this purpose is ASTEC3.[42]

3.2 ASTEC3 Software

ASTEC3 is a circuit analysis software package capable of performing transient, a.c. small signal, and d.c. steady state simulations of analogue electrical circuits [41,42]. The program uses an iterative method for solving the circuit equations, in which the number of iterations, accuracy of solution, and the simulated duration of analysis can be specified by the user. To aid conversion within each iterative loop, the Newton-Raphson method is used, but the algorithm has an improvement over the traditional method in that it logarithmically attenuates the speed of the iterations. This improves global convergence properties albeit at the expense of increased processing time. Using ASTEC3, it is also possible to perform repeated analysis using a number of different initial conditions during the analysis of a single system, the resulting data being output in tabular and/or graphical form. It has powerful modelling

facilities where sub-circuits or system components can be described and stored in libraries in the form of models, and then called as required to simulate more complex systems.

The simulation of a circuit using ASTEC3 proceeds in three independent stages:

* circuit description
* simulation
* presentation of results

Each of these three stages may be individually repeated as required, allowing results to be obtained from several sets of initial conditions and presented in a variety of formats from one simulation.

The circuit description is an electrical circuit equivalent with component types, values and connections being entered as a net list.

Dc, ac or transient conditions can be simulated. In dc analysis the steady state conditions of the circuit are determined. For the ac analysis, a dc analysis is firstly performed to establish the operating points of the circuit. The circuit is then linearised about these working points and a small signal ac analysis performed. The transient command performs a transient circuit analysis. The initial values of all variables and the duration of the simulation can be set by the user.

Output from the simulator can include node voltages, voltages between nodes, branch currents and component values. The results from a simulation may also be used to generate more complex parameters, which may then be output in graphical form. Component models exist for most analogue devices, and those which do not exist can be generated by the user and stored in personal libraries.

In addition to the simulation of standard electrical circuits, ASTEC3 permits the solution of sets of simultaneous differential equations. This facilitates the simulation of electro-mechanical and electro-thermal systems, and enables the investigations of such operating characteristics as the temperature rise of electrical components.

The development of thermal/electrical analogues, and the use of ASTEC3 to model thermal systems has been described by Poole, Sarvar, Witting and McKenzie [40].

ASTEC3 software thus offers the possibility of modelling and hence determining the mutual relationships between the current flowing in a fuse element, the temperature rise of the section of the element containing the M-effect alloy, and the diffusion of the alloy through the element.

Consider, for example, a simple one dimensional system represented by a resistor-capacitor "ladder" as shown in Fig. 3.1. This system may also be used to represent a thermal or diffusive system, where the flow of heat or

diffusing substance is simulated by the flow of electrical charge, and the potential gradient represents the temperature or concentration gradients. In other words, the flow of heat through a thermal resistance or the flow of material through a diffusive resistance is analogous to the flow of current through an electrical resistance, and any heat or material entering or leaving a system can be modelled as current sources or sinks. Similarly, using the analogy between temperature in a thermal system, concentration in a diffusing system and voltage in an electrical system, fixed temperatures or concentrations at a boundary may be modelled as voltage sources of the same value.

Poole [40] has extended this one dimensional analogy to two and three dimensions for thermal systems. The analogy has been further extended by the author to include two and three dimensional diffusion modelling. The model parameters are determined as follows:

Consider a sub-volume of side lengths Δx, Δy and Δz enclosing a volume ΔV. The "resistance" to flow in the x direction for the flow of current, material or heat through the volume may be determined by comparing:

Fick's first law for mass diffusion.

$$F(x) = -D\Delta y\Delta z\frac{\partial C}{\partial x} \qquad \text{- - - - (3.5)}$$

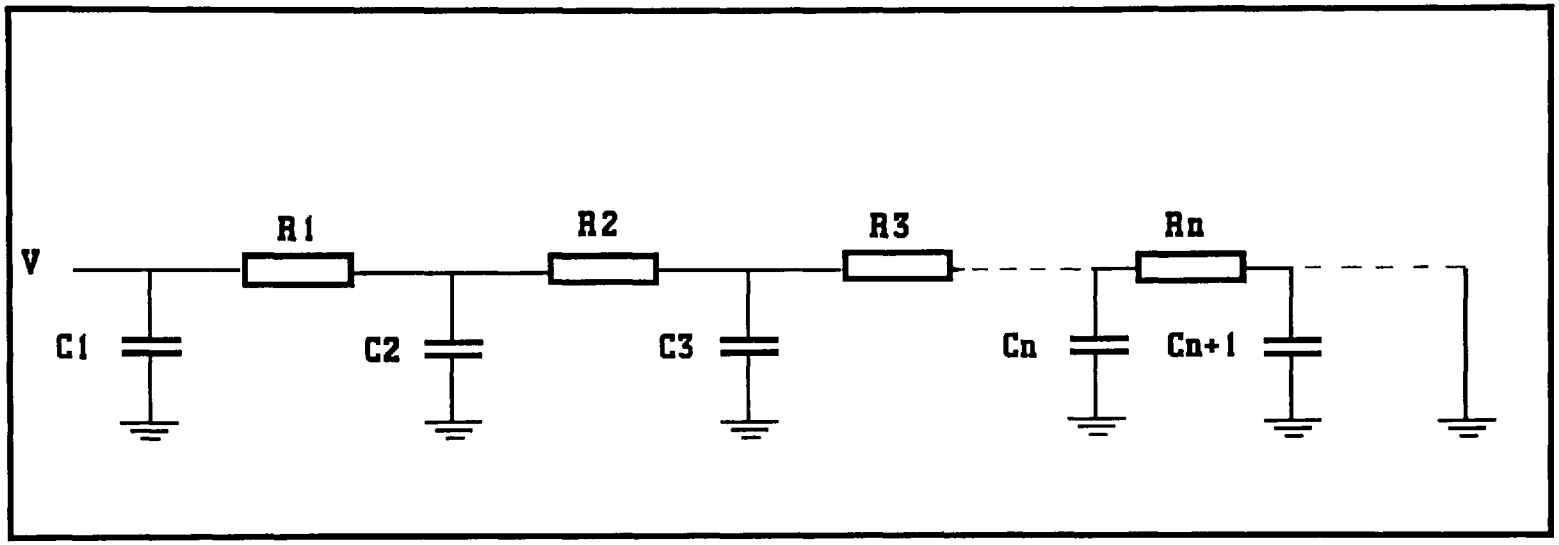

Modelling One Dimensional Diffusive And Thermal Systems

Using An Electrical R-C Ladder Diagram

Fig.3.1

and Fourier's law for heat conduction

$$q(x) = -K\Delta y\Delta z\frac{\partial T}{\partial x} \qquad \text{- - - - (3.6)}$$

with Ohm's law for the current flow

$$I(x) = -\frac{\Delta x}{\mathrm{R}}\frac{\partial V}{\partial x} \qquad \text{- - - - (3.7)}$$

From these three equations, it can be seen that:

$$R_{(\text{Thermal})} = \frac{\Delta x}{K\Delta y\Delta z} \qquad \text{- - - - (3.8)}$$

$$R_{(\text{Diffusion})} = \frac{\Delta x}{D\Delta y\Delta z} \qquad \text{- - - - (3.9)}$$

Similar expressions can also be written for the y and z directions.

The value of the equivalent capacitor may be determined in a similar manner as follows.

The rate of change of thermal energy stored in a volume element Δ V is given by:

$$\rho C_p\Delta x\Delta y\Delta z\frac{\partial T}{\partial t} \qquad \text{- - - - (3.10)}$$

where ρ and C_p are the density and specific heat respectively.

The rate of change of mass of a volume element ΔV is given by:

$$\Delta x \Delta y \Delta z \frac{\partial C}{\partial t} \qquad \text{- - - - (3.11)}$$

Comparing equations 3.10 and 3.11 with the equation for the current in a charging capacitor,

$$I = C \frac{\partial V}{\partial t} \qquad \text{- - - - (3.12)}$$

it can be seen that equivalent electrical capacitances can be used to represent the thermal and diffusive capacitances of a cell of volume ΔV of a body, given by:

$$C_{(\text{Thermal})} = \rho C_p \Delta V \qquad \text{- - - - (3.13)}$$

$$C_{(\text{Diffusion})} = \Delta V \qquad \text{- - - - (3.14)}$$

Simple electrical equivalent models for thermal and diffusion characteristics can be written using the analogous thermal and diffusive resistance and capacitance quantities.

The ASTEC3 input language is based on a conventional circuit diagram with the positions of each element defined by the nodes at its connections. Figs. 3.2 to 3.4 show the electrical configurations used for cells or sub-volumes in 1, 2 and 3 dimensional systems. In each model the equivalent resistance in each direction is divided by two and resistors of such values are connected from the node at the centre of the cell to nodes at the mid-point of each side. The equivalent capacitances of value $C_{THERMAL}$ and $C_{DIFFUSION}$ and the optional current source representing heat or mass generation in the cell are connected between the centre node and ground. Cells of any dimensions may be

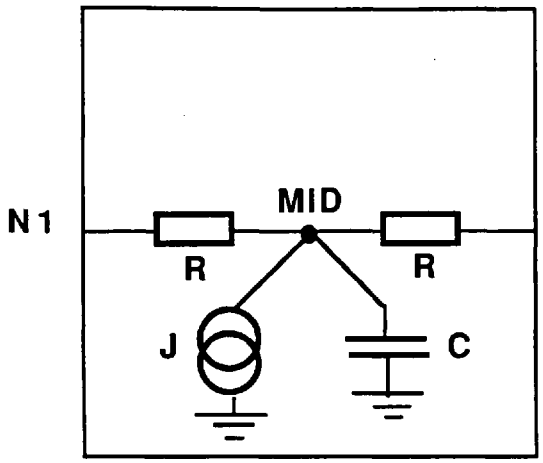

$$R = \frac{1}{2} R_{ELECTRICAL}$$

ELECTRICAL CELL

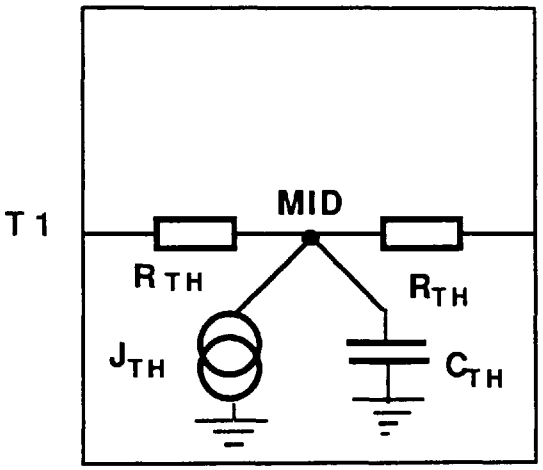

$$R_{TH} = \frac{1}{2} R_{THERMAL}$$

THERMAL CELL

(After Poole [40])

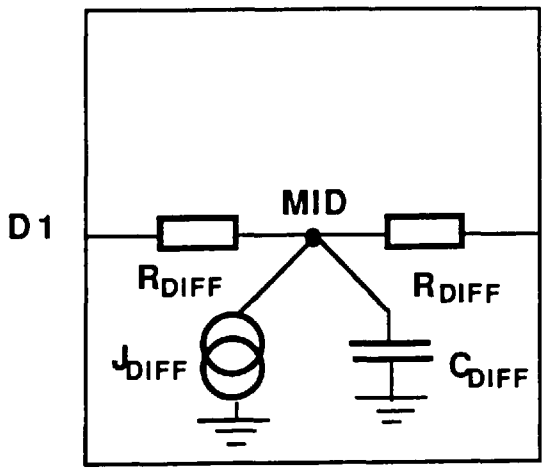

$$R_{DIFF} = \frac{1}{2} R_{DIFFUSION}$$

DIFFUSION CELL

Modelling Analogous Systems Using One Dimensional Cells

Fig. 3.2

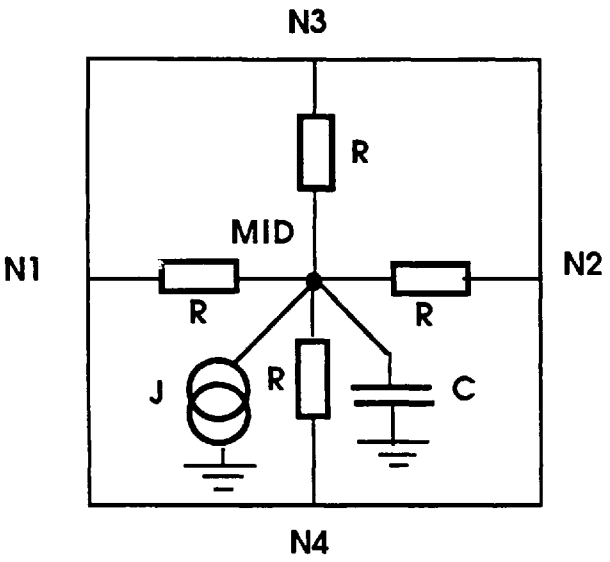

$$R = \frac{1}{2} R_{ELECTRICAL}$$

ELECTRICAL CELL

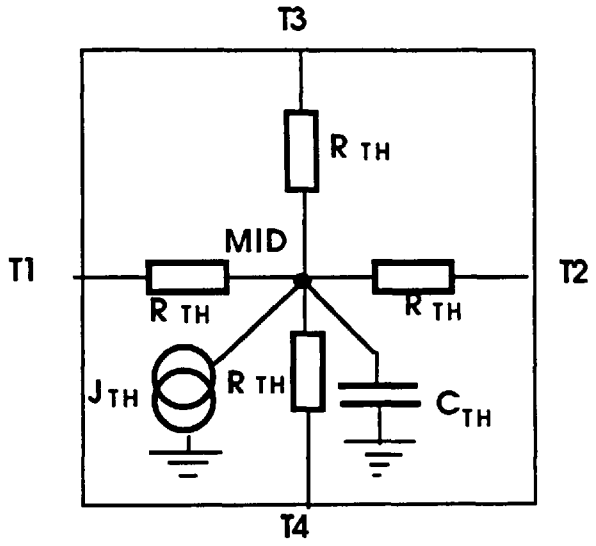

$$R_{TH} = \frac{1}{2} R_{THERMAL}$$

THERMAL CELL

(After Poole [40])

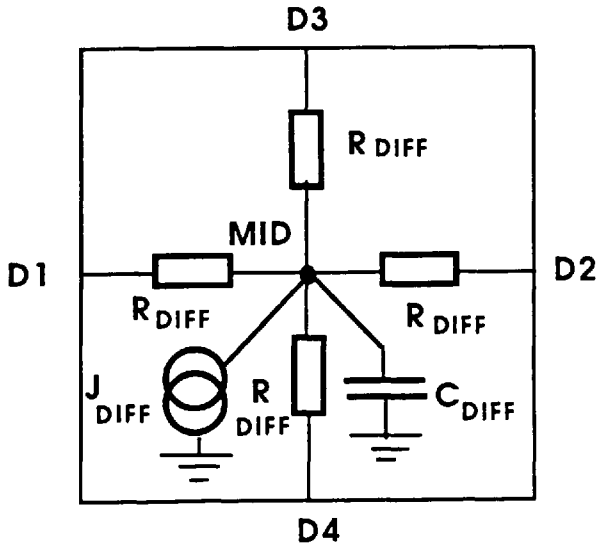

$$R_{DIFF} = \frac{1}{2} R_{DIFFUSION}$$

DIFFUSION CELL

Modelling Analogous Systems Using Two Dimensional Cells

Fig. 3.3

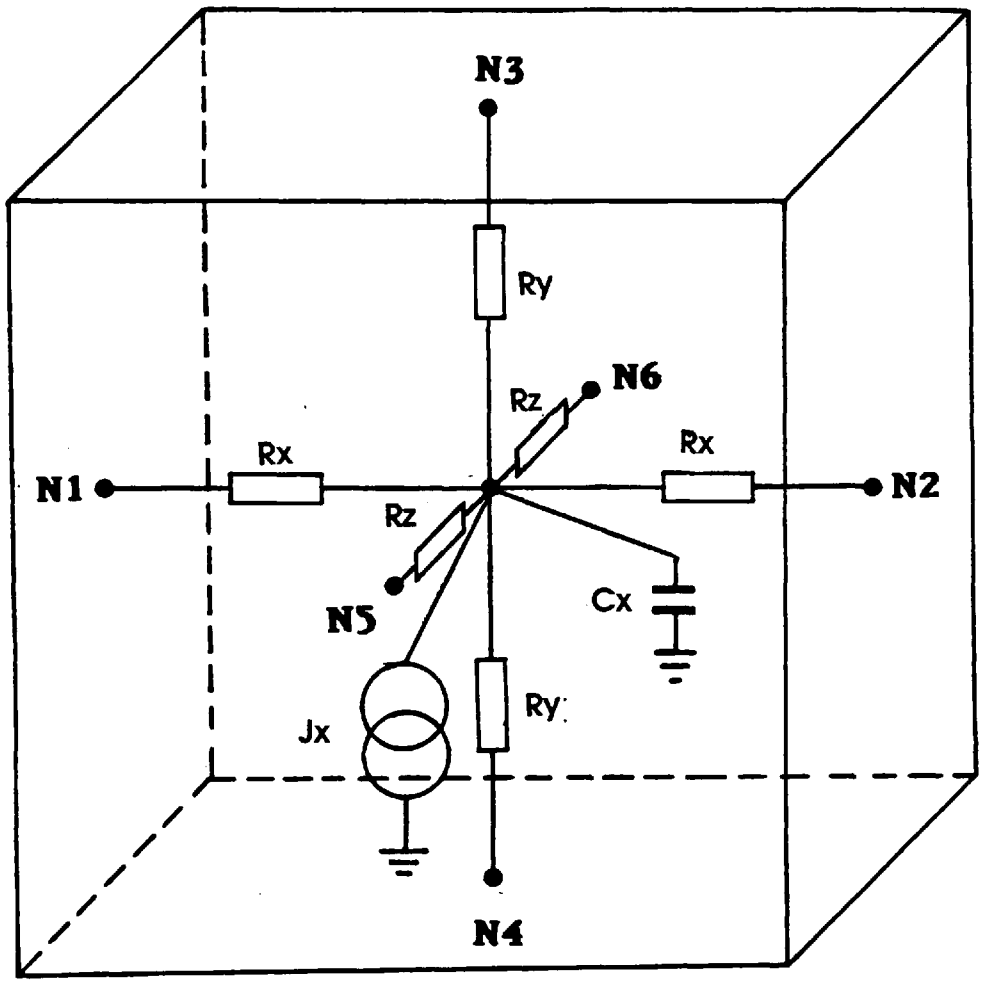

GENERAL THREE DIMENSIONAL CELL.

Rx, Ry, Rz may be R, R_{TH}, or R_{DIFF}

Jx may be J, J_{TH}, or J_{DIFF}

Cx may be C, C_{TH}, or C_{DIFF}

Modelling Analogous Systems Using Three Dimensional Cells
(Thermal Model After Poole [40])

FIG. 3.4

used, but in this illustration the cells are assumed to be of equal dimensions and consequently to have equal resistances in all directions.

Once the cell model has been established, cells may be linked together to form one, two or three dimensional circuits, depending on the particular system being studied. Inputs to and outputs from the system to the surrounding media may also be modelled. These may, for example in the case of thermal modelling, be of the form of fixed resistors of appropriate value connected from nodes on the outside surface of the model to ground to represent heat loss at system boundaries, or fixed voltages to denote constant temperature heat sources or sinks.

3.3 Evaluation of ASTEC3 Software Modelling

Before applying ASTEC3 to modelling fuse operation it is necessary to verify the validity of this modelling technique in thermal, thermal/electrical and diffusion modelling. To do this ASTEC3 was used to model some simple systems, and the results obtained compared with those obtained using well established independent techniques.

3.3.1 Thermal Modelling

To assess the performance of modelling thermal systems, ASTEC3 was used to model a two dimensional heat transfer problem.[40]

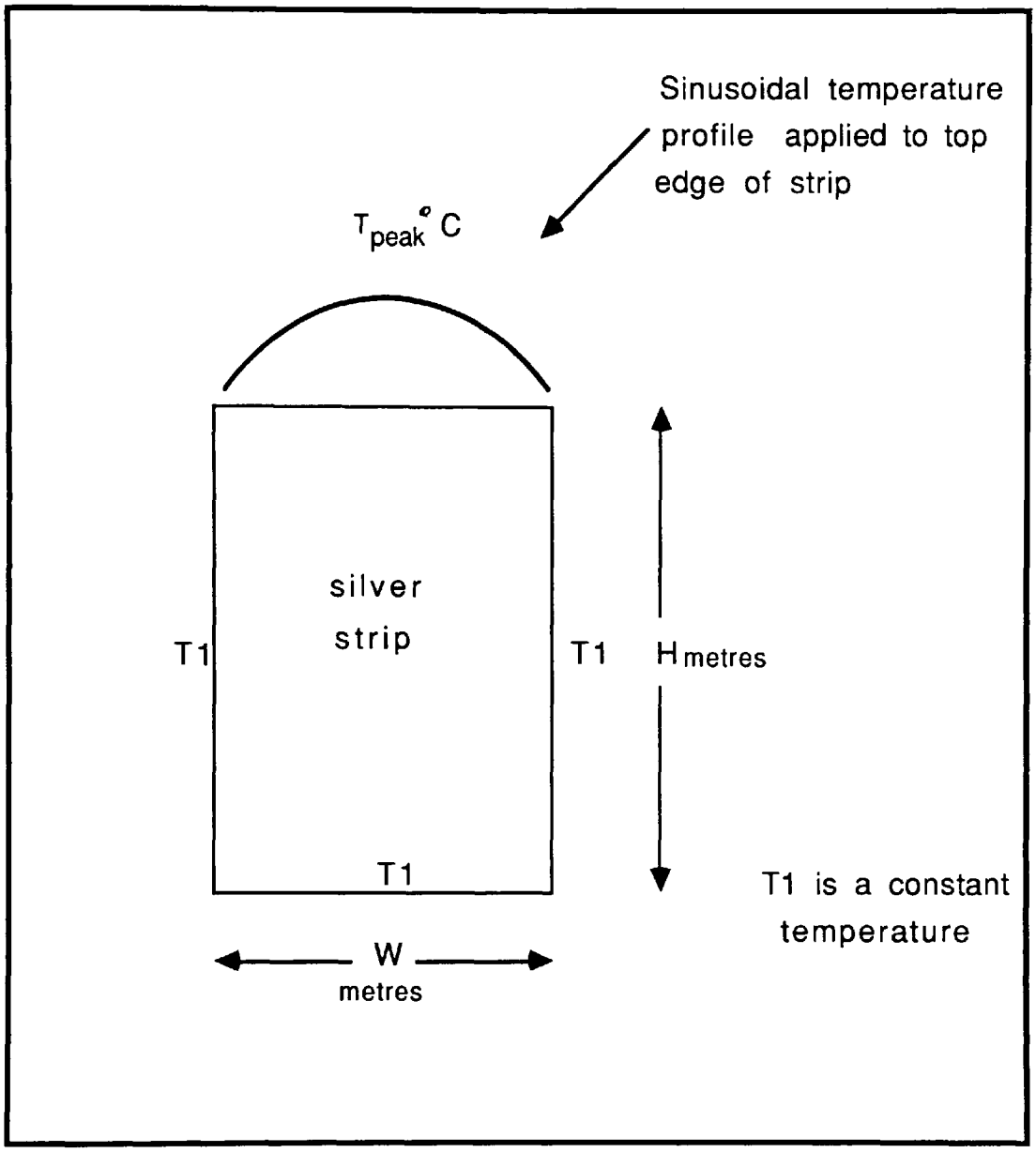

The Determination Of The Temperature Distribution Of A Fully Insulated Silver Strip When A Sinusoidal Heat Source Is Applied To One Edge. All Other Edges Are Assumed To Be At A Constant Temperature T1

Fig.3.5

Consider a plain silver strip 14mm x 10mm which has three sides maintained at a constant temperature T_1. The top side has a sinusoidal temperature distribution impressed upon it, as shown in Fig. 3.5. In order to use ASTEC3 to determine the steady state temperature distribution, the strip was divided into thirty five cells, each 2mm x 2mm. The values of the cell constants were determined from equations 3.8 and 3.13 and an equivalent electrical network constructed as shown in Fig. 3.6. Voltage sources were applied to the five nodes on the top side of the strip to represent average values of the sine function temperature distribution, and the three remaining sides earthed to represent a temperature T_1 of 0°C.

The general solution to this problem has been derived analytically in standard heat transfer textbooks [43]. A method of separation of variables was used to solve the two dimensional steady state heat conduction equation, the temperature at any point x, y in the strip being T(x,y) where:

$$T(x,y) = Tpk.\frac{\sinh(\frac{\pi y}{W})}{\sinh(\frac{\pi H}{W})}.\sin\left(\frac{nx}{W}\right) \qquad - - - \ (3.15)$$

where Tpk represents the amplitude of the sinusoidal temperature distribution, and W and H the breadth and length respectively of the silver strip.

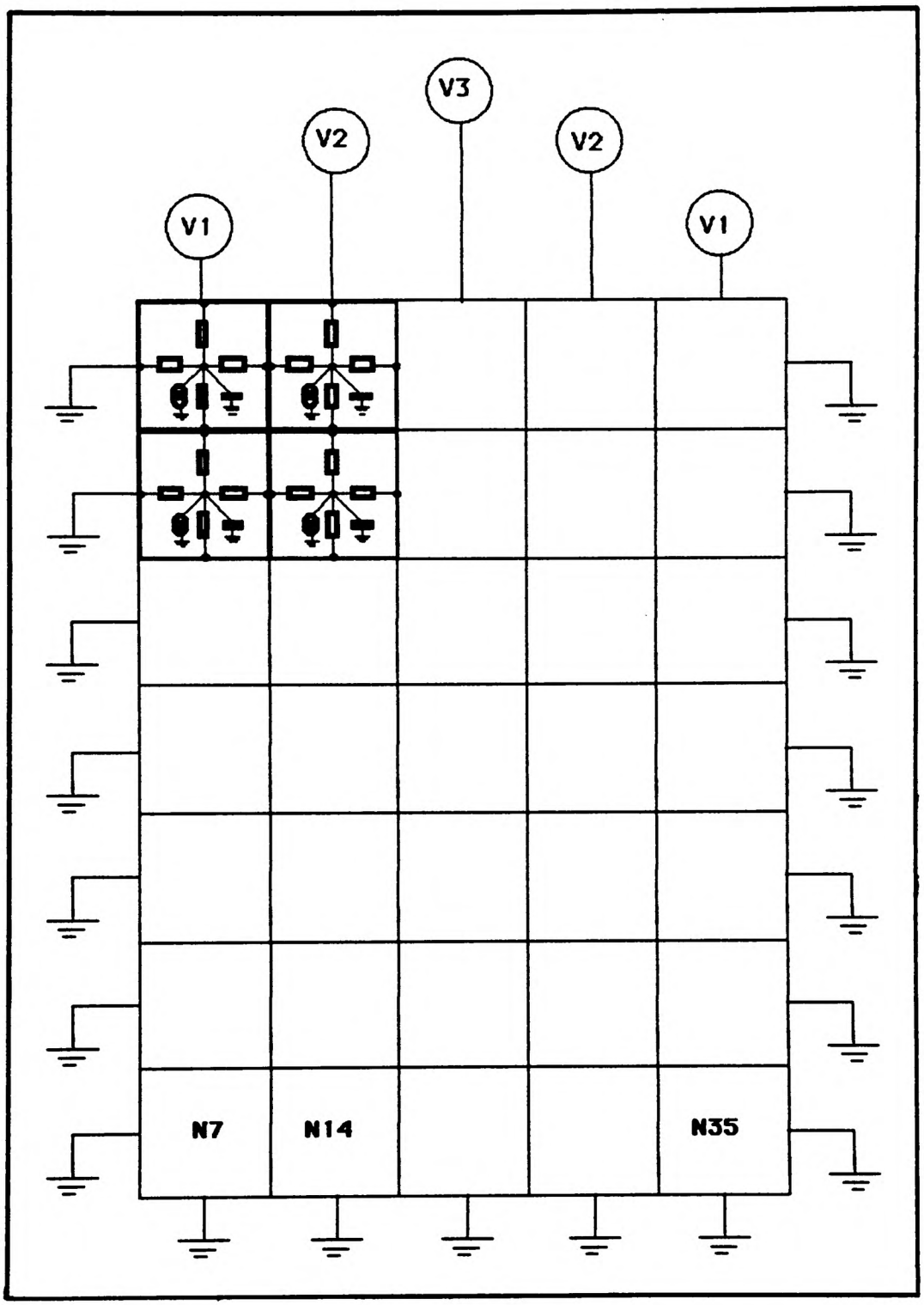

Equivalent Electrical Circuit For The Thermal Problem Described In Fig.3.5

Fig. 3.6

Table 3.1 shows a comparison between the results obtained using ASTEC3 and the exact analytical solution for the temperatures of the mid-nodes of the cells. It can be seen that the ASTEC3 results vary from -3.7% to +5.8% of the exact values.

The variation between the exact solutions and ASTEC3 are due solely to the resolution errors involved in these methods, namely the cell dimensions. These errors can be reduced by using a finer mesh whereby the strip is divided into a larger number of smaller cells. This may be achieved by dividing each cell into four, eight, sixteen etc. smaller ones, and recalculating the new values of the cell parameters.

Table 3.2 shows the results of the same simulation, but this time using a mesh size in which each original cell was replaced by four small cells as shown in Fig. 3.7. As expected, the finer resolution produced a marked improvement in the ASTEC3 results, these now being within 1% of the exact values. For clarity, the results of tables 3.1 and 3.2 are shown as error diagrams in Fig. 3.8. It may thus be concluded that the smaller the cell size, the greater the accuracy of the solution. Unfortunately, the rate of solution convergence using ASTEC3's iterative method to solve the differential equations, decreases as the number of cells increases, and the computing time can become prohibitively large. A trade off thus exists between solution accuracy and computing time. In many cases, particularly for non-linear configurations, a mixture of

Node	Temperature (°C) Exact	ASTEC3	Difference %
N1	22.57	21.77	-3.7
N2	12.03	11.84	-1.6
N3	6.40	6.42	+0.3
N4	3.39	3.46	+2.1
N5	1.75	1.82	+4.0
N6	0.83	0.87	+4.8
N7	0.25	0.26	+4.0
N8	59.08	57.01	-3.6
N9	31.50	30.99	-1.6
N10	16.76	16.81	+0.3
N11	8.86	9.06	+2.3
N12	4.58	4.76	+3.9
N13	2.17	2.28	+5.1
N14	0.64	0.66	+3.1
N15	73.03	70.46	-3.6
N16	38.93	38.31	-1.6
N17	20.72	20.78	+0.3
N18	10.96	11.19	+2.0
N19	5.66	5.99	+5.8
N20	2.68	2.82	+5.2
N21	0.79	0.84	+6.3
N22	59.08	57.01	-3.6
N23	31.50	30.99	-1.6
N24	16.76	16.81	+0.3
N25	8.86	9.06	+3.0
N26	4.58	4.76	+3.9
N27	2.17	2.28	+5.0
N28	0.64	0.66	+4.1
N29	22.57	21.77	-3.7
N30	12.03	11.84	-1.6
N31	6.40	6.42	+0.3
N32	3.39	3.46	+2.1
N33	1.75	1.82	+4.0
N34	0.83	0.87	+4.8
N35	0.25	0.26	+4.0

Comparison of calculated temperatures with those obtained using the ASTEC 3 model for the thermal distribution problem shown in Fig. 3.5 and Fig. 3.6

Table 3.1

NODES	TEMPERATURE (°C) EXACT	ASTEC3	DIFFERENCE (%)	NODES	TEMPERATURE (°C) EXACT	ASTEC3	DIFFERENCE (%)	NODES	TEMPERATURE (°C) EXACT	ASTEC3	DIFFERENCE (%)
1,127	13.37	13.32	-0.4	25,123	1.49	1.50	+0.7	49,91	11.46	11.51	+0.4
2,128	9.75	9.70	-0.5	26,124	0.97	0.98	+1.0	50,92	8.30	8.36	+0.7
3,129	7.13	7.09	-0.5	27,125	0.55	0.55	0	51,93	5.97	6.03	+1.0
4,130	5.20	5.19	-0.2	28,126	0.18	0.18	0	52,94	4.24	4.28	+0.9
5,131	3.80	3.79	-0.3	29,99	60.43	59.78	-1.0	53,95	2.93	2.96	+1.0
6,132	2.77	2.77	0	30,100	44.13	43.77	-0.8	54,96	1.90	1.92	+1.0
7,133	2.01	2.02	+0.5	31,101	32.22	32.04	-0.6	55,97	1.07	1.08	+0.9
8,134	1.46	1.47	+0.7	32,102	23.52	23.44	-0.3	56,98	0.35	0.35	0
9,135	1.05	1.06	+0.8	33,103	17.16	17.15	-0.1	57,71	84.40	83.80	-0.7
10,136	0.74	0.74	0	34,104	12.50	12.53	+0.2	58,72	61.64	61.13	-0.8
11,137	0.51	0.51	0	35,105	9.10	9.13	+0.3	59,73	45.01	44.75	-0.6
12,138	0.33	0.33	0	36,106	6.59	6.63	+0.6	60,74	32.85	32.75	-0.3
13,139	0.19	0.19	0	37,107	4.74	4.78	+0.8	61,75	23.47	23.95	-0.1
14,140	0.06	0.06	0	38,108	3.36	3.40	+1.0	62.76	17.47	17.50	+0.2
15,113	38.78	38.38	-1.0	39,109	2.32	2.34	+1.0	63,77	12.70	12.76	+0.5
16,114	28.33	28.10	-0.8	40,110	1.51	1.52	+0.7	64,78	9.21	9.23	+0.2
17,115	20.69	20.57	-0.6	41,111	0.85	0.85	0	65,79	6.62	6.68	+0.9
18,116	15.10	15.05	-0.3	42,112	0.27	0.27	0	66,80	4.70	4.73	+0.8
19,117	11.02	11.01	-0.1	43,85	76.14	75.33	-1.0	67,81	3.24	3.26	+0.6
20,118	8.03	8.04	+0.1	44,86	55.06	55.15	+0.2	68,82	2.11	2.12	+0.5
21,119	5.84	5.86	+0.3	45,87	40.60	40.37	-0.6	69,83	1.21	1.21	0
22,120	4.23	4.26	+0.7	46,88	29.64	29.54	-0.3	70,84	0.39	0.39	0
23,121	3.04	3.06	+0.9	47,89	21.62	21.60	-0.1				
24,122	2.16	2.17	+0.5	48,90	15.76	15.78	+0.1				

Comparison of calculated temperatures with those obtained using the ASTEC3 model for the thermal distribution problem shown in Fig 3.5 and Fig 3.7

Table 3.2

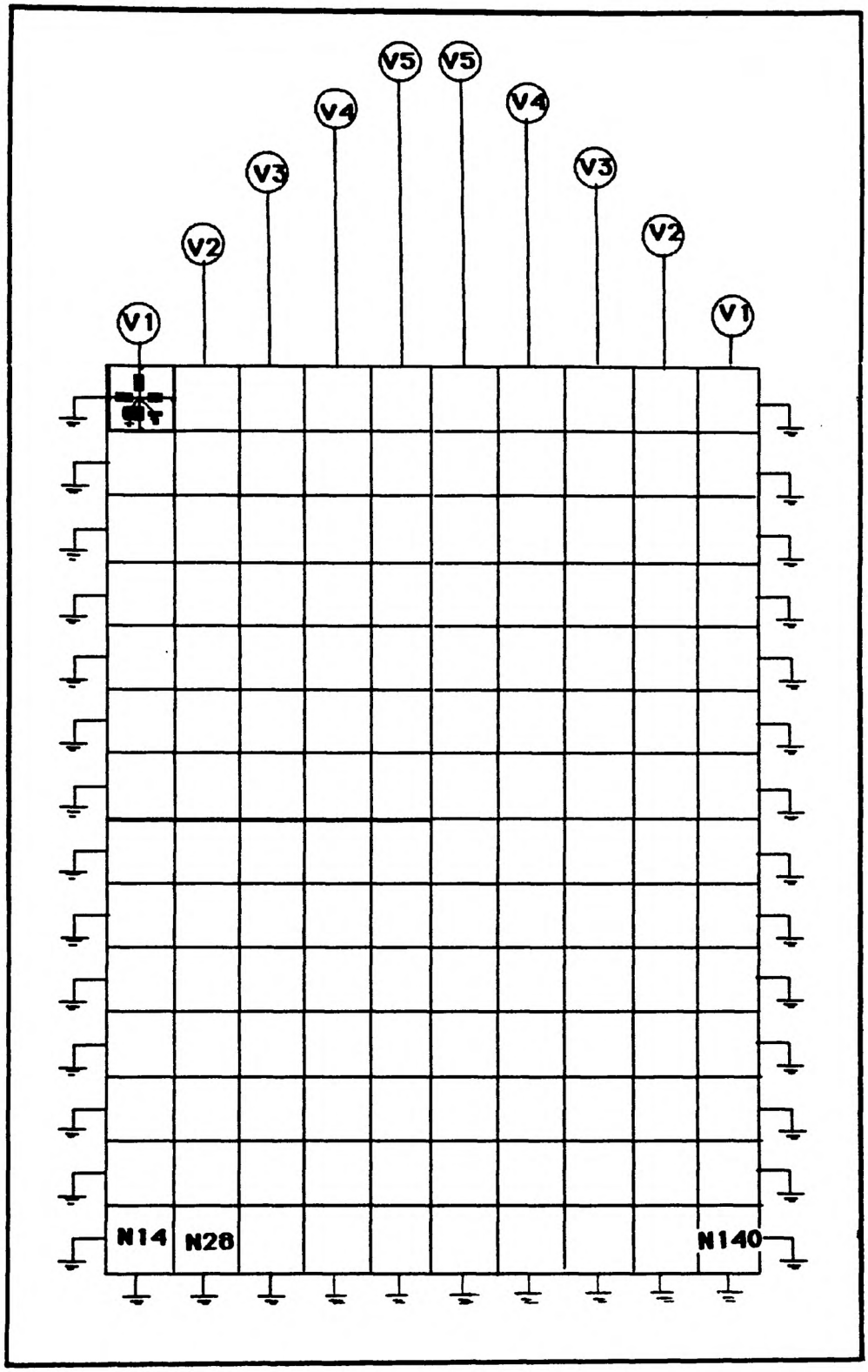

Equivalent Electrical Circuit For The Thermal Problem Described In Fig.3.5, But Using A Fine Mesh.

Fig. 3.7

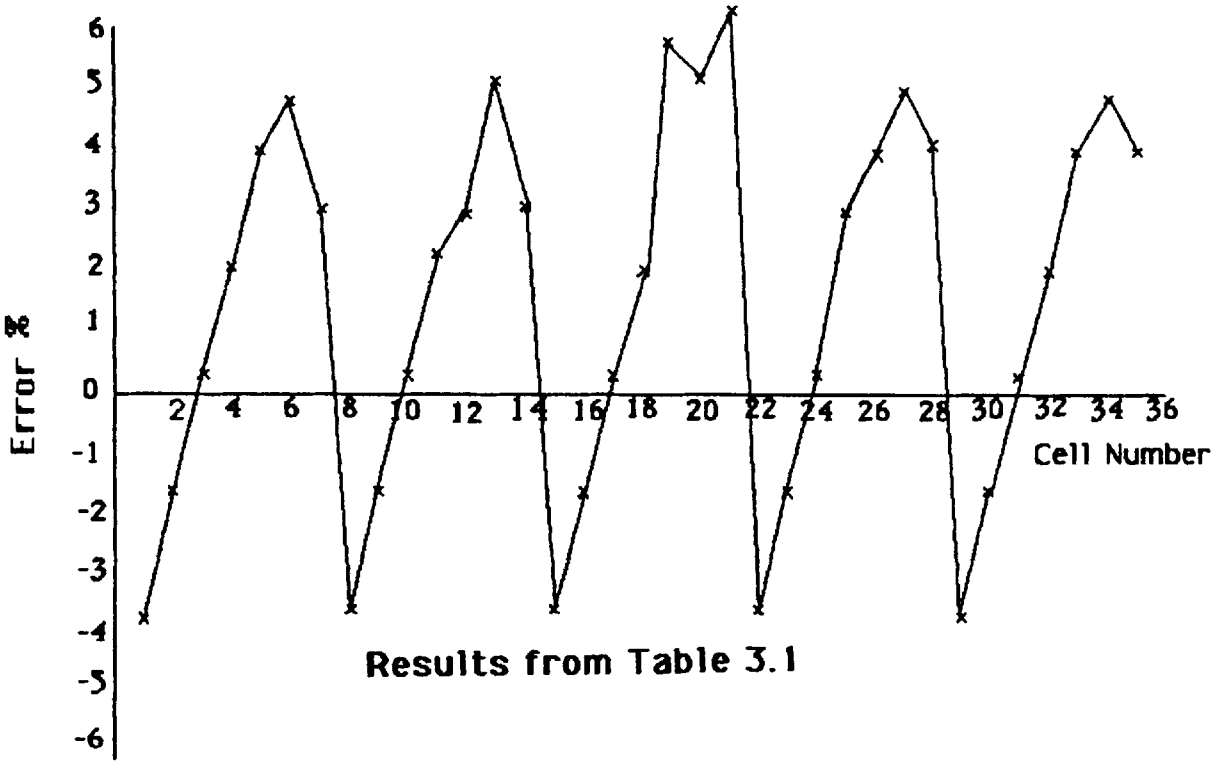

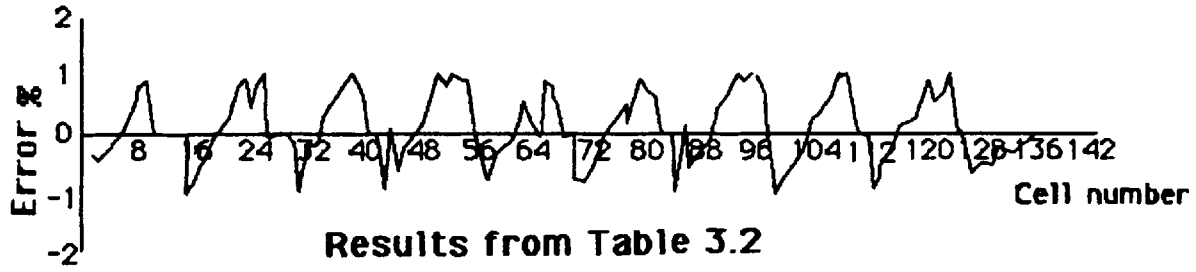

Error Diagrams Showing The Deviation Of Astec3 Results From Calculated Values.

Fig. 3.8

coarse and fine cells may be used to obtain the required accuracy within a reasonable computing time, and this is utilised in the next section.

3.3.2 Electrical Modelling

ASTEC3 was primarily designed as a circuit simulation package, and its ability to accurately determine the values of current in circuit conductors and voltages at circuit nodes is well documented [41,66]. One electrical application of particular interest to the fuse design engineer is the determination of resistance of a non-uniform conductor, such as a notched fuse element. In industry, element resistances are mainly determined either experimentally, by direct measurement using a commercial bridge, or graphically using field plotting techniques due to the difficulty in obtaining theoretical values using classical methods.

Fig. 3.9 shows three typical fuse elements used in commercial fuses. When a notched strip possesses symmetry, the problem may be simplified. Lines of symmetry will be either equipotentials (across the strip width), or the longitudinal centre line, which will be a current flow line. The ends of the element where it is attached to a substantial conductor, will also be equipotentials. Thus, owing to the symmetry of the designs, only one quarter of the element section need be modelled, the other three sections giving identical results. Each element section was divided into a number of two dimensional cells, the current being uniform in the third dimension.

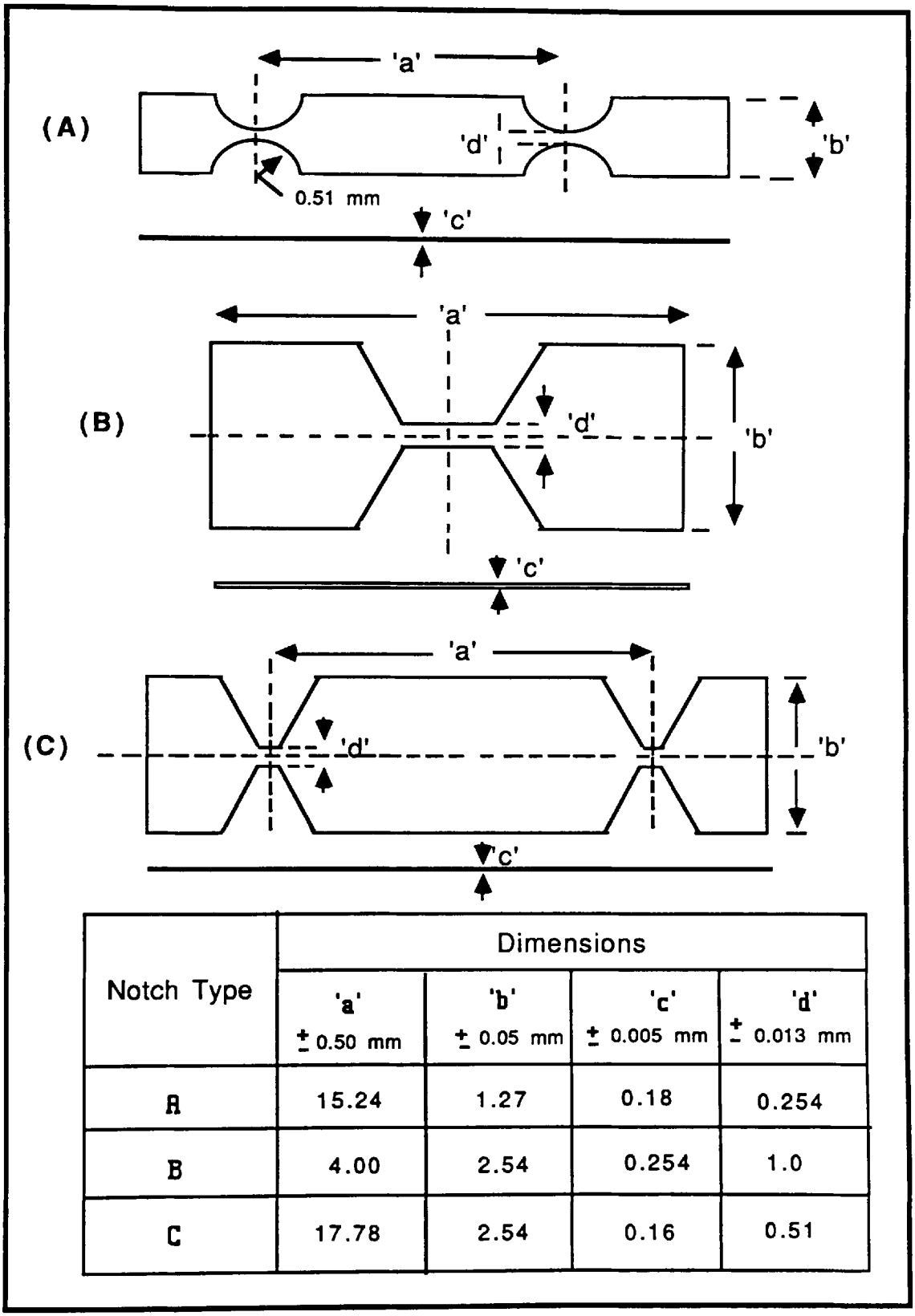

Notch Type	Dimensions			
	'a' ± 0.50 mm	'b' ± 0.05 mm	'c' ± 0.005 mm	'd' ± 0.013 mm
A	15.24	1.27	0.18	0.254
B	4.00	2.54	0.254	1.0
C	17.78	2.54	0.16	0.51

Typical Fuse Elements Used In Commercial Fuses

(A) &(C) - High Voltage Distribution Fuse Elements
(B) - Low Voltage Industrial Fuse Element

Fig.3.9

The finer the cell structure chosen, the greater the resolution and hence the more accurate the solution. Around the contour of the notch itself a fine mesh is desirable, whilst in the bulk strip where the current is more uniform a coarser mesh will suffice. ASTEC3 can accommodate this by allowing both coarse and fine meshes to be used in one simulation. Fig. 3.10 shows how intermediate cells may be used to connect a large cell to two or four smaller cells. This combines the accuracy of the finer mesh around the areas of greatest interest without the large increase in computer time which would be required if the whole section were covered in a fine mesh.

The actual simulation for each of the three elements involved the mixture of coarse and fine cells. As an example Fig. 3.11 shows the cell configuration for the element shape given in Fig. 3.9(a). The cell resistance values were determined from the dimensions of the cell and the physical properties of the element material. Having determined the cell parameters and constructed the electrical circuit mesh, a computer program was written in ASTEC3 format to simulate the notch configuration. By applying a small voltage to one end of the notched section and computing the resulting total current flowing out of the opposite end, the resistance may be determined by simply applying Ohm's law. As there are no known analytical solutions to this problem, the results of the simulations were compared with both experimentally measured values of standard commercially produced elements measured using a commercial bridge for measuring low impedances and

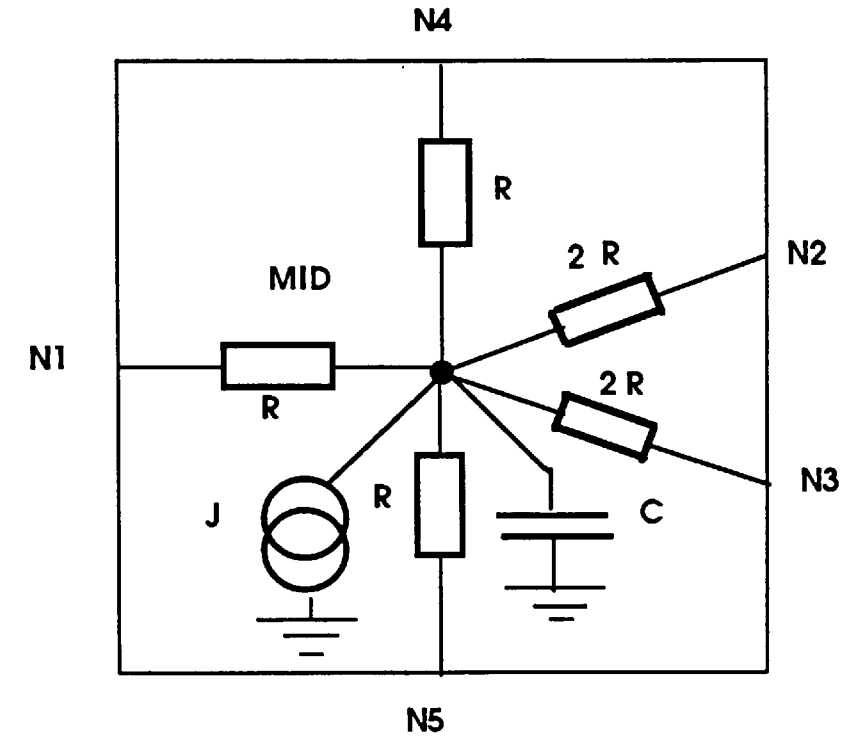

(a)

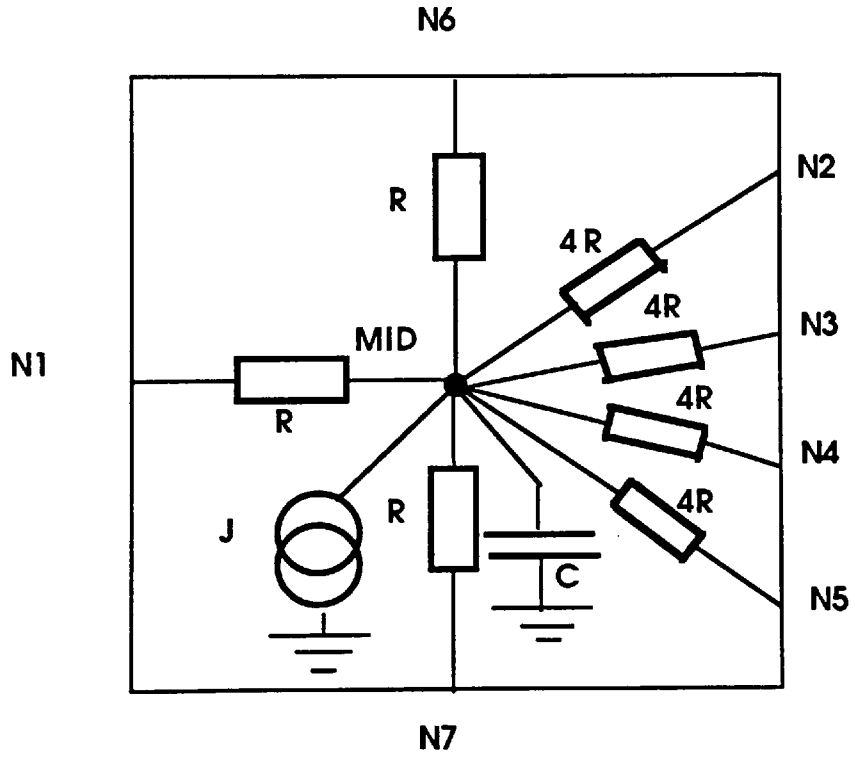

(b)

Method Of Connecting a Large Cell To: (a) Two Smaller Cells.

(b) Four Smaller Cells.

Fig. 3.10

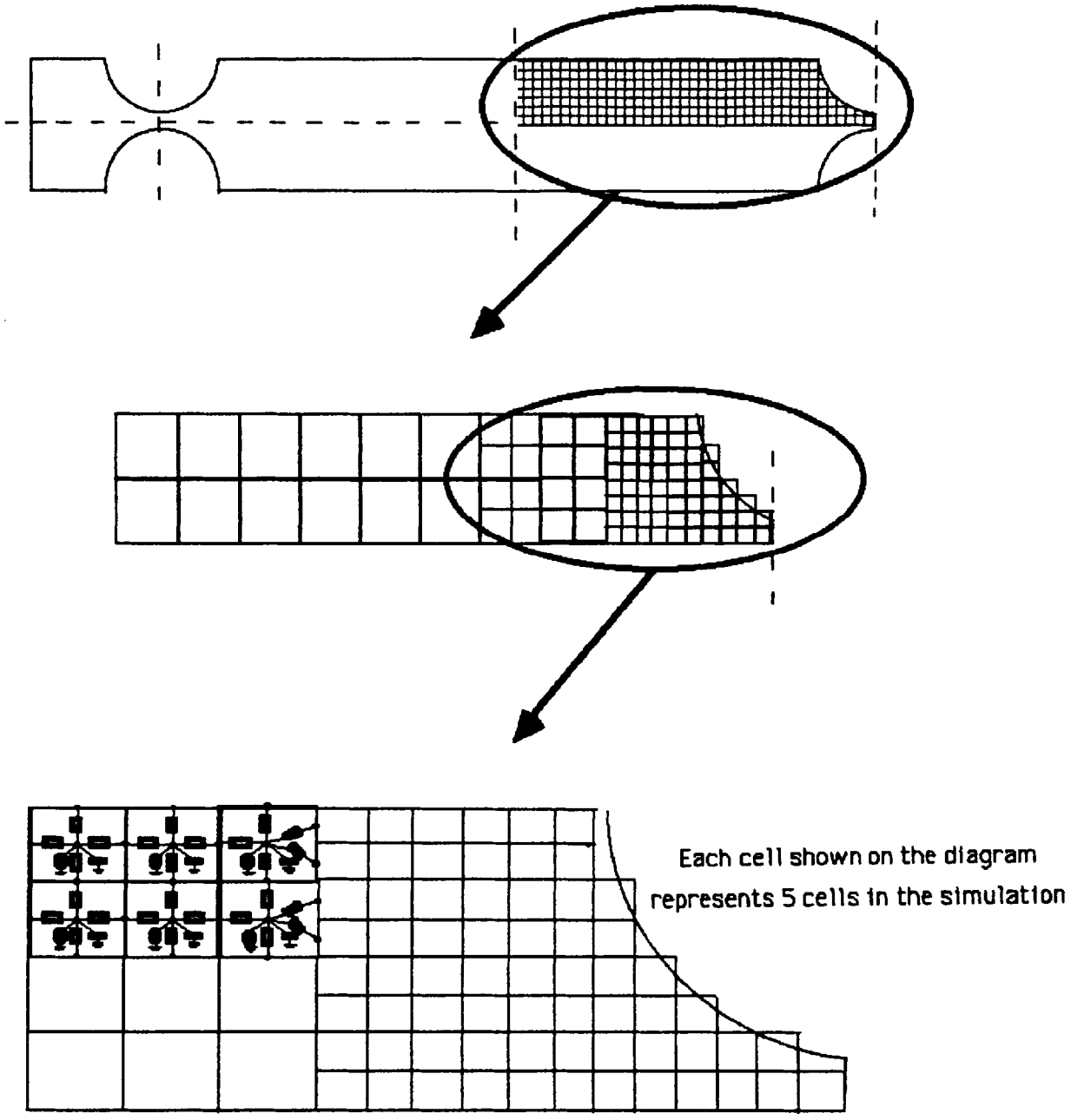

Due to the symmetry of the design only one quarter of the element need be modelled

Modelling a Notched Fuse Element

Fig. 3.11

also with values obtained from finite difference simulations using a method due to Leach [44]. The results are shown in Table 3.3 from which it may be seen that the ASTEC3 simulation results compare closely with both the finite difference results and also the measured values.

For both the ASTEC3 simulation and also the finite difference calculation, the resistivity of silver at 20°C was taken as 1.66 x 10^{-8} ohms-metres, which is the resistivity of commercially pure (99.97%) fully annealed silver strip. Some work hardening of the silver strip occurs during element manufacture, however, which may result in an increase in resistivity values to typically 1.70 to 1.75 x 10^{-8} ohms-metres [45]. This, along with slight dimensional variations between the elements tested probably accounts for the spread in measured values.

3.3.3 Combined Electrical and Thermal Modelling

The preceding sections have shown that ASTEC3 can be used to simulate both electrical and thermal systems. In fuse modelling, however, the thermal and electrical systems are inter-related, and it is necessary to confirm that these two systems can be successfully combined. To verify this, the temperature rise of a simple plain silver fuse element was modelled. The element was heated from the ohmic heating produced by applying a constant voltage source at one end and grounding the other. Heat loss from the element was assumed to occur by conduction only to massive heat sinks at each end of the element, maintained at ambient temperature (Fig. 3.12).

Notch Type	Element Resistance At 20°C (milli-ohms)*		
	ASTEC3	Finite Difference	Experimental Values **
A	1.352	1.359	1.26 - 1.41
B	0.174	0.174	0.17 - 0.19
C	0.896	0.910	0.87 - 0.99

*Resistance of notched strip of length 'a' (see Fig. 3.9)

**Average value of 100 notches.

Comparison Of Astec3 And Finite Difference Models With Experimental Values For Silver Strip Punched With Notches Described In Fig. 3.9

Table 3.3

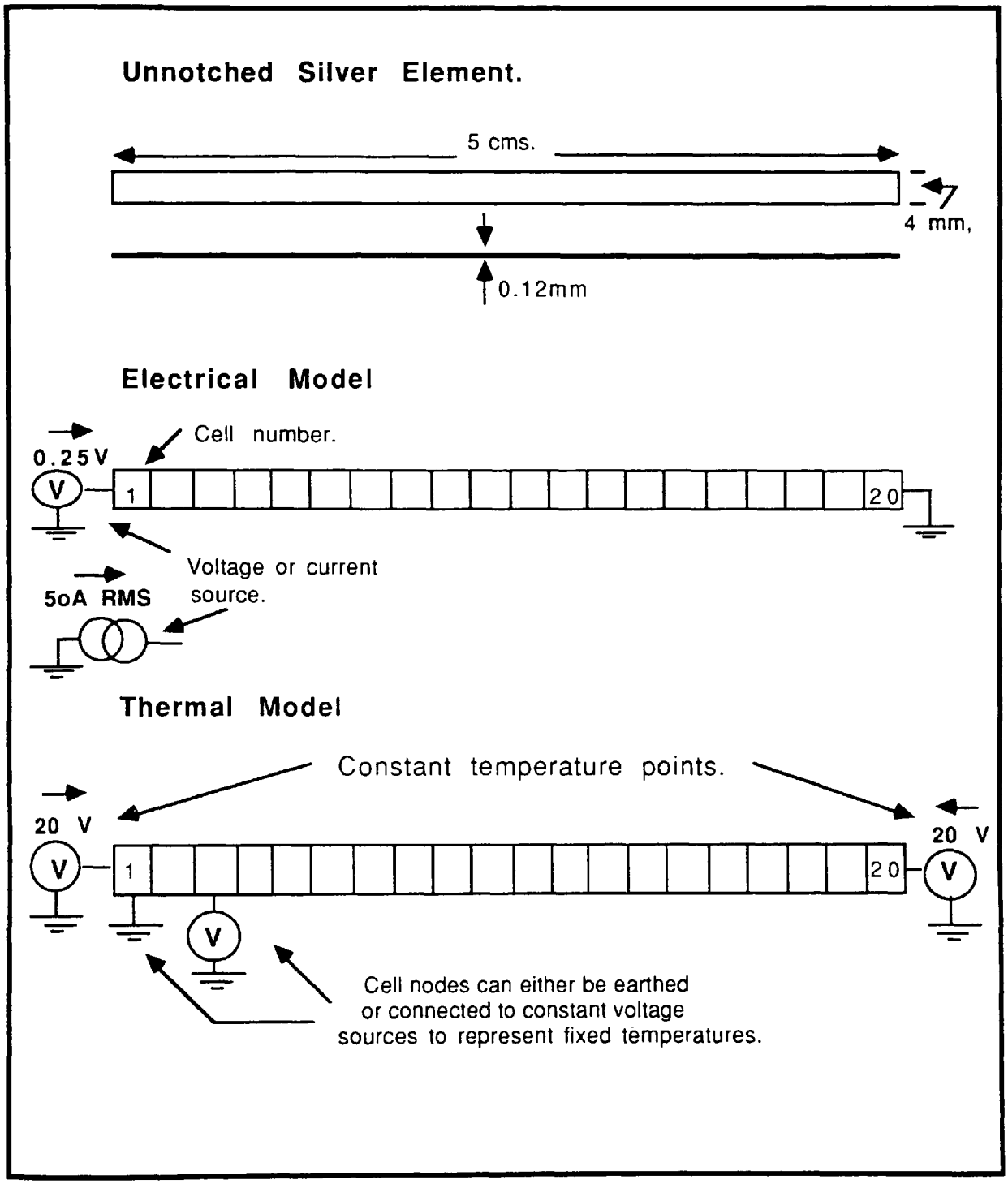

Electrical And Thermal Models For An Unnotched Silver Element

Fig. 3.12

The formula derived by Butts and Cox [46] was used to determine the variation of silver resistivity with temperature, that is

$$\rho_T = 1.54(1 + (4.1T + 0.00055T^2)x10^{-3})x10^{-8} \text{ ohms-metres}$$

where ρ_T is the resistivity at some temperature T.

The specific heat and thermal conductivity of silver were taken as 234 Joules kg^{-1} K^{-1} and 375 watts m^{-1} K^{-1} respectively [47].

Integration of the electrical and thermal characteristics of the circuit was achieved by combining both models within each cell. Cross-referencing between thermal and electrical models then automatically occurs during each iterative loop, ensuring that the influence of temperature rise on resistance, and hence circuit current was taken into account during the simulation.

The element modelled was a 5cm x 4mm x 0.12mm silver strip, which, for simulation purposes, was divided into twenty, three dimensional cells. A drive voltage of 0.25 volt was assumed to be applied to one end and the other end earthed. A simulated heat sink temperature of 20°C was achieved in the thermal model by connecting constant voltage supplies of 20 volt D.C. to each end of the strip. The cell constants were calculated, the electrical mesh constructed and a computer program written in ASTEC3 format. Cross-correlation between the electrical and thermal models occurs in each iterative loop. Hence, the influence of temperature rise on

the resistance of each cell, the corresponding effect on the total element resistance, and the current flowing in the element, can be obtained from the simulation.

Simulation of this simple model produced the expected linear voltage drop along the element and also the initial resistance value of the silver element (1.611 mΩ), which agreed closely with the calculated value (1.604 mΩ). The simulation also gave the temperature rise distribution along the fuse element for various points in time, as well as the effect that this increase in temperature has on both the element resistance and hence current flowing in the element. The element temperature rise distribution is shown in Fig. 3.13(a) and the variations of element current, element resistance and element mid-point temperature rise are shown in Fig. 3.13(b). The simulation was then repeated, but this time a more realistic case was chosen in which the voltage source was replaced with a 50 ampere R.M.S. constant current source. The resulting voltage drop along the element again agreed exactly with calculated values, indicating that the simulation was functioning correctly. The element temperature rise profile, resistance variation and element mid-point temperature rise are shown in Figs. 3.14(a) and 3.14(b).

The finite difference model developed by Leach [44] was again used to confirm the validity of the ASTEC3 results. Comparisons of results for both constant voltage and constant current sources are also shown in Figs. 3.13(a) and 3.14(a) respectively, and again good agreement was obtained.

Element Dimensions - 5cmsx4mmx0.12mm - Drive Voltage 250 mV.

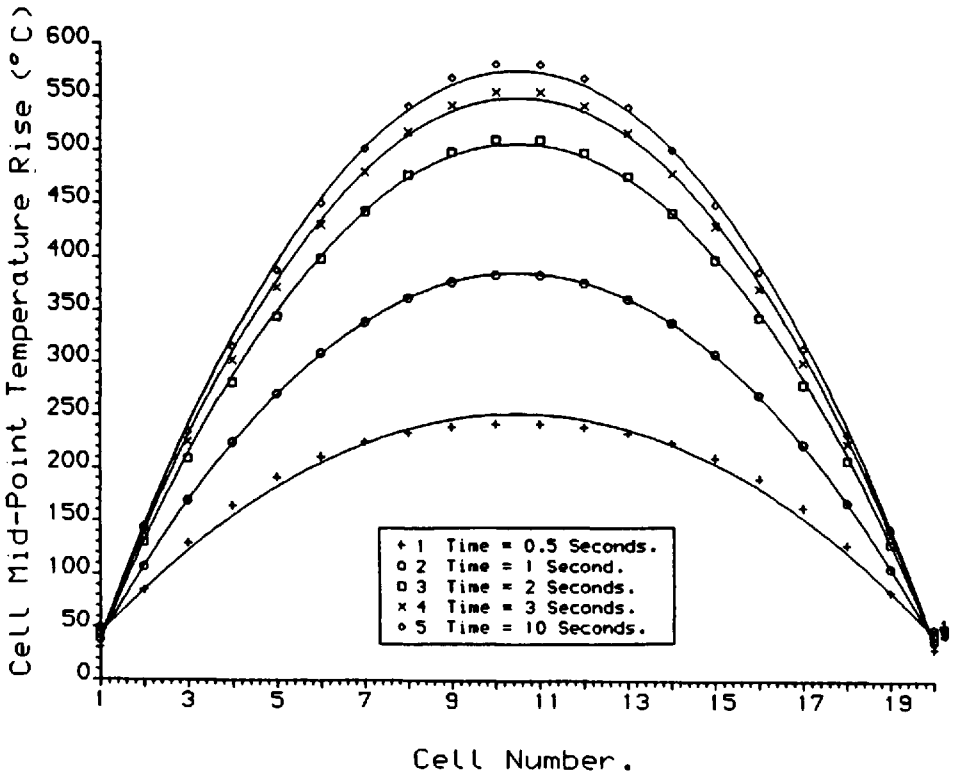

Time (Seconds)		Cell Number (Temperature Rise in °C)									
		1&20	2&19	3&18	4&17	5&16	6&15	7&14	8&13	9&12	10&11
0.5	ASTEC 3	31	85	129	164	191	211	225	234	239	242
	FINITE DIFF.	28	83	128	163	190	208	223	233	236	240
1	ASTEC 3	38	107	169	224	270	309	339	362	377	384
	FINITE DIFF.	36	105	167	222	266	301	335	357	369	379
2	ASTEC 3	45	130	209	281	344	399	443	477	499	511
	FINITE DIFF.	43	128	204	279	339	391	438	472	489	508
3	ASTEC 3	48	139	225	302	372	431	480	518	543	556
	FINITE DIFF.	45	138	221	300	369	428	471	509	531	549
10	ASTEC 3	50	145	234	315	388	451	502	542	569	582
	FINITE DIFF.	47	141	228	307	380	443	496	534	560	576

Silver Element - Constant Voltage Source

Element Temperature Rise

Fig. 3.13 (a)

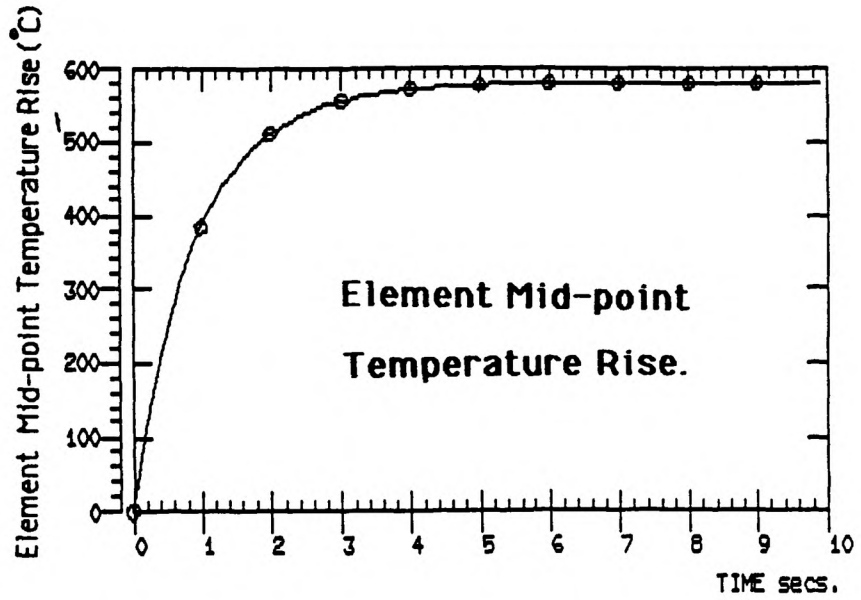

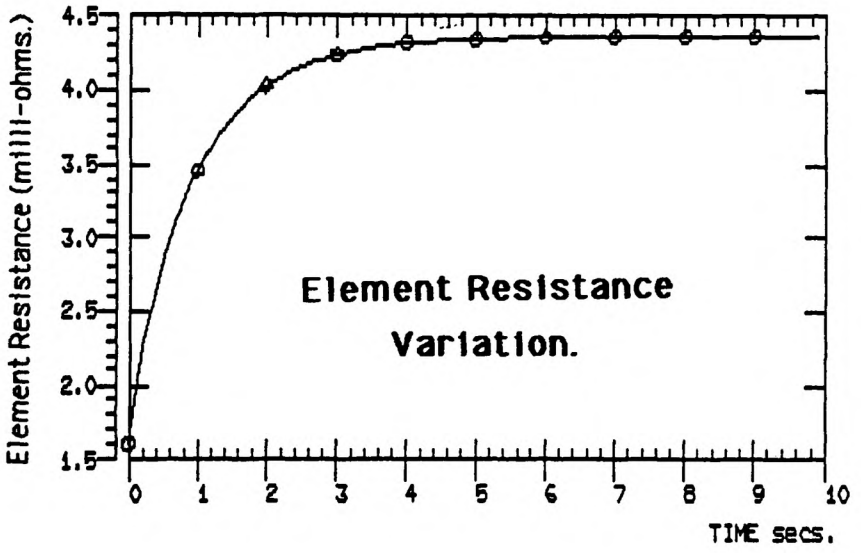

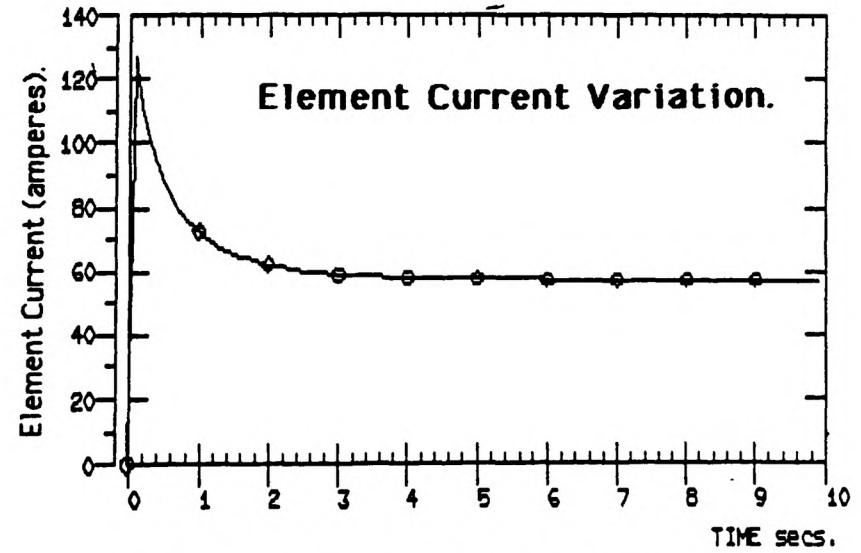

Silver Element - Constant Voltage Source.

Fig. 3.13(b)

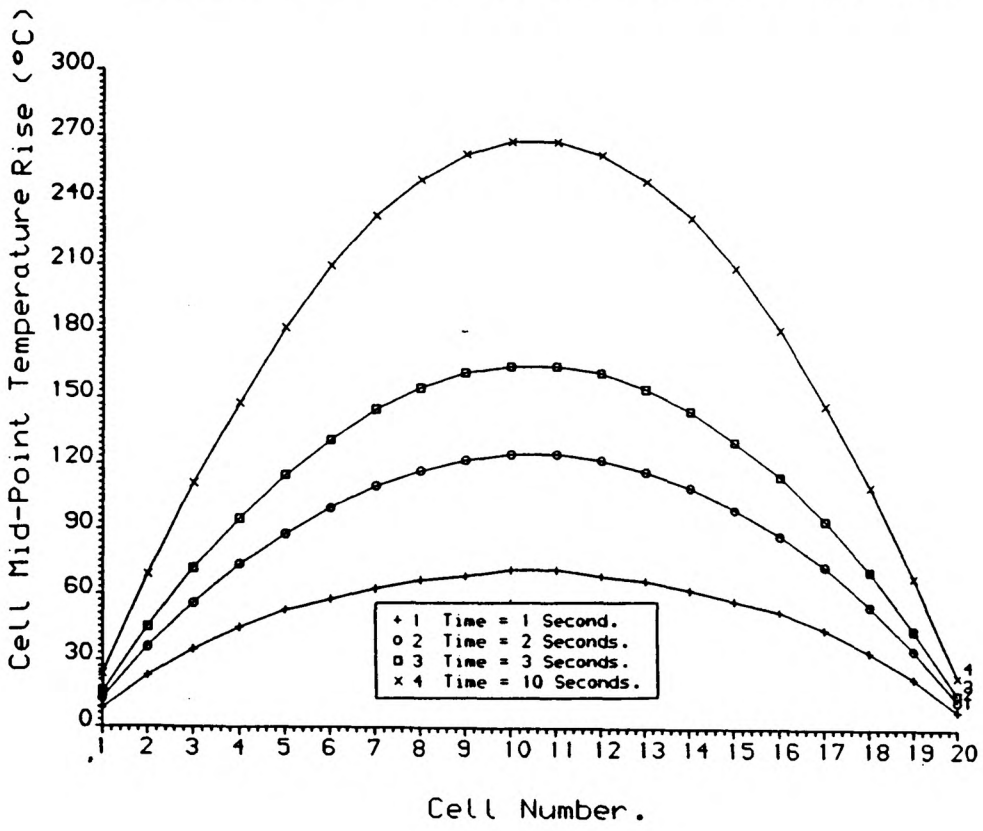

Time (Seconds)		Cell Number (Temperature Rise in °C)									
		1&20	2&19	3&18	4&17	5&16	6&15	7&14	8&13	9&12	10&11
1	ASTEC 3	8	23	35	45	53	58	63	67	69	72
	FINITE DIFF.	6	22	34	45	53	57	63	67	68	71
2	ASTEC 3	13	36	56	74	88	100	110	117	122	125
	FINITE DIFF.	9	34	55	74	87	99	108	116	121	124
3	ASTEC 3	16	45	72	95	115	131	145	155	162	165
	FINITE DIFF.	13	41	68	91	113	131	144	155	160	165
10	ASTEC 3	24	69	111	148	182	210	233	250	262	268
	FINITE DIFF.	19	66	109	147	179	209	233	249	258	267

Silver Element - Constant Current Source.
Element Temperature Rise.

Fig. 3.14(a).

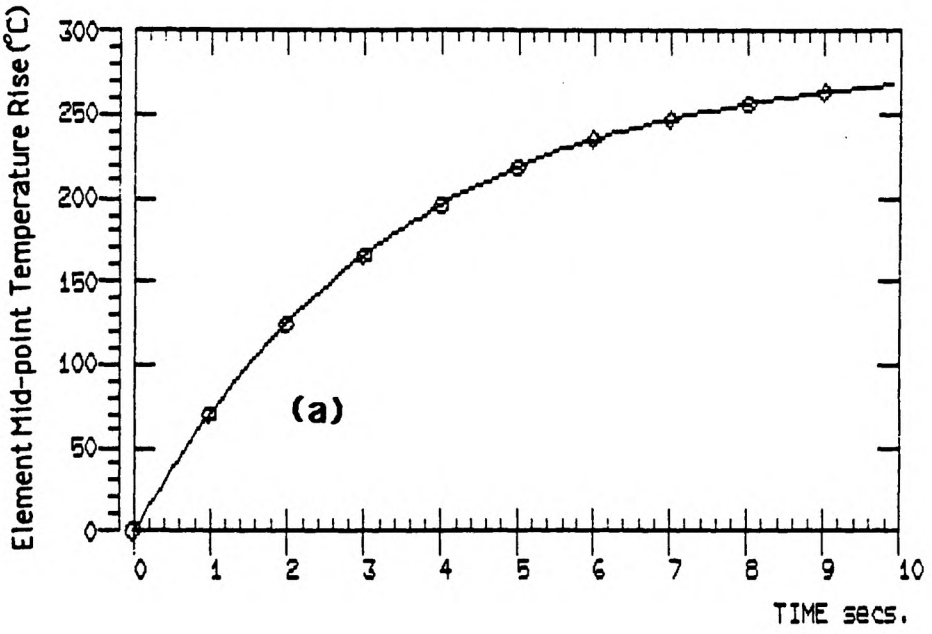

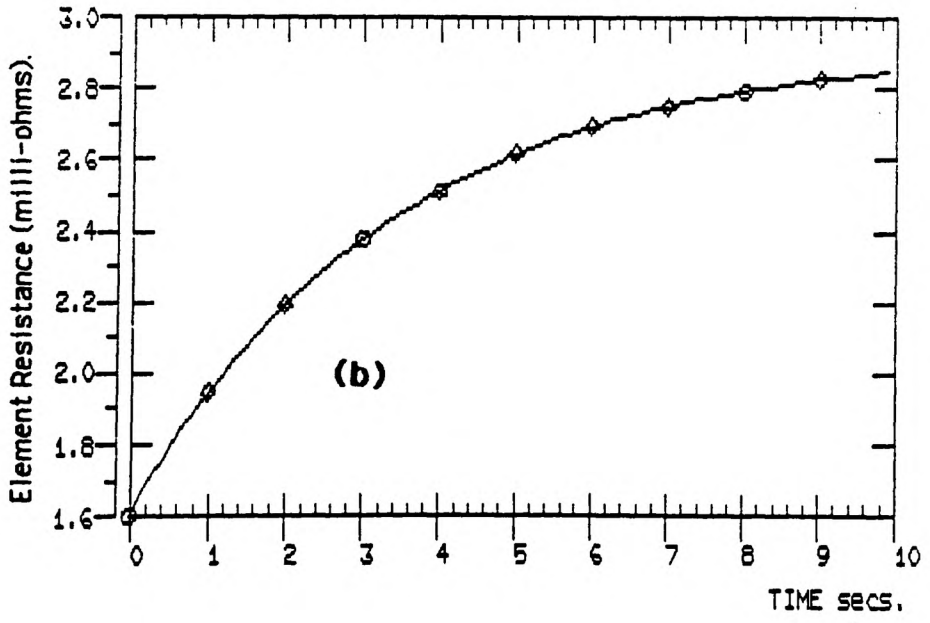

Silver Element - Constant Current Source.

(a) Element Mid-point Temperature Rise.

(b) Element Resistance Variation.

Fig. 3.14(b).

Having established that the thermal and electrical models could be combined within each cell, and valid results obtained from the ASTEC3 simulation of the system, the model was extended to include the cooling effect of the silica sand filler. In addition to losing heat by conduction along the element to the end connections, heat is also lost by conduction to the granular filler. To accommodate this, additional cells were arranged either side of the element in the thermal model to represent the filler. Values of density, specific heat and thermal conductivity of the silica sand filler were taken as 1.80×10^3 kg m^{-3}, 1.20×10^3 Joules kg^{-1} K^{-1} and 0.51 watts m^{-1} K^{-1} respectively [13,48].

The three dimensional arrangement so formed is shown in Fig. 3.15. This three dimensional model allows the properties of the filler to be studied. The relative thinness of the element allowed it to be assumed that, to a first approximation, heat would only be lost to the filler from the large side faces of the element, the heat lost from the strip edges being considered negligible. The dimension of the filler cell perpendicular to the element was chosen to be several times the dimension of the element cell to enable the temperature rise at points well removed from the element to be determined. To simulate a 20°C ambient temperature, 20V voltage sources were either connected directly to the outside nodes of the filler cell, or through a suitable resistor. In the latter case the value of this resistor effectively determined the thickness of the sand filler between the element and the inside surface of the fuse

barrel, which in this simple case is assumed to remain at ambient temperature. In this manner, results for several sand filler thicknesses may be obtained.

The results of the simulation including the effect of the filler for the 50 Ampere RMS current source are shown in Figs. 3.16(a) and 3.16(b). As can be seen, the cooling effect of the silica sand filler effectively reduces the mid-point element temperature by over 100°C and, as expected, the thermal time constant of the filler is very much slower than that of the silver element. Fig. 3.17 shows how the temperature profile of the sand a distance 1 cm away from the centre of the fuse element varies with time. The addition of different resistance values can simulate different sand thicknesses between the element surface and a constant ambient temperature, and Fig. 3.18 shows the variation in sand temperature a distance of 1cm away from the element for various total filler thicknesses. Assuming a constant surface temperature, it can be seen that whilst the initial effect of the addition of the silica sand filler is to cool the fuse element, once the fuse assembly has reached thermal equilibrium greater sand depths around the element cause the element to run slightly warmer, for any given ambient temperature. The simulation shows that for this particular fuse element and operating conditions, increasing the sand depth from 2 to 5 cms causes the sand temperature a distance of 1 cm away from the centre of the element to increase by 21°C after 1000 seconds. These results will be compared with experimental values in later chapters .

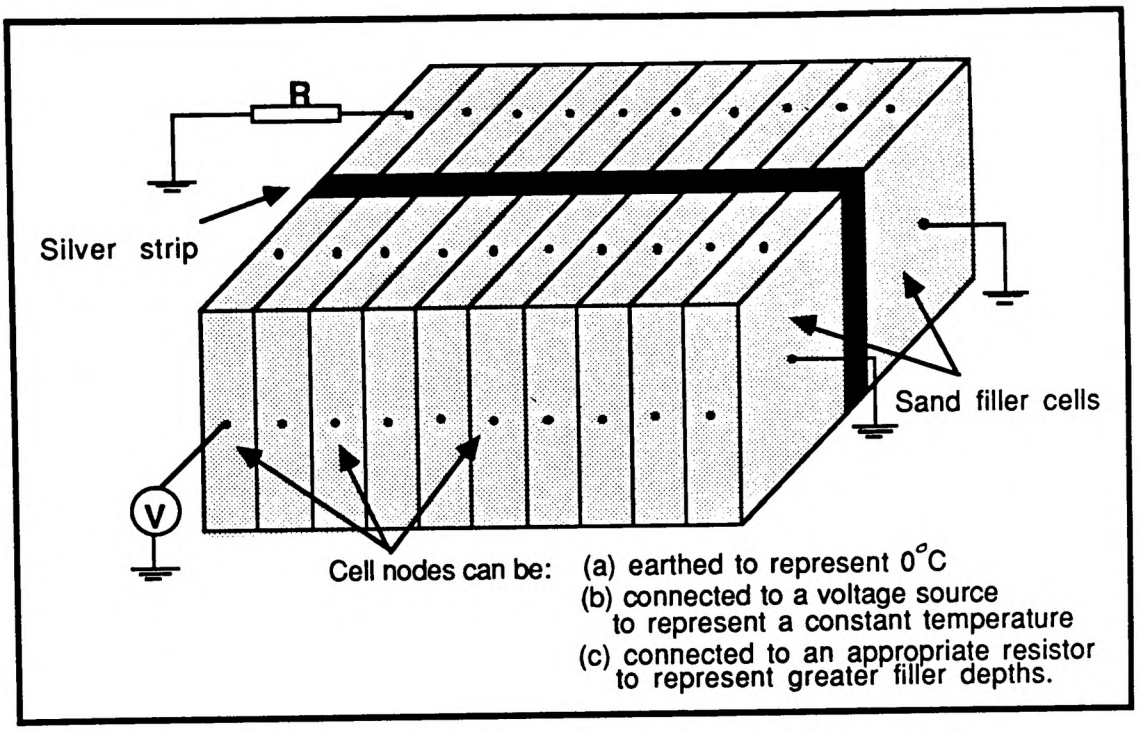

Schematic Arrangement of Sand Filler Cells Around the Silver Element.

Fig. 3.15

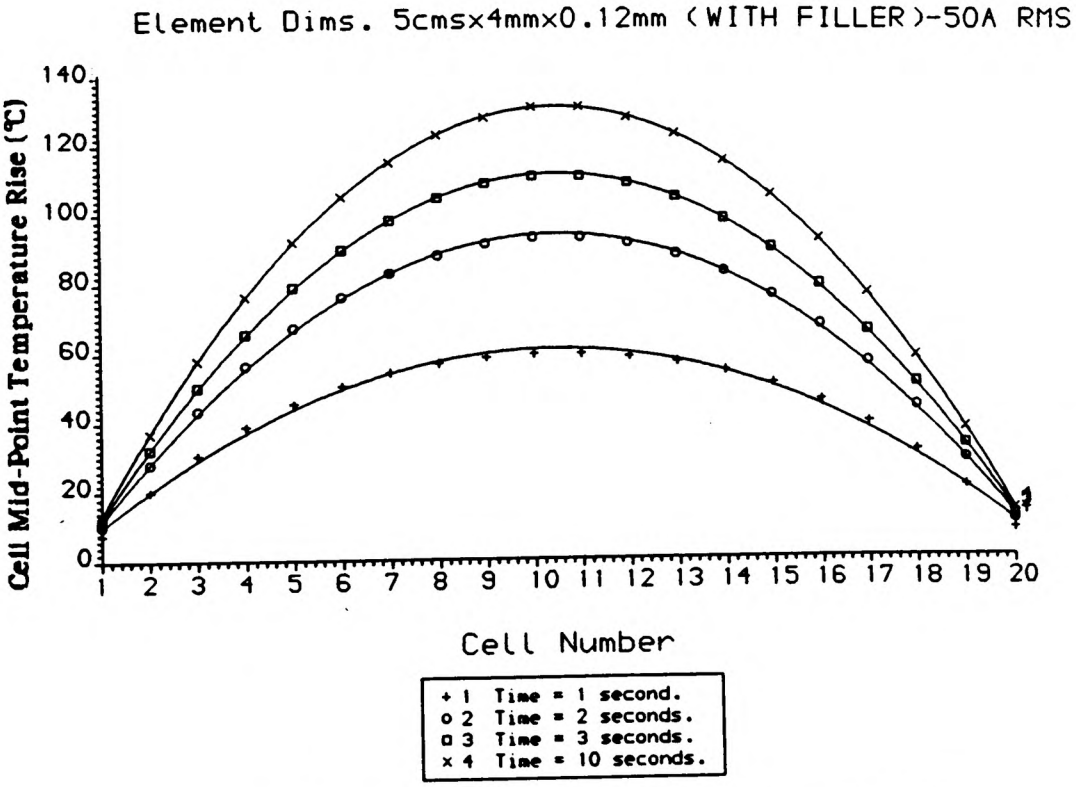

Temperature Rise of Silver Element Surrounded with Granular Filler.

Fig. 3.16(a)

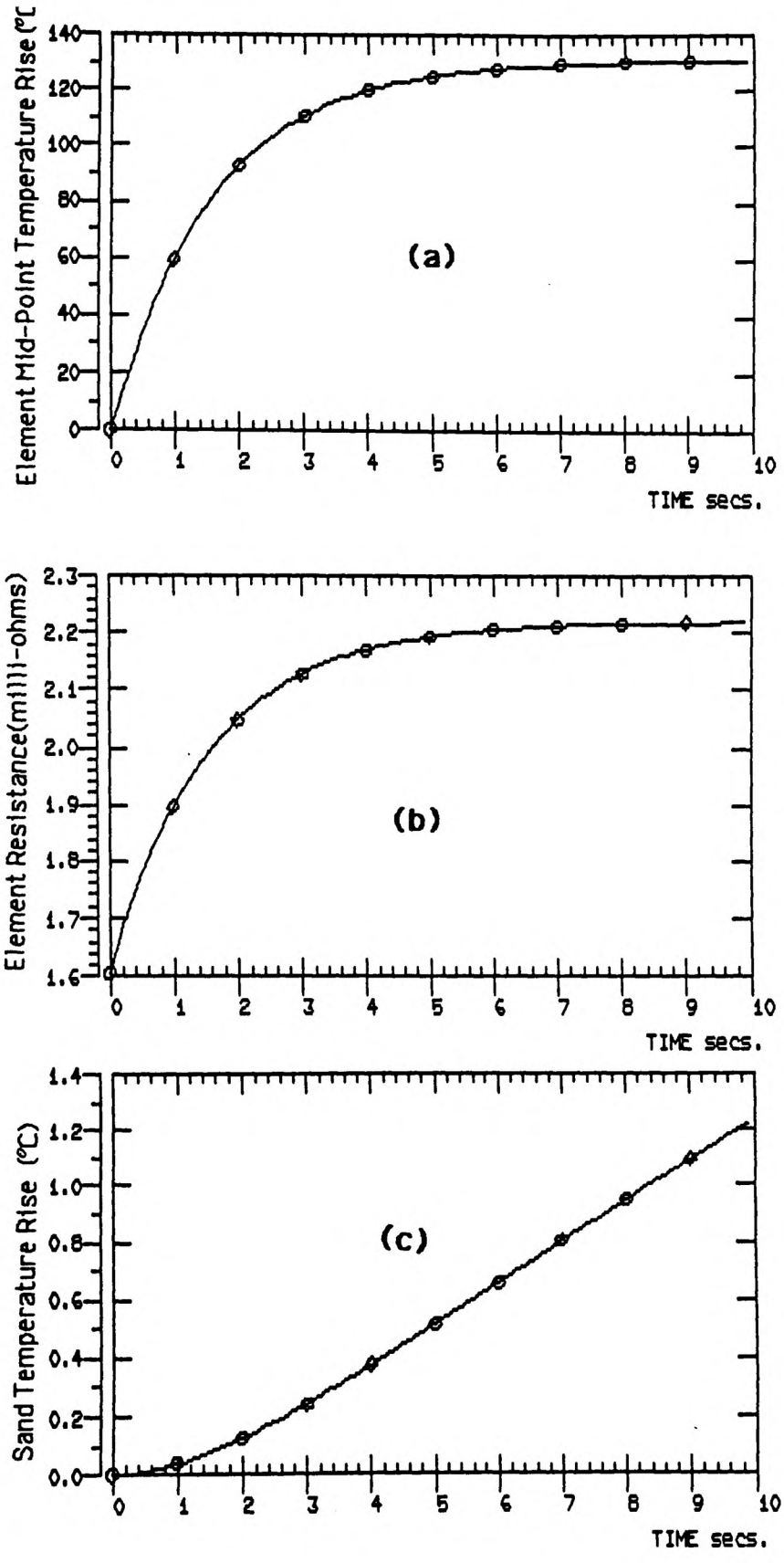

Silver Element Surrounded with Granular Filler

(a) Element Mid-point Temperature Rise.
(b) Element Resistance Variation.
(c) Sand Temperature Rise.

Fig. 3.16(b)

The ASTEC3 modelling technique was then applied to determine the rapid temperature rise of notched fuse elements when subjected to a high fault current. The fuse elements used were two of those whose 'cold resistance' was determined in section 3.3.2. The same mesh distribution of coarse and fine cells was used, but this time a thermal model was included. The effect of the filler was not included in this simulation, since for times of this order (<10 milliseconds) the temperature rise can, to a first approximation, be assumed to be adiabatic.

Owing to the relatively low impedance of the element the current is usually independent of fuse impedance. A constant current source rather than a constant voltage source was thus used to provide the drive current. In order to simulate the rapid temperature rise of the notch section when subjected to high values of current under typical fault conditions, the characteristics of the prospective current, that is the current which would have flowed in the circuit if the fuse were replaced with a solid link, had to be closely modelled. The prospective current is usually at power frequencies (50 or 60 Hz) and its value at any point in time is determined by both the power factor of the circuit and the point on the voltage wave at which the fault is initiated. The power factor in a fault situation is typically less than 0.15 and maximum asymmetry of the current is achieved by initiating the fault near a voltage zero. A prospective current with these characteristics may thus be represented by [49]:

$$I = Ip(\sin(wt + P.O.W. - \cos^{-1} pF) - \sin(P.O.W. - \cos^{-1} pF) \exp\left(\frac{-t\omega}{\tan(\cos^{-1} pF)}\right)$$

where I is the instantaneous current after a time t, w is the angular frequency of the supply, I_p is the 'steady state' peak value of the prospective current, POW is the point on wave switching angle in radians and PF the power factor of the circuit.

ASTEC3 is capable of representing current sources of this type, and thus the effect of power factor and point on wave variation can be determined. Fig. 3.19 shows the simulated applied prospective currents for different power factor values and different point-on-wave closing angles.

From practical tests made on actual fuse elements (see Chapter 4), the test current was chosen so as to cause fuse operation in approximately ten milliseconds. Figs. 3.20 and 3.21 show the notch temperature profile obtained from the ASTEC3 simulation after 8 milliseconds and 10 milliseconds respectively for a 250 ampere prospective current with a circuit power factor of 0.15 and a point on voltage wave closing angle of 0°. In each figure, (a) shows the temperature contour map of the notched section, (b) shows the three dimensional temperature distribution of the cells and (c) shows a smoothed three dimensional temperature profile which has been computer interpolated from the cell mid-point temperatures.

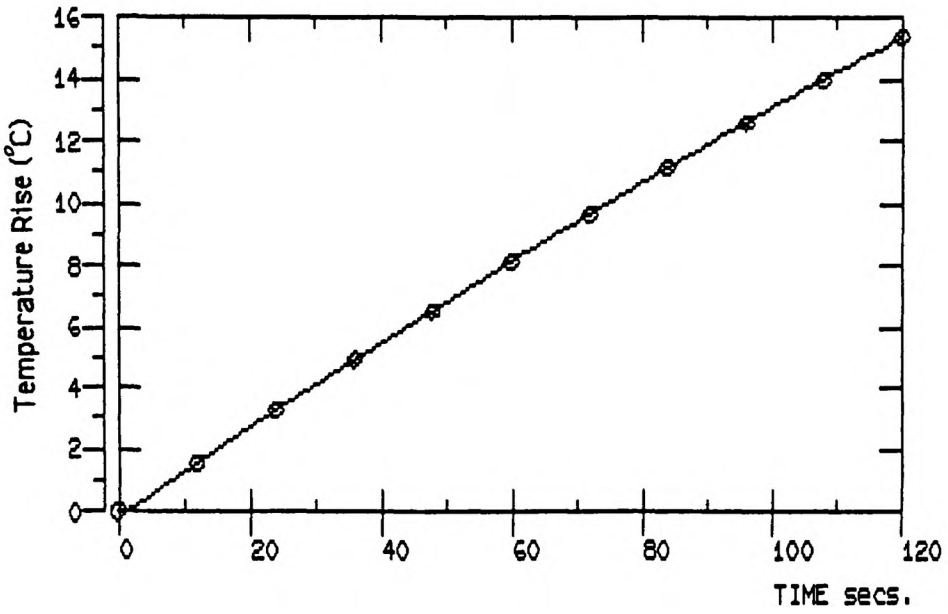

Sand Filler Temperature Rise

Fig. 3.17

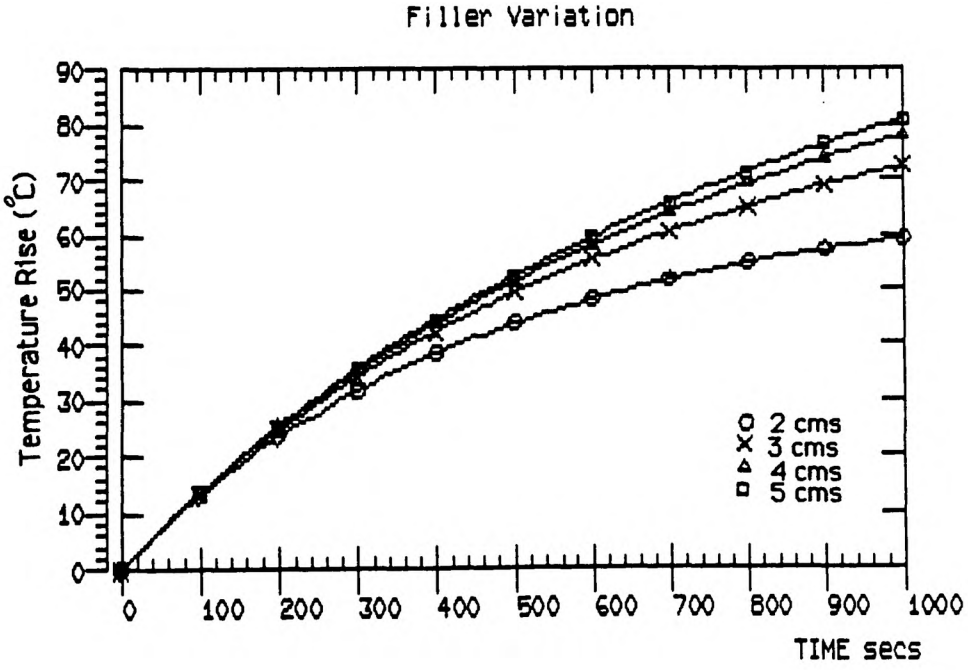

Temperature Rise For Different Sand Filler Depths

Fig. 3.18

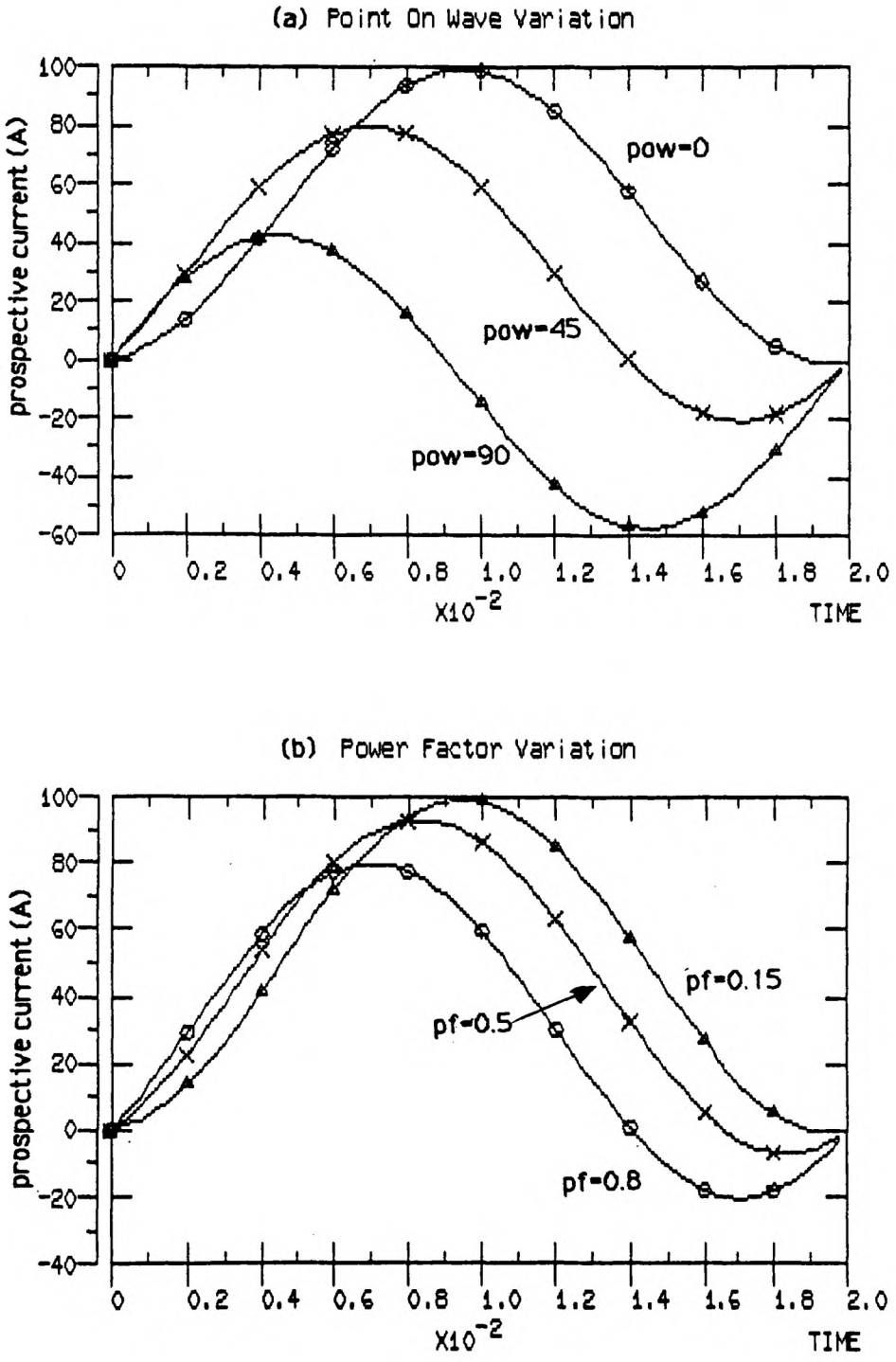

Variation Of Applied Prospective Currents With:

(a) Point On Wave

(b) Power Factor

Fig.3.19

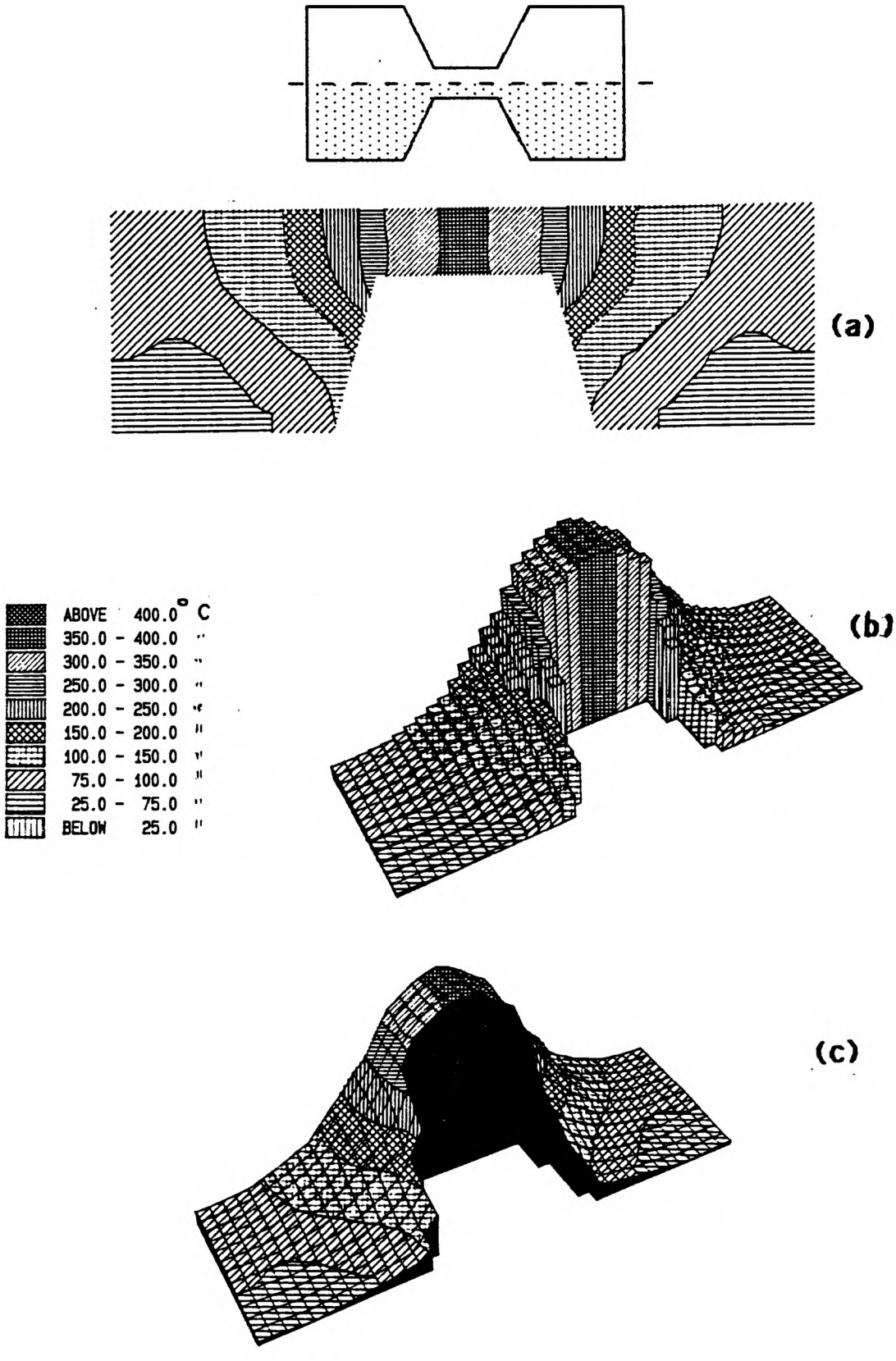

Notch Temperature Profile After 8 Milli-seconds.
Applied Prospective Current 250 Amperes R.M.S

Fig.3.20

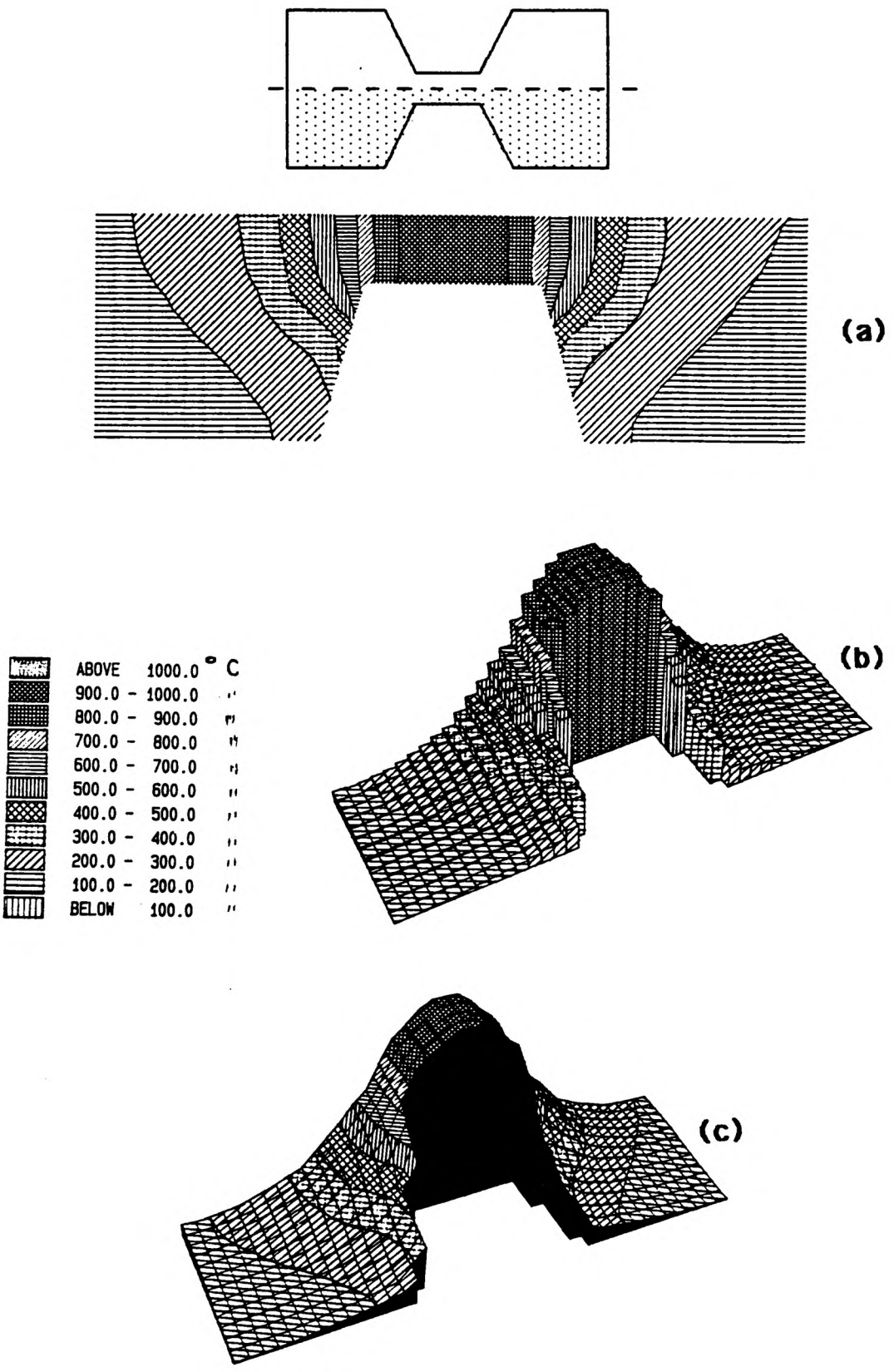

Notch Temperature Profile After 10 Milli-seconds.
Applied Prospective Current 250 Amperes R.M.S

Fig.3.21

As a final check on the validity of the ASTEC3 modelling and the accuracy of its solution, the results were compared with spot results obtained from the finite difference model [44], and agreed within 1%.

3.3.4 Modelling Diffusion

Verification of the software's ability to model diffusion was achieved by simulating diffusion from a plane source and the results again compared with results obtained from established techniques. Analytical solutions to the diffusion equation have been derived by Crank [36], and the ASTEC3 results were compared with these values as well as with results from a finite difference model.

Consider the one dimensional diffusion from an infinite source of concentration C_O to an infinite sink a distance 1 metres away, through a medium with a diffusion coefficient D.

An analytical solution to this problem can be obtained by solving the one dimensional diffusion equation given by equation 2.6, namely:

$$\frac{\partial C}{\partial t} = D \frac{\partial^2 C}{\partial x^2}$$

for the boundary conditions that C = Co (the initial concentration) at x = 0 and C = 0 at x = 1 for all values of time and the initial condition that C = 0 throughout the system at time t = 0.

By firstly converting to dimensionless variables, and then using a method of separation of variables, Crank has shown that the solution to this problem is given by:

$$C = C_o\left(1 - \frac{x}{l} - \frac{2}{\pi}\sum_{n=1}^{\infty}\frac{1}{n}\sin\frac{(n\pi x)}{l}\exp\left(-(n\pi)^2\frac{Dt}{l^2}\right)\right) \qquad --(3.16)$$

and thus involves the summation of an infinite series. Owing to the factors 1/n and n^2 in the negative exponential, however, each term of the series is smaller than the previous one, and a very accurate solution can be obtained using only a relatively small number of terms.

By choosing suitable values for D and l, setting Co = 1 and truncating the series after (say) ten terms, accurate values of C can be obtained at various points in time.

A second method of solving this problem is to use a numerical finite-difference model based on the Crank-Nicolson implicit method [50]. By developing a high level computer program from a method described by Crank, McFarlane, Newby and Pedley [50], finite difference approximations were obtained for various values of D, l and t, and these were directly compared with both the analytic and ASTEC3 results.

The ASTEC3 model to simulate this one dimensional problem merely consists of a number of cells in series, as shown in Fig. 3.22. The values of the equivalent resistances and capacitances were calculated from equations 3.9 and 3.14 respectively using nominal values for D and l, the diffusion

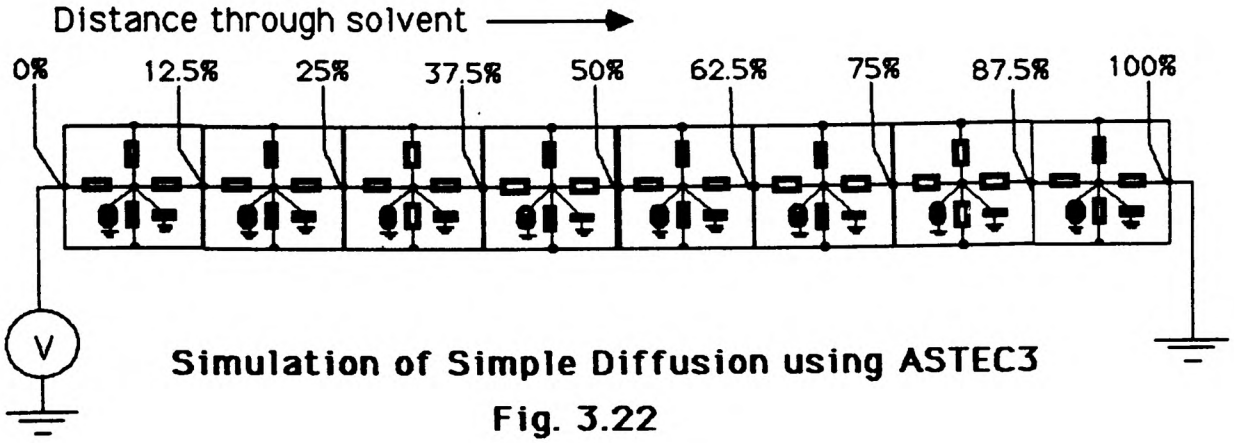

Simulation of Simple Diffusion using ASTEC3

Fig. 3.22

Distance through solvent % →		0	12.5	25	37.5	50	62.5	75	87.5	100
Time (% of steady state) ↓		← Concentration % →								
Exact Solution	3.125	100	61.7	31.7	13.4	4.6	1.2	0.3	0.04	0
Finite Difference	"	100	62.9	33.2	14.3	4.9	1.3	0.2	0	0
ASTEC3	"	100	61.4	31.8	13.9	4.8	1.3	0.3	0.02	0
Exact Solution	6.25	100	72.4	47.9	28.9	15.7	7.7	3.3	1.2	0
Finite Difference	"	100	72.8	48.7	29.6	16.3	8.0	3.5	1.2	0
ASTEC3	"	100	72.2	47.8	28.9	16.0	8.0	3.6	1.3	0
Exact Solution	12.5	100	80.2	61.7	45.2	31.5	20.5	12.1	5.6	0
Finite Difference	"	100	80.4	62.0	45.6	31.8	20.9	12.4	5.7	0
ASTEC3	"	100	80.2	61.6	45.1	31.4	20.5	12.1	5.6	0
Exact Solution	25	100	85.4	71.3	57.3	44.5	32.5	21.2	10.4	0
Finite Difference	"	100	85.4	71.1	57.4	44.5	32.4	21.1	10.4	0
ASTEC3	"	100	85.4	71.1	57.4	44.5	32.4	21.1	10.4	0
Exact Solution	50	100	87.3	74.7	62.1	49.6	37.1	24.7	12.3	0
Finite Difference	"	100	87.3	74.7	62.1	49.6	37.1	24.7	12.3	0
ASTEC3	"	100	87.3	74.7	62.1	49.6	37.1	24.7	12.3	0
Exact Solution	100	100	87.5	75.0	62.5	50.0	37.5	25.0	12.5	0
Finite Difference	"	100	87.5	75.0	62.5	50.0	37.5	25.0	12.5	0
ASTEC3	"	100	87.5	75.0	62.5	50.0	37.5	25.0	12.5	0

Comparison of Results for the Diffusion Problem shown in Fig. 3.22

Table 3.4

coefficient and diffusing distance respectively. The concentrations at any point in space and time are obtained directly from the simulation, being represented by the cell node voltages.

The ASTEC3 results are compared in Table 3.4 with the values obtained from the finite difference simulation and also the analytic solution. Good agreement was once again obtained for this simple problem.

3.4 Interim Conclusions.

The results of the electrical, thermal and diffusion modelling confirm that ASTEC3 software is suitable for simulating and predicting measurements in these three systems. Furthermore it is capable of simulating systems with inter-related electrical and thermal properties and it thus offers the possibility of being equally suitable for systems in which the electrical, thermal and diffusion properties vary simultaneously. One such system is the operation of a fuse with M-effect alloy, and this system will be modelled using the software package. There are, however, no known analytical solutions or finite difference models of the M-effect with which to compare the results of the simulation. The results will, instead, be directly compared with measured values obtained under closely controlled experimental conditions.

CHAPTER 4

EXPERIMENTAL METHODS

4.1 Introduction

Pre-arcing time-current characteristics supplied by fuse manufacturers are used by system design engineers to choose the required fuse current ratings to ensure that complete system protection and coordination is achieved. These fuse characteristics are produced by manufacturers in accordance with the relevant national or international standards. In Britain these include BS 88 Part 1, 1988 - "Cartridge fuses for voltages up to and including 1000 V a.c. and 1500 V d.c.", and BS 2692 Part 1 1986 - "Current limiting fuses exceeding 1000 volts a.c.". All fuses supplied by the manufacturer must comply with their published curves within the tolerance band given in the relevant standard, typically $\pm$20%. As stated in Chapter 1, the shape of these time-current curves for pre-arcing times greater than a few seconds is dictated, in the main, by the speed of operation of the M-effect alloy. It is important, therefore, that the fuse design engineer is fully conversant with the M-effect parameters which affect the shape of the time-current curve to allow him to develop the optimum curve for any given application. There has also been some concern that the use of the M-effect may adversely affect fuse performance by causing element degradation and premature 'ageing' and the design engineer must also be fully aware of any possible limitations of his design. The fuse production engineer

also needs to know the effect of these M-effect parameters to ensure consistency of manufacture and hence compliance with the required standards.

Although the advantages of using M-effect alloy is well known to fuse manufacturers, its use has been mainly on an empirical basis, and since Metcalf's original work in 1939 [9] there has been, until recently, very little research into the M-effect mechanism. As a result of this, little test evidence exists to establish what parameters such as alloy quantity, position, composition and temperature have on fuse operation. Indeed, conflicting results have been obtained by different researchers. In order to develop a sound model the degrees to which these variables influence fuse performance must be determined, and a series of tests were thus performed to obtain reliable data under typical fuse operating conditions. These results were then compared with those of other researchers and used to confirm the validity of the ASTEC3 software model. Before describing these tests, however, it is useful to review, very briefly, previous research into diffusion in metals in general and into the M-effect in particular.

4.2 Diffusion in Metals

Whilst equations 2.6 and 2.7 generally hold true for simple diffusion systems, diffusion in solid and liquid metals is generally far more complex. In solid metals the diffusion or transport of atoms through the metal's atomic lattice may occur in several ways. In metals of similar atomic weight, such as silver and tin, the most usual method of diffusion

is by a substitutional or vacancy mechanism [51]. Due to their thermal energy the atoms in the lattice are continually in motion, each vibrating about their normal lattice point. Occasionally, vacancies or unoccupied sites occur, and these vacancies then become occupied by an adjacent atom and the vacancy's neighbouring site then becomes vacant. In this way a particular atom can slowly move or diffuse through the lattice. In a similar manner, when two metals are in intimate contact, atoms from one metal can move by the vacancy mechanism through the other metal and thus a mutual interchange of atoms occurs. Energy is required for this process to occur and is composed of two terms. If E_f is the energy of vacancy formation and E_m the energy of migration, then the total energy required for an atom to migrate or diffuse through the lattice is given by

$$Q = E_f + E_m$$

where Q is the activation energy.

When considering diffusion in an alloy consisting of metal A and metal B, it is important to realise that the diffusion rates of A atoms in B and B atoms in A are generally not equal, (the so-called Kirkendall effect [51]).

In solid metals it has been empirically found [51] that diffusion in the vast majority of metals is a function of temperature and follows the Arrhenius equation namely:

$$D = D_o \exp.\left(\frac{-Q}{RT}\right)$$

where Do is the diffusion constant for the medium, T the absolute temperature, R the universal gas constant and Q the activation energy.

The problem of predicting, correlating and extrapolating diffusion data in liquid metals is very difficult because of the general lack of understanding of their structure. Diffusion is a structure-sensitive property and D would thus be expected to increase with increasing lattice irregularity. Once molten, the atoms are no longer tied to their lattice formation and can move more freely, resulting in much higher values of diffusion coefficient. Diffusion rates in liquid metals are, indeed, much greater than in the solid state, but the large increase in the value of D on melting is much higher than can be explained by the vacancy theory.

It is generally accepted that in liquid metals, the two most important factors affecting the value of the diffusion coefficient are temperature and concentration. Diffusion rates increase rapidly with temperature whilst both the diffusion coefficient D and the activation energy Q appear to vary with concentration.

The variation of D with temperature in liquid metals is not clearly understood. Both Swalin [52] and Reynick [53] proposed a linear temperature dependency of the form

$$D = a + b\,T$$

where a and b are constants for the diffusing metals, whilst Saxton and Sherby [54] examined a large amount of liquid metal data and concluded that diffusion almost invariably followed an Arrhenius tendency.

Little data exists on the variation of D and Q with concentration. If D is concentration dependent then equation (2.7) must be replaced with the more general equation [36].

$$\frac{\partial C}{\partial t} = \frac{\partial}{\partial x}\left(\frac{D\partial C}{\partial x}\right) + \frac{\partial}{\partial y}\left(\frac{D\partial C}{\partial y}\right) + \frac{\partial}{\partial z}\left(\frac{D\partial C}{\partial z}\right) \qquad - - (4.1)$$

The M-effect, being in the main the diffusion of a liquid metal through a solid metal, embraces both solid metal and liquid metal diffusion theory. It is thus an extremely complex process, and little information exists on the dependency of D on either temperature or concentration in such a system.

4.3 Previous Research into the M-Effect

The first in-depth study of the M-effect was made by Sletterink, Vlutters and Zwaag in 1972 [55]. The investigation consisted of two parts. Firstly, silver elements with tin deposits were placed in a temperature controlled oven and the rate of diffusion of the tin through the silver measured for various oven temperatures. The diffusion depth was measured by sectioning the element sample and measuring the diffusion depth using an optical microscope. The tests showed that with the oven set at 140°C, the diffusion depth was not detectable even after

2000 hours. After 2000 hours at 215°C, however, a distinct diffused layer could be seen. At temperatures above 221°C the diffusion rate increased considerably, although no measurements of the diffusion rate were made. Once in the molten state they observed that the diffusion rate appeared to increase with temperature according to the Arrhenius equation.

They also deduced that the diffused layer, being a compound of silver and tin, should have a different resistivity to both pure tin and pure silver, and thus the resistance of the fuse should change as the tin diffused through the silver. This change in resistivity, however, could not be detected experimentally.

The second part of their investigation was to determine whether the diffusion of the tin through the silver caused by fuse heating, due to temporary overloads, would lead to a change in the fuse time-current characteristic. Tests were made at several values of overload current, the current being applied for short time periods to ensure the fuse did not operate. Tests were made on 160 ampere fuses with currents which would cause melting in the range 10 seconds to 1000 seconds, but with the currents only applied for 40%, 60% and 80% of the expected melting time. The fuse elements were sectioned and examined using a X25 optical microscope. They detected "hardly any diffusion visible" after applying a load current for 40% of the time which would normally cause the fuse to operate. After 60% of the expected operating time they "clearly observed" that silver had

diffused into the tin, whilst after 80% "almost the entire cross-section had dissolved". It is interesting to note that even when these overload tests were repeated up to 10,000 times on the same fuses, the variation in operating times were still within the $\pm$ 20% tolerance allowed in the international standards.

Daalder, Kulsetas and Rondeel [32] also studied the diffusion rate of tin through silver elements by placing elements in an oven held at various constant temperatures both below and above the melting point of tin. Again they found that whilst diffusion was negligibly small below the melting point of tin, it increased dramatically above it. In contrast to Sletterink, Vlutters and Zwaag, however, their results showed that the diffusion rate did not follow the Arrhenius temperature dependency. They identified the diffused layer as the inter-metallic compound Ag_3Sn, and by growing a sample of the compound determined it to have a resistivity of 20.5 x 10^{-8} ohms-metres at 20°C and a temperature coefficient of resistance of 1.46 x 10^{-3} K^{-1}.

Rondeel, Kulsetas and Bodsberg [56] investigated the effect of the dimensions of the tin deposit on the operating time-current characteristic of the fuse. They found that varying the thickness of the applied tin from 0.25 mm to 1.5 mm had only limited influence on the shape of the time-current curve and produced less than 5% variation in the fuse operating speed.

Both Klepp [57] and Hofmann and Lindmayer [30] studied a range of M-effect alloys on both silver and copper elements. Tests were carried out both on samples in a temperature controlled oven and also in a test circuit with known currents passed through the fuse elements. The elements were tested in air and the element temperature rise measured using an infra-red thermometer. At temperatures below 221°C no significant diffusion had occurred after 20 days. At temperatures above 221°C the diffusion rate was considerably higher. The diffusion rate of the M-effect alloy through the element material increased with temperature, but at any given temperature, diffusion started off quickly but then slowed down as if it were becoming saturated. They concluded that the diffusion rate was a function of both temperature and concentration gradient, and thus the thickness of the M-effect deposit had to be greater than a certain minimum thickness otherwise an undesirable stabilisation at high temperature levels resulted.

Ovland, Kulsetas, Forstel and Rondeel [58] studied the effect of M-effect alloy on silver plated copper fuse elements. Elements were placed in temperature controlled ovens in the range 147°C to 222°C for times up to 2800 hours. Tests were also made on complete fuses with currents in the range 25 Amps to 66 Amps, with fusing times ranging from 17 seconds to 3 hours. Examination of the M-effect region on both types of samples revealed the presence of two intermetallic compounds Cu_3Sn and Cu_6Sn_5 at the copper-tin interface. They found, however, that the growth rate of

inter-metallic compounds at any given temperature was slower than in the tin-silver system and whilst some fuse ageing was apparent, its rate was "acceptably slow".

Several researchers have thus studied the M-effect, but whilst this research has provided a qualitative assessment of M-effect action, most of the quantitative work was merely to confirm that any ageing which occurred did not vary the fuse operating characteristics by more than that allowed in the international standards, and made no attempt to obtain fundamental information on M-effect action such as diffusion rate and diffusion rate temperature dependency. In order to obtain the coefficients required for the software model it is necessary to obtain reliable test data under known test conditions. Once this has been obtained, the relationship of the speed and mode of fuse operation during M-effect action to the metallurgical processes occuring between the element material and the alloy may be determined. It is clear, therefore, that to obtain a full understanding of the mechanism of the M-effect, it is necessary to study this metallurgical alloying process. Fig. 4.1 shows the phase equilibrium diagram for silver and tin [59]. In this system there is a critical composition where the 'alloy' has just one melting point rather than the more usual range of melting temperatures spanning the solidus and liquidus points. This critical composition, known as a 'eutectic', occurs at 96.5% Tin, 3.5% Silver, and the eutectic temperature of 221°C is below that of both the melting point of silver (961°C) and the melting point of tin (231°C). The

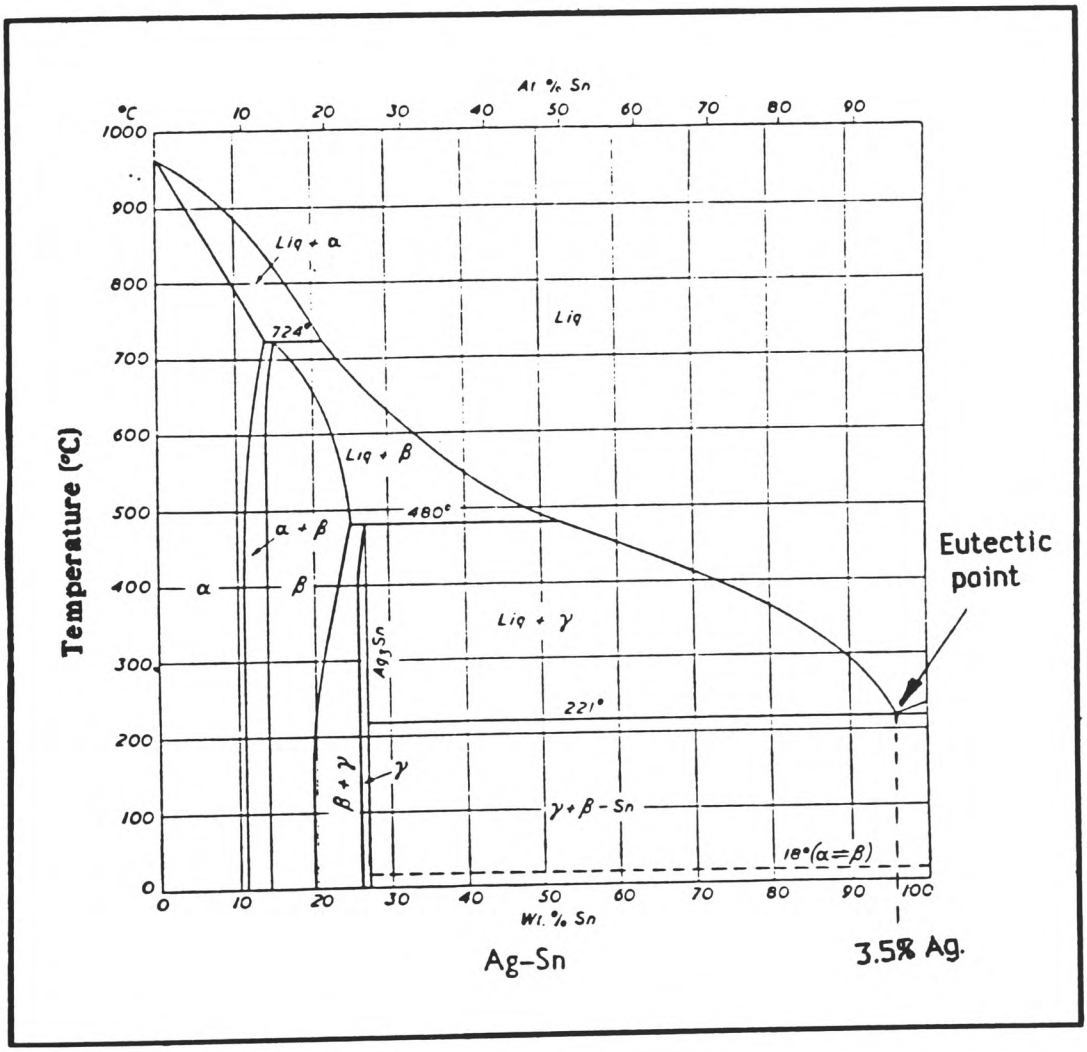

Equilibrium Phase Diagram For The Silver/Tin System.

Fig. 4.1

α and β phases shown on the diagram are various mixtures of the two metals, whilst the γ phase is a constant ratio of the two metals known as an inter-metallic compound.

The general conclusion of all the previous researchers was that the rate of diffusion of tin through silver in the solid state was negligible, and thus for significant M-effect action to occur there must be some liquid present. The eutectic point is the lowest temperature at which liquid can be present and since, as a general rule, the rate of diffusion for liquid phases is much higher than that for solid phases [33], it is reasonable to estimate that the onset of significant M-effect action occurs at temperatures above 221°C, a result concurred by all the researchers.[30,52,57,58].

The relationships between the composition of the various compounds formed and their respective melting temperatures can thus be determined from the equilibrium phase diagram, and this can be used, with caution, to estimate what will happen under various experimental conditions. It should be remembered, however, that M-effect action is a dynamic process with diffusion rate, temperature and changing alloy composition being the key variables. Equilibrium diagrams are not dynamic in the same sense as they represent 'equilibrium' conditions, which means very slow heating or cooling conditions must be maintained. Nevertheless, their use can give a useful guide to M-effect operation.

The equilibrium phase diagram to represent the M-effect action of tin on silver plated copper elements would clearly be far more complex as three metals are involved. This tertiary system would be far more difficult to model, and in view of this the following experiments were confined to the binary tin-silver system.

4.4 Experimental Work

Previous research [30,55] has shown that the diffusion rate of the alloy through the element material is a function of temperature (see Section 4.3) and thus during fuse operation under low-overcurrent fault conditions the temperature and diffusion rate vary simultaneously until the fuse operates. One method of studying the M-effect would thus be to apply a series of low over-currents and monitor both the M-effect temperature and diffusion depth until fuse operation occurs. In this way the relationship between current, temperature and operating time could be determined.

An alternative method would be to hold the fuse at a series of known constant temperatures, and measure the corresponding diffusion depth as a function of time. This would give the diffusion rate at any given temperature, therefore enabling the relationship between temperature and diffusion rate to be determined.

Experiments were carried out using both these modes of testing, the former referred to as 'constant current' testing and the latter 'constant temperature' testing. The constant current tests were made on both single elements

placed in a test box and also on specially constructed fuses connected to a low voltage test circuit. The constant temperature tests were made on elements placed in a temperature controlled oven for various time periods. In both cases the element samples were sectioned, mounted and polished, and examined using both optical and scanning electron microscopes.

4.4.1 Constant Current Testing

When a fuse is subjected to a low over current fault, the relatively low impedance of the fuse ensures essentially constant current conditions, with element temperature increasing until fuse operation occurs. One of the main reasons for using M-effect alloy is to optimise the shape of the time-current characteristic. Factors relating to the alloy which may influence this shape are its quantity, composition and position on the element, and initially the tests concentrated on these three variables. For example, by applying a known current to a fuse, and measuring the time the fuse takes to melt and break the circuit, one point on the time-current curve may be determined. A series of tests, each at a different applied current, would thus allow the complete time-current curve to be constructed. Also, at any given test current point, by keeping the current constant, but varying the quantity and/or position of the alloy on the fuse, the effect of these parameters on fuse melting time could be determined. Similarly, if several sets of fuses were manufactured, identical in every respect except that each set used a different M-effect alloy, then

the effect of M-effect composition on the time-current curve could be established. In this way, data regarding alloy composition, position and quantity may be determined.

Test Equipment

This section describes the test equipment used to carry out these tests.

Tests were made on both fully assembled fuses and also on single fuse elements mounted in a test box. The test box, shown in Fig. 4.2, was designed to accommodate a range of typical fuse element sizes. The elements were surrounded by 60-100 mesh fuse grade silica sand which was vibrated for a given period prior to each test to ensure uniform compaction and thus consistent test conditions. Removable partitions enabled the sand depth around the element to be varied. Large copper mounting pads and connecting cables limited the temperature rise of the pads which were monitored using chromel-alumel thermocouples. The thermocouples were connected to Status Instruments GPM 2000 cold junction compensated thermocouple indicators with a measurement accuracy of better than $\pm$ 1°C. The output from the GPM 2000 was connected to a Rikadenki KB multi-channel chart recorder so that any temperature changes were recorded. The thermocouples and the chart recorder were calibrated against a standard potentiometer voltage source both prior to use and at frequent intervals during the tests. The test box was connected to the low voltage (30 volt) test circuit shown in Fig. 4.3. The a.c. power supply (230V, 50Hz) was fed through an auto-transformer (T1), contactor

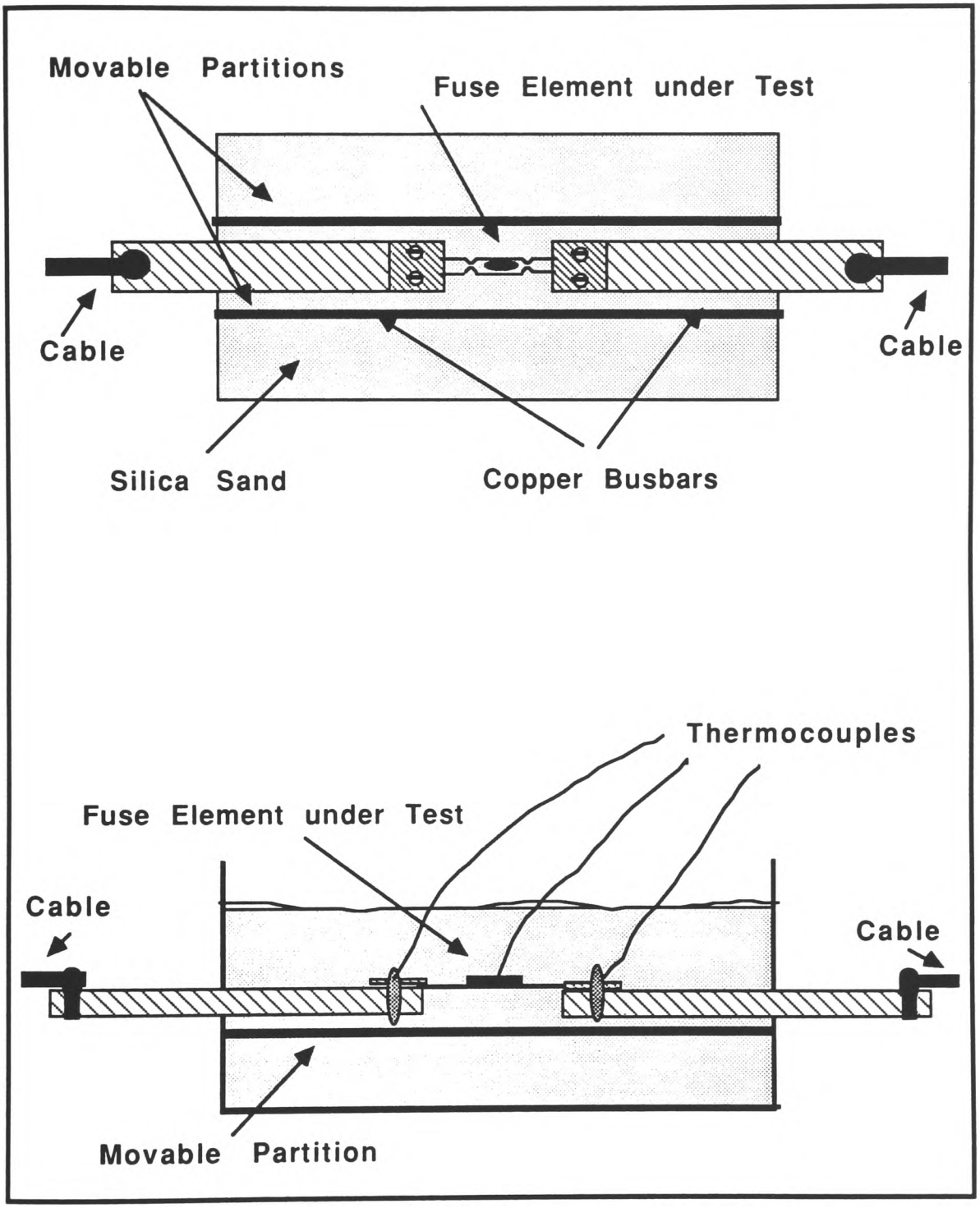

Fuse Test Box

Fig. 4.2

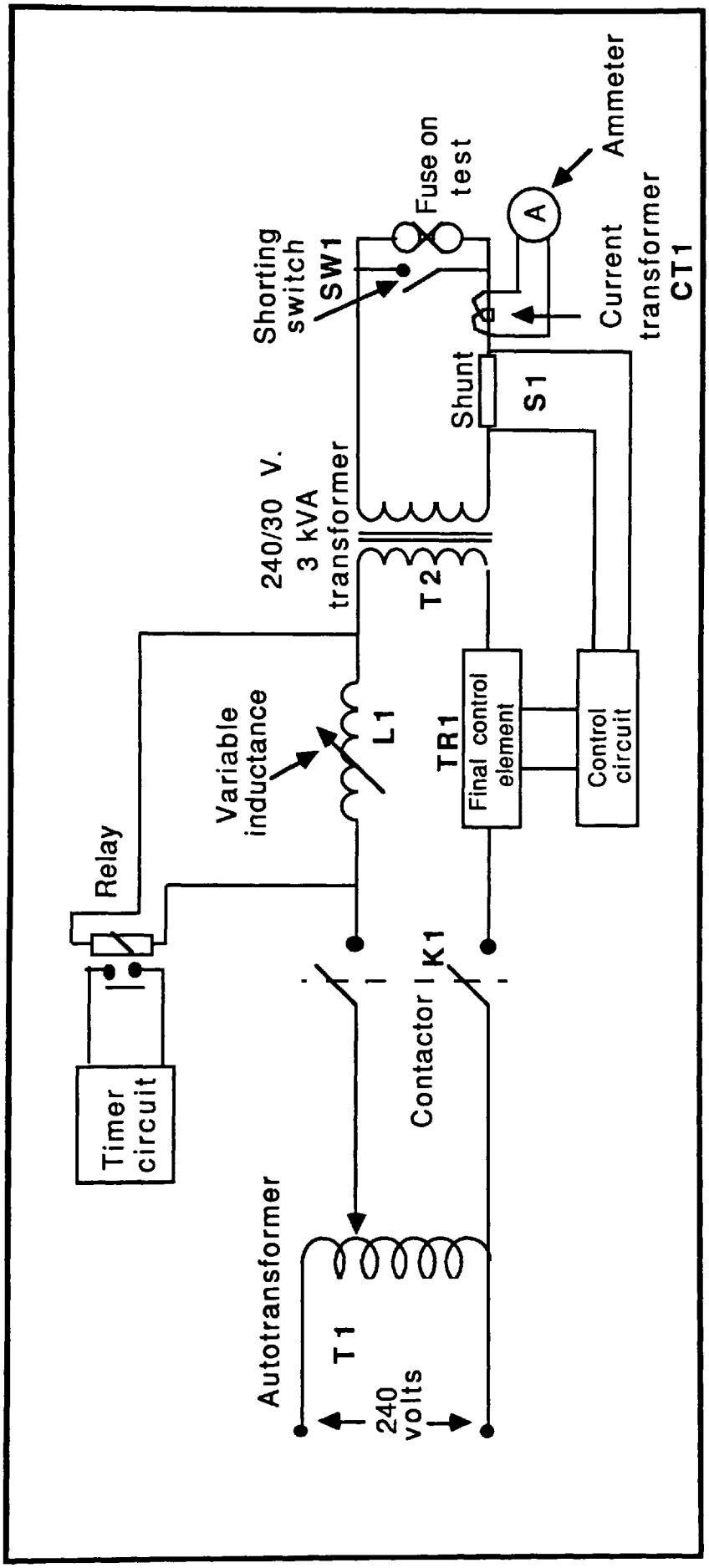

Circuit Diagram Of Test Equipment

Fig. 4.3

(K1), ballast inductor L1 and final control element (TR1) to the 3kVA transformer (T2) where the voltage was reduced to the test voltage of 0-30 volts. The secondary circuit of T2 supplied the control shunt (S1), the current measurement transformer (CT1) and the test box. For calibration purposes the test box was shunted by a high power, off-load switch (SW1). The final control element was a power triac whose switching angle could be varied by the control circuitry. The current in the secondary circuit was monitored by an ammeter and chart recorder connected via the current transformer (CT1).

The tests were made in a current range of 30 to 160 Amperes RMS, with the currents kept constant to within $\pm$1 ampere by the control circuit. The control circuit held the fuse current constant by monitoring the voltage drop across the control shunt (S1) and adjusting the firing angle of the power triac and hence controlling the power to the transformer, T2. Preliminary investigations showed that chopping the input voltage produced no adverse heating of transformer T2 which stayed within temperature rise limits throughout the investigations. A timing circuit using a clock and chart recorder monitored long fuse operating times, whilst short operating times ($<$ 1 sec) were measured using an ultra-violet recorder and storage oscilloscope.

The Effect of varying the Quantity of M-Effect Alloy

Before describing the tests, it is useful to review the methods of manufacture of fuse elements.

Industrial fuse elements are manufactured by mechanically punching out the required element profile prior to the addition of M-effect alloy. Depending upon the type of element being made, alloy may be applied mechanically or manually. Some element designs have well-shaped recesses stamped in during the element forming process to receive the alloy, and the complete element is manufactured automatically on a multi-stage fabrication line as follows. After the element form has been punched out and the well-shaped recess formed, a measured quantity of alloy is mechanically cropped from a reel and dropped into the recess. A gas torch then melts the alloy which flows to fill the recess, after which the alloy is rapidly cooled by an air jet (Fig. 4.4).

In other element designs, the alloy is not contained in a recess but is merely applied to the surface of the element by an operator using a hand soldering iron. The automatic method ensures the quantity and position of the alloy, and also the alloy melting and solidifying times, are fixed by the machine settings, whilst in the manual operation, the quantity and position of the alloy is determined by the skill and experience of the operator.

The first series of tests was to determine what effect the quantity of alloy had on fuse operating time, and also whether there was any difference in the mode of fuse operation between the two methods of manufacture.

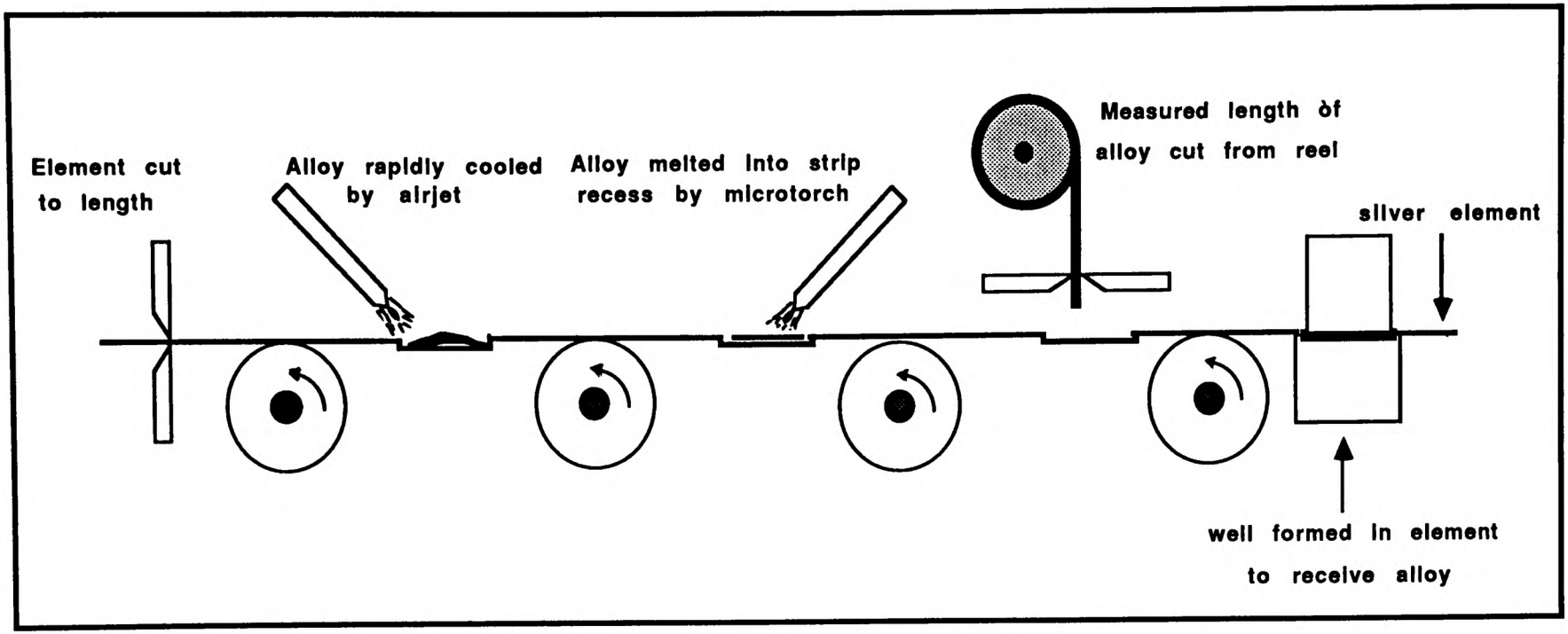

Mechanical Application Of M-effect Alloy In Production Process

Fig. 4.4

Measured quantities of alloy were applied to elements using both manufacturing techniques. For this series of tests the "alloy" used was commercially pure tin (99.97%). The quantity of alloy added in commercially manufactured elements is typically measured by volume rather than weight, this being the length of wire cropped from a reel. In order to investigate how consistent this operation is, and thus determine typical quantities of M-effect alloy used on elements, several commercially manufactured elements were weighed with and without alloy and the alloy weight determined. The results of the measurements on three popular element sizes, with the range of weights tested are given in Table 4.1. It is interesting to note that approximately the same quantity of alloy is added, regardless of the thickness of the element.

Element Dimensions	Alloy Weight
Low voltage industrial fuse-link 4mm x 0.10 mm	65 mg ± 8 mg
Low voltage industrial fuse-link 4mm x 0.15 mm	68 mg ± 8 mg
High voltage distribution fuse-link 2.54 x 0.16 mm	80 mg ± 14 mg

Weight of M-effect Alloy used on Commercially Manufactured Fuse-links.

Table 4.1

For the mechanically produced elements, measured quantities of tin were melted into the pre-formed recess and rapidly cooled using an air jet in a similar manner to commercially produced elements. For the manually produced elements, a gas torch was used in preference to a copper bit soldering iron to preclude the possibility of the copper bit contaminating the tin. Flux is never used, as this may leave harmful residues. Although in industry, operator skill and experience alone is used to judge the correct quantity and position of the tin, it was felt that some technique should be introduced to ensure a measure of control, and thus obtain consistent results. A method had to be devised to confine a measured quantity of the M-effect metal to a small area of the element. Initially a thin mica sheet with a slot cut in it was used as a template for positioning the weighed quantity of tin, the object being to cover the element with the template and then to melt the tin through the slot so that it would be accurately positioned on the element. Unfortunately, surface tension effects prevented the molten metal from flowing through the narrow slot, and no variation of this technique proved successful. After trying several different methods it was concluded that if a fine flame gas micro-torch was used it was possible, with sufficiently low flame and skill, to control the heat input and to accurately position the tin globule. The flame was played onto the tin just long enough for it to melt onto the element, a period of two to three seconds, after which it was quickly removed. Elements were compared during manufacture so that they were visually similar with regard to the shape of and position of the tin.

Both mechanically and manually produced elements were tested using the test box and low voltage test circuit described earlier. Fuse grade silica sand was poured around the element to a depth of 2.0 cms. and vibrated for one minute to ensure uniform compaction, a technique used in commercial fuse manufacture. The elements were tested by passing a fixed current through them until melting occurred and the circuit broken. Test currents were chosen so as to cause fuse operation in approximately 100, 1000, and 10,000 seconds, covering the range of melting times over which M-effect operation typically occurs.

The results of the tests, shown in Fig. 4.5 indicate that for each element thickness there is a minimum quantity of tin required to obtain consistent M-effect action. This minimum quantity corresponded to an amount of tin which left residual tin on the element surface after the element had melted. In practice this required an original tin thickness of approximately four to five times the thickness of the element under test. Increasing the weight above this critical value produced no noticeable change in the fuse element operating time. Also, in general, no significant difference was detected between mechanically produced elements in which the tin was confined to a well, and the manually produced elements to which the tin had been merely applied to the surface. An exception to this was observed when using large amounts of tin, particularly on the thickest element. Under these conditions, on manually produced elements, the tin would occasionally run to a notch and produce an untypically fast operating time. It was also

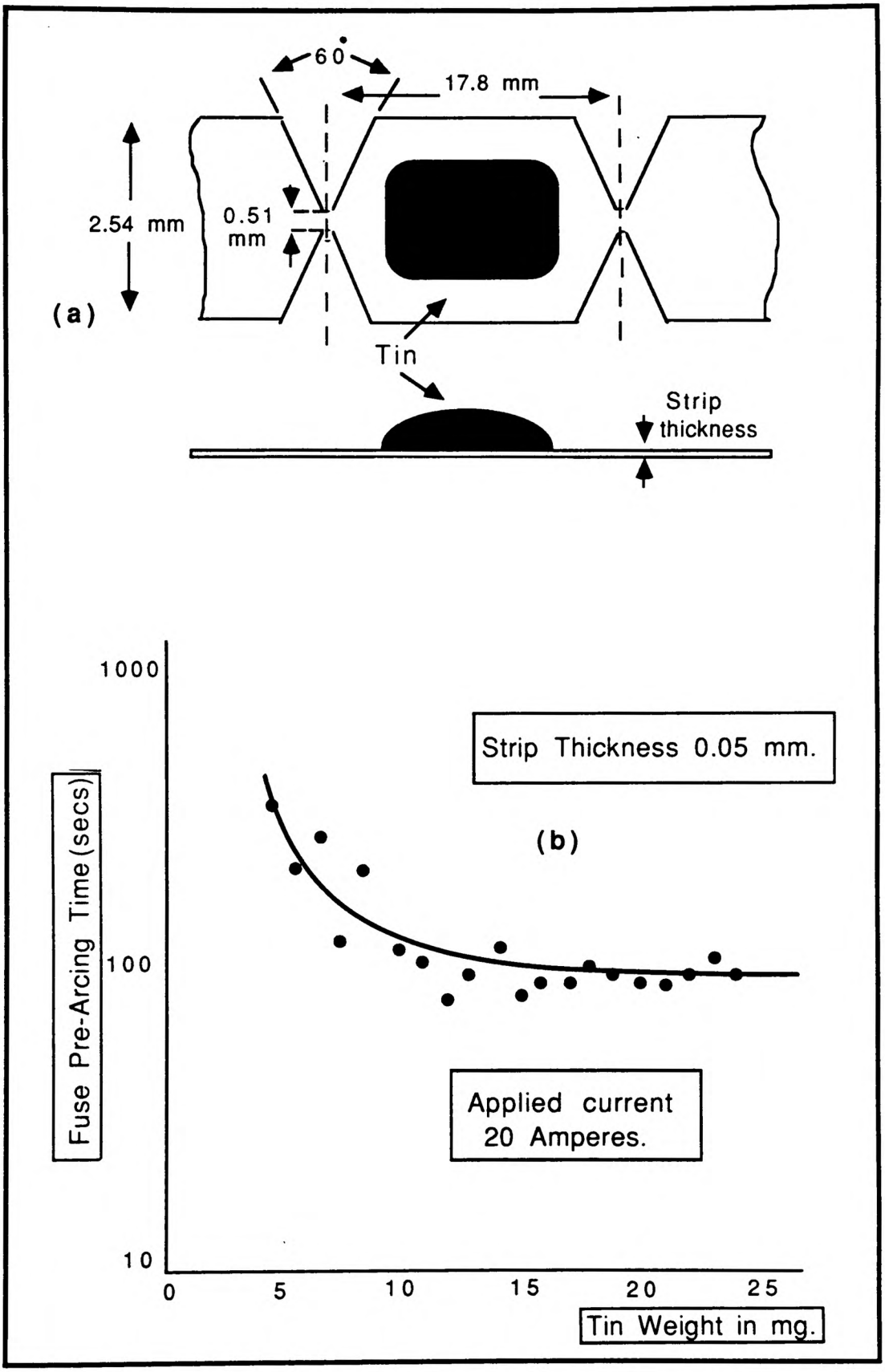

(a) Element Arrangement.

(b) Fuse Pre-Arcing Time for Various Weights of Tin.

Fig. 4.5.(a & b)

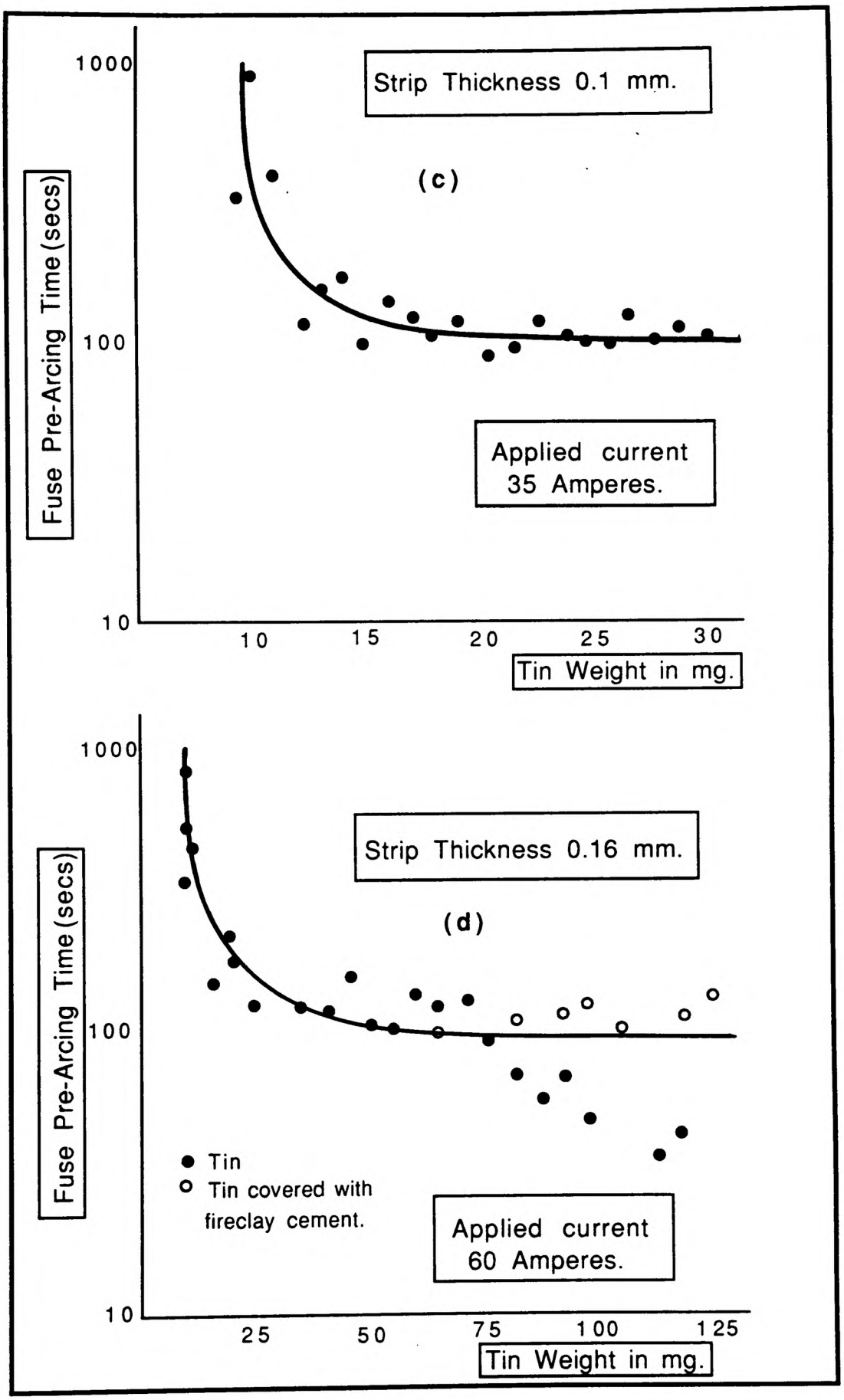

Fuse Pre-Arcing Time For Various Weights Of Tin.

Fig. 4.5.(c & d)

noticed that on these thick elements the molten tin would spread over the surface of the silver element and again produce inconsistent results (see Fig. 4.5(d)). It was found that covering the tin surface with a thick solution of fireclay cement during element manufacture retained the molten tin in one spot and consistent results were again achieved. The cement is quite inert and has no detectable adverse effect on the operation of the fuse.

The Effect of Varying the Position of M-Effect Alloy

M-effect alloy is usually placed at the centre of the fuse-element, mid-way between notches, as this is usually the hottest point of the element under low-overcurrent fault conditions [60]. The effect of alloy position was determined by testing a series of elements in which the tin globule was positioned at varying points along the fuse element, and also at varying points between two adjacent notches at the element centre.

As expected, fuse operation always occurred at the tin deposit at the centre point of the fuse. It was found that the actual position of the tin between adjacent notches was not critical, except that with the manually soldered elements, if it were placed too near a notch (within approximately 2mm) it would run to the notch and give premature operation. The mechanically produced elements did not suffer from this problem, since in this design the tin is contained in a well.

The Effect of Varying the Composition of the M-Effect Alloy

Although pure tin is often used as the low melting point 'alloy', some fuse manufacturers usually add small quantities of silver to the tin, typically up to a maximum of 10% silver. This is to overcome the manufacturing problem that pure tin will not 'wet' the surface of the silver element and adding small quantities of silver improves the 'solderability'. In order to determine the effect on fuse performance of varying the tin/silver alloy composition in this way, a number of alloys of different tin/silver composition were produced by weighing the constituent metals and alloying them together. To confirm that complete alloying had taken place, 'cooling curves' (Fig. 4.6) were plotted to determine the solidus and liquidus points of the various alloys, and these compared with standard published values [59].

Elements using no M-effect alloy and also different compositions of alloy were made and tested in the test box. In each case the quantity of alloy was carefully weighed to ensure consistency. Time-current curves were plotted as described earlier and are shown in Fig. 4.7. It can be seen that the alloy composition has a marked effect on the time-current characteristic of the element, the addition of more silver to the alloy effectively moving the fuse curve to the right. That is, the higher the silver content, the slower the operating speed. It was also noted that fuse operation usually occured at the edge of the alloy deposit rather than, as might be expected, at its centre. This will be considered further in section 4.4.4.

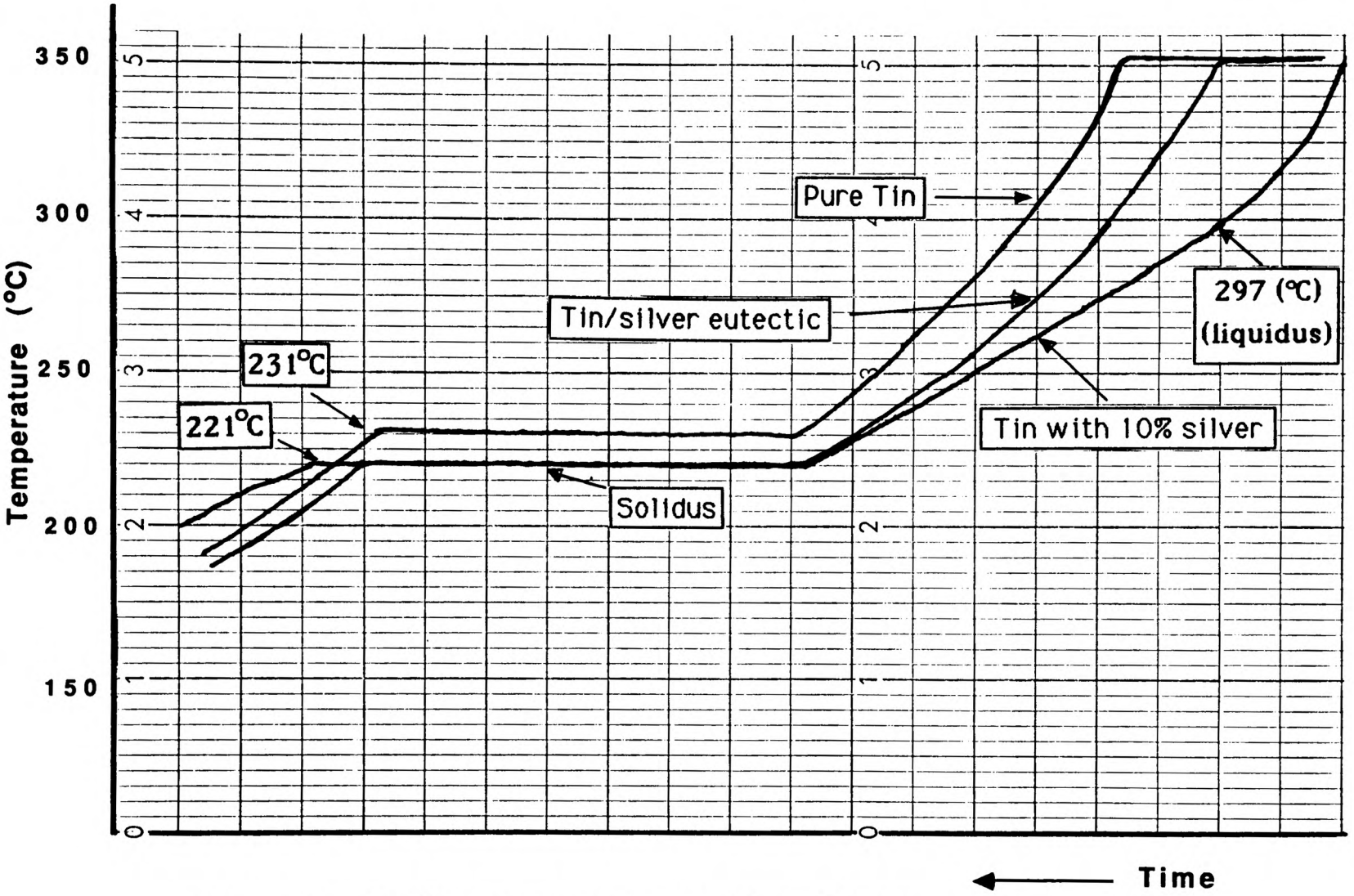

Fig. 4.6. Cooling curves for M-effect Alloys.

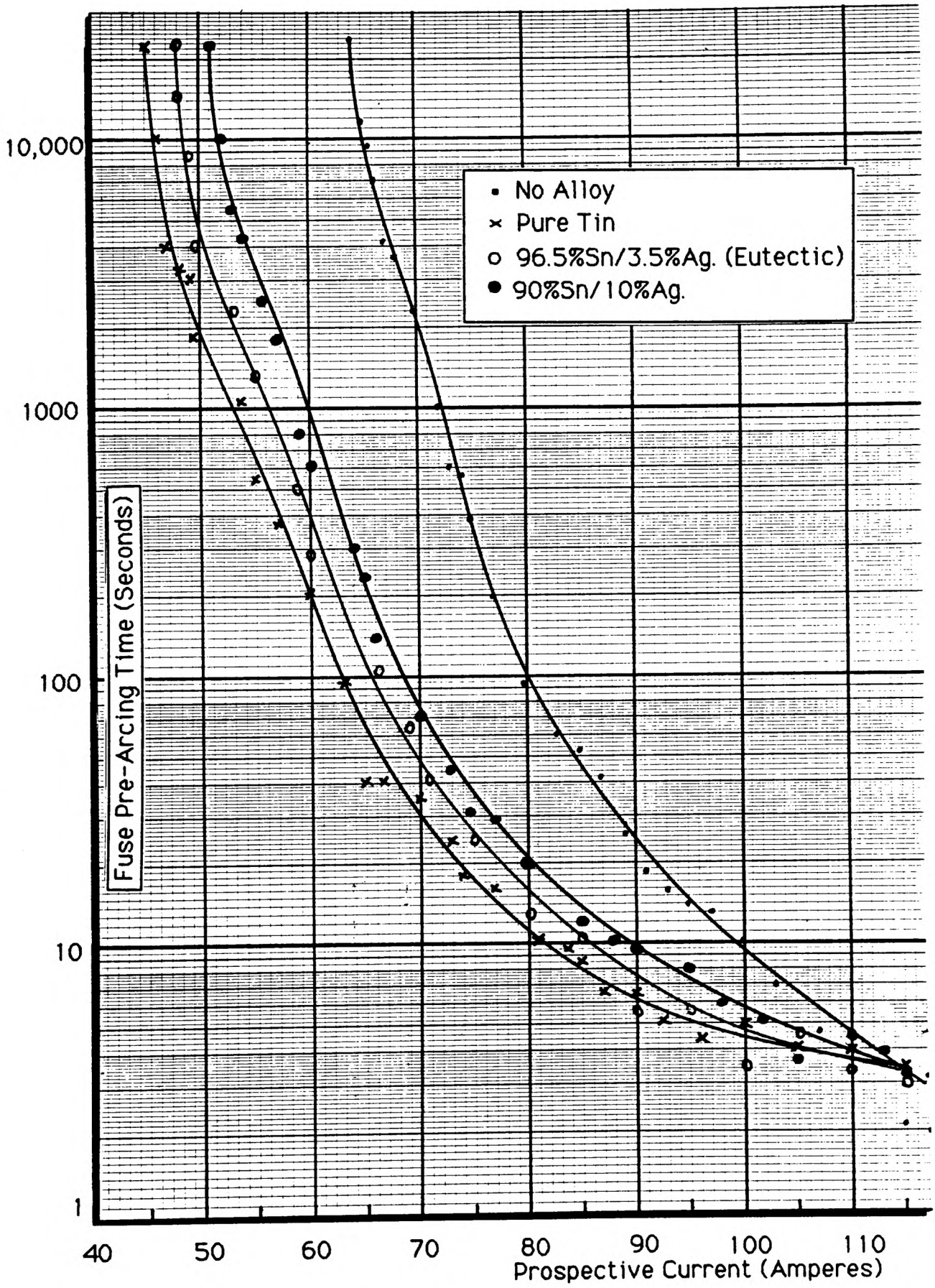

The Effect of Alloy Composition On the Fuse Time-Current Characteristic.

Fig. 4.7

During these tests the temperature rise of the elements was also studied. In addition to the thermocouples monitoring the temperature rise of the connecting pads, fine chromel-alumel thermocouples (0.3 mm diameter) were connected to the centre portion of the alloy on the element under test. Two methods of attachment were tried. Initially the thermocouple was crimped into a groove cut in the alloy. It was found, however, that during sand vibration, the thermocouple occasionally came away from the alloy. In view of this a second method was developed in which the thermocouple was fused into the alloy during element manufacture, giving a stronger mechanical connection. Preliminary tests showed that temperature rise results obtained were identical for each method of attachment under the same test conditions, and the use of the smallest wire gauge available for the thermocouples minimised temperature disturbance.

Fig. 4.8 shows a typical temperature rise plot for the alloy centre when a constant current is passed through the element. By a series of tests in which the element was inspected at various points in time, it was determined that points a, b and c represent the alloy melting point, the fuse operating point and the alloy solidifying point respectively.

Whilst the shape of the temperature rise plot was essentially the same for the three alloy compositions tested, a series of tests showed that the final element temperature was lower, as well as the operating time being

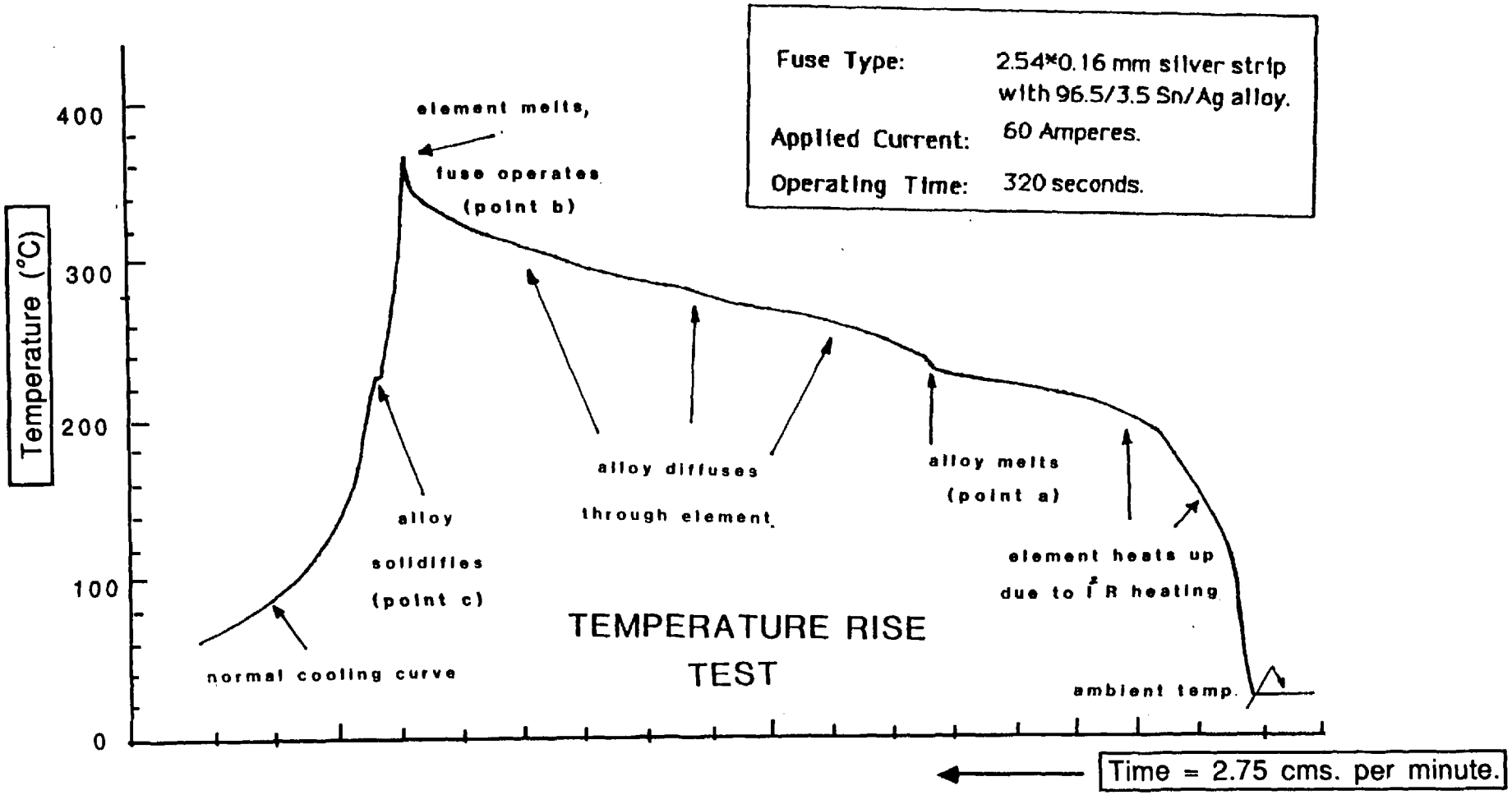

Monitoring Of M-effect Alloy Temperature Rise During Fuse Operation

Fig. 4.8

shorter for the higher tin content alloys. (see Table 4.2). Values of standard deviation also show that the higher the tin content, the more consistent the operation.

M-effect Alloy Composition	FUSE OPERATING TEMPERATURE	FUSE OPERATING TIME (SECS)
100% TIN	Mean Value = 325°C 6n-1 = 18.6°C	Mean Value = 180 6n-1 = 46
96.5% TIN - 3.5% SILVER	Mean Value = 347°C 6n-1 = 26.5°C	Mean Value = 330 6n-1 = 83
90% TIN - 10% SILVER	Mean Value = 390°C 6n-1 = 37°C	Mean Value = 595 6n-1 = 233
APPLIED CURRENT 60 AMPERES RMS		

Variation of Fuse Operating Temperature with M-effect Composition

Table 4.2

In order to investigate further the effect of alloy composition, tests were made on specially prepared "standard" 12kV distribution fuses. These fuses were identical in every respect except that some fuses had deposits of pure tin at the centre of each element and some had tin/silver alloys. In each case the weights and positions of the alloy on the elements were as identical as possible. The fuses were connected in series in the low voltage test circuit and the same current passed through them. The fuse barrel temperatures were monitored using chromel-alumel thermocouples. The results, given in Table 4.3, generally confirm that increasing the silver content, makes the fuse slower acting, and operate at higher temperatures.

Operating Time/Temperature Rise Tests on 12 kV Distribution Fuses to BS 2692

(a) 12kV 40 Amp Fuses

Alloy	Applied Current	Operating Time	Barrel Temperature (Centre)
10% Silver/90% Tin	58A	151 minutes	174°C
		162 ..	176°C
		150 ..	176°C
3.5% Silver/96.5% Tin	58A	128 minutes	135°C
		120 ..	132°C
		132 ..	138°C
Pure Tin	58A	130 minutes	130°C
		118 ..	132°C
		116 ..	128°C
10% Silver/90% Tin	55A	260 minutes	177°C
		281 ..	181°C
		274 ..	174°C
3.5% Silver/96.5% Tin	55A	175 minutes	153°C
		178 ..	152°C
		182 ..	146°C
Pure Tin	55A	173 minutes	148°C
		169 ..	146°C
		182 ..	146°C
(b) 12kV 100 Amp Fuses			
10% Silver/90% Tin	125A	360 minutes	192°C
		374 ..	193°C
		388 ..	196°C
3.5% Silver/96.5% Tin	125A	210 minutes	177°C
		225 ..	173°C
		178 ..	178°C
Pure Tin	125A	212 minutes	176°C
		206 ..	174°C
		186 ..	170°C
10% Silver/90% Tin	160A	65 minutes	202°C
		66 ..	204°C
		68 ..	201°C
3.5% Silver/96.5% Tin	160A	59 minutes	170°C
		61 ..	174°C
		57 ..	173°C
Pure Tin	160A	56 minutes	168°C
		62 ..	173°C
		57 ..	167°C

Table 4.3

Measurement of Alloy Diffusion

Tests were then made to investigate the rate of alloy diffusion through a silver fuse element under constant current conditions. Fuse elements to which a weighed amount of tin M-effect alloy had been added were mounted in the test box. Test currents were chosen which would normally have caused the fuse elements to operate after approximately ten minutes and one hundred minutes, but in these tests the currents were disconnected prior to fuse operation to enable partial operation of the fuse to be studied. To do this a constant test current was passed through a number of identical fuse elements for varying times, all of which were less than the anticipated operating time of the fuse element. The elements were then removed, sectioned through the alloy, and metallurgically examined. In this way the diffusion rate of the tin through the silver element could be measured.

The elements were notched silver strips 2.54 mm wide of various thicknesses, to which a weighed amount (85 mg) of tin was added, this weight being chosen as it was well above the 'minimum requirement' discussed earlier. To localise the tin at one point on the element it was covered with fireclay cement. Test currents were applied for 20%, 40%, 60% and 80% of the anticipated operating time. The elements were then removed from the test box and sectioned through the alloy. After mounting in cold curing compound, the samples were polished using various grades of abrasive paper and pastes until a surface finish of better than one micron was obtained, and then etched slightly to remove any surface

smearing. The samples were examined using a Cambridge Instruments S240 scanning electron microscope (S.E.M.). The S.E.M. bombards the sample with electrons and uses the secondary electron emission from the sample material to build up a visual picture. The secondary electron coefficients of tin and silver are so similar, however, that the S.E.M. is not able to easily distinguish between the two in its normal visual mode. In order that the interface between the two metals could be studied, the S.E.M. was fitted with a Link 860 Series 2 X-ray micro-probe analyser which was able to easily detect the metal boundaries. The approximate tin/silver boundary was firstly detected visually and then a scan for both tin and silver across the boundary was made. The presence of each element is represented by a trace whose amplitude changes in relation to the element concentration. The approximate boundary was firstly located near the edge of the M-effect alloy (Fig. 4.9(a)). A micro-probe scan across that boundary then confirmed that the visual boundary and micro-probe boundary coincided (Figs. 4.9(b) & (c)). Having located the boundary, it was then possible using the X-Y table on the S.E.M. to scan for both tin and silver at various boundary points through the sample. Fig. 4.10 shows such a scan.

Clearly, if the boundary is not a straight transition from pure tin to pure silver due to the formation of any silver/tin compounds then this should be easily seen from the traces as a widening of the boundary region. (See Figs. 4.11(a) to 4.11(f)). By careful interpretation of the

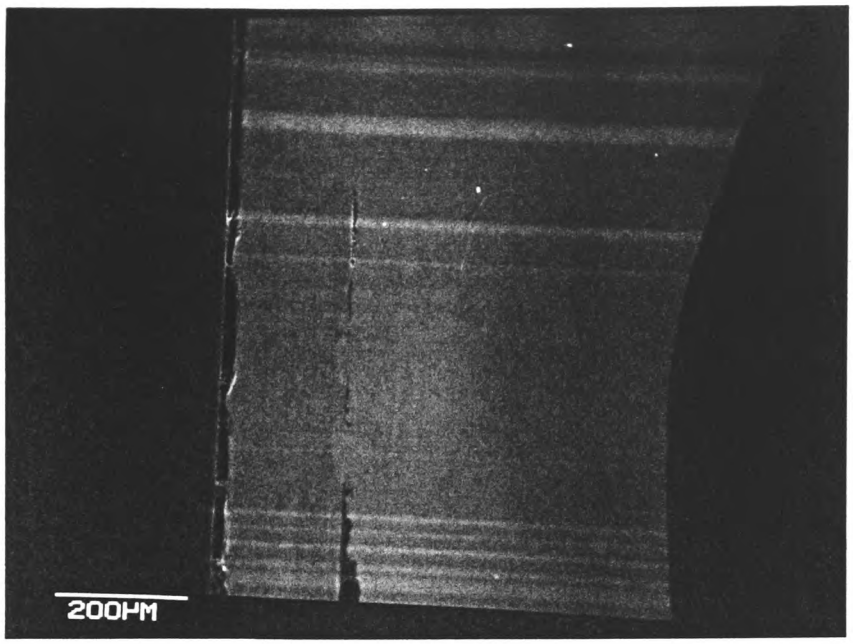

(a)

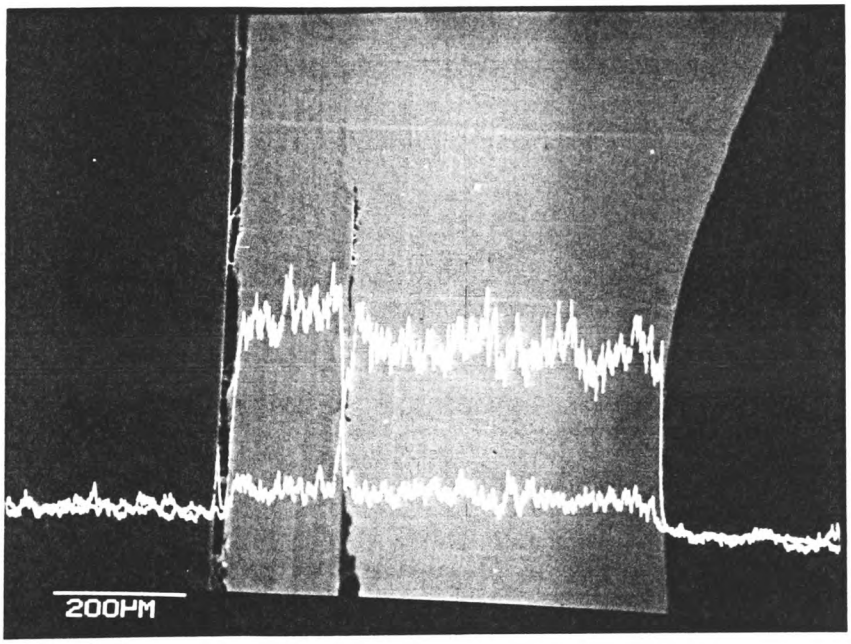

(b)

Comparison Of Physical and Micro-scan Boundaries.
(a) Physical Boundary. (b) Micro-scan Boundary.

Fig. 4.9.

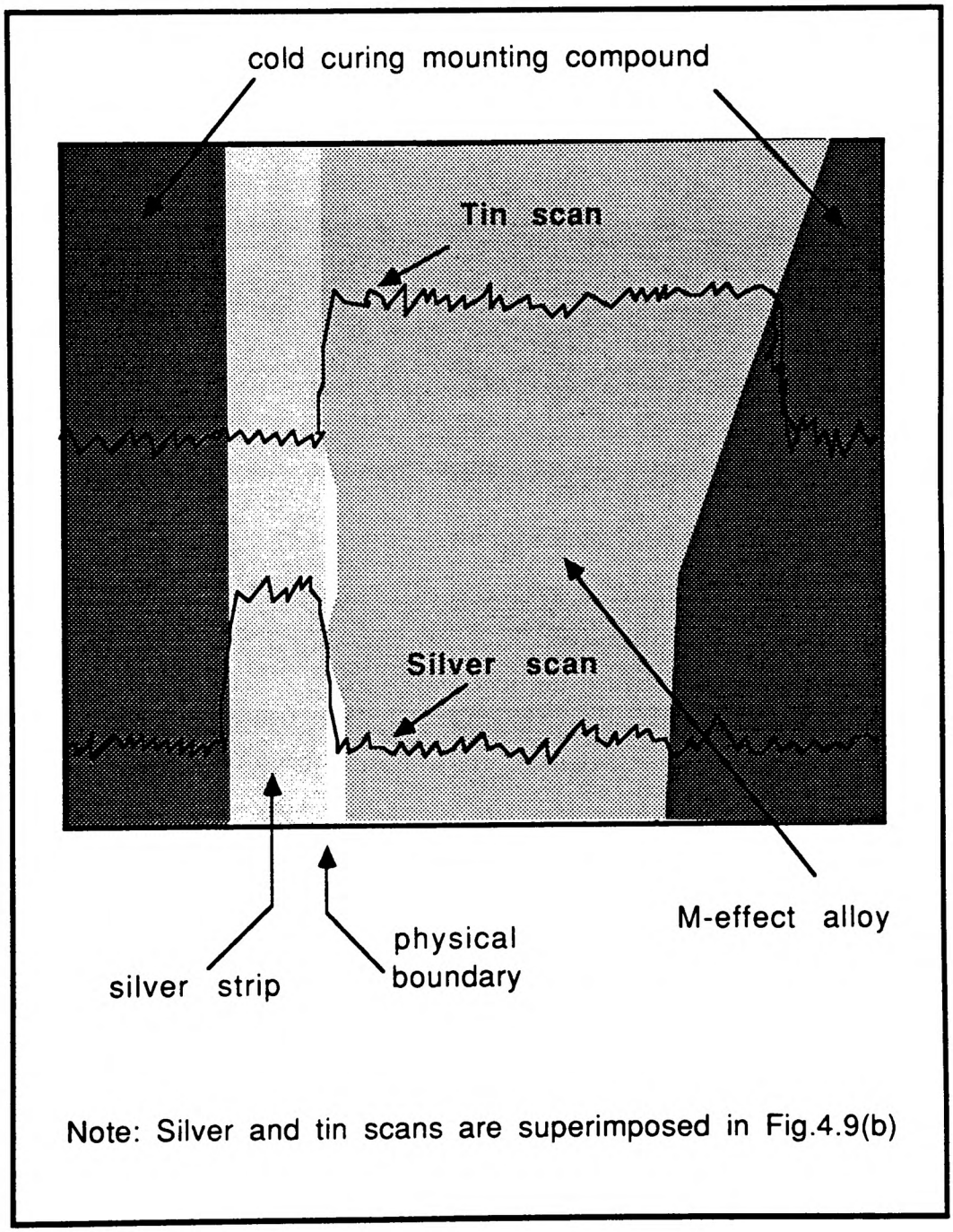

Note: Silver and tin scans are superimposed in Fig.4.9(b)

Interpretation of Figs. 4.9(a) & 4.9(b)

Fig. 4.9(c)

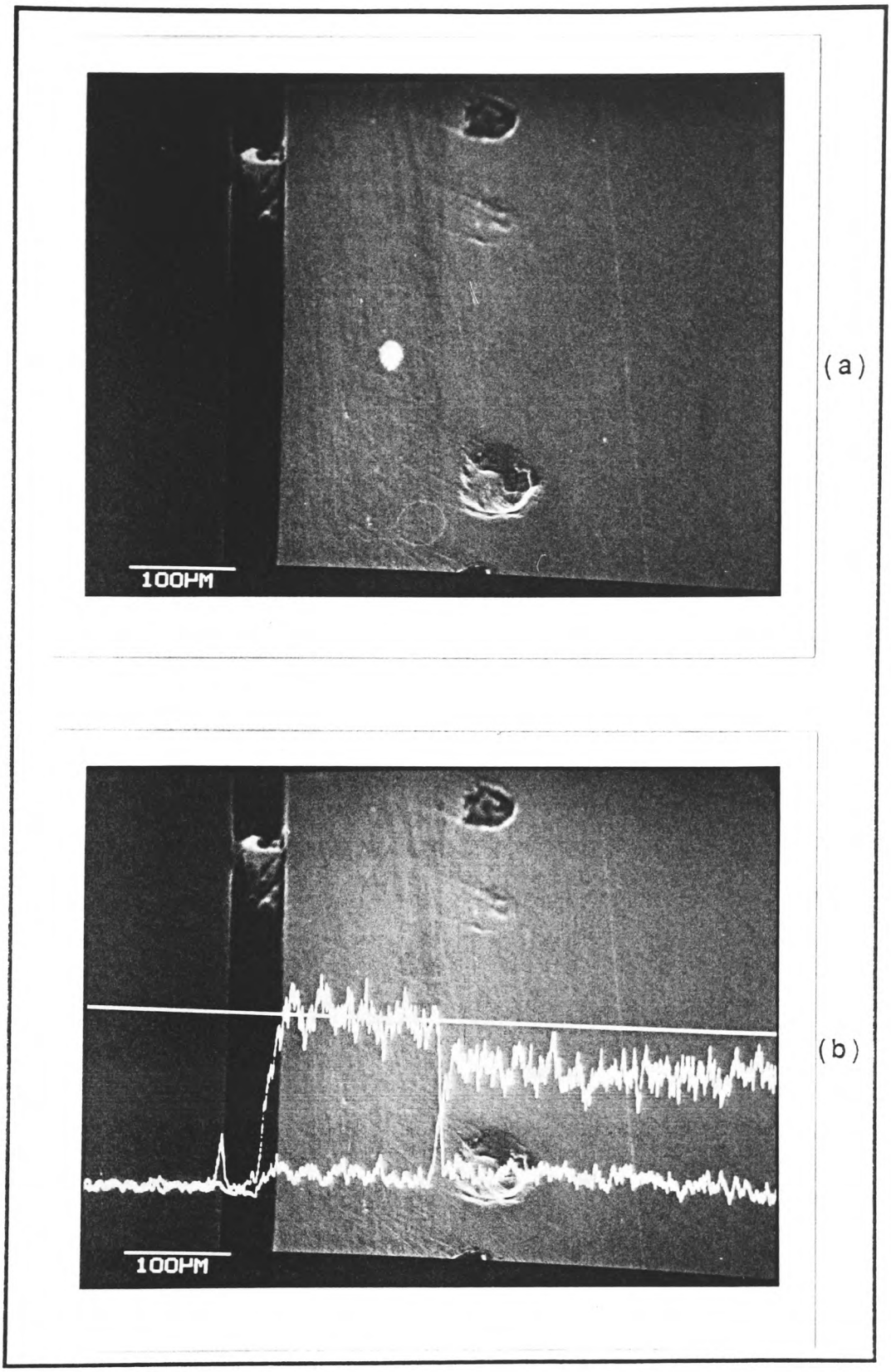

The Physical Boundary, Not Easily Seen In The Visual S.E.M. Scan (a) Is Clearly Picked Out By The Micro-probe Scans For Tin & Silver Shown In (b).

Fig. 4.10

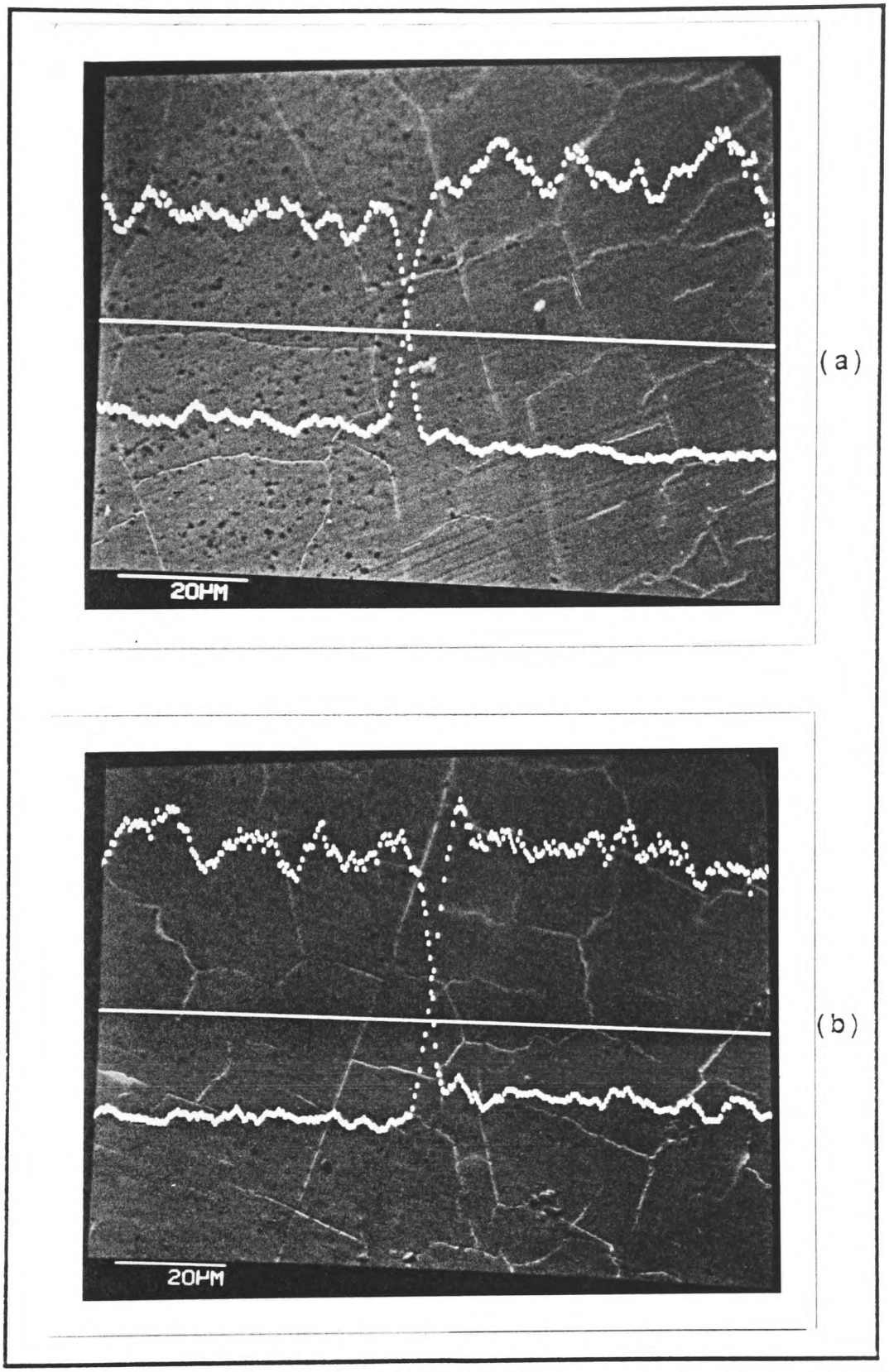

Measuring the Depth of Diffusion Using Micro-probe Traces.
(a) Total Diffusion Depth = 6 microns.
(b) Total Diffusion Depth = 8 microns.

Fig. 4.11(a&b)

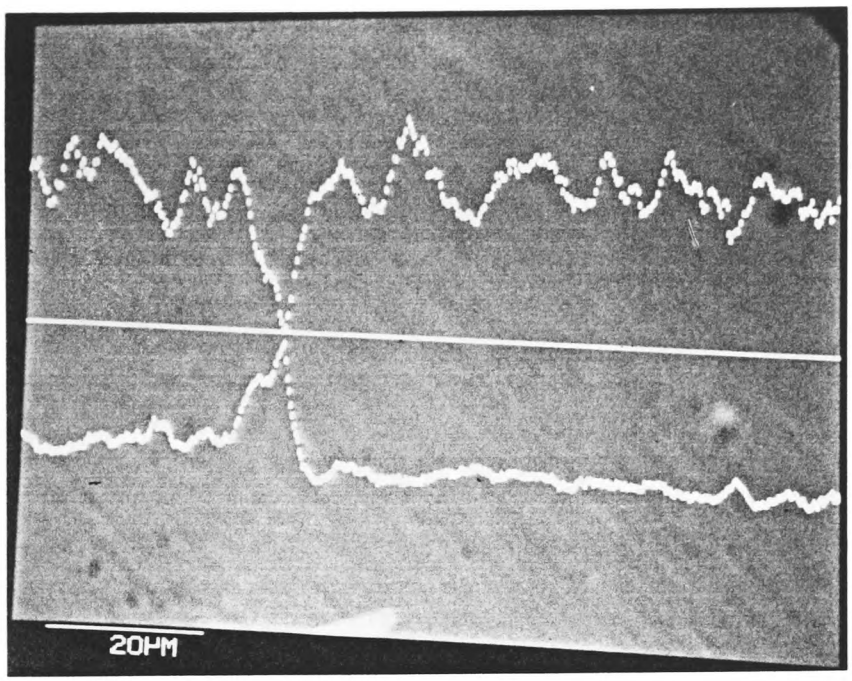

(c)

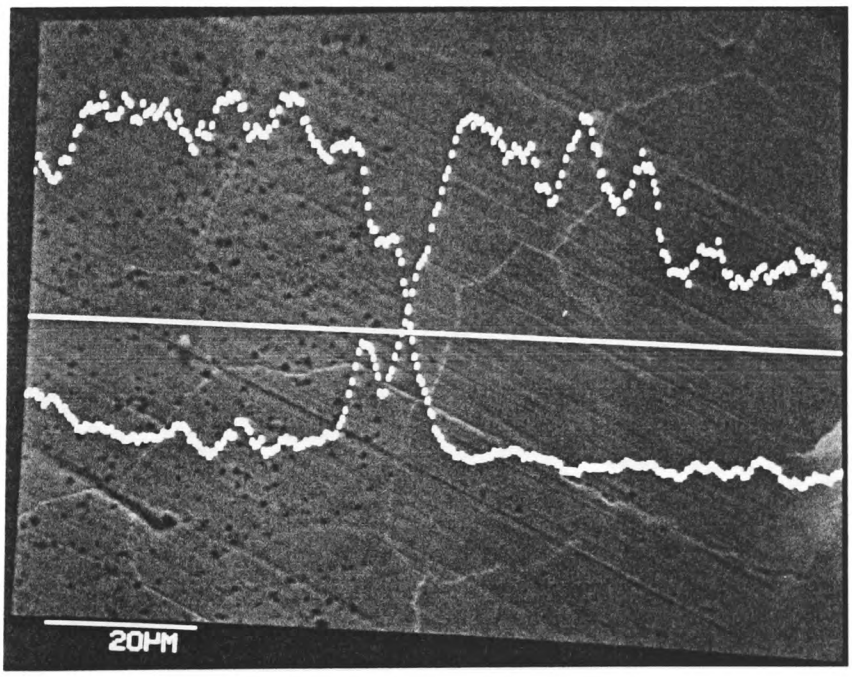

(d)

Measuring the Depth of Diffusion Using Micro-probe Traces.

(c) Total Diffusion Depth = 9 microns.

(d) Total Diffusion Depth = 12 microns.

Fig. 4.11 (c&d)

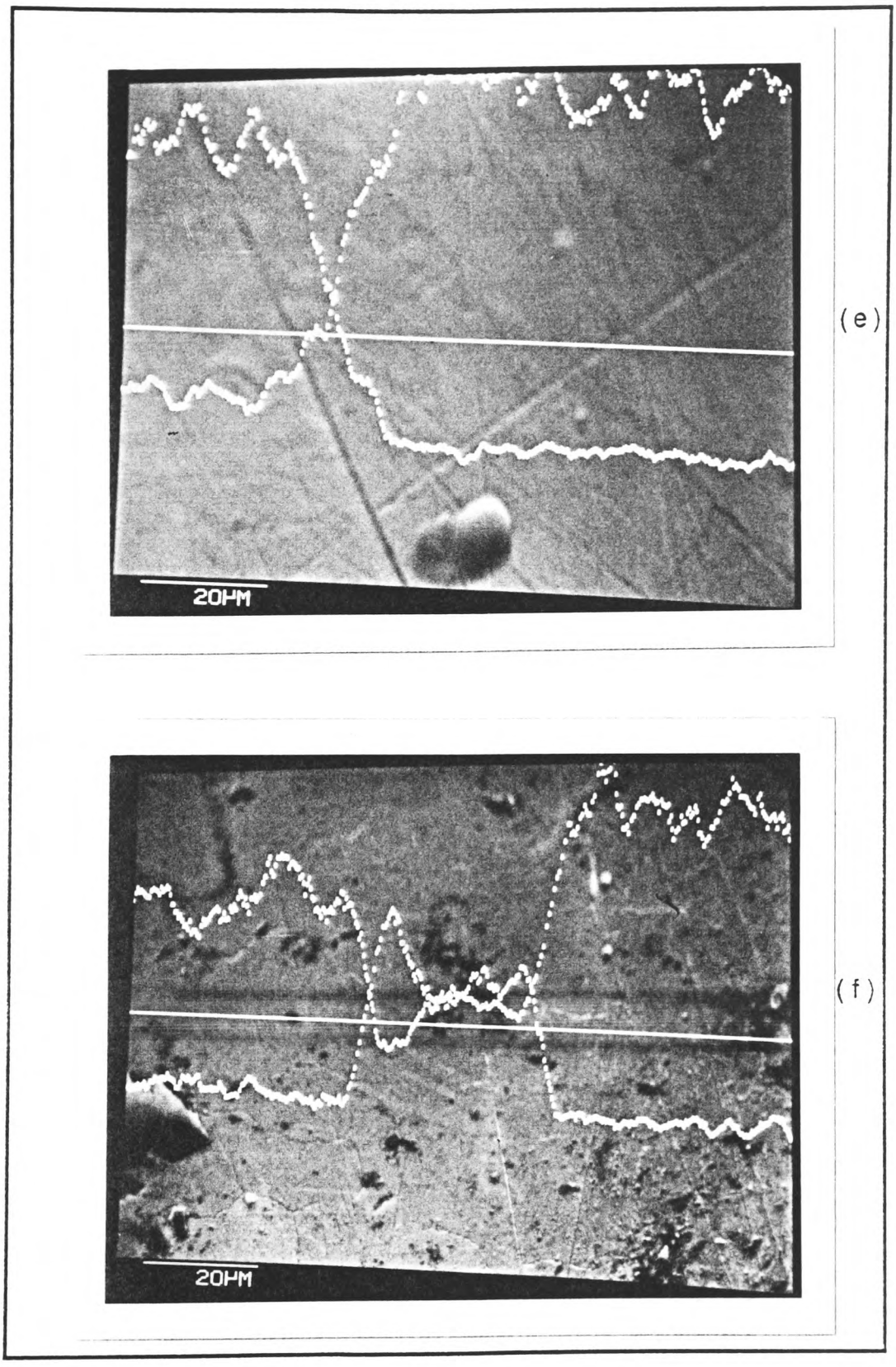

Measuring the Depth of Diffusion Using Micro-probe Traces.
(e) Total Diffusion Depth = 22 microns.
(f) Total Diffusion Depth = 37 microns.

Fig. 4.11 (e&f))

traces, it was possible in this way to measure the width of the boundary region and thus determine the rate of diffusion of one metal into the other. (See Section 4.4.3)

Although the micro-probe scans give an excellent graphical representation of the change from one metal to another at the boundary, the actual composition of the boundary region cannot be determined from them. To do this a detailed point by point quantitative analysis was made using the micro-probe analyser in which the calibrated electron beam incident current, reflected current, and background electron count were noted at each point.

The results of these analyses were then fed into a computer program developed by C. Davies [61] from which the actual tin and silver compositions at each point were obtained.

Using the qualitative scan and quantitative point by point tests it was thus possible to determine both the width and actual composition of the boundary region, not only for a variety of samples but also at various points across each sample.

The element size, test current and test results are shown in Table 4.4 Each test was repeated five times and thus the spread in values represents the results obtained on five separate samples, three sectioned longitudinally and two transversely (see Table 4.4). Both mechanically produced and hand produced elements were used, and in each case several new elements, i.e. elements which had not been

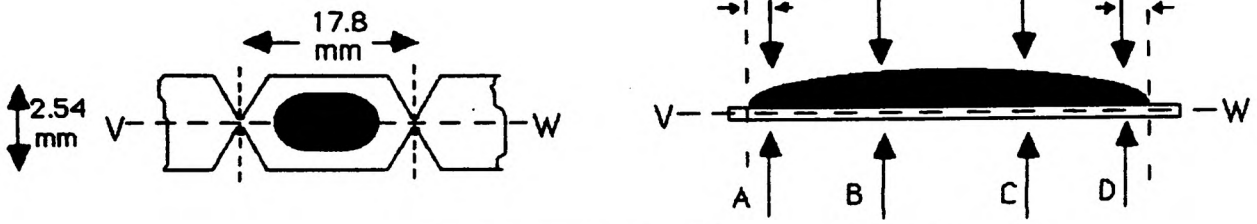

Longitudinal Section Scanning paths

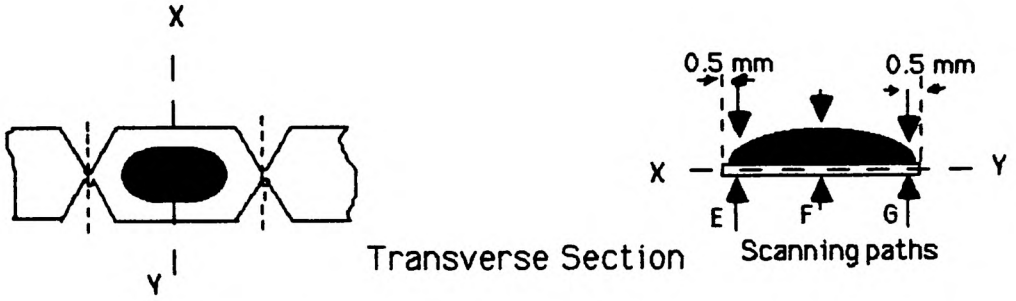

Transverse Section Scanning paths

Current (Amps)	Time (mins.)	Element Thickness	Diffusion Depth (microns.) A	B	C	D	E	F	G
54 **	0	0.16 mm	1-2	1-2	1-2	1-2	1-2	1-2	1-2
	2	"	3-4	1-4	1-4	3-4	1-3	2-4	2-3
	4	"	10-13	5-10	6-9	9-12	5-9	5-9	5-10
	6	"	40-55	30-46	32-39	42-58	33-40	30-40	33-42
	8	"	61-100	43-72	40-67	63-160*	40-58	42-56	42-58
46	0	0.16 mm	2-4	2-4	2-4	2-4	2-4	2-4	2-4
	20	"	6-8	4-8	4-8	8-10	3-6	2-5	3-5
	40	"	8-9	5-7	6-8	7-10	5-11	6-9	8-10
	60	"	36-66	30-39	32-48	34-52	28-40	27-39	32-39
	80	"	78-93	55-68	50-58	80-90	53-62	55-67	55-59
36	0	0.1 mm	1-5	1-5	1-5	1-5	1-5	1-5	1-5
	2	"	2-7	2-7	2-7	2-8	2-8	2-7	2-7
	4	"	9-13	4-9	4-10	9-13	4-8	4-9	4-9
	6	"	38-56	27-47	28-46	42-60	27-46	29-38	27-39
	8	"	82-100*	48-68	60-76	88-94	47-59	48-53	46-60
30	0	0.1 mm	2-5	3-5	3-5	4-5	1-5	3-5	4-5
	20	"	3-11	5-7	5-8	6-10	4-9	5-7	5-7
	40	"	7-16	8-11	9-12	9-13	8-11	—	—
	60	"	38-42	34-39	30-42	37-51	34-38	29-36	30-41
	80	"	68-82	46-60	42-48	83-86	41-57	39-48	44-59
28	0	0.08 mm	3-5	4-5	3-5	3-5	3-5	3-5	4-5
	2	"	3-4	4-7	4-7	4-8	4-7	5-7	5-7
	4	"	8-14	8-9	8-9	9-11	8-11	7-9	7-8
	6	"	20-23	18-20	16-22	21-24	17-19	16-23	14-17
	8	"	30-47	26-39	25-40	36-63	28-37	26-39	28-38
25	0	0.08 mm	4-5	3-5	4-5	4-5	4-5	4-5	4-5
	20	"	4-11	4-7	5-6	5-12	4-8	7-10	2-6
	40	"	7-13	6-12	8-13	9-14	6-10	8-11	4-9
	60	"	21-26	19-23	23-25	21-29	20-29	18-23	22-27
	80	"	44-62	32-47	36-40	48-71	36-46	32-47	31-40

* Sample operated prior to end of test. ** mechanically produced elements

Diffusion Depth Versus Applied Current, Constant Current Testing

Table 4.4

subjected to any test current, were sectioned and mounted to determine whether appreciable diffusion had been caused purely due to manufacture. It is interesting to note that the initial boundary layers varied between one and two microns for mechanically produced elements and one and five microns for manually produced elements, the latter being clearly less consistent in manufacture. Notice also that the thinnest element had the widest boundary layer and hence the highest initial diffusion.

Table 4.4 also shows that the results were very variable, the diffusion depth varying by up to 60% between successive samples. This might have been anticipated since, owing to the asymptotic nature of the time-current characteristic at these long times, and slight unavoidable variations in test samples, the actual operating time of the particular fuse element under test could not be accurately predicted. Indeed some samples operated after what should have only been 80% of their anticipated operating time.

One clear result which did emerge, however, was that the depth of the boundary layer varied across the sample. Four scans were made on each longitudinally sectioned sample, one scan approximately one millimetre in from each edge and two scans near the centre. In every case the boundary layer was deeper at the edges of the sample, indicating that the diffusion rate was greater at the edges than at the centre. No similar effect was noticed on the transversely sectioned samples.

Area Scanned	Composition (wt. %)
5 micron x 5 micron	100% silver
5 micron x 5 micron	100% silver
5 micron x 5 micron	65.3% silver 34.7% tin
1 micron x 1 micron	72.4% silver 27.6% tin
1 micron x 1 micron	74.3% silver 25.7% tin
5 micron x 5 micron	62.7% silver 37.3% tin
5 micron x 5 micron	61.3% silver 38.7% tin
5 micron x 5 micron	100% tin
5 micron x 5 micron	100% tin

Quantatative Analysis Across the Boundary Layer

Table 4.5

The results of the quantitative analysis are shown in Table 4.5. The element composition across the width of the boundary region was determined at five micron intervals on several samples. Whilst this in the main was reasonably constant at approximately 60% by weight silver and 40% by weight tin, occasionally points approximating to the inter-metallic compound Ag_3Sn were found. The significance of this result, along with the results obtained from all the constant current tests will be discussed further in section 4.4.4.

Whilst the constant current tests give valuable information regarding the operation of fuse links under typical operating conditions, small variations in element dimensions and test current ($\pm$ 1 ampere) lead to wide variations in fuse temperature and hence diffusion rate and operating

time. In order to study the diffusion mechanism under more stable conditions, constant temperature tests were made on a variety of samples.

4.4.2 Constant Temperature Testing.

Identical fuse elements to those described earlier in the constant current tests (section 4.4.1) were placed in an oven at known constant temperatures for various periods of time. No current was passed through the elements in these tests. The elements were then removed, sectioned, mounted and polished as described earlier prior to being examined under both optical and scanning electron microscopes. In this way the diffusion rates at various constant temperatures could be determined.

The oven used in the tests was a Gallenkamp plus series fan-assisted oven which could be set and controlled to within $\pm 1^{\circ}C$. To verify the actual temperature of the sample under test and also to plot any local temperature fluctuations during the test period, a thermocouple element was placed adjacent to each sample and the thermocouple indicator connected to a chart recorder. The tests covered temperature ranges from 225°C to over 400°C and for time periods ranging from less than one hour to several days. In all, over 100 samples were examined. The results are shown in Table 4.6 and will be discussed in detail in section 4.4.4.

Temperature (°C)	Test Duration (hours)	Mean Diffusion Depth (microns)	Test Duration (hours)	Mean Diffusion Depth (microns)
225	0	1	0	2
"	0	4	4	21
"	9	24	16	30
"	49	40	94	61
"	144	105	189	108
240	6.25	35	16	52
"	25	62	36	85
"	49	112		
275	0	1	0	1
"	0	1	0	2
"	1	22	3	40
"	6.25	60	10	65
"	10.5	85	11.5	67
"	12.25	93	12.25	110
"	14	94	14	115
"	20	125	25	128
300	0	3	0	1
"	0	2	1	30
"	2	40	3	54
"	4	47	4	61
"	5	68	5	60
"	5.75	89	10	91
"	10	82	12.25	110
350	0	2	0	4
"	0	3	0.25	60
"	1	85	2.25	105
"	4	149		
410	0	4	0	2
"	10 minutes	50	15 minutes	80
"	20 "	73	30 "	85
"	30 "	79	45 "	104
"	1 hour	134	1 hour	160
"	1 "	104		

Diffusion Depth Versus Time, Constant Temperature Testing.

Table 4.6

Whilst the S.E.M. was again used to provide both diffusion depth measurements and quantitative analysis of the diffused layer, excellent visual representation of M-effect action was obtained by viewing the samples under an optical metallurgical microscope. The results obtained are typified by Fig. 4.12(a)to (i) which show a series of samples heated to 275°C for times ranging from one hour to seventeen hours. The diffused layer is quite visible and its growth through the silver element may be plotted as a function of time. It can be seen that the layer does not grow evenly throughout the sample, maximum growth rate occurring at the sample edges. (Fig. 4.13).

4.4.3 Diffusion Depth Measurements

Both constant current and constant temperature testing have shown that the depth of the diffused layer is not constant but varies across the width of the M-effect alloy. In order, therefore, to obtain meaningful results some measurement criteria were needed to determine the average diffusion depth for any given set of conditions. The criteria used were:

(i) for micro-probe analyser scans.

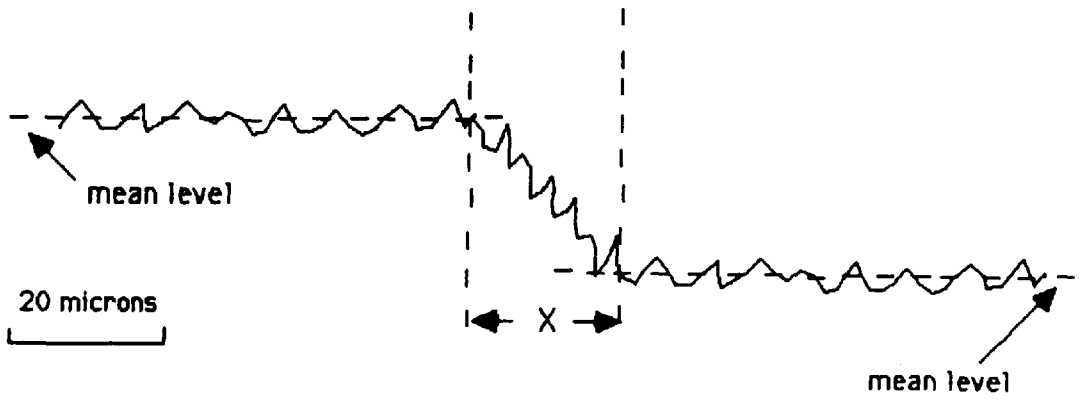

Both silver and tin scans were examined and the distance x obtained. The depth of diffusion is given by the avarage value of Xsilver and Xtin.

That is total diffusion depth = $x = \frac{X_{silver} + X_{tin}}{2}$

If, to a first approximation, it is assumed that diffusion occurs equally in both directions, then the diffusion depth of tin into the silver is half this value.

The diffusion depth of the tin into the silver is thus given by:

$$\bar{x} = \frac{X_{silver} + X_{tin}}{4}$$

(ii) for optical photographs.

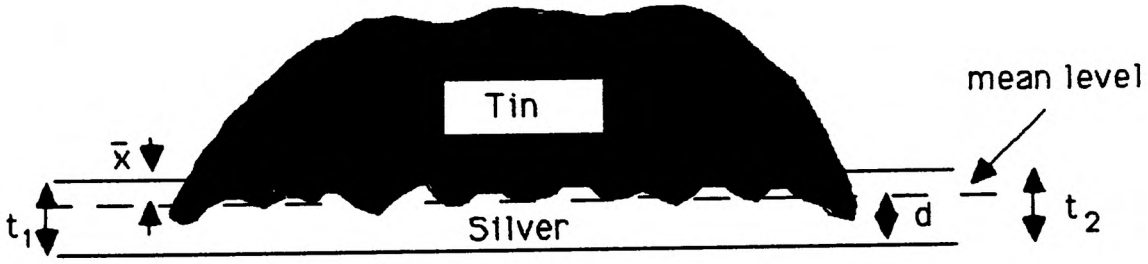

$$\bar{x} = \frac{t_1 + t_2}{2} - d$$

t1, t2 and d were measured using a calibrated graticule.

This was the method used by Hofmann and Lindmayer [30] and thus allows direct comparison of results.

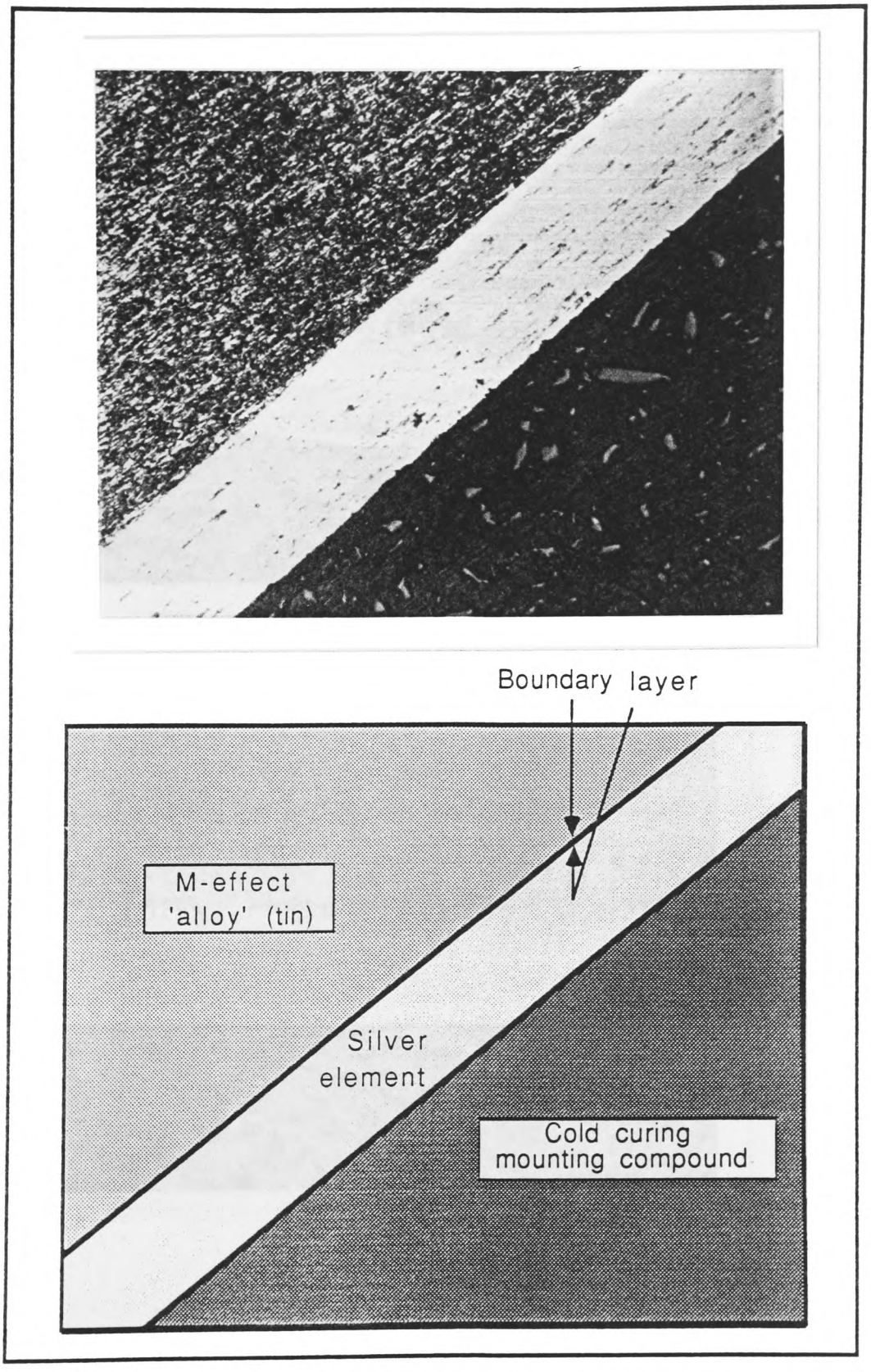

Sectioned Sample of a 2.54*0.12 mm Silver Element with M-effect Prior to Heat Treatment.
(Boundary Layer < 1 micron.)

Fig. 4.12(a)

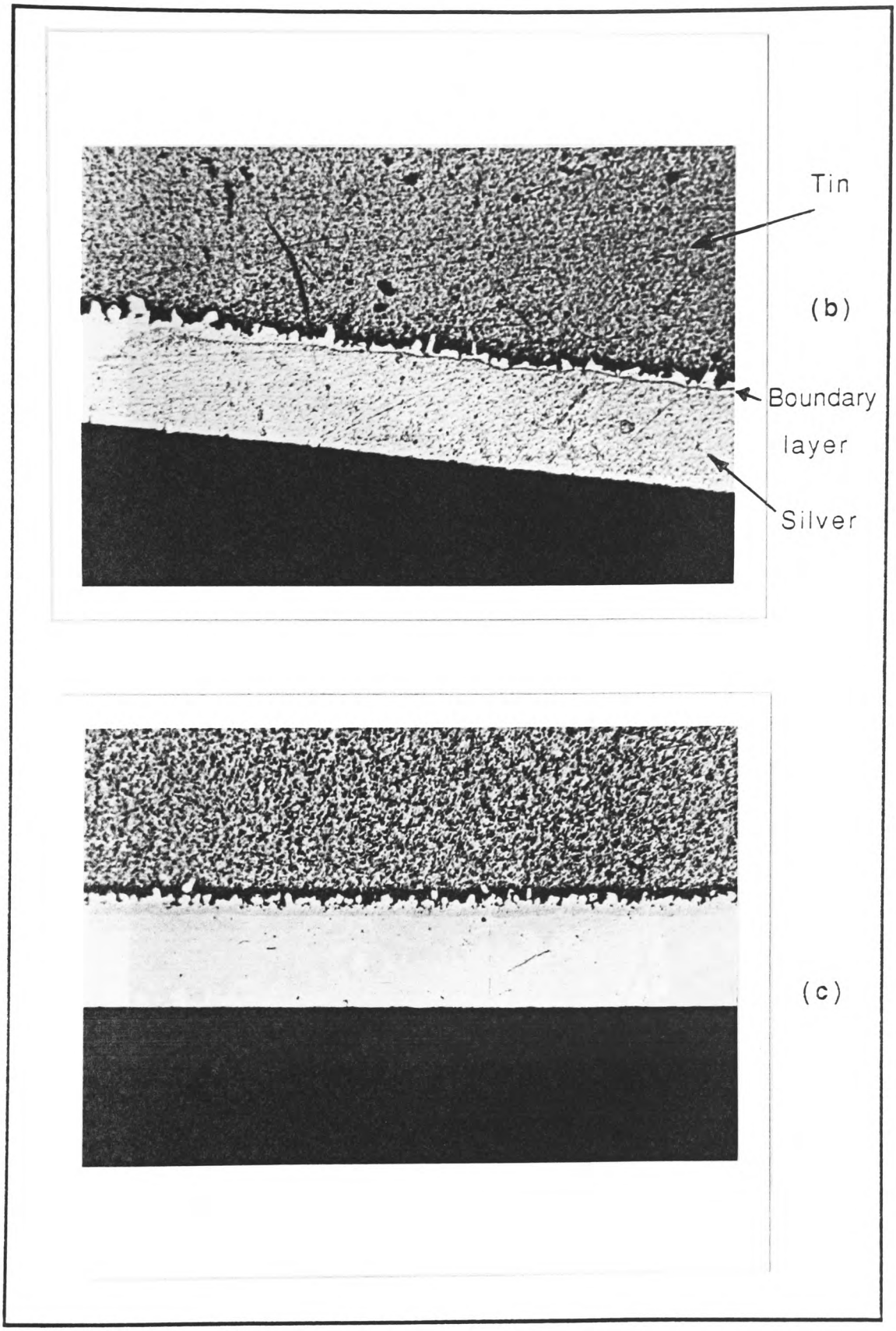

Samples after Heat Treatment at 275 C for 1 Hour.

Fig. 4.12(b&c)

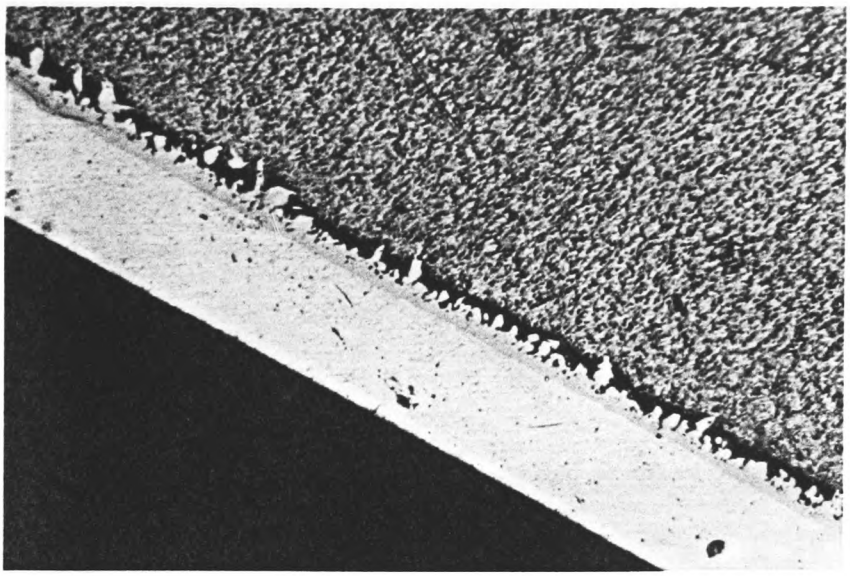

(d)

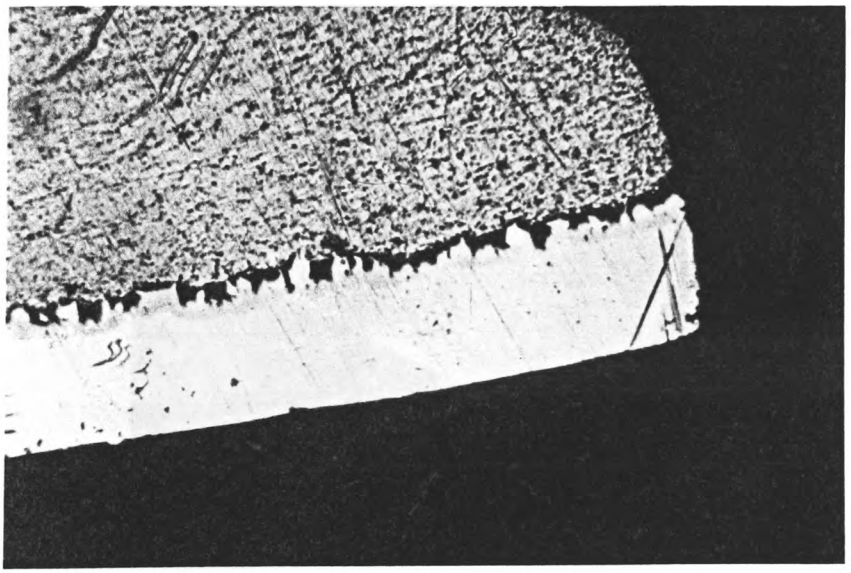

(e)

Samples after Heat Treatment at 275° C for 3 Hours.

Fig. 4.12(d&e)

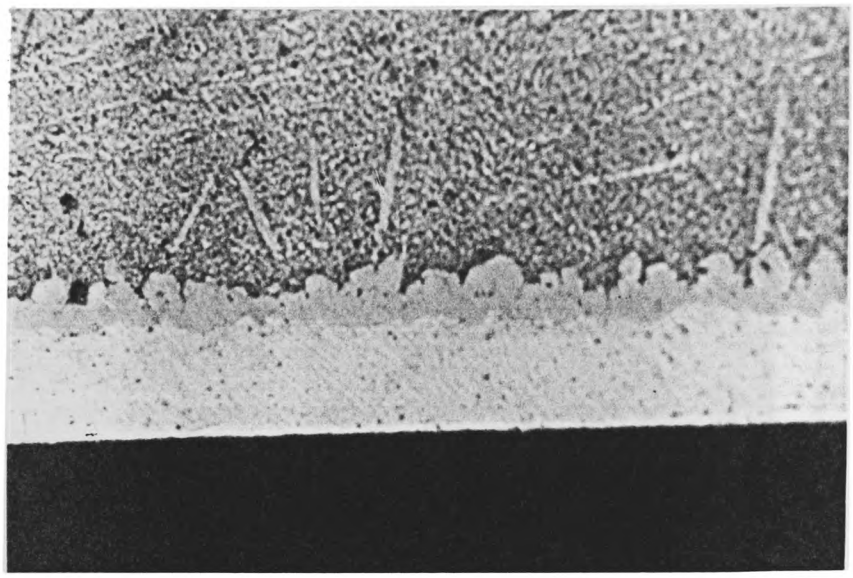

(f)

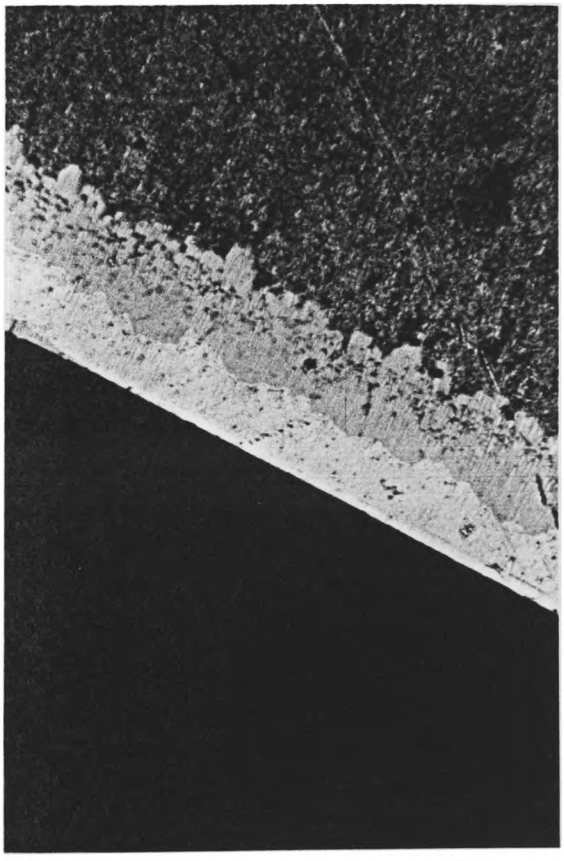

(g)

Samples after Heat Treatment at 275°C for (f) 6.25 Hours: (g) 10.5 Hours.

Fig.4.12(f&g)

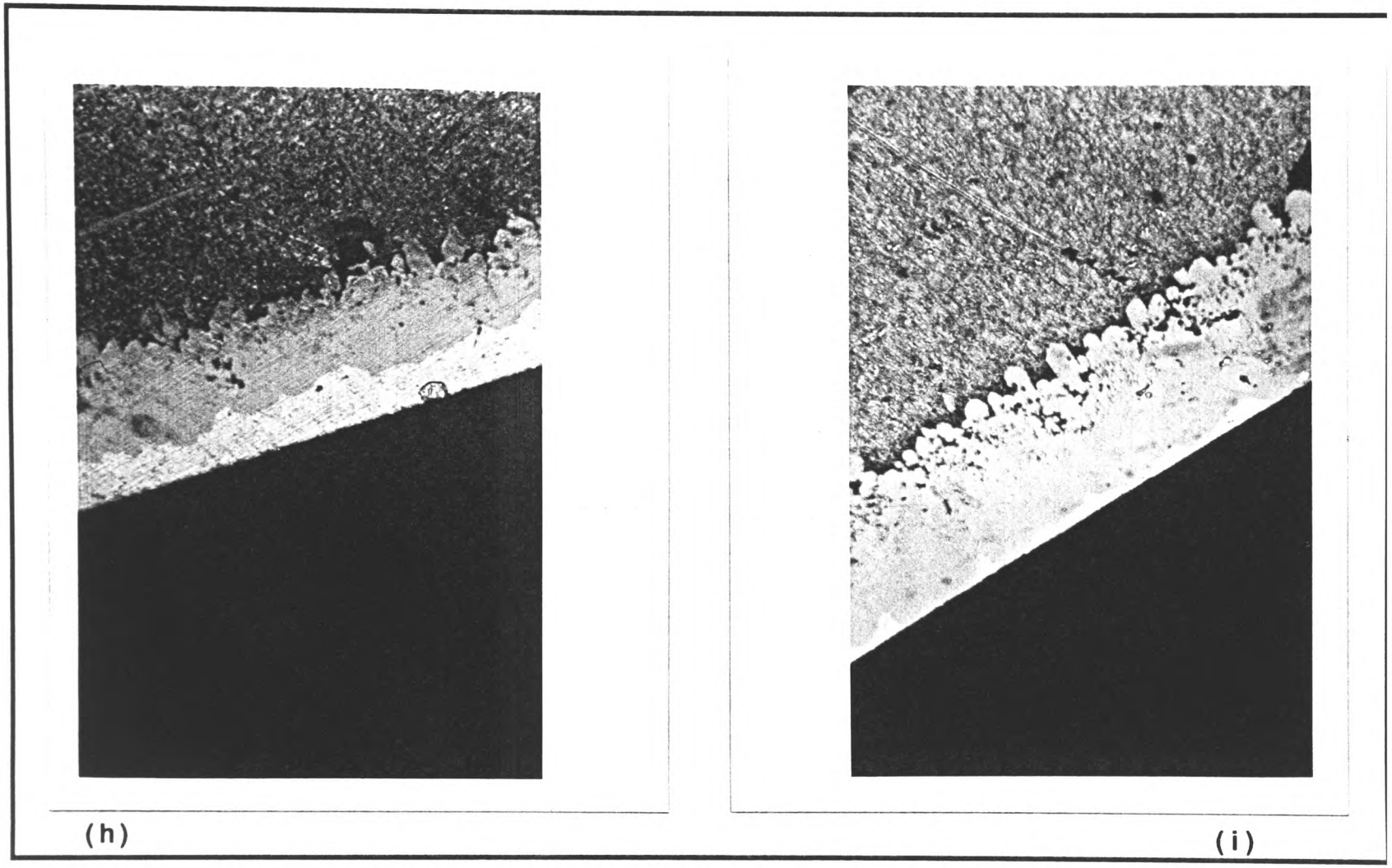

Samples after Heat Treatment at 275 C for:
(h) 14 Hours (i) 25 Hours.
Fig.4.12(h&i)

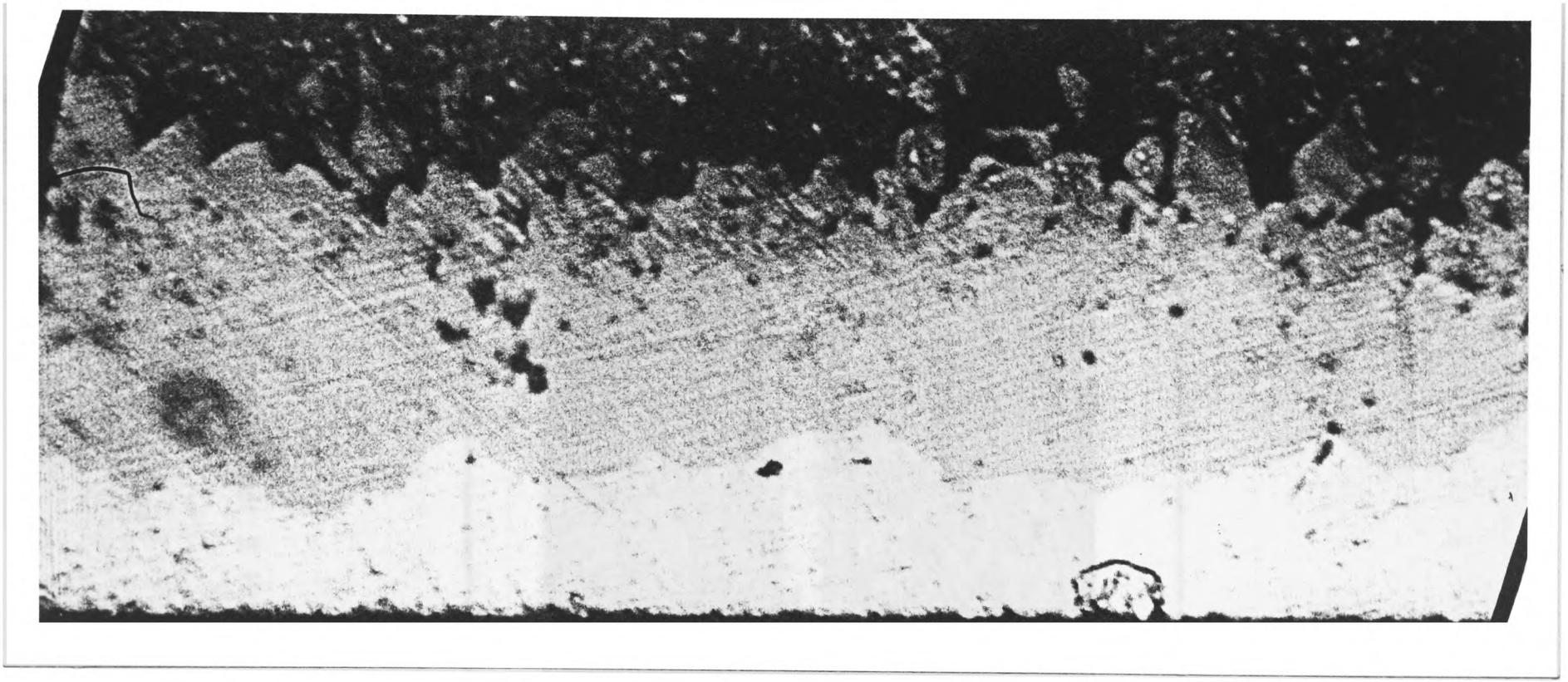

Enlargement of Fig. 4.12(h) To Show More Clearly the Boundary Region.

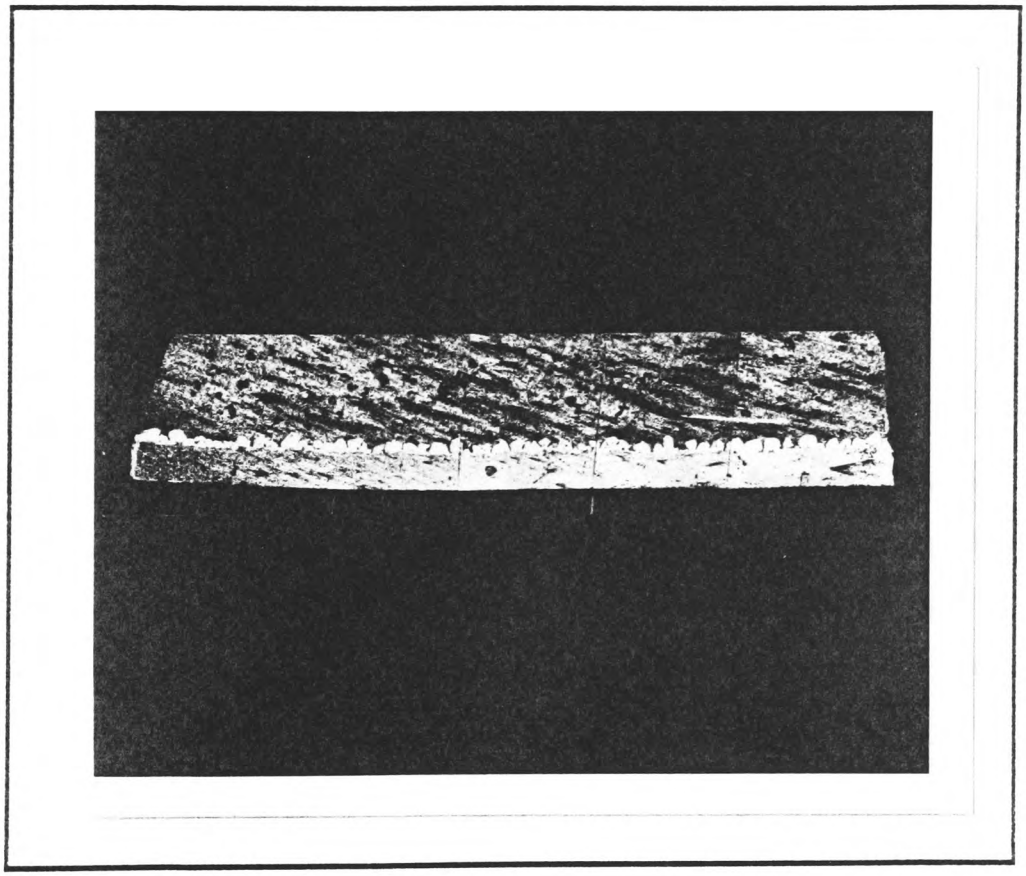

Complete Section of Sample after 3 Hours Heat Treatment at 275 °C.

Fig. 4.13.

4.4.4 Analysis of the Results

The results of the tests may be summarised as follows:

Quantity of M-effect Alloy -

(a) there is a definite minimum quantity below which effective M-effect action will not proceed. Once this minimum value has been exceeded, however, the actual quantity of M-effect alloy appears to have little direct bearing on the speed of alloy diffusion. Too much alloy may, however, cause secondary problems due to the alloy running to an adjacent notch and causing premature operation.

(b) locating the alloy in a pre-formed well or alternatively covering it with fireclay cement and thus containing it at one point on the fuse element gives more consistent operation, particularly on thicker elements (> 0.1 mm).

Since diffusion activity only occurs at the boundary of two metals then, provided there is sufficient free tin (the M-effect alloy) at the boundary to enable unrestricted diffusion to take place, any additional free tin is surplus to requirement, and this indeed is what was found in the tests.

Too little tin, however, would not allow unrestricted diffusion to take place. Thicker silver elements would require correspondingly more free tin to enable complete

diffusion to proceed, and in tests on these elements it was found that the tin would run along the element, reducing the tin thickness to below the minimum requirement and thus impairing M-effect action. Placing the tin in a well, or alternatively covering it with fireclay cement prevented running and hence maintained the minimum thickness requirement.

Position of the Alloy - it may be expected that since the element notches are generally at a higher temperature than the intermediate bulk strip then a temperature variation will exist along the strip between adjacent notches, and this temperature variation would influence the diffusion rate and hence operating time. It was found, however, that provided the alloy was not positioned within 2 mm of a notch, then for all practical purposes, on the notched elements examined, the exact position of the alloy between adjacent notches was not found to be critical.

Alloy Composition - although adding small quantities of silver (≤10%) to the tin improves the wetting properties of the tin, it has the adverse effect of increasing the operating time and raising the overall fuse temperature during operation on low-overcurrents.

Reference to Fig. 4.1 enables the reasons for this occurrence to be postulated. When a current is passed through the element, ohmic heating occurs until the temperature rise of the element is sufficient to melt the alloy. Once molten, the alloy starts to diffuse more

rapidly through the silver element, increasing its resistivity and creating a local hot spot. Ohmic heating increases the temperature of the hot spot, which in turn increases the diffusion rate, this being a function of temperature, until the alloy diffuses completely through the element and fuse operation occurs.

If pure tin is used, then after melting at 231° C, any alloying with the silver ensure the mixture remains in the liquid phase, since the liquidus temperature drops with increasing percentage silver until the eutectic point is reached.(Fig. 4.1) Since the M-effect alloy is in the liquid phase then the diffusion rate remains high.

If the alloy used is the eutectic then the alloy becomes molten at at a lower temperature (221° C) and diffusion starts earlier. Addition of silver to the alloy, however, raises the liquidus temperature, requiring more heat to maintain the alloy in the liquid phase. The diffusion rate thus procedes less quickly than with pure tin.

The alloy with 10% silver has a liquidus temperature of approximately 295°C, and thus the rate of diffusion is low until this temperature is reached. As the alloy starts to diffuse through the silver element, the percentage of silver in the alloy increases and the alloy melting temperature thus increases, moving to the left along the liquidus curve. This requirement for a higher initial melting temperature

and slower diffusion rate may thus account for the fact that fuses using alloys with a high silver content were slower acting.

Measurement of Alloy Diffusion - It can be seen from the results (Figs. 4.11 & 4.12) that both constant current and constant temperature testing demonstrate the presence of the diffused boundary layer and enable the growth of this layer to be studied. The results of these tests have been reported in Tables 4.4 and 4.6 respectively. In both sets of tests, micro-probe analyser results confirmed that the boundary region was composed of free tin and silver and the intermetallic compound Ag_3Sn. This was achieved by firstly scanning several areas of the boundary approximately five microns square and the average composition of the boundary determined. By reducing the scanned area it was then possible to analyse areas down to one micron square, and whilst the overall composition of the boundary region was shown to be approximately 60% by weight silver and 40% by weight tin, much of the smaller areas scanned were approximately 72% silver 28% tin corresponding to an atomic ratio of 3:1 clearly showing the presence of the inter-metallic compound Ag_3Sn.

The constant current tests enabled the variation in the depth of the diffused boundary layer with time across the length of the sample to be studied. This boundary layer was reasonably constant throughout the sample except at the edges adjacent to the silver strip where the diffused layer at any point in time was appreciably greater. This was

confirmed by observations made during the time-current tests reported in section 4.4.1 where the fuse element frequently operated at the edge of the M-effect alloy rather than at its centre. If this variation in diffusion rate can be attributed to a temperature variation then clearly the edges of the alloy must be at a higher temperature. This will be investigated further in the next chapter.

The constant current tests also showed that the diffusion of the tin through the silver rapidly increases with time. During these tests the voltage drop across the element (representing the element resistance under constant current conditions) was also monitored. Fig.4.14 shows how the voltage drop across the fuse increases with time, increasing rapidly as the fuse approaches its operating point. The shape of this curve mirrors the element temperature rise results shown in Fig. 4.8., and enables the mean element temperature to be determined.

Whilst these tests represent fuse operation under typical operating conditions, the constantly changing temperature of the boundary layer prevents the diffusion rate at any given temperature to be determined. The constant temperature tests, on the other hand, whilst not truly reflecting typical fuse operation, nevertheless enable fundamental data on diffusion rates and the temperature dependency of the diffusion coefficient to be determined. Assuming there is sufficient tin to ensure a constant concentration of tin on the silver element then an analytical solution to the diffusion equation can be obtained.

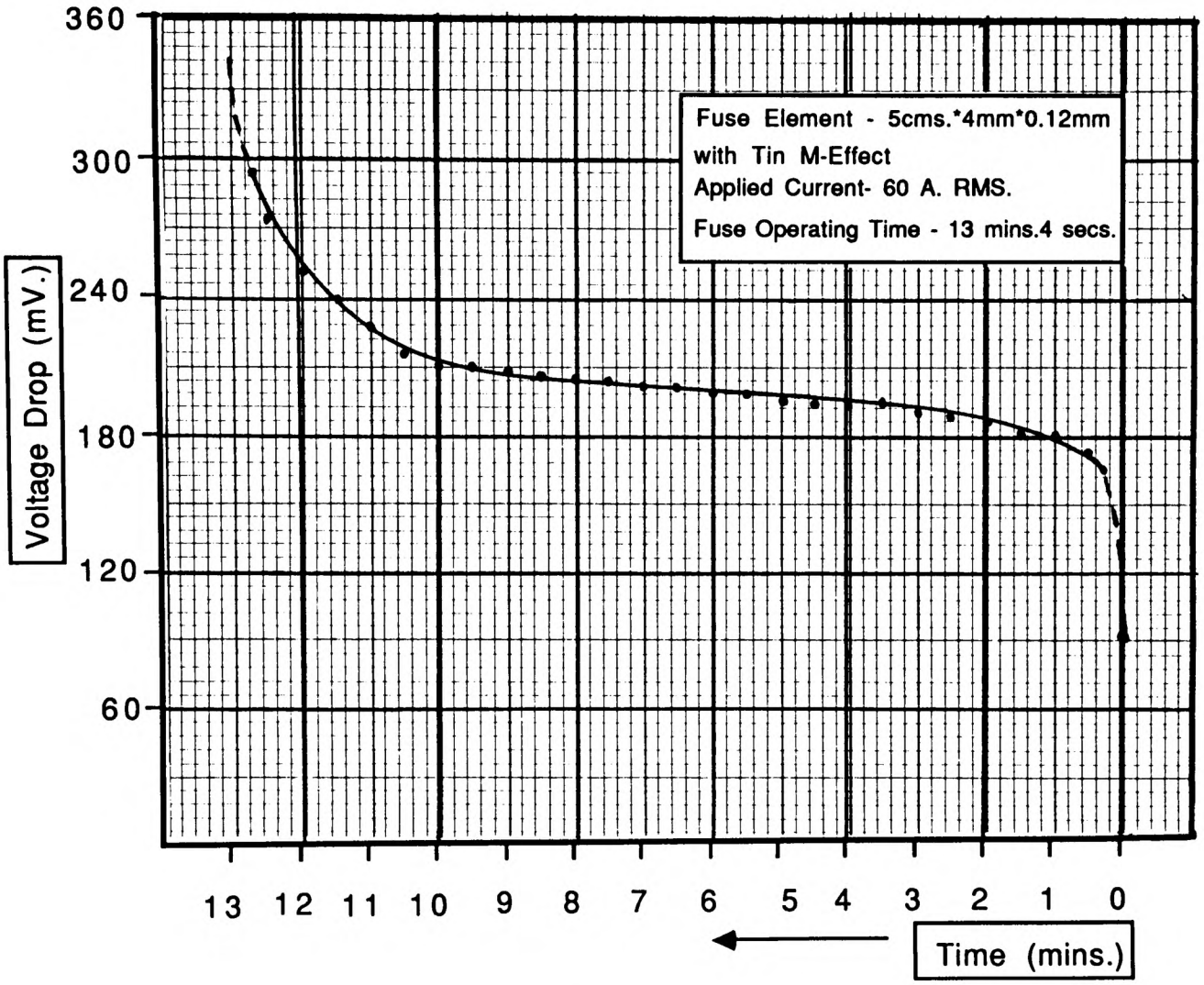

Voltage Drop Across a Fuse Element during M-Effect Action.

Fig. 4.14

Jost [22] has shown that solving the one dimensional diffusion equation:

$$\frac{\partial C}{\partial t} = D\frac{\partial^2 C}{\partial x^2}$$

under these conditions enables the mean square of the diffusion depth $\overline{x^2}$ of one metal diffusing into the other during a time t to be approximated to

$$\overline{x^2} = 2Dt$$

from which the average diffusion depth $\overline{x}$ is given by

$$\overline{x} \simeq \sqrt{\overline{x^2}} = \sqrt{(2Dt)}$$

where D is the coefficient of diffusion at any given constant temperature T.

A plot of x against $\sqrt{t}$ should thus give a straight line and enable the diffusion coefficient D to be obtained. The results of the tests listed in Table 4.6 are shown in Figs. 4.15 to 4.20 and are summarised, along with results obtained by other researchers, in Fig. 4.21. It can be seen that the results can be approximated to straight lines and from these the diffusion coefficient D has been calculated at various temperatures. These are shown in Table 4.7.

Temp°C	D cm sec^{-1}
225	8.9×10^{-11}
240	4.1×10^{-10}
275	1.2×10^{-9}
300	1.3×10^{-9}
350	5.3×10^{-9}
410	1.3×10^{-8}

Table 4.7

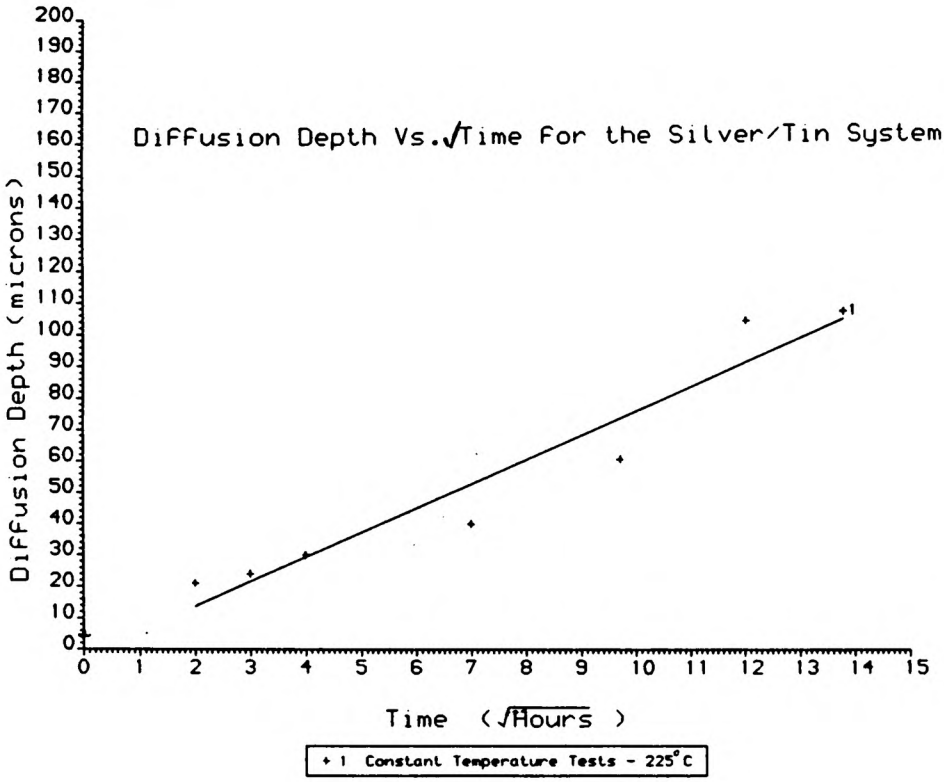

Fig. 4.15 - Diffusion at 225°C.

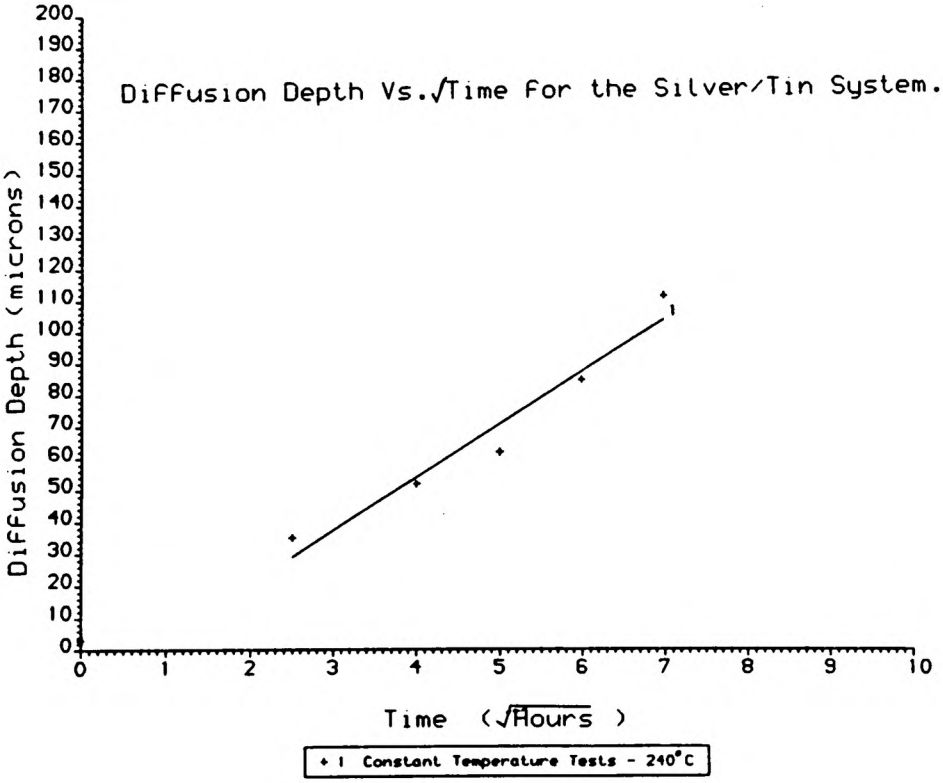

Fig. 4.16 - Diffusion at 240°C.

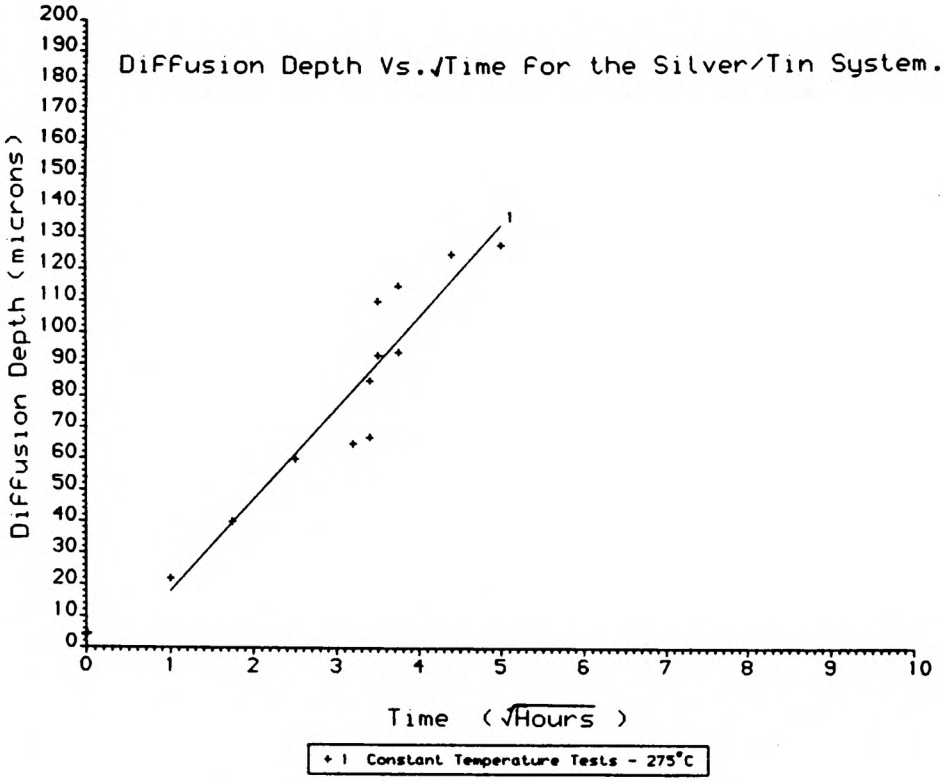

Fig. 4.17 - Diffusion at 275°C.

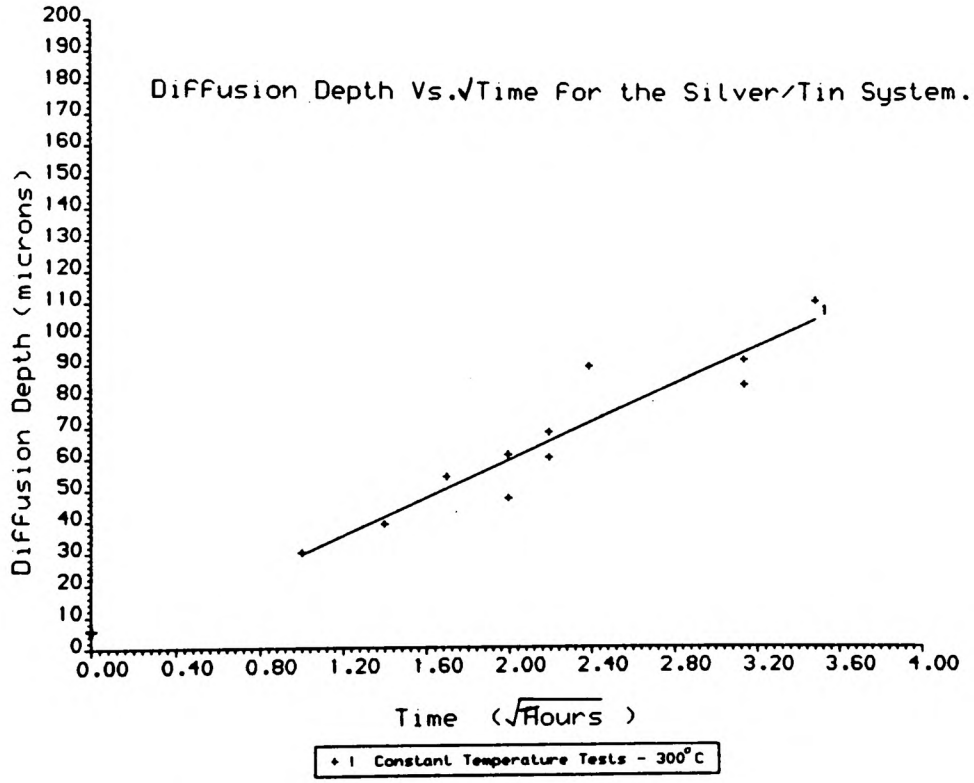

Fig. 4.18 - Diffusion at 300°C.

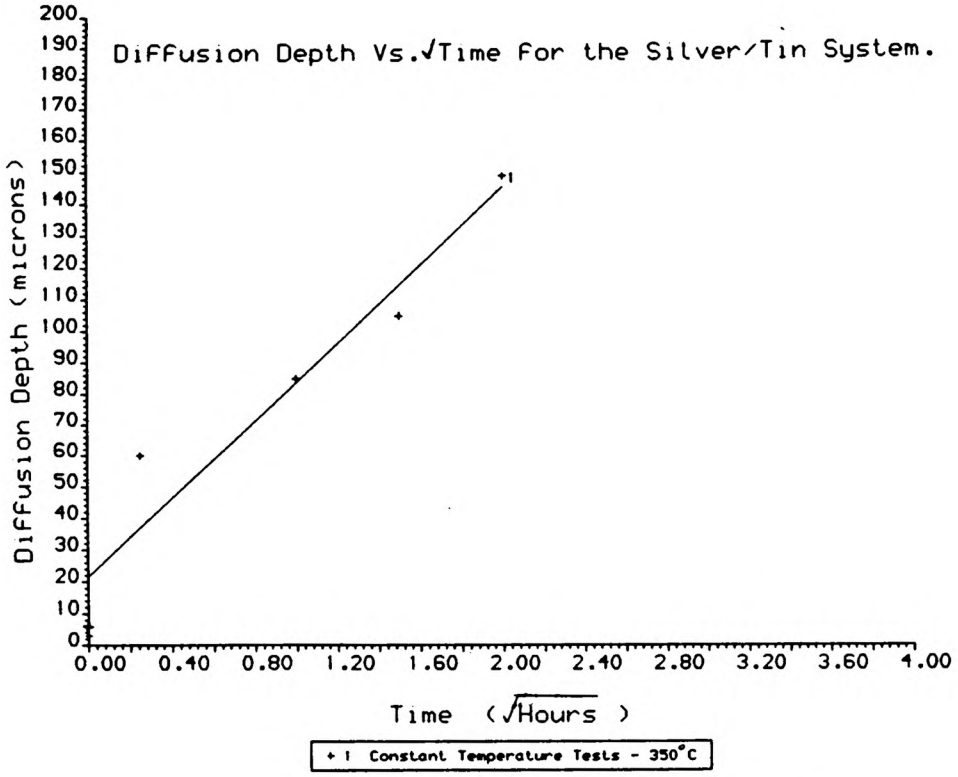

Fig. 4.19 - Diffusion at 350° C

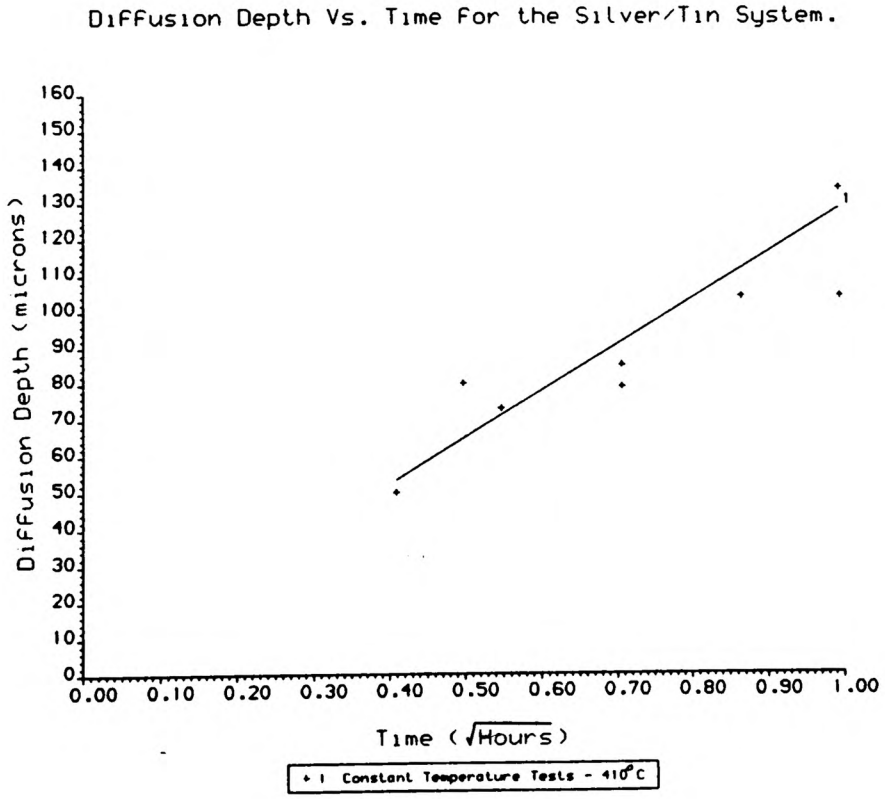

Fig. 4.20 - Diffusion at 410° C

Diffusion Depth Vs.√Time For the Silver/Tin System.

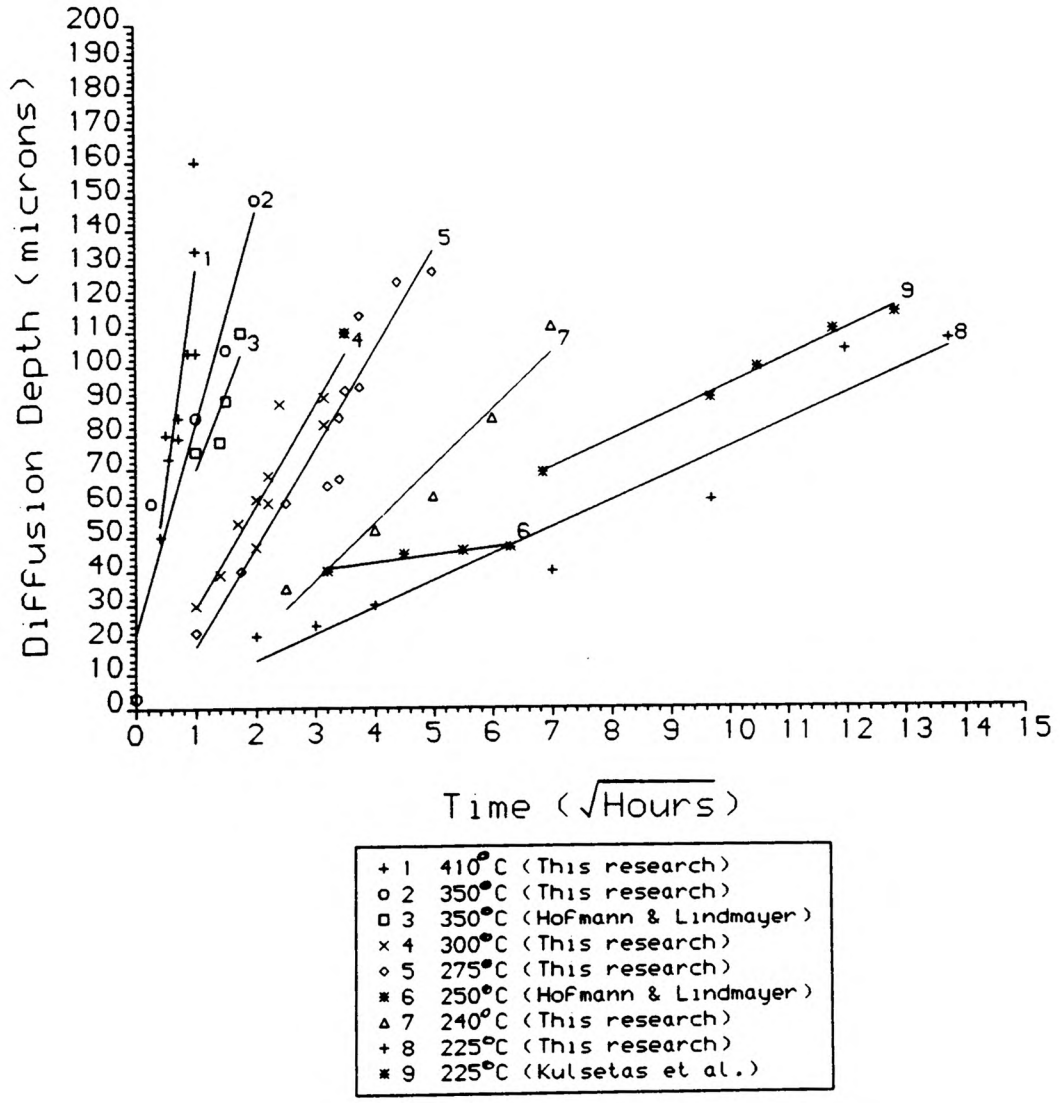

Compilation of the Results Presented in Figs. 4.15 - 4.20 along with those of Other Researchers.

Fig. 4.21.

If the variation of the diffusion rate with time follows an Arrhenius tendency, as do most diffusing systems, then the results should lie on the Arrhenius curve, given by equation 2.8

$$D = Do \exp\left(-\frac{Q}{RT}\right)$$

If this expression is valid for the silver/tin system then a plot of ln D against 1/T should give a straight line, enabling D_O and Q to be obtained from the intercept and slope respectively. Fig. 4.22 shows that the points lie approximately on a straight line, from which the diffusion coefficient D_O was computed to be 2.1×10^{-4} cm^2 sec^{-1} and Q the activation energy 55,400 Joules Mol^{-1}.

Due to the wide variation in experimental results used to obtain diffusion measurements, the calculation of errors in the diffusion coefficient and activation energy is a difficult task. D_O has been obtained from the best straight line graph of values of D at different temperatures, which have themselves been computed from best straight line approximations. By studying the scatter in values about the best straight lines the errors in D and D_O were estimated to be $\pm$ 28%.

That is: $D_O = 2.1 \times 10^{-4} \pm 28\%$ cm^2 sec^{-1}

$Q = 55,400 \pm 28\%$ Joules Mol^{-1}

in the temperature range 225°C to 410°C.

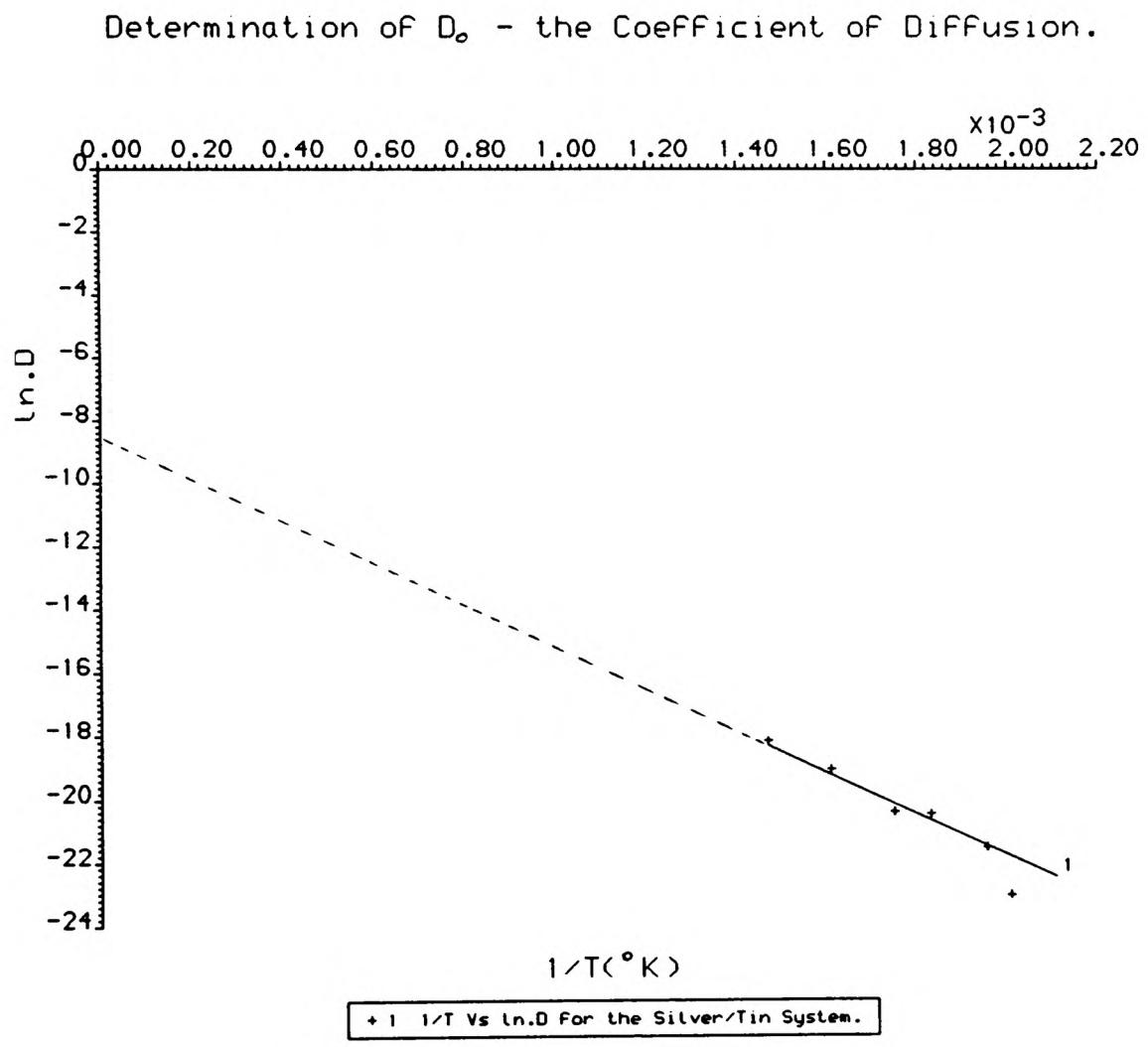

Graph of ln D versus 1/T°K for the Silver/Tin System.

Fig. 4.22.

There are no published results on fuse investigations with which to compare these values, but general published data on silver/tin diffusion give the following values.

D_O = 2.6 x 10^{-4} cm^2 sec^{-1} ; Q = 17,640 Joules Mol^{-1} - temperature range 280°C - 500°C (Ma & Swalin [62]).

D_O = 7.8 x 10^{-5} cm^2 sec^{-1} ; Q = 89,450 Joules Mol^{-1} - temperature range 650°C - 895°C (Seith & Peretti[63]).

Controlling and measuring the diffusion process is a difficult task and this is clearly reflected in the wide spread of values obtained by the researchers.

4.5 Interim Conclusions.

The effect of M-effect parameters such as quantity, position and composition, have been studied and their influence on fuse operation determined. By measuring the diffusion rate of the M-effect alloy under both constant current and constant temperature conditions, values for D_0, the diffusion constant, and Q, the activation energy, have been obtained, as well as values of D, the coefficient of diffusion, at various discrete temperatures. With this information, it is possible to construct a model of M-effect action to predict diffusion rates and eventual fuse operating times under long-time operating conditions. Chapter 5 describes the development of such a model.

CHAPTER 5

Modelling the M-Effect

5.1 Introduction

Chapter 3 showed how an analogue circuit simulation package, ASTEC3, could be successfully used to model electrical, thermal and diffusion phenomena. In this chapter an ASTEC3 program will be developed to model M-effect operation in fuses, a process which involves all three transport properties. It is thus useful at this stage to review the operational requirements of such a model. During fuse operation on low over-current faults, ohmic heating causes the fuse element temperature to rise. Once the M-effect alloy reaches its melting temperature it starts to diffuse through the silver element forming compounds with comparatively high values of resistivity. This causes increased ohmic heating which in turn causes greater diffusion. A hot spot is thus formed and catastrophic heating-diffusion, increased heating-increased diffusion, rapidly follows, until the fuse eventually operates at the alloy deposit. In order to use ASTEC3 to simulate such a process the electrical, thermal and diffusion processes have to be modelled, and these models then nested to ensure cross-referencing occurs during the simulation. Any variations with temperature in the electrical, thermal or diffusive properties must also be taken into account, as too must the cooling effect of the granular filler. The problem may thus be broken down into discrete stages as follows.

(i) Divide the fuse element and adjacent filler into a three dimensional array of cells and calculate the electrical, thermal and diffusion parameters for each cell at ambient temperature.

(ii) Connect the cells together to form an electrical circuit and apply an electrical current to represent the fault current flowing through the fuse.

(iii) Determine the temperature rise of each cell, taking into account the variation of resistivity and thermal conductivity with temperature and cell composition.

(iv) Calculate the alloy diffusion depth and hence determine the alloy concentration in each cell.

(v) Recalculate the electrical resistance of each cell, the cell resistance varying with alloy concentration.

(vi) Continue the heating/diffusion cycle until the alloy has diffused completely through the base element.

Each stage of the process is dependent upon previous conditions and thus conditional statements have to be introduced into the test program. ASTEC3 allows its normal analogue circuit simulation capabilities to be enhanced by the addition of user written Fortran sub-routines. Conditional statements may thus be easily added to the test program.

5.2 Determination of the Model Parameters

The key model parameters are the resistivity, thermal conductivity, specific heat and coefficient of diffusion of the element and the thermal conductivity of the granular filler.

5.2.1 Resistivity

Whilst researching dilute silver-tin mixtures Linde [64] showed that the presence of a few percent tin in silver led to a substantial increase in resistivity. He showed that for a solution of 2.5% tin in silver, the resistivity at room temperature was approximately the same as that of tin, whereas for concentrations greater than 2.5%, Daalder [32] concluded that the resistivity of the mixture was close to that of the inter-metallic compound Ag_3Sn. These values are, however, for solid phases. During M-effect action, only the underlying undiffused silver strip will be in the solid phase. The residual tin or alloy will be in the liquid phase and the diffusing boundary in a paste form consisting of solid inter-metallic compound Ag_3Sn mixed with a liquid silver-tin composition. Linde has shown that the resistivity of liquid tin at 300°C is 50×10^{-8} ohms-metres with a temperature coefficient of resistance of $5 \times 10^{-3}°C^{-1}$ in the range 300°C to 700°C. The resistivity of the diffusing paste, however, is unknown, but it is most likely that it will be at least of this order, and thus, for modelling purposes, the values for liquid tin were assumed.

5.2.2 Thermal Conductivity

The flow of heat through the element and surrounding granular filler is determined by the thermal conductivities of the silver element and sand filler. Published values of the thermal conductivity of silver at various temperatures [46] enabled a curve fitting method to be used to produce a graph of thermal conductivity against temperature. From this graph an equation relating conductivity and temperature was obtained.

Fig. 5.1 shows the discrete values of thermal conductivity along with the curve fitting approximation. The equation representing this approximation between 0°C and 550°C is given by

$$K = 419.013 - 0.625T + 0.715*10^{-2}T^2$$

where T is the temperature in °C.

The thermal conductivity of the silica sand was assumed to remain constant at 0.51 watts $m^{-1}K^{-1}$. This value refers to a bulk quantity, and assumes a homogenous material. Heat loss from the element to the filler will, however, only occur at points over the element surface where the sand grains actually touch, and thus some errors in the analysis may occur. In all practical tests, the sand filler was vibrated on a vibrating table prior to test commencement to ensure a consistent packing density, and despite the possible inaccuracy described above, the results obtained from the thermal simulation were in good agreement with the experimental results.

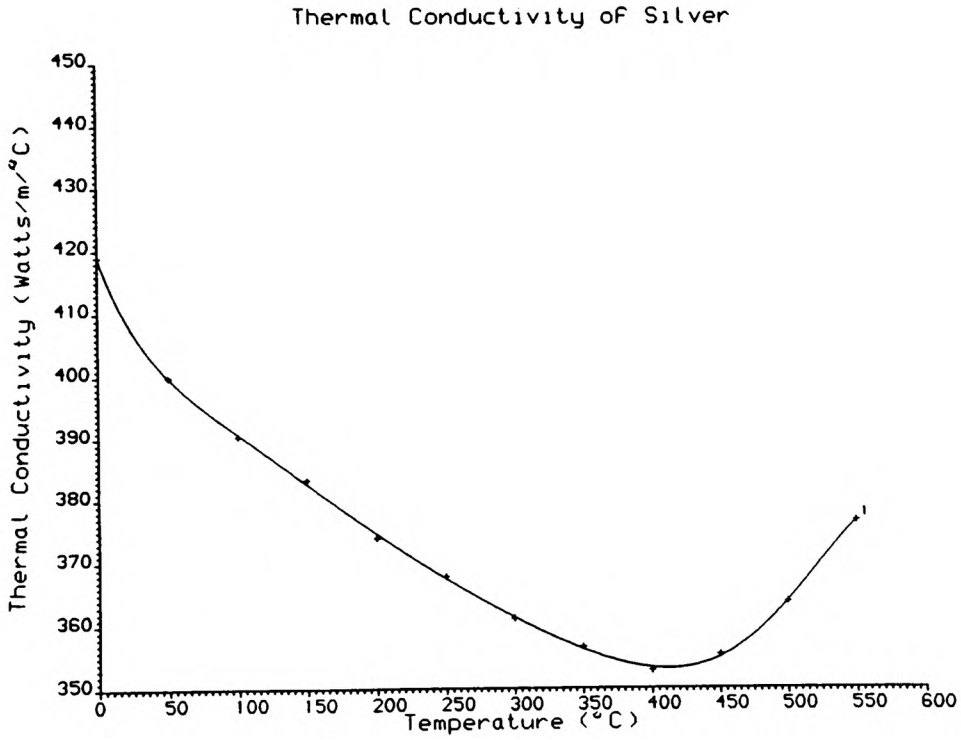

Variation of the Thermal Conductivity of Silver with Temperature.

Fig. 5.1

5.2.3 Coefficient of Diffusion and Activation Energy

The values of diffusion coefficient and activation energy determined experimentally in Chapter 4 were in broad agreement with the little published data which currently exists for diffusion in the silver-tin system, and these values were used in the simulation. The diffusion rate was assumed, as shown experimentally in Chapter 4, to follow an Arrhenius temperature dependency.

The experimental work also showed that the presence of insufficient alloy would reduce the diffusion rate, the process being effectively starved of diffusing alloy. To ensure that there was always free tin available for diffusion at the silver-tin boundary, the concentration of tin at the boundary was assumed to be fixed at 100% in the simulation. This is an approximation, since in practice diffusion occurs from the silver to the tin as well as from the tin to the silver, and thus the actual concentration at the boundary will be somewhat less than 100%. Again, to simplify the model, D_0, the diffusion constant, was initially assumed to be independent of concentration.

5.2.4 Circuit Layout

The actual values of resistance, capacitance and current sources in the electrical, thermal and diffusion models, were calculated in accordance with equations 3.8, 3.9, 3.13 and 3.14 as described in Chapter 3. External voltages, currents and ground planes were added to represent boundary conditions. The cells were then connected together to form a three dimensional array. Increasing the number of cells

per unit volume increases the resolution of the simulation at the expense of computer time. In practice a relatively coarse cell structure was firstly used to verify the correct operation of the simulation, and then each cell subdivided and the simulation repeated to produce a more exact solution. Increasing the number of cells also makes the circuit more complex and increases the likelihood of errors occurring in the manual numbering of cell nodes in the circuit description file. In order to aid the generation of an error free circuit, a computer program was written to generate a three dimensional cell matrix, where all adjacent cell nodes were numbered in the correct sequence. This greatly eased the production of an accurately labelled circuit description file and simplified the generation of the ASTEC3 program. A flow chart of the cell node numbering program is shown in Fig. 5.2.

5.3 Comparison of Simulation Results with Practical Tests

Simulations were made on several element configurations, both with and without M-effect alloy, and the results obtained compared with experimental results obtained by testing elements using the test box and test circuitry described in Chapter 4 Section 4.4.1.

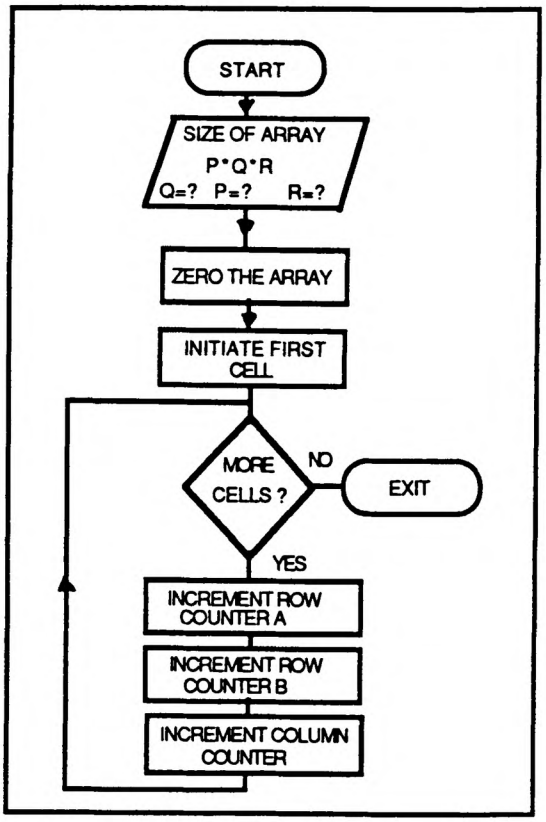

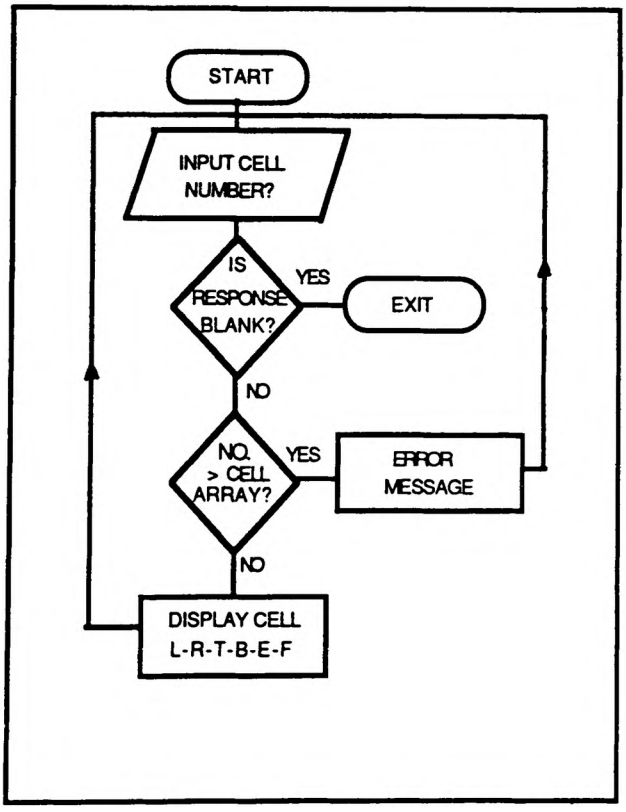

Flowcharts Of : (a) Cell Number Generation Routine.

(b) Cell Number Display Routine.

Fig. 5.2

5.3.1 The Modelling of a Plain Silver Element Without M-effect Alloy.

The temperature rise of a plain (unnotched) silver element 5 cms x 4mm x 0.12 mm has already been modelled using ASTEC 3 and the simulation results reported in Chapter 3, Section 3.3.3, Fig. 3.16. In this simulation, sand was assumed only to be in contact with both sides of the strip, and heat from the strip-edge assumed to be negligible. The temperature of the outside surface of the sand filler and the copper end connections was assumed constant at 20°C.

In order to reproduce these conditions experimentally, a silver element was mounted in the test box and the movable insulation board partitions arranged around the element. During the tests, accurate movement of these partitions enabled the sand depth either side of the element to be varied. The temperature rise of both the silver element and sand filler were measured using fine chromel-alumel thermocouples. The presence of the filler made accurate positioning of the thermocouples difficult, this being compounded by the need to vibrate the sand to ensure compaction. The positioning of the thermocouple in the sand was achieved by attaching it to the side of the partition and securing it using cotton threads so that it was positioned 1.0 cm. away from the centre point of the element. The sand was then added and vibrated. On removal of the sand after the test, the position of the thermocouple was found to be within 1.0 mm. of its original position. Positioning the thermocouple so as to be permanently in contact with the centre point of the element proved to be

more difficult, as any slight movement away from the element caused a dramatic drop in the recorded temperature. The cotton threads method proved unreliable for this measurement and the thermocouple was eventually spot-welded to the centre point of the element. Whilst this ensured element contact and repeatable results it did, however, cause some slight surface deformation of the element.

The voltage drop across the element was also monitored during the tests and from this the element resistance variation calculated.

In the simulation, the free surface of the sand was assumed constant at 20°C. To ensure this remained at ambient temperature throughout the tests, a cooling fan was played onto the sand surface.

A current of 50 amperes, R.M.S., was passed through the element and the temperature rise of both the strip centre and the sand filler noted. The test was then repeated with the sand-filler-depth increased from 2 cms. to 3 cms. and then 5 cms. Fig. 5.3 (a), (b), (c) and (d) shows both the simulation and experimental results and, as can be seen, good agreement was obtained.

The simulation was then used to determine a time-current pre-arcing characteristic for the element. This was achieved by plotting the simulated temperature rise for currents in the range 80 amperes to 120 amperes and noting the time at which the temperature of the mid-point of the

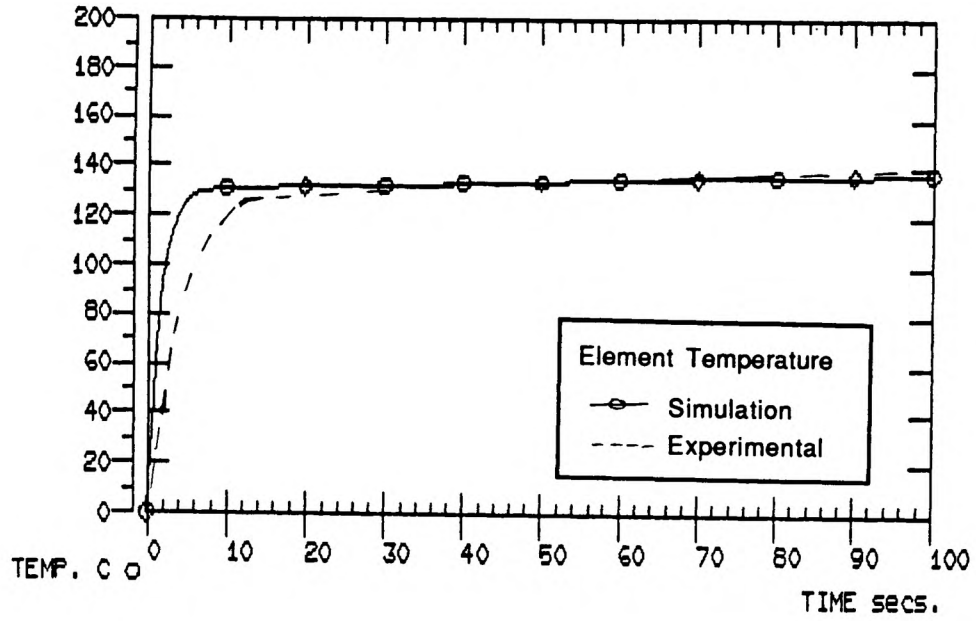

(a)

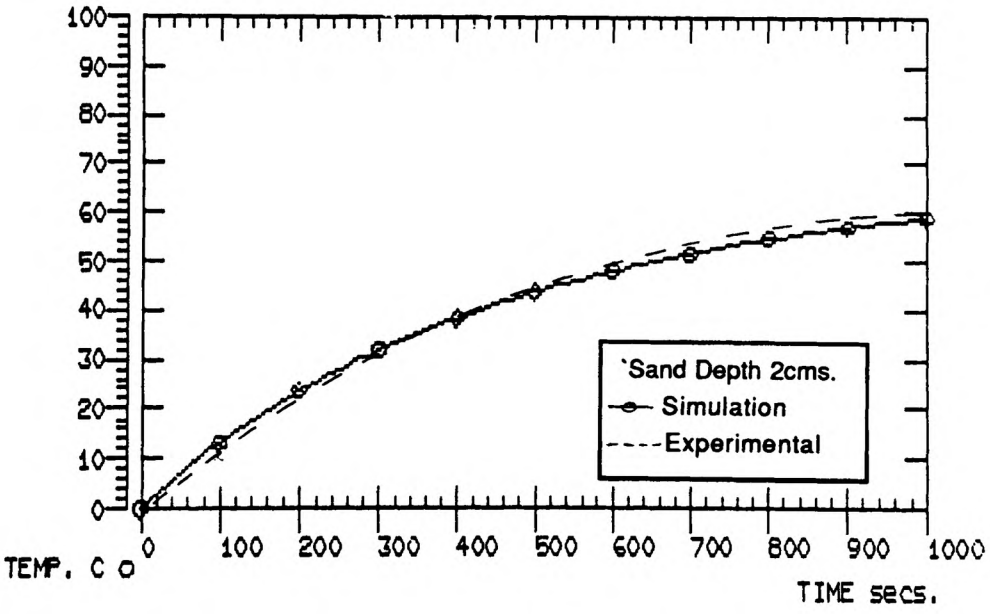

(b)

Comparison of Experimental and Simulation Results.
(a) Element Temperature Rise.
(b) Sand Filler Temperature Rise

Fig. 5.3(a&b)

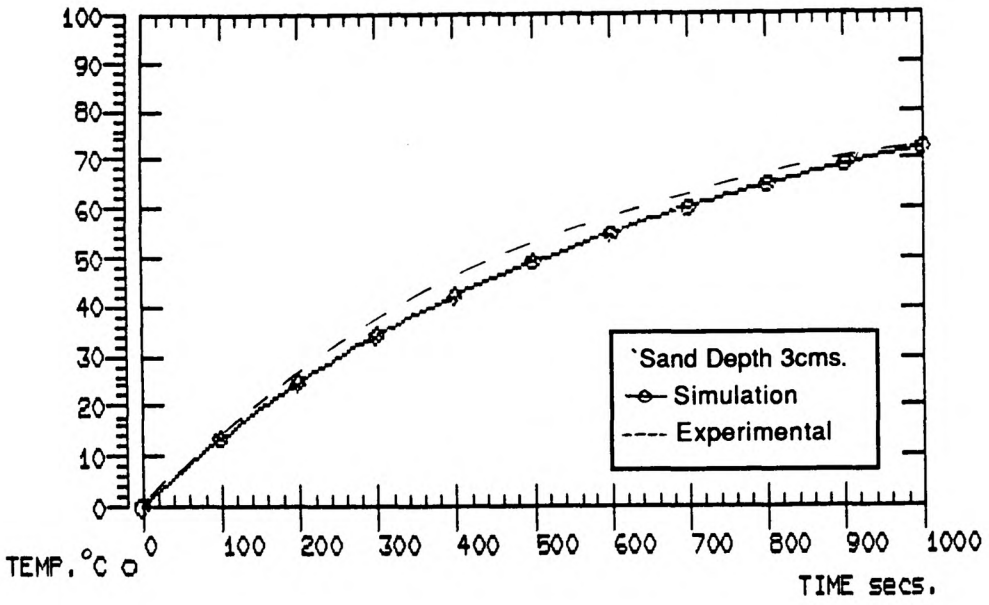

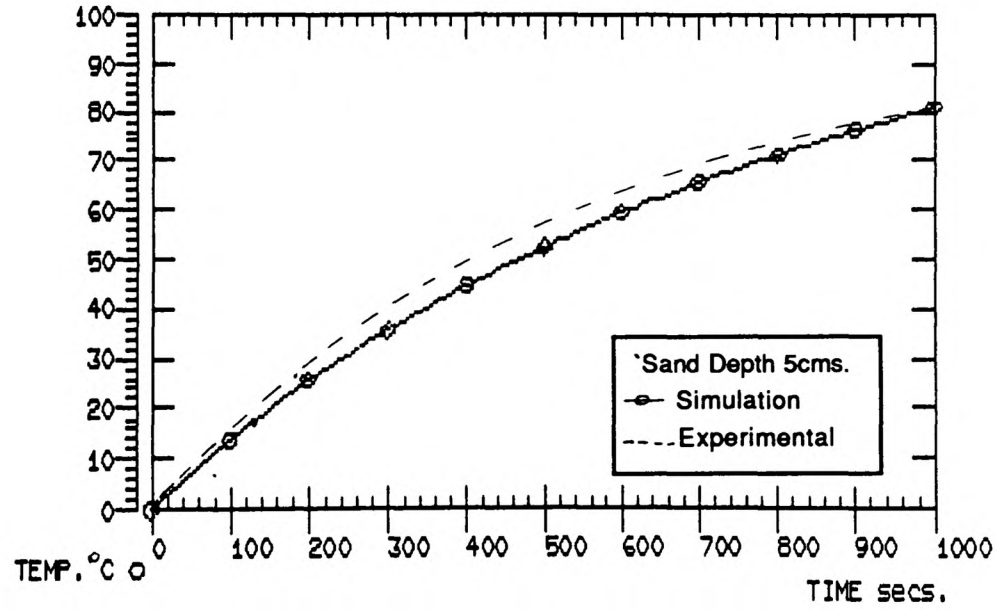

Comparison of Experimental and Simulation Results.
Sand Filler Temperature Rise for Different Sand Depths.

Fig. 5.3(c&d)

element exceeded 961°C, the melting point of silver, this being taken, to a first approximation, as the end point of the pre-arcing period.

To compare the results of the simulation with experimental results, a time-current characteristic for the element was plotted from the results of a series of tests in the test box, as described in Chapter 4, Section 4.4.1. The currents chosen (78A to 120A) gave operating times in the range one second to over two hours, and for times of this magnitude, any arcing time can be ignored.

The simulation and experimental results are shown in Fig. 5.4 and again good agreement was obtained.

5.3.2 The Modelling of a Plain Silver Element with M-Effect Alloy.

The computer simulation determines both the element temperature-rise and the growth of tin concentration in the silver element due to tin diffusion, but what will be the end point of the simulation signifying the end of the pre-arcing period?

The pre-arcing operating point of a fuse element consisting solely of a pure metal can be clearly defined as the point at which the element first melts and then either vapourises or leaves the conducting path by some other means [65], producing an open circuit to the flow of current. A

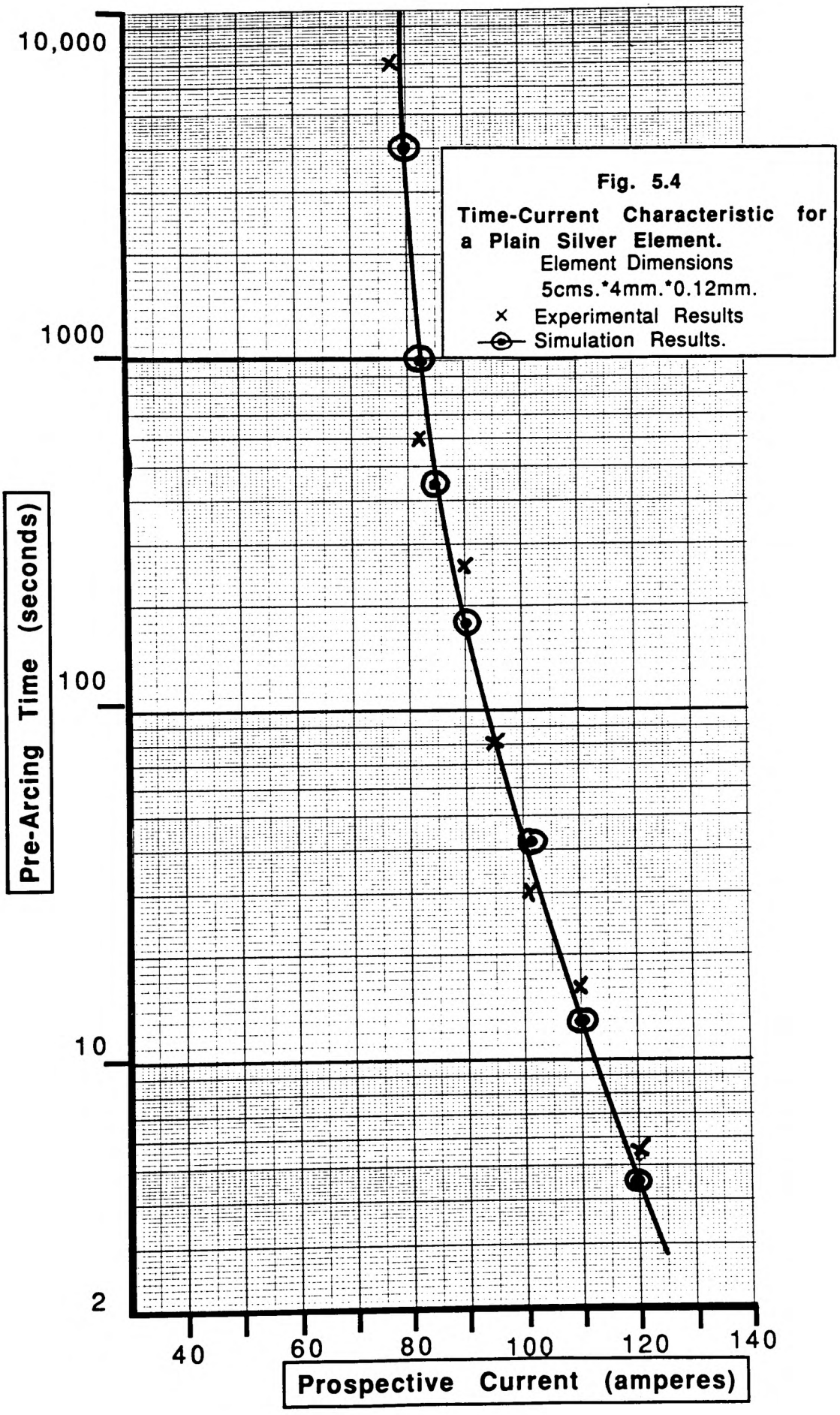
10,000
1000
100
10
2
Pre-Arcing Time (seconds)
40
60
80
100
120
140
Prospective Current (amperes)
Fig. 5.4
Time-Current Characteristic for a Plain Silver Element.
Element Dimensions
5cms.*4mm.*0.12mm.
× Experimental Results
Simulation Results.

computer simulation of such a fuse-link would thus equate heat input and heat losses and determine the resulting temperature rise. The end point of the simulation would then be the attainment of well defined element melting and/or vapourisation temperatures, taking into account, if necessary, any latent heat requirements.

The situation is far less clear, however, when considering the melting and vapourisation of diffusing substances. The element composition, and therefore melting temperature, varies with both temperature and time, and thus there is no simple method of determining the actual temperature of the fuse element when fuse operation occurs. Temperature alone, therefore, cannot be used to determine the end point.

A possible end point may be taken as the condition when the silver element beneath the alloy is fully dissolved in the liquid alloy at one point through the element, that is, the diffusion depth is equal to the thickness of the base element. This was the criterion used by Hofmann and Lindmayer during their investigations into M-effect on copper elements [29].

In order to determine typical values of concentration at the operating point, representing this fully dissolved condition, recourse has to be made to experimental data. The quantitative scanning electron microscope tests, reported in Chapter 4, showed that fuses which had operated under M-effect action had diffused layers whose composition

was reasonably constant at approximately 40% tin. In view of this, and for the purposes of the simulation, the pre-arcing end point was taken as:

(a) the attainment of 40% tin concentration through one point of the cross-section of the element.

or

(b) the silver element reaching its melting temperature of 961°C.

Once again, the element modelled was an unnotched silver strip 5 cms x 4 mm x 0.12 mm, but on this occasion a deposit of tin 5 mm x 4 mm x 2mm was situated at its mid-point. Cells were arranged, as before, to represent a 2 cm depth of sand filler. A relatively coarse mesh structure was initially tried. The element and tin deposit were sub-divided into 76 three-dimensional cells of various sizes as shown in Fig. 5.5. Clearly the area of greatest interest is the tin deposit and the adjacent section of silver element, and this area accounted for 59 of the 76 cells. Once the model was functioning correctly, each cell was sub-divided into eight smaller cells to give a greater resolution (2%) through the thickness of the strip.

Previous work on the element without M-effect alloy has shown that the thermal aspects of the model are functioning correctly. In order to verify that the model can also successfully model diffusion, the diffusion of the tin through the silver element was firstly modelled under constant temperature conditions. The modelling of constant

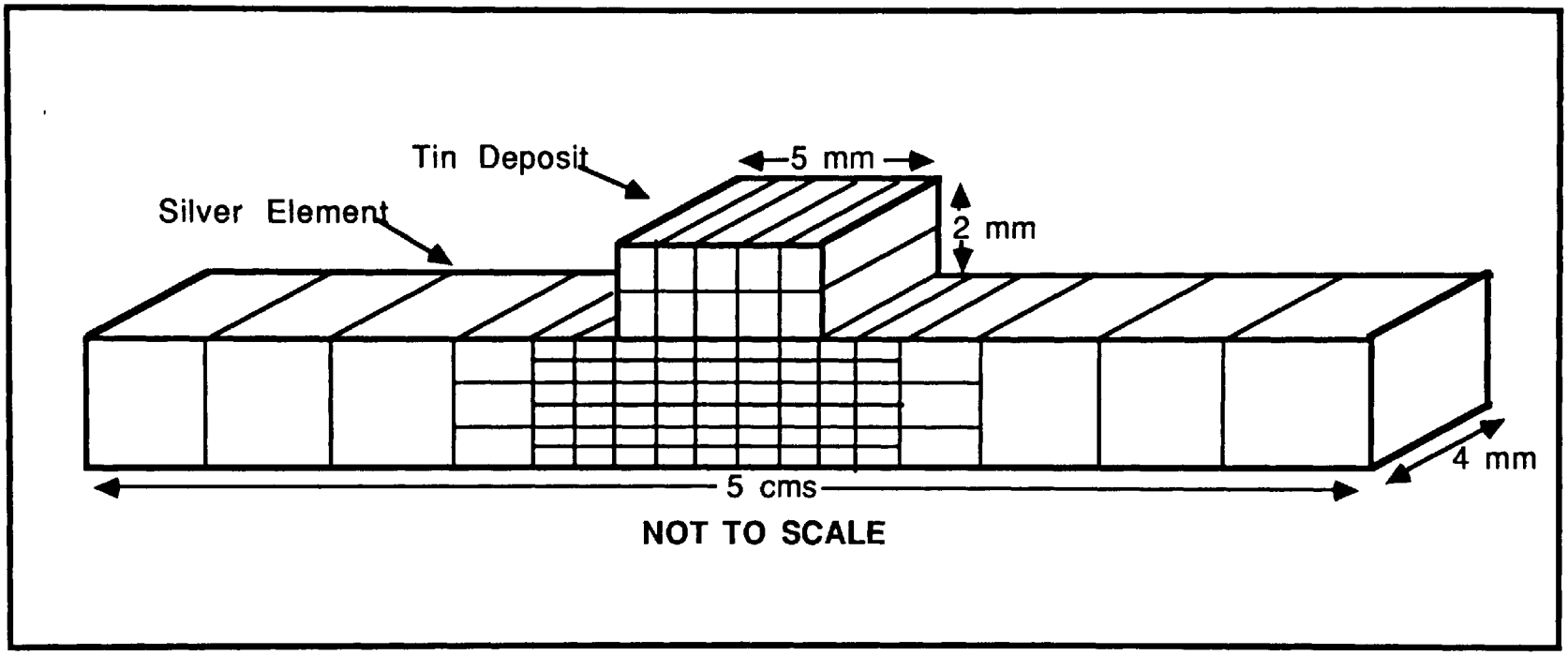

Coarse Cell Arrangement For Modelling A Silver Element With M-effect

Fig. 5.5

temperature conditions can be easily achieved by fixing all circuit nodes in the thermal model at a constant voltage. The results of the simulation can then be compared with the experimental 'constant temperature' results shown in Table 4.6. Fig. 5.6 shows the rate of change of tin concentration with time when the element is held at a constant temperature of 300°C. The graphs show circuit voltage nodes which represent the tin concentration at points in the silver element a distance of 10, 30, 50, 70, 90 and 110 microns depth away from the tin deposit. Using the criterion that the rate of advance of the diffused layer is represented by 40% tin concentration, then the time taken for the tin to diffuse through the silver element can be determined from the graph. Table 5.1 compares these results with the experimental results given earlier in Table 4.6.

Experimental		Simulation	
Diffusion Depth (microns)	Time (secs)	Diffusion Depth (microns)	Time (secs)
		10	1000
30	3600	30	4000
54	10,800	50	10,000
68	18,000	70	17,000
91	36,000	90	22,000
110	44,100	110	24,000

Table 5.1

Diffusion Rate at a Constant Temperature of 300°C

Table 5.1 shows that for times up to approximately six hours, good agreement is obtained with experimental results, but for longer times the simulation gives much faster diffusion rates.

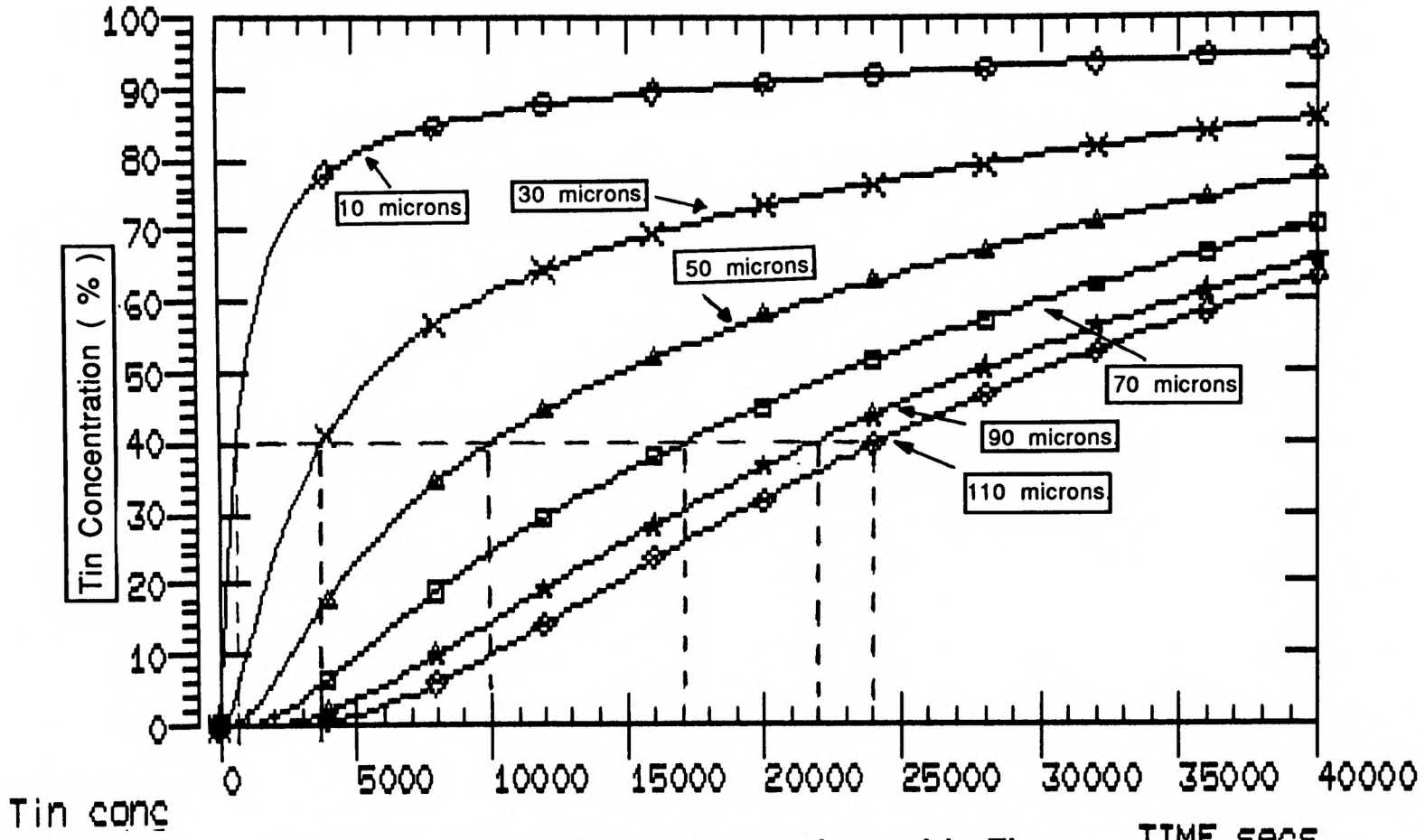

Variation of the Tin Concentration with Time at Various Depths through the Silver Element- Constant Temperature Testing (300 ^{o}C)

Fig. 5.6

The constant voltage sources applied to each circuit node to represent a constant temperature were then removed, and the circuit nodes left to assume values determined by the simulation when a series of R.M.S. values of current were applied to the fuse element.

As an example, Figs. 5.7 and 5.8 respectively show the variation of tin concentration with time at various depths through the silver element, and also the corresponding element temperature rise which occurs when a current of 73 amperes is applied to the fuse element. It can be seen that both the tin concentrations (representing the diffusion depth) and element temperature both rise rapidly towards the end of the pre-arcing period, and in this particular case, the fuse operated after 183 seconds.

Fig. 5.9 shows an experimental temperature rise curve carried out on the element when a current of 73 amperes was applied. The fuse operated after 203 seconds, in good agreement with the simulation. The temperature rise and general shape of the time-temperature curve aligned with the simulation results, although the final temperature was less than that predicted. This can possibly be explained by the fact that the thermocouple measures the temperature of the surface of the liquid alloy, whilst the simulation gives the temperature of the centre of the silver element, or more probably, it may be due to the relatively slow response of the chart recorder.

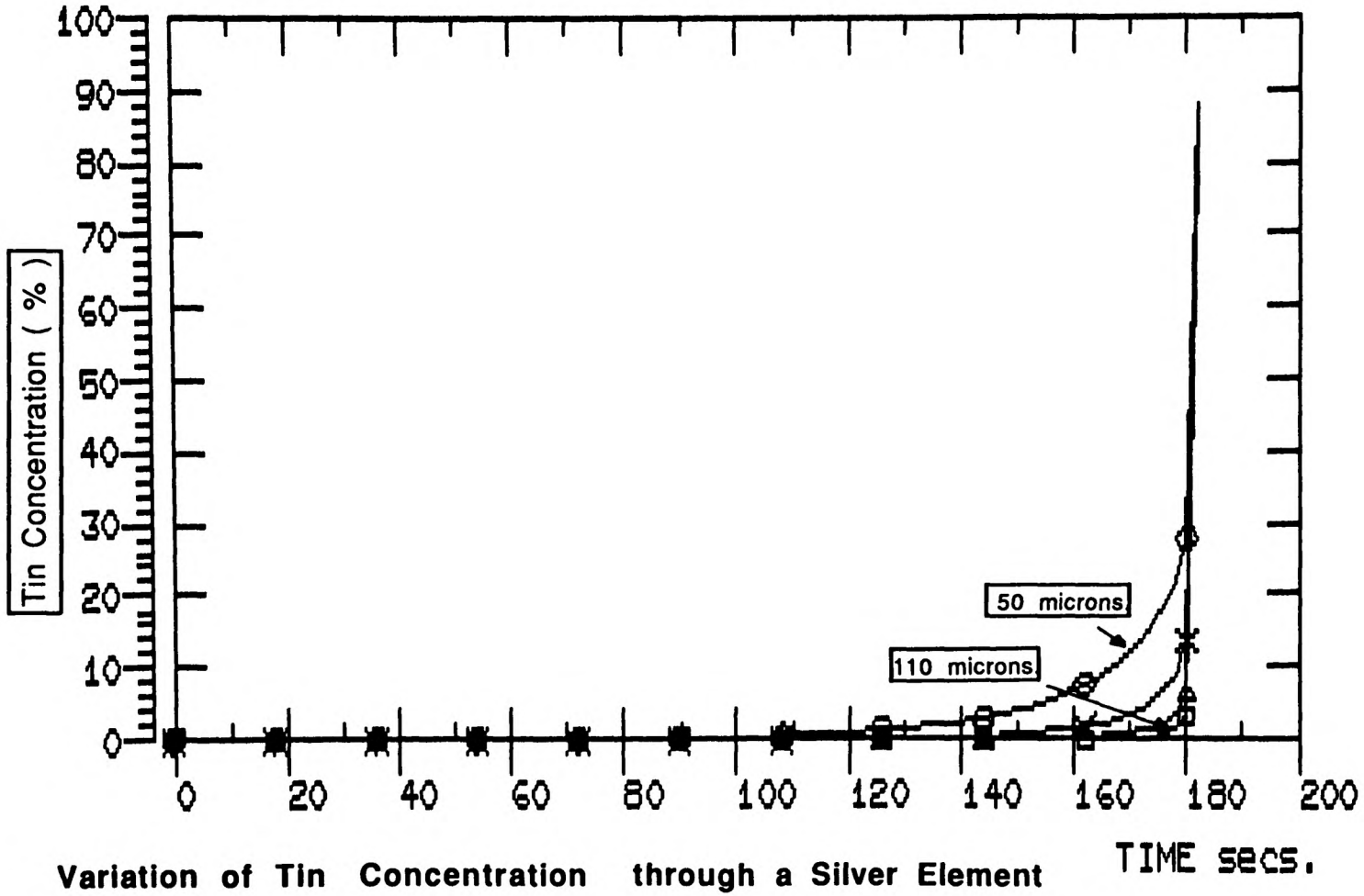

Variation of Tin Concentration through a Silver Element during M-Effect Action - Applied Current 73 Amperes RMS

Fig. 5.7

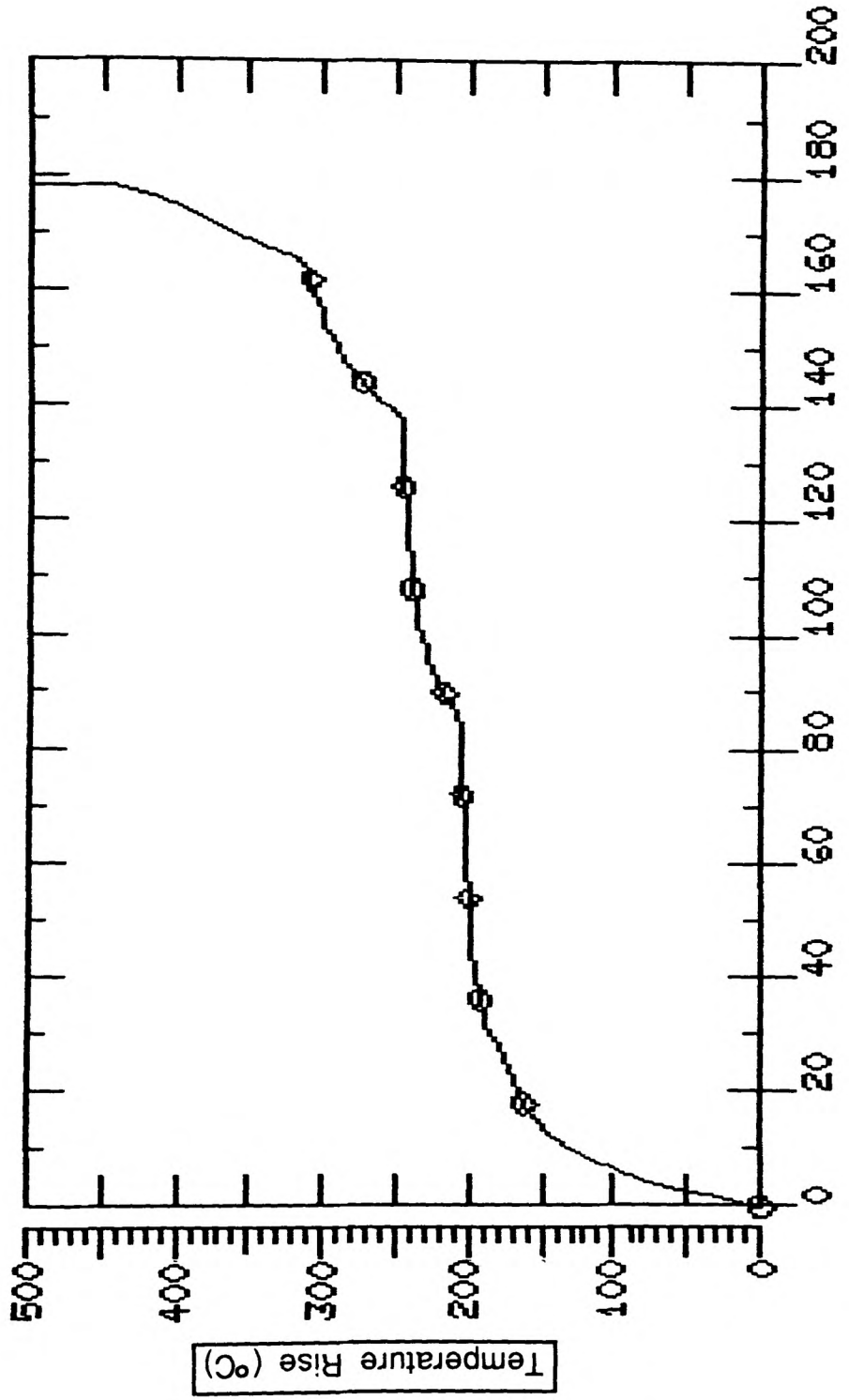

Simulated Temperature Rise of a Silver Element during M-Effect Action - Applied Current 73 Amperes RMS

Fig. 5.8

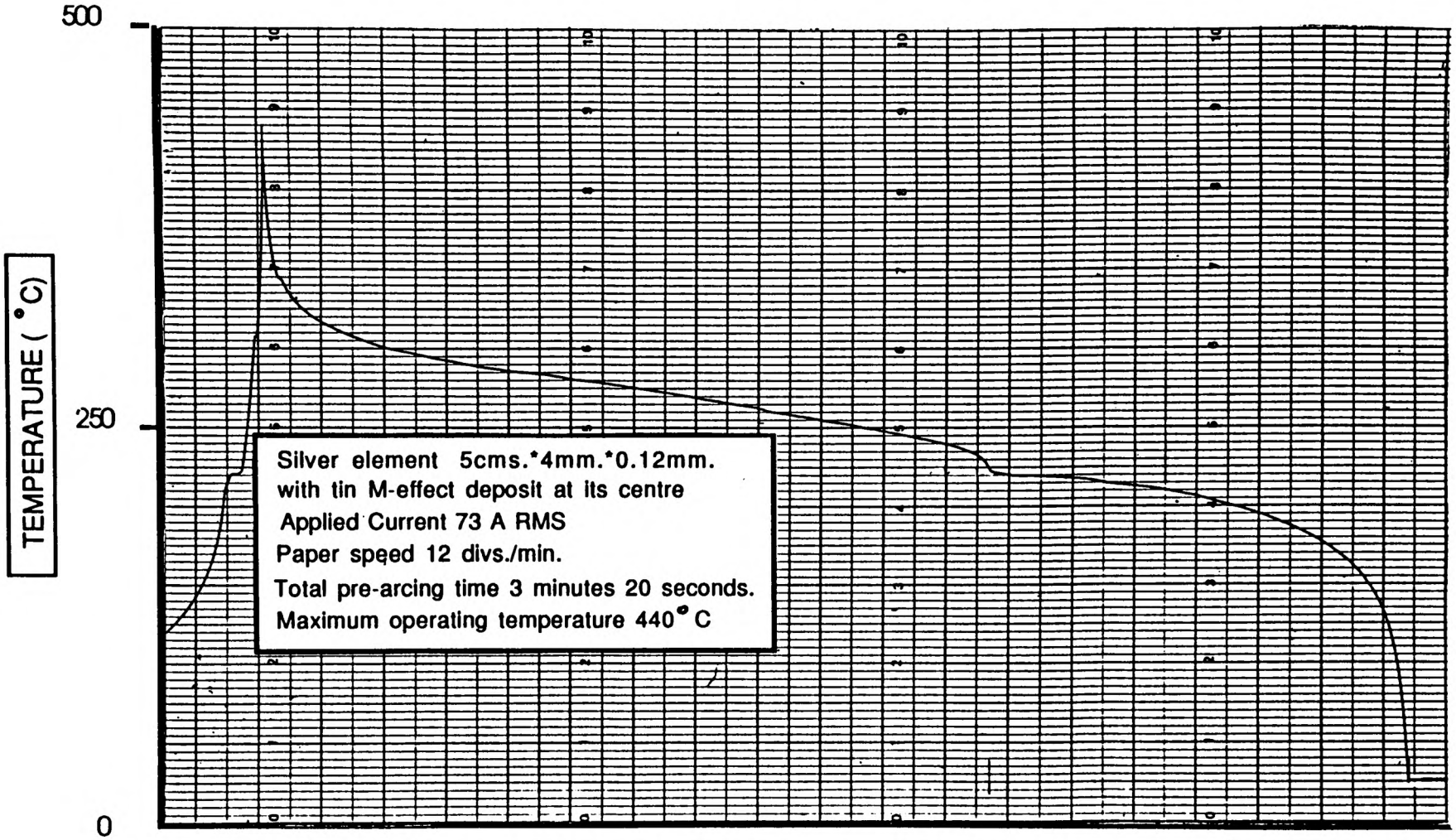

Temperature Rise Test on a Plain Silver Element

Fig. 5.9

The experimental work presented in Chapter 4 showed that the rate of diffusion was faster at the edges of the alloy than at its centre. The simulation results show that the silver cells adjacent to the edges of the alloy were indeed at a higher temperature than those at the element centre, by approximately 12°C.

A series of simulations were then carried out for a range of currents corresponding to operating times ranging from a few seconds to three hours.

Elements were made by applying a weight of tin (300 mg) equivalent to the weight of tin deposit in the simulation and covering it with a layer of fireclay cement to prevent running. The elements were tested in the test box and an experimental time-current characteristic constructed from the results. The simulation and practical tests are compared in Fig. 5.10, where it can be seen that whilst agreement is good for relatively long operating times (up to approximately thirty minutes), for longer operating periods the simulation predicts faster operation than is achieved in practice. The consequences of this will be discussed further in Section 5.4.

5.3.3 The Modelling of Notched Silver Elements

One method of simulating a notched silver element would be to model each notch as described in Chapter 3, Section 3.3.2 and include models of each notched section in the overall element simulation. The use of such a method would,

however, involve considerable computer storage and result in a prohibitively long program execution time. Since the notches under consideration have already been separately modelled, and remembering that the simulation should be no more complex than is required to produce acceptable results, then a simplified method was employed.

During the long pre-arcing times associated with M-effect action, the only effect the notches will have on the simulation is to increase the strip resistivity and produce local hot spots along the element where the notches occur. The effect of these notches can thus be taken into account in the form of cells of increased resistance at regular points along the element length. Once a particular single notch configuration has been modelled, the results obtained from this simulation can be used to determine the value of these resistors.

The element modelled was a 5 cm x 2.54 mm x 0.16 mm silver strip shown in Fig. 3.9(c). This element was modelled in Chapter 3, Section 3.3.2. The ASTEC3 results obtained, given in Table 3.3, show that for this particular notch configuration, notching the strip increases its resistivity over an equivalent unnotched strip by 26%. Fig. 5.11(a) shows the dimensions of the element under test, and from the geometry of the strip, the resistances of the notched sections and the remaining unnotched sections were calculated. The equivalent resistances are shown in Fig. 5.11(b).

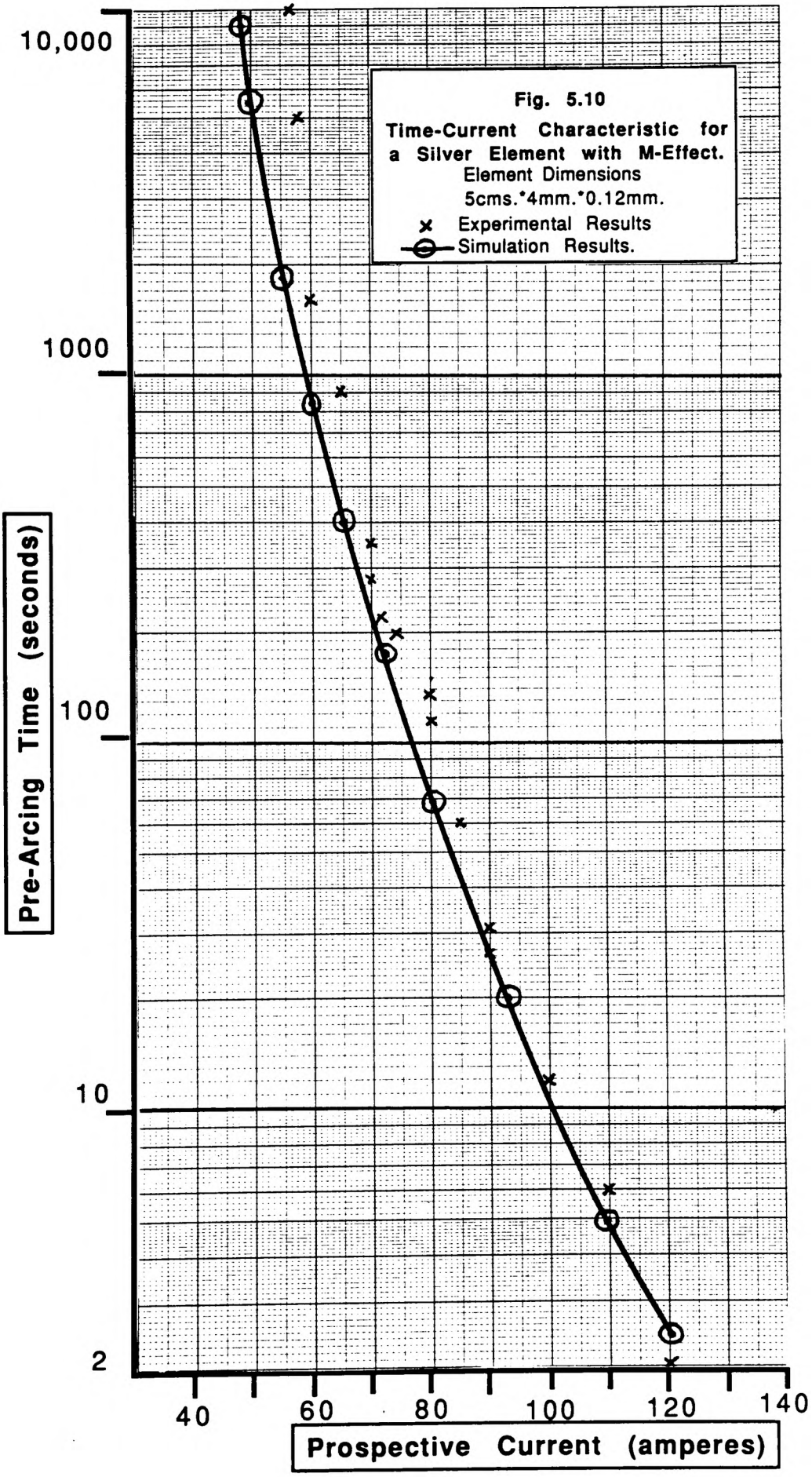
10,000
1000
100
10
2
Pre-Arcing Time (seconds)
40
60
80
100
120
140
Prospective Current (amperes)
Fig. 5.10
Time-Current Characteristic for a Silver Element with M-Effect.
Element Dimensions
5cms.*4mm.*0.12mm.
Experimental Results
Simulation Results.

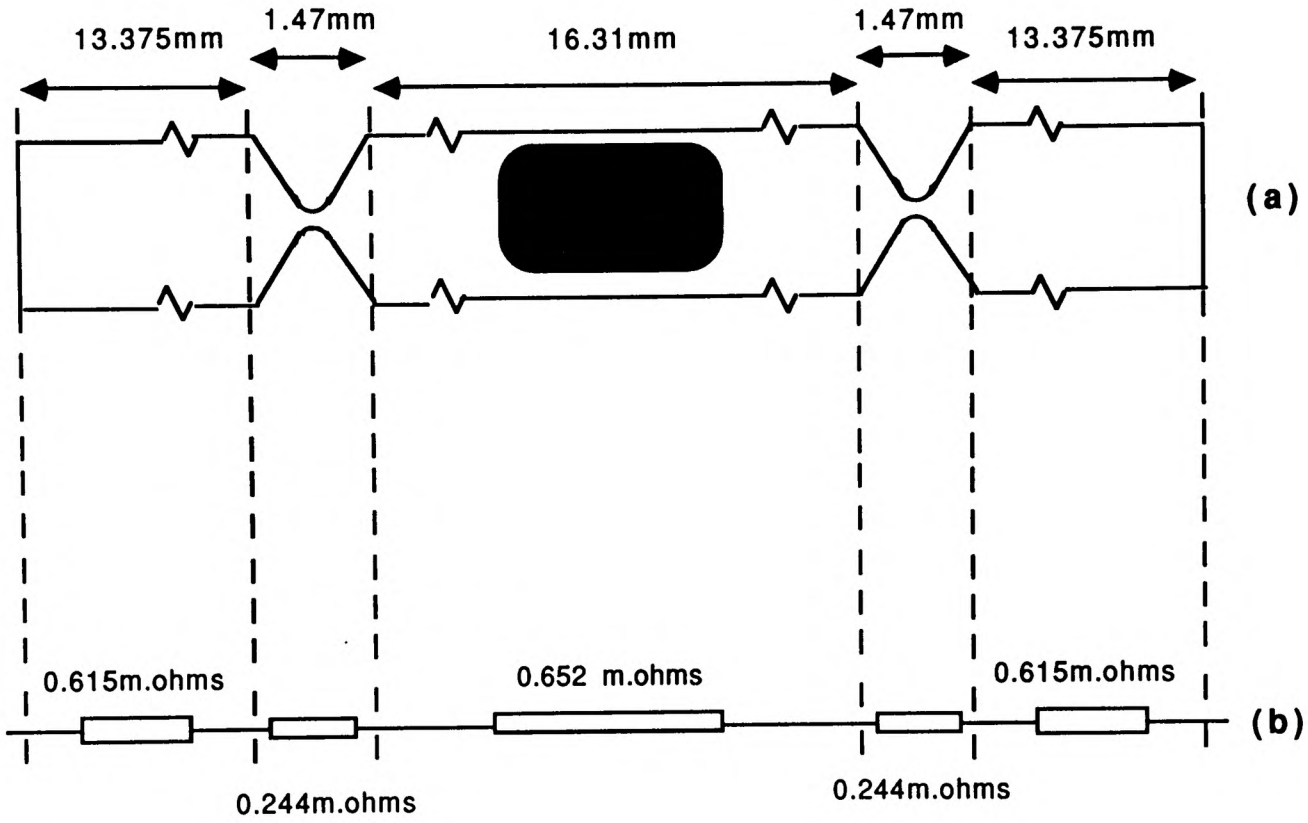

The Modelling of Notches as Resistors.
(a) The Element Dimensions.
(b) The Equivalent Resistor Network.

Fig. 5.11

The element was modelled, as before, using a mixture of coarse and fine cells, the fine cells being concentrated in the silver element beneath the tin deposit. The notched sections were modelled as single coarse cells, the electrical resistance being calculated as described above, and the thermal resistance and thermal capacity calculated, taking into account the reduced element mass. Each cell was subsequently divided into eight smaller cells to improve the model's resolution. Sand filler cells were grouped on both sides of the element to represent a 2.0 cm. depth of compacted sand.

The experimental and simulation results are compared in Fig. 5.12. Again it can be seen that good correlation is achieved for shorter operating times, but the results deviate for longer times.

5.4 Discussion of the Results

Both the simulated temperature rise test (Fig. 5.3) and time-current characteristic for fuse elements without M-effect (Fig. 5.4) give excellent agreement with experimental results, and it can be concluded that from the thermal aspects, the theory adequately describes the physical problem.

For fuses with M-effect, when temperature and diffusion are actively involved, agreement is reasonable for operating times up to approximately thirty minutes, but for longer times the simulation predicts faster operating times than are achieved in practice. This was confirmed by the

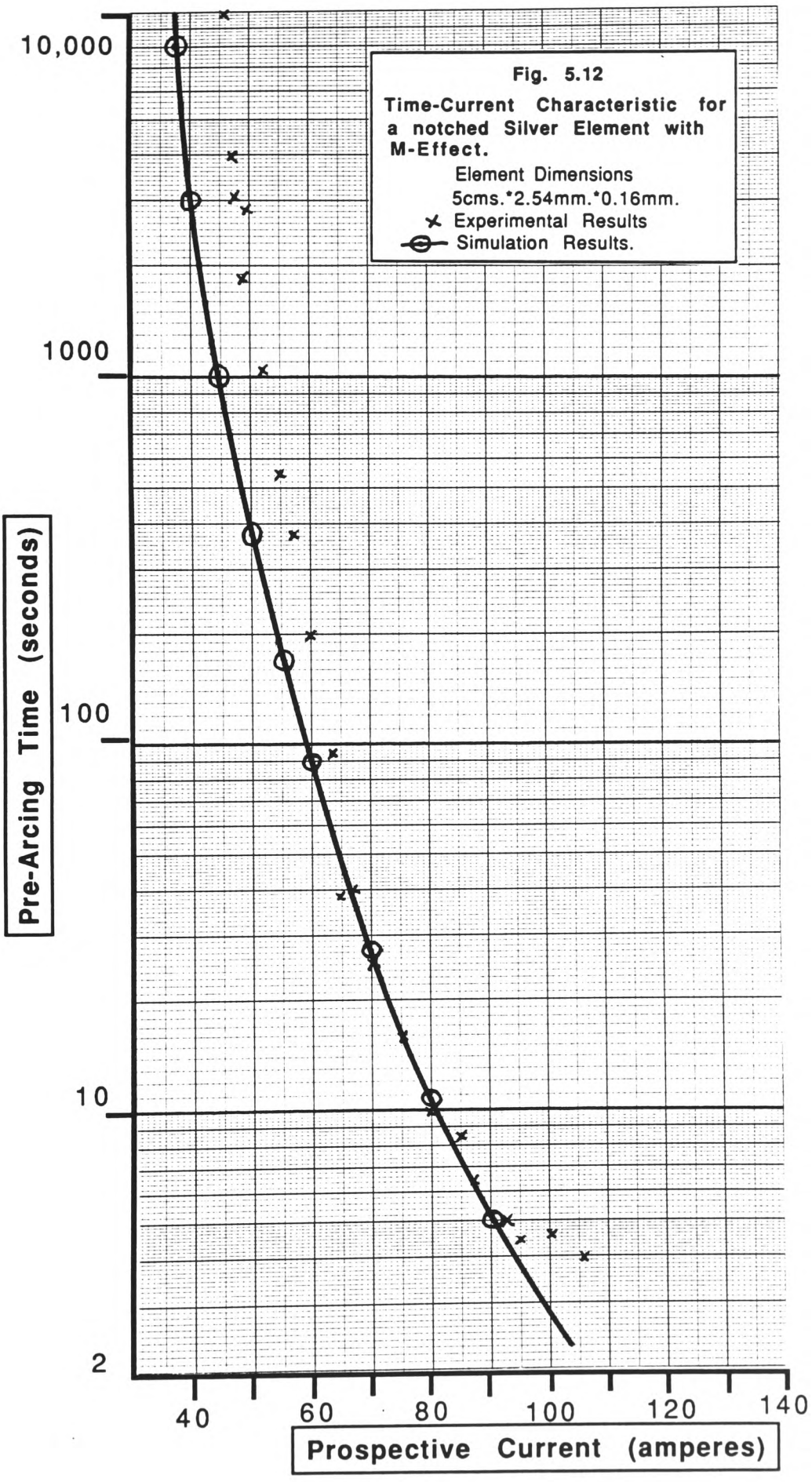
Fig. 5.12
Time-Current Characteristic for a notched Silver Element with M-Effect.
Element Dimensions
5cms.*2.54mm.*0.16mm.
Experimental Results
Simulation Results.
10,000
1000
100
10
2
Pre-Arcing Time (seconds)
40
60
80
100
120
140
Prospective Current (amperes)

constant temperature tests which also showed the simulated results to deviate from those obtained experimentally for longer diffusing periods. Several assumptions have been made wher formulating the computer model, but the variable with the greatest influence is the rate of diffusion. The assumption in the model that the rate of diffusion is dependent only on temperature is clearly an over simplification. In their work on the M-effect, Hofmann and Lindmayer [30] observed that a form of saturation set in which restricted further dissolution of the element in the molten alloy and dramatically slowed down the rate of diffusion. From the results presented here, however, it would appear that this apparent concentration dependency of the diffusion rate is less marked at shorter operating times, possibly due to the turbulent reaction which takes place at these high current densities, preventing local saturation occurring.

Clearly modifications have to be made to the diffusion aspects of the model to take into account variations in the rate of diffusion with concentration if accurate results are to be obtained for longer operating times. There appears to be, however, no information available in the literature to give guidance as to what form this concentration dependency should take. Further research is required to determine the variation of D_0, the diffusion constant, with concentration, and this would then allow refinement of the model to accurately predict pre-arcing times over the complete operating range.

5.5 The Ageing of Fuses

Once a fuse has been correctly selected for a particular application then it should have a useful service life of many years in a fault-free circuit. There are several factors, however, which may cause fuse fatigue, possibly resulting in premature operation. Usually this is referred to as 'nuisance blowing' with no harmful consequences other than the loss of supply. In some situations, however, the premature operation of a fuse can cause serious damage to other circuit components. Consider, for example, the loss of one fuse in a three phase motor circuit. Single phasing results, leading to possible motor damage. High voltage fuses protecting such motors are usually fitted with striker pins, and used in conjunction with a three-phase switch. Loss of one fuse, for any reason, causes its striker pin to operate the trip-all-phase switch mechanism, disconnecting the motor and thus preventing any damage.

The striker pin operated fuse-switch can also save a damaged fuse from self destruction. For example, if a multi-element fuse loses one or more of its elements, for whatever reason, then this may effectively reduce its current carrying capability to such a degree that it is no longer capable of carrying its rated full load current. It is thus possible that this fuse would operate in a fault-free circuit. If the circuit current is less than the minimum breaking current of the fuse, then it may be unable, alone, to clear

the circuit. However, as soon as the fuse starts to arc, the striker pin operates the fuse-switch mechanism, and the switch contacts clear the circuit, thus relieving the fuse.

Unfortunately, not all fuse-gear is fitted with striker pin operated switch mechanisms. Such fuse-gear then rely on the fuse successfully clearing all currents. If a damaged fuse were to operate on a current below its minimum breaking current in these circumstances, there is a possibility that serious failure may result. It is most important, therefore, that fuse elements are not damaged prior to, or during their service life. There are several factors which might cause element damage. These include:

(i) Physical damage due to handling. Fuses are, in particular, susceptible to axial forces, when one or more elements may break at an element notch.

(ii) Metal fatigue due to cyclic loading. The continual expansion and contraction of fuse elements during cyclic loading, due to, say, direct-on-line motor starting applications, can cause elements to fracture. Special motor start fuses with corrugated elements have been designed to overcome this problem.

(iii) Partial operation of the M-effect during transient overloads or gradual operation under normal full load current conditions.

Factors (i) and (ii) are beyond the scope of this thesis, but factor (iii) will be considered further.

The effect of transient overloads on the M-effect has been considerably researched [55, 56, 58]. During these investigations it was shown that, whilst some M-effect action was apparent, no fuse degradation occurred which in any way impaired the subsequent performance of the fuse.

The effect of prolonged operation at or near full load current is however, more difficult to determine experimentally, as under normal conditions this would require the examination of fuses which have been in service for many years, to see whether any element degradation had occurred.

Previous research [30] has shown that the current corresponding to the asymptote of the element time-current characteristic corresponds with the minimum current which will cause the M-effect alloy to become molten. Since the full load current of a fuse would be typically 20% to 30% below this value, the M-effect alloy would never reach melting temperature. This has been confirmed by Leach [34] who showed that typical 60 ampere low voltage fuses carrying full load current have an element centre temperature of 170°C, well below the alloy melting temperature.

Using the simulation it is possible to determine the growth of tin concentration through the silver element, and hence predict any fuse degradation due to ageing.

The element was set at a constant temperature of 200°C, to allow for fuse designs which may run at higher temperatures than those tested by Leach, and a tin concentration plot with time obtained. Fig. 5.13 shows the growth in tin concentration at a depth of 50 microns from the tin deposit. This distance was chosen as it represents the thinnest element typically used in fuse designs. Using the criterion that 40% concetration represents the diffused depth, the simulation predicts a life expectancy of over six years.

For longer operating times the model has been shown to predict faster diffusion rates than are achieved in practice, and thus any errors due to model inaccuracy would err on the side of caution. Fuses would thus be expected to have a useful life of many years longer than this predicted life.

5.6 Interim Conclusions.

A combination of the software modelling techniques developed in Chapter 3, and the experimental data on diffusion rates obtained in Chapter 5, have enabled computer simulations to be produced for a range of fuse elements. Plain silver elements, both with and without M-effect alloy, and also notched silver elements have been successfully modelled, and, in the main, good agreement obtained with experimental results.

The model has also enabled the effect of fuse ageing to be studied, and predictions of fuse service life to be made.

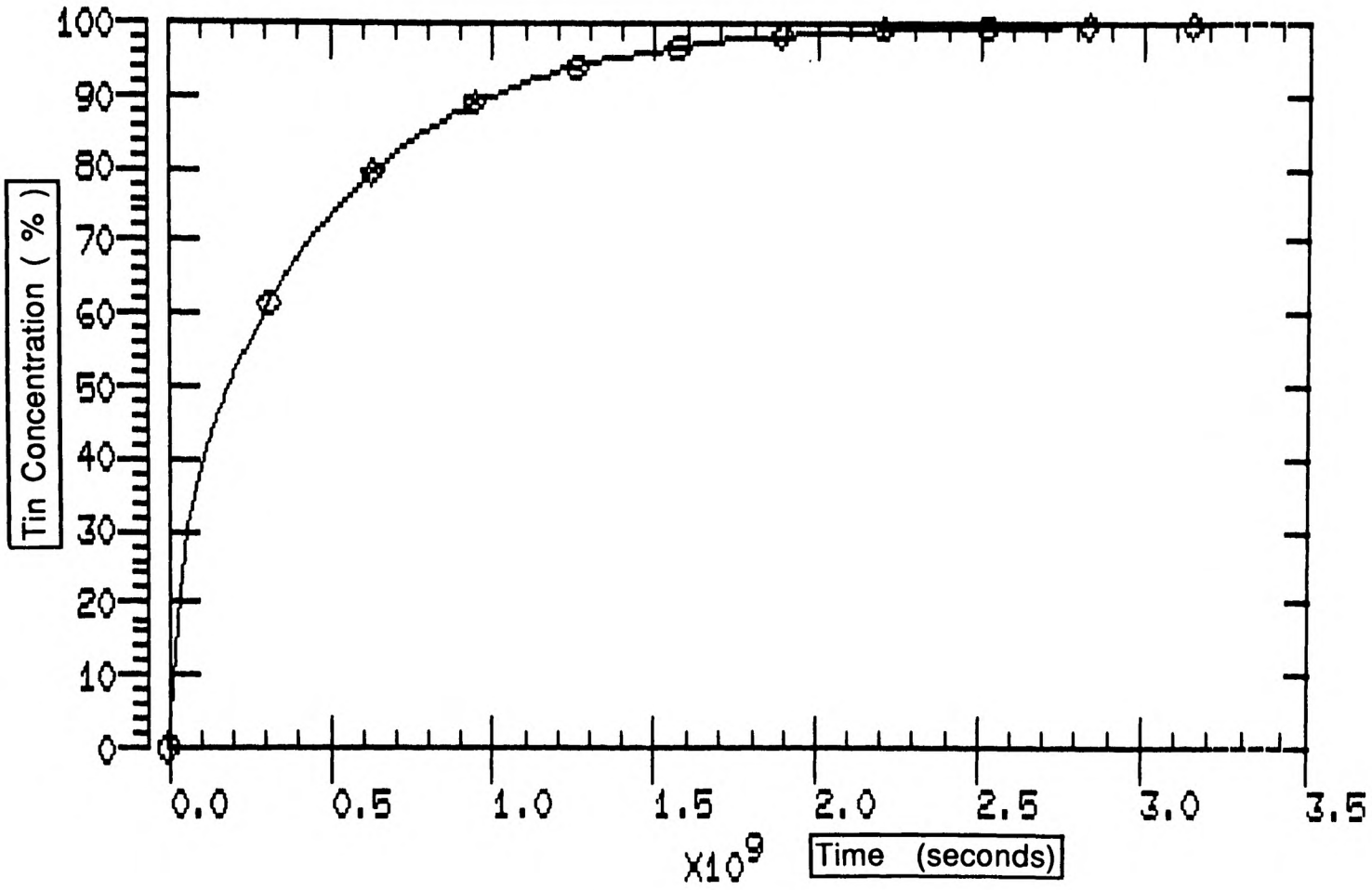

Growth of Tin Concentration with Time a Distance of 50 Microns from the M-Effect Deposit when subjected to a Constant Temperature of 200 °C

Fig. 5.13

Chapter 6

Conclusions and Recommendations for Further Work

The pre-arcing operation of the high rupturing capacity fuse has been extensively studied, and several novelties identified, regarding both its mode of operation and the way in which this operation can be successfully modelled. These novelties include:

* the simulation method
* the effect of varying the depth of granular filler
* the effect of varying both the composition and quantity of the M-effect alloy
* the determination of fundamental diffusion parameters relevant to fuse operation
* the prediction of fuse service-life

A novel method has been developed to analyse the heat flow and diffusion effects which simultaneously occur during the pre-arcing operating period of a fuse with M-effect. By describing heat flow and mass diffusion in terms of electrical analogues, it has been possible to model fuse operation as an electrical circuit, and to analyse the operation of this circuit using a commercial analogue circuit simulation package. Although such packages have been

available for several years, they have never been used, as far as it is known, to model fuse operation. Their use permits fuse parameters to be studied to depths previously not possible, and offers unrivalled possibilities in the fields of fuse design and fuse applications.

The method developed has enabled plain elements, notched elements and elements both with and without M-effect alloy to be modelled, and also the cooling effects of the fuse's silica sand filler to be determined. At high current densities, the effects of the characteristics of the prospective current, such as circuit power factor and point on wave closing angle, can be taken into account, and notch temperature profiles and element resistance variations with temperature obtained.

At lower current densities, both radial and axial heat loss to the silica sand filler can be successfully modelled. It was found that whilst the initial effect of the addition the filler was to cool the fuse element, increasing the filler depth around the element actually caused the element to run warmer.

Practical tests were made to determine what effect the quantity, location and composition of the M-effect alloy have on the operating characteristics of the fuse.

It was found that there is a definite minimum quantity of alloy, below which M-effect action will not successfully proceed. Once this minimum value has been exceeded,

however, the actual quantity of alloy appears to have little bearing on the speed of alloy diffusion. Too much alloy may cause secondary problems by running to an adjacent notch and causing premature operation. This can be obviated by placing the alloy in a pre-formed well in the element,or alternatively, covering it with a layer of fireclay cement.

The practice of adding small quantities of silver to the tin to improve 'solderability' on silver elements adversely affects the operating characteristics of the fuse. It was found that increasing the silver content caused the fuse to operate both slower and at higher temperatures when being subjected low over-current faults.

The parameters for the diffusion model were obtained from experiments to determine both the composition of the diffused M-effect layer and also the rate of diffusion of the layer through the element. Fuse elements were heat treated in a temperature controlled oven (constant temperature testing) and also subjected to low fault over-currents for controlled periods of time (constant current testing). Analysis of these elements, using both optical and scanning electron microscope techniques, enabled the composition of the diffused layer to be determined as approximately 40% Tin, 60% Silver. It was also found that the diffusion rate of tin through silver for temperatures up to 410°C follows an Arrhenius temperature dependency in which the diffusion constant, D_o is equal to $2.1 \times 10^{-4} cm.^2 sec.^{-1}$ and the activation energy, Q is equal to 55,400 Joules $Mol.^{-1}$

The model was used to simulate the time-current characteristics for fuse elements both with and without M-effect alloy, and the results obtained compared with experimental tests. It was found that the simulation of elements without M-effect gave good agreement with practical results for the time periods one second to over three hours. Results on fuses with M-effect were, however, more variable. Reasonable agreement was obtained for pre-arcing operating times up to approximately thirty minutes, but for longer times the simulated results deviated from those obtained experimentally. Several simplifying assumptions were made whilst developing the model, but the most important variable is the rate of diffusion. Although provision was made in the model for the variation of the rate of diffusion with temperature, no account was taken of its variation with concentration, this being assumed fixed at 100%. It is probable that this over-simplification was the cause of the deviation. Unfortunately there is a dearth of knowledge in this area and there appears to be no information available in the literature to give guidance as to what form this concentration dependency should take. Further research is thus required in this area.

The possible ageing of fuses due to progressive diffusion of the M-effect alloy through the fuse element has been studied. Using both constant current and constant temperature modelling techniques, it was found that under normal operating conditions, fuses with M-effect should have a life expectancy of many years in a fault-free circuit.

The model was used to determine temperature rise and time-current characteristics for single fuse elements mounted in a test cell. No account was taken of the loss of heat to the fuse barrel, surrounding air or connecting tags and cables. The model can be extended to cover the barrel and end connections by merely extending the mesh arrangement of the model to include these additional components, provided of course, their thermal properties are known. Loss of heat from the barrel surface by convection can also be modelled as an electrical analogue using ASTEC3 [40] and thus the loss of heat to the surrounding air determined.

Multiple element fuses may also be modelled by duplicating the single element model within the model's mesh array several times, once for each element. Modelling helically wound and concentric elements would, however, severely complicate the model and more research is required in the analysis of multiple element fuses.

In conclusion, the novel modelling techniques described in this thesis enable fuse operation to be examined and evaluated to a depth previously not possible, and fundamental information on fuse operation obtained. This knowledge is invaluable to the fuse design engineer as it will permit the rapid development of new fuses, as well as determining the suitability of existing fuses for new applications. Further research is required at very long pre-arcing times (greater than thirty minutes), however, before fuse operation over the entire fuse pre-arcing period can be accurately predicted.

REFERENCES

1. **Preece W.H.**,'On the Heating Effects of Electric Currents', Proc. Royal. Soc. 1884, 36, p 464

2. **Thompson S.P.**, Reported by Newbery, P.G. & Wright, A. 'Electric Fuses', I.E.E. Power Eng. S2 Peter Peregrins Ltd. 1982, Ch.1.

3. **Boys C.V. and Cunyngham H.H.**, Reported by Newbery, P.G. & Wright, A. 'Electric Fuses', I.E.E. Power Eng. S2 Peter Peregrins Ltd. 1982, Ch.1.

4. **Cockburn A.C.**,'On Safety Fuses for Electric light Circuits and on the Behaviour of the Various Metals usually Employed in their Construction', J. Soc. of Teleg. Eng., 1887, 16 pp 650-665

5. **Edison T.A.**, Reported by Newbery, P.G. & Wright, A. 'Electric Fuses', I.E.E. Power Eng. S2 Peter Peregrins Ltd. 1982, Ch.1.

6. **Mordey, W.M.**,'High-Tension Safety Junctions'. Reported in the Elec. Times Centenary Ed. (1891-1991). Feb. 1991.

7. **Oelschlager**, reported by Schwartz A. and James W.H.N. 'Low-tension Thermal Cut-outs.' Journal I.E.E. 1905,35,p364

8. **Gibson J.W.**,'The High-Rupturing-Capacity Cartridge Fuse, with Special Reference to Short-Circuit Performance', Journal Institution of Electrical Engineers, London, - Vol.88, 1941, pp 2-24

9. **Metcalf A.W.**,'A New Fuse Phenomenon', Beama Journal, 1939, 44, pp 109-151

10. **Rosen P.**,'The Design and Application of High Voltage Fuses', Institution of Engineers (India), lecture presented at Bombay, Madras, Hyderabad, Calcutta and Delhi. February 1979

11. **Newbery P.G. & Wright A.**,'Electric fuses', Proc. IEE, Vol.124, No 11R, November 1977.

12. **Turner H.W. & Turner C.**,'Phenomena Occurring During the Extinction of Arcs in Fuses', 2nd Int. Conf. on Switching Arc Phenomena. Lodz, Poland 25-27th Sept. 1973

13. **Turner H.W. & Turner C.**,'Thermal Constants of Filler and their Influence on the Metallurgical Effects in Fuse Elements during Pulse Duty', Int. Conf. on Electric Fuses and their Applications. Trondheim, Norway 13-15th June 1984

14. **Rosen P.**,'Fuses for Transformer Protection - Continental and U.S. Practice', Electrical Times, 18th May 1979

15. **Turner H.W. & Turner C.**, 'Correct Fuse Selection must be based on Appropriate Standard', Electrical Times, 23rd Feb. 1979 pp 6-8

16. **Gibson J.W.**, 'The Standardisation of High Voltage Current-Limiting Fuses,' Int. Conf. on Electric Fuses, Liverpool Polytechnic, 7-9 April 1976.

17. **Leach J.G., Newbery P.G. & Wright A.**, 'Analysis of High-Rupturing-Capacity Fuselink Prearcing Phenomena by a Finite-Difference Method', Proc. IEE, Vol.120, No 9, Sept. 1973

18. **Turner H.W. & Turner C.**, 'Fuse Standards Demand Tighter Tolerances', Electrical Times, Dec. 1980, pp 9-10

19. **Wilkins R.**, 'Simulation of Fuselink Temperature-Rise Tests.',Int. Conf. on Elec. Fuses and their Applications. Trondheim, Norway 13-15th June 1984.

20. **Wilkins R & McEwan P.M.**, 'AC short Circuit Performance of Notched Fuse Elements', Proc. Inst. Elec. Eng., V122, N3, March 1975 pp 288-292

21. **Ikeda & Yoneta**, 'Mathematical Investigation of Fusing', Engineering Memoirs, Hokkaido Uni., Sappora, Japan, Vol. 2, 1930, pp 147-159

22. **Schubert G.U.**, 'On a Solution of the Heat Conduction Equation which Enters into the Theory of Electrical Fuses', Zeitschrift fur angewandte Physik, Berlin, Vol.2, 1950 pp 174-179

23. **Guile A.E. and Carne E.B.**, 'An Analysis of an Analogue Solution Applied to the Heat Conduction Problem in a Cartridge Fuse', A.I.E.E. Transactions, Vol.72, January 1954 pp 861-868

24. **Guile A.E.**, 'The Calculation of the Complete Time/Current Characteristics of Cartridge Fuses with Single Wire Elements', A.I.E.E. Transactions, Vol. 74, 1955, pp 1108

25. **Guile A.E.**, 'The Calculation of the Complete Time/Current Characteristics of Certain Cartridge Fuses with Strip Elements', Electrical Energy, Dec. 1956, pp 114-119

26. **Novotny B.**, 'Theory of Current Limiting Fuses', Elektrotech Abyor, Vol. 49 No 11, November 1960

27. **Wilkins R. and McEwan P.M.**, 'AC Short-circuit Performance of Uniform Section Fuse Elements', Proc. Inst. Elec. Eng., V122, N3, March 1975, pp 285-288

28. **Xian-Zhong and Ji-Mei**, 'The Simulation of Pre-arcing Characteristics of Fuse Elements in the Finite Element Method', Proc. 3rd Int. Conf. on Electric Fuses and their Applications, Eindhoven, The Netherlands, 11-13th May 1987, pp 24-29

29. **Hofmann M. and Lindmayer M.**, 'Pre-calculation of Time/Current Characteristics of "M"-effect Fuse Elements', Proc. 3rd Int. Conf. on Electric Fuses and their Applications, Eindhoven, The Netherlands, 11-13th May 1987, pp 30-38

30. **Hofmann M. and Lindmayer M.**, 'Fusing and Ageing Behaviour of Fuse Elements with "M"-Effect at Medium-and-Long-Time Overload', Int. Conf. on Electric Fuses and their Applications, Trondheim, Norway, 13-15th June 1984, pp 280-296

31. **'ADINAT** - A Finite Element Program for Automatic Dynamic Nonlinear Analysis of Temperature', ADINA Engineering AB, Vasteras, Sweden

32. **Daalder J.E., Kulsetas J. and Rondeel W.G.J.**,'Ageing in Fuses with M-Effect', 4th Int. Symposium on Switching Arcs, Lodz, Poland, 22-24th Sept. 1981

33. **Jost W.**, 'Diffusion in Solids, Liquids, Gases', Academic Press Inc. New York, Revised Edition 1960

34. **Leach J.G.**, 'The Analysis of H.R.C. Fuse-link Pre-arcing Phenomena', PhD Thesis, Nottingham Uni. Oct.1972

35. **Allen, D.N.**,'Relaxation Methods', McGraw-Hill, 1954

36. **Crank, J.**, 'The Mathematics of Diffusion', Clarendon Press, Oxford, 1975

37. **Fick, A.**,'Ueber Diffusion', Ann. Phys. Lpz 170(1855), 59

38. **Cornwell, K.**,'The Flow of Heat', Van Nostrand Reinhold, 1977, pp 113-116

39. **Fourier, J.B.**, 'Theorie Analytique de la Chaleur', Euvres de Fourier, 1822

40. **Poole, N.J., Sarvar, F., Witting, P.A. and McKenzie, W.H.**,'Thermal Modelling using ASTEC3 Software, Int.J. of Num. Mod. Vol 1, 1988, pp 103-113

41. **Witting P.A.** 'Electronic Circuit and System Simulation with ASTEC3.' Computer-Aided Eng. J. Vol 2 No6,1985 pp 186-191.

42. **'ASTEC3 User Manual'**, Sia Computer Services, France, 1984

43. **Chapman, A.J.**,'Heat Transfer', Collier-Macmillan Ltd., 1974 pp 110-113

44. **Leach, J.G.,** 'Pre-Arcing Analysis of Fuses', Brush Fusegear Ltd., Internal Report No 705, 1976

45. **'Resistivity of Work Hardened Silver Strip'**, Private Communication: Johnson-Matthey Ltd., 1988

46. **Butts, A. and Cox, E.,** 'Silver Economics, Metallurgy and Use', Van Nostrand, 1967

47. **Weast, R.C.,** 'Handbook of Chemistry & Physics', 70th Edition, CRC Press Inc., USA, 1989-90

48. **'Pre-Arcing Analysis of Fuses using the HP1000 Computer'**, Brush Fusegear Ltd. Internal Report, June 1986

49. **Stevenson, W.D.,** 'Elements of Power System Analysis', McGraw-Hill, 2nd Edition, 1962, pp 251-252

50. **Crank, J., McFarlane, N.R., Newby, J.C. Paterson, G.D. & Pedley, J.B.,** 'Diffusion Processes in Environmental Systems', The Macmillan Press Ltd., London, 1981

51. **Geiger, G.H. and Poirier, D.R.,** 'Transport Phenomena in Metallurgy', Adison-Wesley Pub. Co. 1973 Ch 13

52. **Swalin, R. and Leak, V.G.,** 'Diffusion of Hetrovalent Solutes in Liquid Silver', Acta Met. 13, May 1965, pp 471-478

53. **Reynik, R.J.**, 'Self Diffusion in Liquid Metals', Applied Physics Letters 9, Sept. 1966, pp 239-240

54. **Saxton, H. and Sherby, O.**, 'Viscosity and Atomic Mobility in Liquid Metals', Trans. ASM 55, Sept. 1962, pp 826-843

55. **Sletterlink, A. Vlutters, H. and Zwaag, H.V.D.**, 'The Influence of Diffusion Phenomena on Time/Current Characteristics of Fuse-Links', Holectechniek 2, 1972, No 3 pp 117-123

56. **Rondeel, W.G.J., Kulsetas, J. and Bodsberg, K.**, 'Dimensioning Criteria for Fuses with M-effect', 4th Int. Symposium on Switching Arcs, Lodz, Poland, 22-24th Sept. 1981

57. **Klepp, G.**, 'Uber das Zeit/Strom-Verhalten von gealterten Sicherungsschmelzleitern mit Lotauftrag', ETZ Archiv Bd. 3 (1981) H.8

58. **Ovland, S., Kulsetas, J., Forster, A. and Rondeel, W.**, 'Metallurgical Deterioration of Copper Fuse Elements in High Voltage Fuses', Int. Conf. on Electric Fuses and their Applications, Trondheim, Norway 13-15th June 1984, pp 270-27

59. **Brandes, E.A.**, 'Smithells Metals Reference Book', 6th Ed, Butterworths, London, 1983

60. **Howe, A.F., de Cogan, D., Webb, P.W. and Nurse, N.P.M.,** 'Measuring the Pre-arcing Temperature of High Breaking Capacity Fuselinks by Thermal Imaging', Int. Conf. on Electric Fuses and their Applications, Trondheim, Norway 13-15th June, 1984

61. **Davies, C.,** 'Quantative Measurements using the S.E.M.', Polytechnic of Wales Internal Report

62. **Ma, C.H. and Swalin, R.A.,** 'A Study of Solute Diffusion in Liquid Tin', Acta Metallurgica, Vol. 8, June 1960 pp 388-395

63. **Seith, W. and Peretti, E.,** 'Diffusion in Festen Metallen und Deren Beziehungen zu anderen Eigenslaften', Z, Elektrochem 42, 570, 1936

64. **Linde, J.O.,** 'Effect of Impurities on the Resistivity of Silver', Ann. Physik 14, 1932, pp 352

65. **Wright, A. and Beaumont, K.J.,** 'Analysis of High-Breaking-Capacity Arcing Phenomina', Proc. IEE Vol. 123 No 3, March 1976, pp 252-260

66. **Charnley, M.,**'A Model Design Approach for Electronic CAE', Computer-Aided Eng. Journal, Dec. 1985, pp 192-199